

Platelet proteomic progress and restraining mechanisms in glycoprotein VI-mediated thrombus formation

Citation for published version (APA):

Huang, J. (2022). *Platelet proteomic progress and restraining mechanisms in glycoprotein VI-mediated thrombus formation*. [Doctoral Thesis, Maastricht University, Universidade de Santiago de Compostela]. Maastricht University. <https://doi.org/10.26481/dis.20221220jh>

Document status and date:

Published: 01/01/2022

DOI:

[10.26481/dis.20221220jh](https://doi.org/10.26481/dis.20221220jh)

Document Version:

Publisher's PDF, also known as Version of record

Please check the document version of this publication:

- A submitted manuscript is the version of the article upon submission and before peer-review. There can be important differences between the submitted version and the official published version of record. People interested in the research are advised to contact the author for the final version of the publication, or visit the DOI to the publisher's website.
- The final author version and the galley proof are versions of the publication after peer review.
- The final published version features the final layout of the paper including the volume, issue and page numbers.

[Link to publication](#)

General rights

Copyright and moral rights for the publications made accessible in the public portal are retained by the authors and/or other copyright owners and it is a condition of accessing publications that users recognise and abide by the legal requirements associated with these rights.

- Users may download and print one copy of any publication from the public portal for the purpose of private study or research.
- You may not further distribute the material or use it for any profit-making activity or commercial gain
- You may freely distribute the URL identifying the publication in the public portal.

If the publication is distributed under the terms of Article 25fa of the Dutch Copyright Act, indicated by the "Taverne" license above, please follow below link for the End User Agreement:

www.umlib.nl/taverne-license

Take down policy

If you believe that this document breaches copyright please contact us at:

repository@maastrichtuniversity.nl

providing details and we will investigate your claim.

Platelet proteomic progress and restraining mechanisms in glycoprotein VI-mediated thrombus formation

Jingnan Huang

Platelet proteomic progress and restraining mechanisms in glycoprotein VI-mediated thrombus formation

Thesis: Maastricht University

ISBN: 978-94-6469-111-5

Cover design: Jingnan Huang; cover layout: proefschriftmaken.

Lay-out: Jingnan Huang

Printed by ProefschriftMaken II [www. Proefschriftmaken.nl](http://www.Proefschriftmaken.nl)

© Jingnan Huang

Platelet proteomic progress and restraining mechanisms in glycoprotein VI-mediated thrombus formation

DISSERTATION

To obtain the degree of Doctor at Maastricht University and
Doctor at La Universidad de Santiago de Compostela,
on the authority of the Rector Magnificus, Prof. dr. Pamela
Habibović, in accordance with the decision of the Board of
Deans, to be defended in public
on

Tuesday, 20 December 2022 at 13:00 hours

by
Jingnan Huang

Promotors

Prof. Dr. Johan W.M. Heemskerk, Maastricht University

Prof. Dr. Albert Sickmann, Leibniz-Institut für Analytische Wissenschaften-ISAS-e.V.

Co-promotors

Dr. Ángel García, Universidade Santiago de Compostela

Prof. Dr. Hugo ten Cate, Maastricht University

Assessment Committee

Prof. Dr. Edwin C. M. Mariman, Maastricht University (Chair)

Dr. Ezequiel Alvarez-Castro, Universidade Santiago de Compostela

Dr. Anika Grüneboom, Leibniz-Institut für Analytische Wissenschaften-ISAS-e.V.

Dr. Francisco Javier Salgado-Castro, Universidade Santiago de Compostela

Prof. Dr. Monika Stoll, Maastricht University

Prof. Dr. Ulrich Walter, Johannes Gutenberg-Universität Mainz

This research in this thesis was supported by a joint PhD scholarship of European Union's Horizon 2020 research and innovation program under the Marie Skłodowska-Curie grant agreement TAPAS No. 766118.

The printing of this thesis was supported by Hart Onderzoek Nederland.

This thesis is submitted as a result of the joint doctorate programme of Jingnan Huang at the Universities of Maastricht University and Santiago de Compostela, for obtaining a double PhD degree. Admission to the joint doctorate programme has been confirmed in the Individual Joint PhD Learning Agreement between the two universities and postgraduate researcher Jingnan Huang, which was signed on 28 February 2020

Contents

Chapter 1	7
<i>General introduction</i>	
Chapter 2	23
<i>Molecular proteomics and signaling of human platelets in health and disease</i>	
Chapter 3	65
<i>Assessment of a complete and classified platelet proteome from genome-wide transcripts of human platelets and megakaryocytes covering platelet functions</i>	
Chapter 4	123
<i>A classified reference genome-wide transcriptome and proteome of human and mouse platelets revealing high qualitative similarity</i>	
Chapter 5	165
<i>Impaired iloprost-induced platelet inhibition and phosphoproteome changes in patients with confirmed pseudohypoparathyroidism type Ia, linked to genetic mutations in GNAS</i>	
Chapter 6	213
<i>Non-redundant roles of platelet glycoprotein VI and integrin $\alpha\text{IIb}\beta\text{3}$ in fibrin-mediated microthrombus formation</i>	
Chapter 7	261
<i>Restrained glycoprotein VI-induced platelet signaling by tyrosine protein phosphatases independent of phospholipase Cγ2</i>	
Chapter 8	283
<i>Roles of focal adhesion kinase PTK2 and integrin $\alpha\text{IIb}\beta\text{3}$ signaling in collagen- and GPVI-dependent thrombus formation under shear</i>	
Chapter 9	333
<i>General discussion</i>	
Chapter 10	349
<i>Summary, Samenvatting, Resumo, 总结, Impact, Curriculum vitae, Publications, Acknowledgements</i>	

Chapter 1

General Introduction

Platelets are the smallest blood cells, being released from megakaryocytes in mainly the bone marrow, that are known to play crucial roles in thrombosis and hemostasis¹. Upon vascular injury, platelets encounter exposed collagens and von Willebrand factor (VWF) in the subendothelial matrix. This leads to platelet adhesion, activation and plug formation in order to avoid excessive blood loss. At a ruptured atherosclerotic blood vessel or undesired platelet activation can promote pathological arterial thrombosis. Apart from hemostasis and thrombosis, platelets are also involved in other physiological and pathological processes, including inflammation and cancer metastasis^{1,2}. A central mechanism of platelet activation under flow is by direct binding of collagen to fibers via the receptors glycoprotein VI (GPVI) and integrin $\alpha 2\beta 1$, as well as by indirect binding VWF via the glycoprotein complex, GPIb-V-IX. The GPVI is an immunoglobulin receptor on the platelet membrane surface, which is now considered as an antithrombotic target due to its major role in thrombosis but a minor role in hemostasis³. With the development of advanced mass spectrometric techniques, and due to the anucleate structure of platelets, mass spectrometry-based proteomics has become a powerful tool to study the membrane receptor-mediated platelet signaling pathways⁴⁻⁷. In this chapter, I give a general background of GPVI-mediated platelet activation and thrombus formation, as well as of applications of mass spectrometry-based proteomics method for the research to platelet proteome and signaling pathways.

Platelet in thrombosis and hemostasis

In the blood, circulating platelets are normally present in a resting state. However, once a blood vessel becomes damaged, the platelets become exposed to subendothelial elements such as collagens and VWF. This causes platelet adhesion and activation, which can lead to either hemostasis or arterial thrombosis⁸. Under flow conditions, the initiation of transient platelet adhesion is by collagen-bound VWF via GPIb-V-IX. This interaction

allows stable adhesion through the collagen receptors, GPVI and integrin $\alpha 2\beta 1$, to further amplify platelet activation responses (Figure 1)^{9,10}. The GPVI-induced platelet activation via collagen provides a strong signaling trigger, involving the mobilization of intracellular Ca^{2+} , activation of integrins $\alpha 2\beta 1$ and $\alpha \text{IIb}\beta 3$, release of thromboxane A_2 (TXA_2), granule secretion, and the surface exposure of phosphatidylserine (PS)^{1,2,11}. The latter response by a fraction of the platelets allows the binding of coagulation factors and promotes thrombin generation¹². Meanwhile, the release of secondary mediators including ADP and TXA_2 , in synergy with the generated thrombin, stimulates more platelets through the activation of G protein-coupled receptors (GPCRs), thereby amplifying the thrombus formation process¹³. In activated platelets, the conformation of integrin $\alpha \text{IIb}\beta 3$ is switched from a low-affinity state to a high affinity state, which allows or enforces its interaction with the (soluble) ligands fibrinogen, fibronectin, VWF and fibrin¹⁴⁻¹⁶. The activated $\alpha \text{IIb}\beta 3$ is required for platelet aggregation, and further enhances platelet activation through outside-in signaling, which results in platelet spreading and clot retraction¹⁵. As referred to above, many reviews have been written on the signaling mechanisms of platelet activation. Here, I will confine to introduce only those aspects that are relevant for the present thesis, in particular by focusing on the central platelet receptor in this thesis, namely GPVI.

Glycoprotein VI (GPVI) as a central platelet receptor

GPVI is the major signaling collagen receptor that is expressed only on platelets and megakaryocytes. Apart from this, GPVI can also act as a responding receptor for other ligands, including fibrin, fibrinogen, laminin, collagen-related peptides (CRP) or convulxin^{11,17}. The GPVI-induced activation of platelets - with strength depending on the nature of the ligand - involves Src family kinases (SFK), which phosphorylate the dimeric GPVI co-receptor FcR γ -chain at its downstream immunoreceptor tyrosine-based activation motifs (ITAM). This recruits the tyrosine kinase Syk to

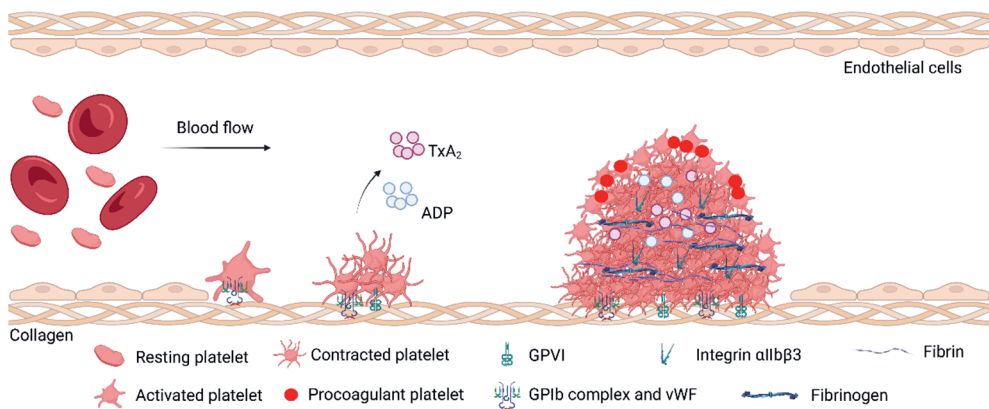


Figure 1. Schematic overview of thrombus formation. Upon vascular damage, resting platelets become activated by binding to collagens in the extracellular, followed by the release of secondary mediators to activate more platelets to build up a thrombus via fibrinogen interactions. Figure created by Biorender.com.

phosphorylate and activate multiple target proteins, including linker for activated T-cells (LAT) (Figure 2). The phosphorylated LAT acts as a recruitment protein for a series of adaptors and kinases, including Tec family kinases (Tec, Btk), SLP76 and phosphoinositide 3-kinases (PI3K). A major outcome of this signaling cascade is the phosphorylation, recruitment and activation of phospholipase $\text{C}\gamma 2$ (PLC $\gamma 2$) to generate the second messengers inositol 1,4,5-trisphosphate (IP_3) and diacylglycerol (DAG); the generated IP_3 evokes mobilization of intracellular Ca^{2+} from the internal stores in platelets. Both the PLC $\gamma 2$ and PI3K activation routes can promote integrin activation and integrin outside-in signaling^{11,18-20}.

In 2009, the first two patients with a compound heterozygous GPVI deficiency were reported. Both patients showed ecchymoses, i.e. only mild bleeding symptoms with a normal platelet count, despite different mutations in the *GP6* gene^{21,22}. In 2013, four additional patients from Chile with novel *GP6* mutations were discovered, who had a somewhat prolonged bleeding time and showed epistaxis. *In vitro* experimentation revealed that the platelets from these patients were completely unresponsive to collagen

and convulxin²³. The findings with Chilean patients suggested that the frequency of GPVI deficiency is higher than was previously estimated. In addition, the observed minor role of GPVI in hemostasis raised the possibility that GPVI can be a suitable anti-thrombotic target with limited bleeding side effects.

Considering that GPVI may be a novel antithrombotic target, the possibilities to suppress GPVI-mediated thrombus formation have been extensively studied. This has led to several inhibitors of the collagen-GPVI interaction. Revacept (a soluble dimeric GPVI-Fc fusion protein) was found to interfere with the GPVI-dependent platelet aggregation through its competitive binding to collagen^{24,25}. On the other hand, the anti-GPVI Fab 9O12 directly interferes with the interaction of GPVI with collagen. The Fab thereby prevents the GPVI-mediated platelet adhesion²⁶. In addition, GPVI-induced platelet activation and signaling can be suppressed through pharmacological inhibition of downstream kinases or adaptors. For example, the compound PRT-060318 is a well-known inhibitor of the tyrosine kinase Syk, while ibrutinib is clinically applied to suppress Btk in cancers, and the drug TGX-221 works to block the class I PI3K β isoform²⁷⁻²⁹.

On the other hand, much less is known of the restraining mechanisms of GPVI-induced platelet activation. Several ITIM-containing (immunoreceptor tyrosine-based inhibitory motif) receptors are expressed in platelets, which signal through receptor and non-receptor protein tyrosine phosphatases, such as Shp1 and Shp2. The receptors which signal through an ITIM include PECAM1 and G6b-B. By convention, this signaling suppresses ITAM-mediated platelet activation by dephosphorylating the key regulators of this signaling, including Src, Syk and LAT³⁰.

Another way of downregulating GPVI activity on the platelet surface is via its cleavage by proteases of the ADAM (A Disintegrin And Metalloprotease) family. Both ADAM7 and ADAM10 become activated upon platelet stimulation, which results in the release of soluble GPVI into the plasma³¹⁻³⁴.

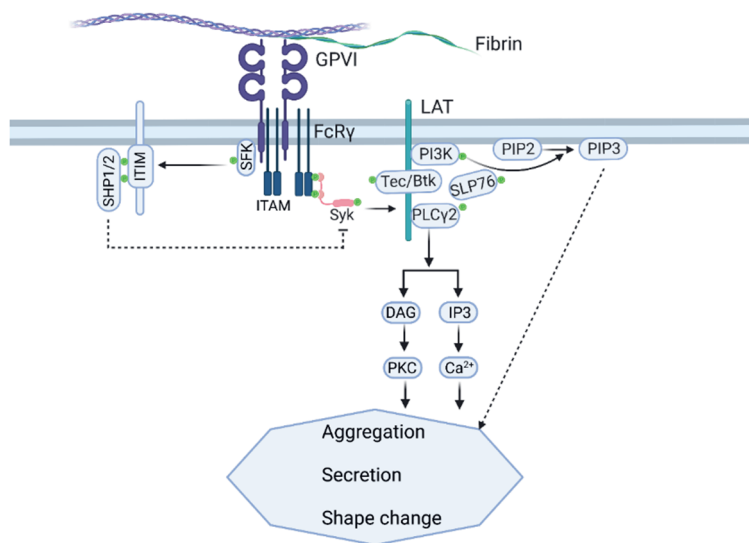


Figure 2. Schematic representation of GPVI-related platelet signaling cascades upon stimulation via collagen of fibrin. The binding of collagen (fibrin) to the dimeric ITAM-containing co-receptor FcR γ -chain activates Src family kinases (SFK) and Syk, resulting in the assembly of a LAT signalosome to recruit executive proteins like PLC γ 2, PI3K and Tec/Btk. The activated PI3K catalyzes the generation of PIP₃ (3-phosphorylated phosphoinositide), while the PLC γ 2 activation results in Ca²⁺ mobilization. As a result, platelets can aggregate, secrete and change shape. For abbreviations, see text. Figure created by Biorender.com.

Soluble GPVI is considered as a potential biomarker for platelet activation, due to the unique expression of GPVI on platelets and megakaryocytes. Increased levels of soluble GPVI have been detected in the plasmas from patients with acute ischemic stroke, sepsis or deep venous thrombosis³⁵.

Remaining questions related to GPVI that are still partly unanswered are: (i) the extent to which integrin α IIb β 3 - as a fibrin(ogen) receptor - adds to the GPVI signaling pathway; (ii) including a known α IIb β 3-dependent signaling rout of calcium- and integrin-binding protein 1 (CIB1) and the focal adhesion kinase PTK2. And furthermore, to which extent Shp1 and Shp2 are really

capable to downregulate platelet activation in response to different GPVI agonists. These questions I aim to answer in the present thesis.

Introducing platelet omics

Because of their anucleate structure, the processes of transcription and translation are restricted in platelets³⁶, implying that the biologic functions of a platelet are mainly regulated by post-translational protein modifications (PTMs), in particular by protein phosphorylations. In recent years, mass spectrometry-based proteomic techniques have been applied to investigate the platelet protein composition (global proteome) as well as the regulatory signaling pathways inside of activated platelets (phospho-proteome)³⁷.

With the development of better and better mass spectrometers and improved spectral resolvment techniques, many publications have appeared to understand the platelet proteome, to identify new platelet signaling cascades, and to better understand the biology of platelet-related disorders. Initially, in 2004, García *et al.* detected 62 (phospho)regulated proteins from the platelets, which were stimulated by thrombin receptor activating peptide-6 (TRAP6), and separated by 2-dimensional gel electrophoresis (2-DE). Of these proteins, 41 were identified by tandem liquid chromatography-mass spectrometry (LC-MS/MS)³⁸. A next breakthrough came in 2012, when Burkhardt *et al.* identified more than 4,000 proteins in platelets, of which the majority with estimated copy numbers, which effort thereby provided a first comprehensive analysis of the human platelet proteome⁶.

Only to a limited extent, mass spectrometry-based analyses have been used for detecting alterations in protein abundance and changes in PTMs of platelets from specific patients, for instance carrying a platelet-related bleeding disorder. The combination of global proteomics, N-terminomics and phosphoproteomics analysis was applied to platelets from a rare Scott syndrome patient (mutated *ANO6* gene, and platelet defect in phosphatidylserine exposure). The proteomics analyses identified some

differential expressed proteins, including anoctamin-6 and the catalytic subunit of calpain-1, and furthermore revealed major changes in protein phosphorylation⁷. In the platelets from a patient with Glanzmann's thrombasthenia (mutated *ITGA2B* gene of integrin subunit), using quantitative and targeted proteomics methods, it was found that the integrin chains α IIb and β 3 were absent, as well as plasmatc proteins that can bind to this integrin (fibrinogen, factor XIII and plasminogen)³⁹. Another example is the syndrome pseudohypoparathyroidism type Ia (PHP Ia)⁴⁰. This is linked to mutations in the *GNAS* locus, which expresses the G-protein subunit G α s. This G-protein is a major positive regulator of the platelet-inhibitory protein kinase A (PKA). However, for many other patients in whom the functions of platelets are expected to be altered, no proteomics information is available to better understand the disease. Since an overview of the overall progress in platelet (phospho)proteome analysis in relation to signaling and health/disease was missing, this information is provided in the present thesis.

At present, several precise proteomics quantification methods are available for monitoring the protein changes in biological samples. The widely used bottom-up proteomics method enables high sensitivity and reproducibility for identifying thousands of proteins and detecting biomarkers⁴¹. A typical platelet proteomics method includes protein extraction, LC-MS/MS analysis, data processing and validation (Figure 3). The application of either isotopic-label or label-free quantification methods on large scale sample sets now ensures a sensitive way of detecting potential novel biomarkers and drug targets in CVD. In this thesis, we have applied these methods to better understand the functional alterations in platelets from patients with mutations in the *GNAS* gene.

While platelets themselves only limitedly synthesize RNAs due to the absence of a nucleus, they inherit substantial amounts of RNA species from the megakaryocytes. This inheritance includes mRNAs, pre-mRNAs, pseudogene RNAs, long non-coding RNAs (lncRNAs), microRNAs (miRNAs) and

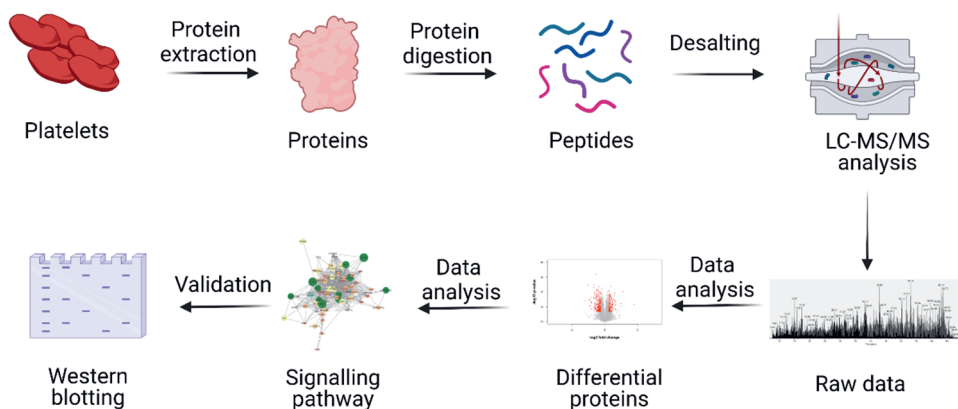


Figure 3. Typical bottom-up workflow of global platelet proteomics. Proteins from well-purified platelets are lysed and extracted, followed by reduction and alkylation steps to remove reactive groups and to allow accessibility for proteolysis. Then the proteins are digested to small peptides, commonly by trypsin. The digested samples are analyzed by a chosen type of LC-MS/MS to obtain the raw mass-spectrometry data. From the obtained spectra, differentially expressed proteins and specific signaling pathways can be determined by bioinformatics analyses. Common enrichment and linkage steps are carried out with the Perseus program from MaxQuant and the Cytoscape network tool. Finally, identified potential biomarkers or drug targets needs to be validated by regular biology experiments. Figure created by Biorender.com.

circularRNAs. Several of these RNAs species have been considered as diagnostic and therapeutic biomarkers, because they are associated with certain diseases⁴²⁻⁴⁵. In the last decades, a terrific amount of such transcripts has been mapped in platelets (>57,000)^{46,47} with advanced novel techniques like cDNA-based next-generation RNA-sequencing (RNA-seq). One megakaryocytic cell is supposed to shed thousands of platelets into the blood stream, and provide these with mRNA species during the process of thrombopoiesis⁴⁸⁻⁵⁰. Therefore, one can consider that a precise comparison of the platelet and megakaryocyte transcriptomes with the platelet proteome will provide a better understanding of the platelet structures and functions. As this comparison has not been made yet, in this thesis we

performed this effort, also extending it to compare human and mouse platelets. We envisioned that this work will help to fully understand the complexity of platelets, and to make a solid prediction model for the still missing part of the platelet proteomes in man and mouse.

Aims and outline of this thesis

For this thesis, my aims are to provide better insight into the composition of the platelet proteome and to use this knowledge for determining the mechanisms by which GPVI-induced thrombus formation can be restricted.

Chapter 1, as a general introduction, provides relevant background knowledge of platelets in hemostasis and thrombosis explains key signaling pathways induced by the collagen receptor glycoprotein VI. The following **Chapter 2** compares and discusses 67 publications on the human platelet proteome. It also recapitulates recent technical and scientific developments of global proteomics and phosphoproteomics analyses. The chapter furthermore gives an overview of reported changes in the (phospho)proteome upon platelet activation via the receptors GPVI, CLEC2 or the receptors for thrombin or ADP. **Chapter 3** provides a first quantitative analysis of the identified platelet proteome, such in comparison to recently obtained genome-wide transcriptomes of platelets and megakaryocytes. In this chapter, it is also aimed to provide a protein classification system to better understand the complexity of the platelet structure and functions, and furthermore to establish a prediction model to come to the full platelet proteome. **Chapter 4** adds to this by the inclusion of additional genome-wide platelet transcriptomes, and by an extended comparison of the human and mouse platelet proteomes and transcriptomes.

In the second part of my thesis, the omics knowledge is used to unravel signaling pathways by which the GPVI-mediated thrombus formation under flow can be restricted. **Chapter 5** reveals the changes in phosphoproteome of platelets from patients with Albright hereditary osteodystrophy (AHO) a syndrome that is linked to a maternally inherited mutation in the *GNAS* complex gene, encoding for the G-protein subunit Gas. The platelets from

these patients are often impaired in sensing inhibitory signals. We describe a way to assist the difficult diagnosis of a suspected AHO syndrome making use of proteomics and platelet phenotype analysis. **Chapter 6** focuses on a novel ligand of GPVI, fibrin, and studies the relative contributions of GPVI and integrin $\alpha\text{IIb}\beta 3$ to fibrin-dependent thrombus formation under flow conditions. In this chapter, a variety of fibrin and fibrinogen surfaces have been made to compare the effects of immunological or pharmacological blockage of GPVI, integrin $\alpha\text{IIb}\beta 3$ or the downstream tyrosine kinase signaling. **Chapter 7** focusses on a potential signaling pathway that can put a restrain on the GPVI-induced signaling pathway. We determine effects of inhibition of the tyrosine phosphatases Shp1 and Shp2, which are considered to downregulate the GPVI signaling, and thus restrain collagen-induced platelet activation and thrombus formation. In order to fully cover the platelet signaling spectrum, the studies are also performed upon blockage of phosphatidylinositol 3-kinase, which foresees in a GPVI signaling sub-pathway. In **Chapter 8**, a series of peptides is designed and synthesized that interfere with the shear-dependent platelet receptor GPR56, focal adhesion kinase PTK2 and the intracellular calcium-and-integrin binding protein 1 (CIB1). All of these signaling components potentially contribute to the GPVI-mediated platelet responses, including thrombus formation under flow. Of particular interest in the study is to see, whether the peptide inhibitor effects are flow- and shear-dependent. In the last **Chapter 9**, the most important findings of this thesis are critically discussed and placed within the framework of the current literature.

References

1. Van der Meijden PE and Heemskerk JW. Platelet biology and functions: new concepts and clinical perspectives. *Nat Rev Cardiol.* 2019;16:166-179.
2. Perrella G, Nagy M, Watson SP and Heemskerk JW. Platelet GPVI (glycoprotein VI) and thrombotic complications in the venous system. *Arterioscler Thromb Vasc Biol.* 2021;41:2681-2692.
3. Rayes J, Watson SP and Nieswandt B. Functional significance of the platelet

- immune receptors GPVI and CLEC-2. *J Clin Invest*. 2019;129:12-23.
4. Beck F, Geiger J, Gambaryan S, Veit J, Vaudel M, Nollau P et al. Time-resolved characterization of cAMP/PKA-dependent signaling reveals that platelet inhibition is a concerted process involving multiple signaling pathways. *Blood*. 2014;123:e1-e10.
 5. Beck F, Geiger J, Gambaryan S, Solari FA, Dell'Aica M, Lorocho S et al. Temporal quantitative phosphoproteomics of ADP stimulation reveals novel central nodes in platelet activation and inhibition. *Blood*. 2017;129:e1-e12.
 6. Burkhardt JM, Vaudel M, Gambaryan S, Radau S, Walter U, Martens L et al. The first comprehensive and quantitative analysis of human platelet protein composition allows the comparative analysis of structural and functional pathways. *Blood*. 2012;120:e73-82.
 7. Solari FA, Mattheij NJ, Burkhardt JM, Swieringa F, Collins PW, Cosemans JM et al. Combined quantification of the global proteome, phosphoproteome, and proteolytic cleavage to characterize altered platelet functions in the human Scott syndrome. *Mol Cell Proteomics*. 2016;15:3154-3169.
 8. Versteeg HH, Heemskerk JW, Levi M and Reitsma PH. New fundamentals in hemostasis. *Physiol Rev*. 2013;93:327-58.
 9. Du X. Signaling and regulation of the platelet glycoprotein Ib-IX-V complex. *Curr Opin Hematol*. 2007;14:262-9.
 10. Ruggeri ZM and Mendolicchio GL. Interaction of von Willebrand factor with platelets and the vessel wall. *Hämostaseologie*. 2015;35:211-24.
 11. Nieswandt B and Watson SP. Platelet-collagen interaction: is GPVI the central receptor? *Blood*. 2003;102:449-461.
 12. Shen J, Sampietro S, Wu J, Tang J, Gupta S, Matzko CN et al. Coordination of platelet agonist signaling during the hemostatic response in vivo. *Blood Adv*. 2017;1:2767-2775.
 13. Furie B and Furie BC. Mechanisms of thrombus formation. *N Engl J Med*. 2008;359:938-949.
 14. Cosemans JM, Iserbyt BF, Deckmyn H and Heemskerk JW. Multiple ways to switch platelet integrins on and off. *J Thromb Haemost*. 2008;6:1253-61.
 15. Huang J, Li X, Shi X, Zhu M, Wang J, Huang S et al. Platelet integrin $\alpha\text{IIb}\beta\text{3}$: signal transduction, regulation, and its therapeutic targeting. *J Hematol Oncol*. 2019;12:26.

16. Watson SP, Auger JM, McCarty OJ and Pearce AC. GPVI and integrin $\alpha\text{IIb}\beta 3$ signaling in platelets. *J Thromb Haemost.* 2005;3:1752-62.
17. Harbi MH, Smith CW, Nicolson PLR, Watson SP and Thomas MR. Novel antiplatelet strategies targeting GPVI, CLEC-2 and tyrosine kinases. *Platelets.* 2021;32:29-41.
18. Nesbitt WS, Giuliano S, Kulkarni S, Dopheide SM, Harper IS and Jackson SP. Intercellular calcium communication regulates platelet aggregation and thrombus growth. *J Cell Biol.* 2003;160:1151-1161.
19. Estevez B and Du X. New concepts and mechanisms of platelet activation signaling. *Physiology (Bethesda).* 2017;32:162-177.
20. Senis YA, Mazharian A and Mori J. Src family kinases: at the forefront of platelet activation. *Blood.* 2014;124:2013-24.
21. Hermans C, Wittevrongel C, Thys C, Smethurst PA, Van Geet C and Freson K. A compound heterozygous mutation in glycoprotein VI in a patient with a bleeding disorder. *J Thromb Haemost.* 2009;7:1356-1363.
22. Dumont B, Lasne D, Rothschild C, Bouabdelli M, Ollivier V, Oudin C et al. Absence of collagen-induced platelet activation caused by compound heterozygous GPVI mutations. *Blood.* 2009;114:1900-1903.
23. Matus V, Valenzuela G, Sáez CG, Hidalgo P, Lagos M, Aranda E et al. An adenine insertion in exon 6 of human GP6 generates a truncated protein associated with a bleeding disorder in four Chilean families. *J Thromb Haemost.* 2013;11:1751-1759.
24. Ungerer M, Rosport K, Bültmann A, Piechatzek R, Uhland K, Schlieper P et al. Novel antiplatelet drug revacept (dimeric glycoprotein VI-Fc) specifically and efficiently inhibited collagen-induced platelet aggregation without affecting general hemostasis in humans. *Circulation.* 2011;123:1891-1899.
25. Massberg S, Konrad I, Bültmann A, Schulz C, Münch G, Peluso M et al. Soluble glycoprotein VI dimer inhibits platelet adhesion and aggregation to the injured vessel wall in vivo. *FASEB J.* 2004;18:397-399.
26. Lecut C, Feeney LA, Kingsbury G, Hopkins J, Lanza F, Gachet C et al. Human platelet glycoprotein VI function is antagonized by monoclonal antibody-derived Fab fragments. *J Thromb Haemost.* 2003; 1: 2653-2662.
27. Reilly MP, Sinha U, André P, Taylor SM, Pak Y, Deguzman FR et al. PRT-060318, a novel Syk inhibitor, prevents heparin-induced thrombocytopenia and

- thrombosis in a transgenic mouse model. *Blood*. 2011;117:2241-2246.
28. Perrella G, Montague SJ, Brown HC, Garcia Quintanilla L, Slater A, Stegner D et al. Role of tyrosine kinase Syk in thrombus stabilisation at high shear. *Int J Mol Sci*. 2022;23:493.
 29. Barrachina MN, Izquierdo I, Hermida-Nogueira L, Morán LA, Pérez A, Arroyo AB et al. The PI3K δ inhibitor idelalisib diminishes platelet function and shows antithrombotic potential. *Int J Mol Sci*. 2021;22:3304.
 30. Coxon CH, Geer MJ and Senis YA. ITIM receptors: more than just inhibitors of platelet activation. *Blood*. 2017;129:3407-3418.
 31. Gardiner EE, Arthur JF, Kahn ML, Berndt MC and Andrews RK. Regulation of platelet membrane levels of glycoprotein VI by a platelet-derived metalloproteinase. *Blood*. 2004;104:3611-3617.
 32. Gardiner EE, Karunakaran D, Shen Y, Arthur JF, Andrews RK and Berndt MC. Controlled shedding of platelet glycoprotein (GP)VI and GPIb-V-IX by ADAM family metalloproteinases. *J Thromb Haemost*. 2007;5:1530-1537.
 33. Naitoh K, Hosaka Y, Honda M, Ogawa K, Shirakawa K and Furusako S. Properties of soluble glycoprotein VI, a potential platelet activation biomarker. *Platelets*. 2015;26:745-750.
 34. Andrews RK, Karunakaran D, Gardiner EE and Berndt MC. Platelet receptor proteolysis: a mechanism for downregulating platelet reactivity. *Arterioscler Thromb Vasc Biol*. 2007;27:1511-1520.
 35. Perrella G, Nagy M, Watson SP and Heemskerk JW. Platelet GPVI (glycoprotein VI) and thrombotic complications in the venous system. *Arterioscler Thromb Vasc Biol*. 2021;41:2681-2692.
 36. Bray PF, McKenzie SE, Edelstein LC, Nagalla S, Delgrosso K, Ertel A et al. The complex transcriptional landscape of the anucleate human platelet. *BMC Genomics*. 2013;14:1.
 37. Burkhart JM, Gambaryan S, Watson SP, Jurk K, Walter U, Sickmann A et al. What can proteomics tell us about platelets? *Circ Res*. 2014;114:1204-1219.
 38. García A, Prabhakar S, Hughan S, Anderson TW, Brock CJ, Pearce AC et al. Differential proteome analysis of TRAP-activated platelets: involvement of DOK-2 and phosphorylation of RGS proteins. *Blood*. 2004;103:2088-2095.
 39. Loroach S, Trabold K, Gambaryan S, Reiß C, Schwierczek K, Fleming I et al. Alterations of the platelet proteome in type I Glanzmann thrombasthenia caused by different homozygous delG frameshift mutations in ITGA2B. *Thromb*

- Haemost.* 2017;117:556-569.
40. Mantovani G, Bastepe M, Monk D, de Sanctis L, Thiele S, Usardi A et al. Diagnosis and management of pseudohypo-parathyroidism and related disorders: first international Consensus Statement. *Nat Rev Endocrinol.* 2018;14:476-500.
 41. Nieto-Fontarigo JJ, González-Barcala FJ, Andrade-Bulos LJ, San-José ME, Cruz MJ, Veldés-Cuadrado L et al. iTRAQ-based proteomic analysis reveals potential serum biomarkers of allergic and nonallergic asthma. *Allergy.* 2020;75:3171-3183.
 42. Nassa G, Giurato G, Cimmino G, Rizzo F, Ravo M, Salvati A et al. Splicing of platelet resident pre-mRNAs upon activation by physiological stimuli results in functionally relevant proteome modifications. *Sci Rep.* 2018;8:498.
 43. Denis MM, Tolley ND, Bunting M, Schwartz H, Jiang H, Lindemann S et al. Escaping the nuclear confines: signal-dependent pre-mRNA splicing in anucleate platelets. *Cell.* 2005;122:379-391.
 44. Balamurali D and Stoll M. Non-coding RNA databases in cardiovascular research. *Non-Coding RNA.* 2020;6:35.
 45. Gandhi S, Ruehle F and Stoll M. Evolutionary patterns of non-coding RNA in cardiovascular biology. *Non-Coding RNA.* 2019;5:15.
 46. Supernat A, Popęda M, Pastuszek K, Best MG, Grešner P, In 't Veld S et al. Transcriptomic landscape of blood platelets in healthy donors. *Sci Rep.* 2021;11:15679.
 47. Petersen R, Lambourne JJ, Javierre BM, Grassi L, Kreuzhuber R, Ruklisa D, Rosa IM et al. Platelet function is modified by common sequence variation in megakaryocyte super enhancers. *Nat Commun.* 2017;8:16058.
 48. Best MG, Wesseling P and Wurdinger T. Tumor-educated platelets as a noninvasive biomarker source for cancer detection and progression monitoring. *Cancer Res.* 2018;78:3407-3412.
 49. Patel SR, Hartwig JH and Italiano JE. The biogenesis of platelets from megakaryocyte proplatelets. *J Clin Invest.* 2005;115:3348-3354.
 50. Cecchetti L, Tolley ND, Michetti N, Bury L, Weyrich AS and Gresele P. Megakaryocytes differentially sort mRNAs for matrix metalloproteinases and their inhibitors into platelets: a mechanism for regulating synthetic events. *Blood.* 2011;118:1903-1911.

Chapter 2

Molecular proteomics and signaling of human platelets in health and disease

Huang J, Zhang P, Solari FA, Sickmann A, García Á, Jurk K, Heemskerk JWM

Int. J. Mol. Sci. 2021; 22:9860

Reprinted with permission

*I collected the data, made the conceptualization and co-wrote the article
together with P.Z., F.S., A.S., A.G., K.J. and J.W.M.H.*

Abstract

Platelets are small anucleate blood cells that play vital roles in haemostasis and thrombosis, besides other physiological and pathophysiological processes. These roles are tightly regulated by a complex network of signaling pathways. Mass spectrometry-based proteomic techniques are contributing not only to the identification and quantification of new platelet proteins, but also reveal post-translational modifications of these molecules, such as acetylation, glycosylation and phosphorylation. Moreover, target proteomic analysis of platelets can provide molecular biomarkers for genetic aberrations with established or non-established links to platelet dysfunctions. In this report, we review 67 reports regarding platelet proteomic analysis and signaling on a molecular base. Collectively, these provide detailed insight into the: (i) technical developments and limitations of the assessment of platelet (sub)proteomes; (ii) molecular protein changes upon ageing of platelets; (iii) complexity of platelet signaling pathways and functions in response to collagen, rhodocytin, thrombin, thromboxane A₂ and ADP; (iv) proteomic effects of endothelial-derived mediators such as prostacyclin and the anti-platelet drug aspirin; and (v) molecular protein changes in platelets from patients with congenital disorders or cardiovascular disease. However, sample sizes are still low and the roles of differentially expressed proteins are often unknown. Based on the practical and technical possibilities and limitations, we provide a perspective for further improvements of the platelet proteomic field.

Introduction

Platelets circulate as anucleated cells in the blood, where they are kept in a resting state by the vascular endothelium producing platelet inhibitors^{1,2}. Alongside other functions, not addressed in this paper, platelets are of fundamental importance in primary and secondary haemostasis and arterial thrombosis³. An extensive network of molecular signal transduction processes in platelets allows their fast adhesion and secretion upon injury of the vessel wall or damage of an atherosclerotic plaque, and hence allows the formation of a rapidly growing thrombus^{4,5}.

Because of their anucleate structure, gene transcription and ribosomal translation activities are restricted in platelets^{6,7}, resulting in a relatively stable proteome⁸. Given this, mass-spectrometry-based proteomic analyses can be a valuable tool to assess the molecular build-up especially of these out-differentiated cells.

Overview of platelet proteomic literature

In the present paper, we provide a topical overview of how technical developments in the mass-spectrometric technologies are contributing to our knowledge of the basic proteome of freshly isolated and stored platelets, as well as of platelets stimulated via key receptor-dependent signaling mechanisms. Details of the 67 published platelet proteomic analyses are provided in Suppl. Table 1 (search terms PubMed 2021: platelet proteomics, excluding non-human, not original protein lists and reviews). Extracted key characteristics per section are indicated in Table 1.

With an estimated size of ~10k unique proteins in nucleated cells^{9,10}, proteome studies of human platelets have identified variable numbers of 2-6k proteins (Figure 1A). From the 67 registered studies, including six papers with two categories (Suppl. Table 1), many (48%) used isolated, washed platelets of high purity (99-99.99%). Given the small volume of platelets (9-11 fL)² and an abundant open canicular system, this purity cannot exclude

Table 1. *Proceedings and characteristics per section of published proteomic studies regarding platelet purity, sample size, types of proteomes analysed and reported study limitations. For details per study, see Suppl. Table 1. Abbreviation: PRM, parallel-reaction monitoring.*

§	Year	Purity checked	Sample size	Type of (sub)proteomes	Reported limitations	Pathway (GO)
3-Basic	≥2011	6/12	20-250 µg	platelets, granules, palmitoylation, methylation	unclear relation to platelet functions, low sample number	8/12
4-Ageing	≥2012	3/12	4-500 µg	stored platelets, N-terminome, extracellular vesicles	unclear relation to platelet functions, low sample number	7/12
5-GPVI	≥2010	8/11	150-2500+ µg	platelets (label-free), phosphorylation (TiO ₂), acetylation, PRM targeted, ubiquitylation, releasate	limited protein recovery, sample pooling	7/11
6-CLEC-2	≥2012	2/2	150 µg	platelets, phosphorylation	limited protein recovery, second mediator interference	2/2
7-PARs	≥2015	5/13	24-150 µg	platelets (label-free), phosphorylation (TiO ₂), releasate, extracellular vesicles	sample pooling, low sample number, leukocyte contamination, clinical relevance unclear	12/13
8-ASA	≥2017	2/5	5-100 µg	platelets, acetylation, glycosylation	unclear clinical relevance	3/5
9-ADP/INH	≥2014	3/3	100-800 µg	platelets, phosphorylation (TiO ₂)	low sample number, unclear function of phosphorylation	2/3
10-PAT	≥2010	7/15	40-600+ µg	platelets (label-free), targeted, phosphorylation, N-terminome	low patient number, inter-patient variation, unclear relation to platelet functions	8/15

contamination with proteins from plasma, red blood cells and leukocytes, which may affect study outcomes¹¹. A minority of the studies investigated platelet releasates, ultracentrifuged platelet extracellular vesicles, or immuno-affinity fractions from platelets, with the latter providing lower numbers of proteins¹². The early procedure of two-dimensional gel separation of lysed platelets is still in use in some laboratories (12 papers), although this method is now mostly replaced by bottom-up LC-MS/MS analysis without gel separation.

As the most common protein digestion method, about half of the collected papers (49%) use trypsin treatment of total platelet lysates (Figure 1B). The usual sample workup is trichloroacetic acid and/or acetone precipitation and filter-aided sample preparation. Many of the 67 publications describe one or more additional sample treatment steps before uploading onto a column. These include stable isotope labelling (isobaric tags for relative and absolute quantification, iTRAQ or TMT 23%), label-free quantification (30%), enrichment (22%, for phosphopeptides, N-terminal or glycopeptides), or targeted or absolute quantification (5%) (Figure 1C). In recent years, label-free quantification has become possible with state-of-the-art mass spectrometers, but this method is demanding for subsequent data analysis^{13,14}. As we detail below (section 11), novel technical advances are gradually appearing in papers, such as label-free quantification methods, data-independent acquisition, targeted analysis with biomarker peptide references, and well-plate-based sample workup.

The majority of the 67 publications state some study limitations. The most mentioned are: low peptide coverage linked to low protein abundance, complex spectral data analysis and missing (hydrophobic) peptide sequences¹⁵. It has been recognised that inter-lab differences in fractionation and instrumentation limit the comparison of the platelet (phospho)proteomes, published by various groups^{16,17}. So far, all studies have examined low sample sizes (platelets from few subjects of mostly unknown gender); hence, questions about inter-subject variation and

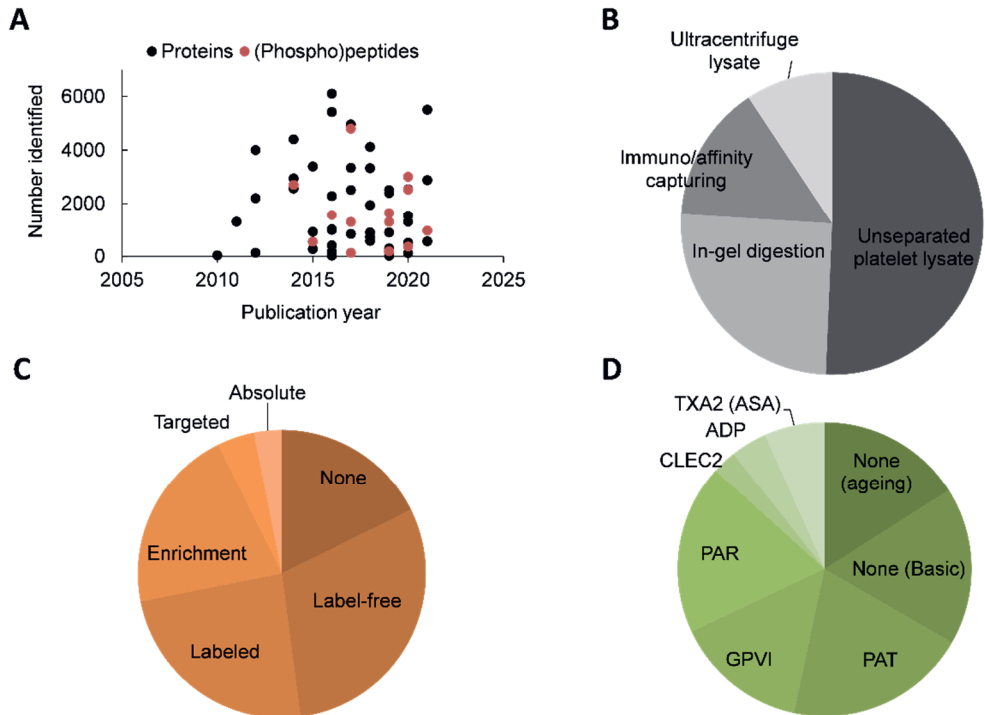


Figure 1. Overview of 67 platelet proteomic publications. **A**, Numbers of identified proteins and (phospho)peptides in human platelets in publications over the years. **B**, Distribution profile over proteomic papers for types of platelet preparations. Half of the collected papers (49%) used trypsin treatment of unseparated platelet lysates; others used prior separation by gel electrophoresis and in-gel digestion (26%), immuno/affinity capturing (15%) or ultracentrifugation enrichment (9%). **C**, Distribution profile of proteomic quantification type. In 67 publications, 20% used no other method, 23% used stable isotope labelling, 30% used label-free quantification, 22% employed special peptides enrichments and 5% employed targeted (4%) or absolute quantification (1%) methods. **D**, Distribution profile of type of (stimulated) platelets used in 67 publications. Most papers used healthy donor platelets without agonist (33%), patient platelets (PAT, 20%) or platelets stimulated via GPVI (15%) or PARs (17%). Rarer was analysis of platelets stimulated via CLEC-2 (3%), ADP (4%) or TXA₂/aspirin (7%).

comparisons of subject cohorts remain to be answered¹⁸⁻²⁰.

Since 2011, with the improvement of mass spectrometric approaches, gradual progress has been made in unravelling of the 'basic' platelet proteome and post-translational modifications (Figure 1D). Markedly, there are a substantial number of studies interested in the ageing-related proteomic changes of *in-vitro* stored platelets. The remaining works studied aspects of platelet signaling in response to key platelet receptors and agonists. As schematised in Figure 2, these concern signaling pathways via the collagen receptor glycoprotein VI (GPVI, ligands: collagen, collagen-related peptide CRP and convulxin); furthermore signaling via the thrombin (co)receptors GPIIb α , PAR1 and PAR4 (ligands: thrombin, thrombin-receptor activating peptides); the C-type lectin receptor CLEC-2 (ligands: podoplanin, rhodocytin); the ADP receptors P2Y₁₂ and P2Y₁; the thromboxane A₂ (TXA₂) mimetic U46619 (a pathway inhibited by aspirin); and the platelet-inhibiting agents prostacyclin and nitric oxide.

Basic platelet proteome

Based on genome-wide platelet transcriptome information, the theoretical platelet proteome (*i.e.* the number of expressed protein-encoding genes) is now estimated at 14.8k proteins. As far as we understand it now, particularly abundant in the identified platelet proteome are mitochondrial, metabolic, signaling/adaptor and transcription proteins¹¹. In the past decade, significant progress has been made in establishing the protein composition of platelets freshly isolated from human blood samples. Numbers of proteins identified by mass spectrometry and by label-free analysis have increased from 1.3k in 2011²² to 5.4k²³, of which 3.7k with estimated copy numbers²⁴. Analysis of the 500 proteins with highest copy numbers indicated highest abundance of proteins in the actin and microtubule cytoskeletons, the α -granules, involved in signaling, and (regulating) small GTPases²⁵. Specific analyses indicated abundant presence of nearly complete 20S and 26S proteasomes, implicating regular protein degradation²⁶. A study of small

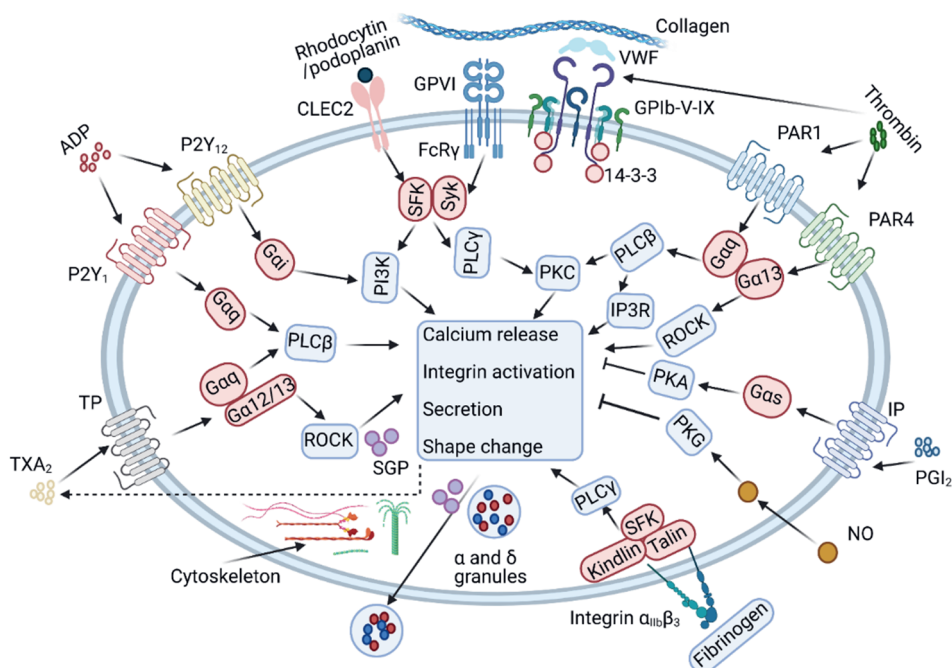


Figure 2. General overview of platelet signaling pathways. Overview of key platelet signaling and responses via key platelet receptors and agonists, examined by platelet proteomic analysis. Indicated are signaling via the collagen receptor glycoprotein (GP)VI, VWF receptor GPIb-V-IX; the proteinase-activated receptor (PAR)1 and PAR4 for thrombin; the podoplanin and rhodocytin receptor C-type lectin receptor 2 (CLEC2); the ADP receptors P2Y₁ and P2Y₁₂; thromboxane (TX)A₂ mimetic U46619 (pathway inhibited by aspirin); integrin α IIb β 3 outside-in signaling; actin and tubulin cytoskeletons; platelet-inhibiting prostacyclin I₂ (PGI₂) and nitric oxide (NO); and α -granule and δ -granule secretion. Other abbreviations: G α , heterotrimeric G proteins; PKA, PKC, PKG, protein kinases A, C, G; PLC, phospholipase C; SGP, small GTP-binding proteins; SFK, Src-family kinase. Refs.^{2, 5, 21}. Figure created by Biorender.com.

and large platelets derived from the same healthy donor revealed that 80 proteins (9%) differed in abundance²⁷. These included signaling proteins, but also several plasma proteins (Table 2).

Several mass spectrometry studies have examined the post-translational modifications of platelet proteins. For the identification of phosphoproteins,

commonly a TiO₂ sample enrichment step was used, often in combination with a calibration label, probe or antibody^{8,20,25}. Reported changes in protein phosphorylation are discussed in the paragraphs below. In another enrichment protocol of platelet membranes, 0.2k palmitoylated proteins could be identified, among which the TREM-like transcript-1 (TLT1) surface receptor²². Distinct enrichment protocols of specific platelet peptides identified 0.2k lysine methylations³² and 1.6k neo N-termini^{28,33}, indicating that protein methylation and cleavage play vital roles in normal platelet function. In a study of unclear physiological significance, a 5.4k platelet proteome was reported, of which ~10% was regulated by the serotonin antagonist sarpogrelate²³. However, the precise role of serotonin in platelet activation still needs to be defined³⁴. Reported limitations of the various studies are unclear relations of the newly identified platelet proteins and the low numbers of proteomes analysed (Table 1).

Proteome changes of ageing platelets

The preferred way to store (ageing) platelets for best preservation of their functions after transfusion is a long-standing issue³⁵. Transcriptome-based studies indicated that freshly isolated platelets have a limited capacity for protein synthesis, along with ongoing degradation of RNA species³⁶. Commonly, platelet concentrates for transfusion purposes can be stored for multiple days, after which the platelets start to lose functional properties, a phenomenon known as platelet storage lesion³⁷. To investigate the cause of this lesion, multiple studies have been carried out to the protein changes of ageing platelets. Since 2018, label-free quantification methods have been used in particular (Suppl. Table 1).

An early paper assessed the extent of protein degradation by determining N-terminal methionines (*i.e.* formed by acetylation or endo-proteolysis)³³. It was reported that the majority (77%) of 2.9k identified proteins contained neo N-termini, which suggested extensive proteolytic processing during platelet storage. Matrix metalloproteinases were found to play an important

Table 2. Selection of protein changes in published platelet proteomes. Confined to papers showing abundant regulated proteins in platelet (fractions from) patients. *Italic: plasma or secretory proteins*¹¹.

proteins			
3-BASIC. Proteomes of large and small platelets (1 subject)	80 up or down (9%)	ADP-ribosylation factor 1/3, GTP-binding protein SAR1a, guanylate cyclase soluble subunit $\alpha 3$, voltage-dependent anion channel protein 3, serotransferrin, immunoglobulins, haptoglobin, hemopexin, $\alpha 1$ -antitrypsin, and vitronectin	27
5-GPVI. Platelet proteome in Scott syndrome (1 patient)	134 up or down (6%)	annectamin 6, annexin A5, calpain 1, protein S100-A8/9, channel aquaporin-1, pregnancy zone protein, myeloperoxidase, serine-pyruvate aminotransferase, platelet glycoprotein 4, cAMP-dependent protein kinase II β regulatory subunit	28
10-PAT. Platelet iloprost phosphoproteome of PHP Ia patients (6 patients)	51 up or down (11%)	phosphorylation of protein kinase A consensus sites: inositol triphosphate receptor associated 1/2, bridging integrator 2, vasodilator-stimulated phosphoprotein, coiled-coil domain-containing protein 9, claudin 5, consorin, Grb2-associated binding protein 2.	29
10-PAT. Platelet proteome in X-linked thrombocytopenia (5 patients)	83 up or down (4%)	prostaglandin G/H synthase 1, solute carrier family 35 member D3, carbonic anhydrase 2, peroxiredoxin 1, tubulin-tyrosine ligase-like protein 12, spectrin α -chain, nexilin, E2 ubiquitin-conjugating enzyme, proteasome subunit α/β type 4, heat shock 70 kDa protein 1b	30
10-PAT. Platelet proteome in Gray platelet syndrome (5 patients)	123 up or down (n.d.)	neurobeachin-like protein 2, SPARC, serglycin, latent-transforming growth factor β -binding protein 1, <i>platelet basic protein</i> , <i>thrombospondin-1</i> , <i>platelet factor 4</i> , <i>multimerin-1</i> , <i>von Willebrand factor</i>	31
10-PAT. Platelet proteome of patients with early-stage cancer (12 patients)	85 up or down (3%)	mitochondrial deoxyribonucleotidase and 39S ribosomal protein, V-type proton ATPase subunit S1, myomegalin, serine/arginine repetitive matrix protein 2, CD34, peptidoglycan recognition protein 1, nuclear ribonucleoprotein A1, histone H2B type 1L, neurochondrin, calmodulin-dependent protein kinase type 1D	19

role in this neo N-terminus formation, pointing to a continued protein cleavage in the platelet granules and in other membrane vesicles. In a platelet apheresis intervention protocol to enrich younger circulating platelets (1 donor and 1.0k identified proteins, hence low power), it was reported that endocytosis- and cytoskeleton-related proteins changes with the platelet age³⁸.

Some studies compared the ageing of platelets in different storage media, using 2D gel-based or pre-labelled proteomic techniques³⁹. While differences in several proteins were observed between storage arms of the studies, the relationship with changes in platelet functions were not always clear. Two quantitative proteomic analyses indicated that, with increasing storage time, modified proteins especially had a role in degranulation^{13,40}. Platelets stored in the cold at 2-6 °C were found to express reduced levels of glycoproteins and increased levels of surface activation markers likely due to stimulation of glycoprotein shedding⁴¹, but the cold storage did not affect platelet viability⁴⁰. An induction of platelet degranulation was caused by pathogen inactivation technologies (*e.g.* with Mirasol) before storage⁴².

A number of groups have been searching for platelet proteins that can explain adverse transfusion reactions affecting the patient's health after the transfusion of ageing platelets. Regarding pathogen inactivation, treatment of platelet concentrates with riboflavin and ultraviolet light for two days - producing reactive oxygen species - resulted in slight increases of oxidised peptides, when compared to the 18% of 9.4k identified platelet peptides that were oxidised anyway^{43,44}. Proteomic studies on extracellular vesicles formed from ageing platelets revealed that metabolic proteins (*e.g.*, glycolysis and lactate production) and proinflammatory cytokines (CCL5, PF4) were upregulated upon ageing⁴⁵. A comparison of pooled platelet concentrates and single-donor apheresis platelets - both of which are preparations that occasionally trigger adverse transfusion reactions - revealed a partly common set of proteome changes (*i.e.*, granular and mitochondrial proteins). On the other hand, signaling pathway analysis also

revealed some differences: altered integrin $\alpha\text{IIb}\beta 3$ signaling in the pooled concentrates and acute phase response pathways in the apheresis platelets^{46,47}.

Collagen receptor glycoprotein VI (GPVI)

GPVI is a key collagen and fibrin receptor on platelets (3-4k copies per cell), which signals via a cascade of protein tyrosine kinases, leading to strong platelet activation^{48,49}. GPVI interaction with subendothelial collagens induces arterial thrombus formation upon vascular injury, such as confirmed in multiple *in vivo* studies with genetically modified mice and in microfluidics studies with mouse or human blood^{50,51}. At high wall shear rates, this interaction is preceded by platelet adhesion to von Willebrand factor (VWF), which avidly binds to collagens, via the GPIb-V-IX complex⁵².

Platelet GPVI binding to collagens and to a lesser extent fibrin induces a profound activation cascade, initiated by tyrosine phosphorylation of immunoreceptor tyrosine-based activation motifs (ITAM) in its co-receptor Fc receptor γ -chain (FcR γ), which ultimately leads to platelet aggregation, secretion and procoagulant activity^{5,53}. The signaling pathway involves Src-family kinases (SFK) and the spleen tyrosine kinase Syk, which triggers the activation of multiple signaling enzymes and adaptors, such as Btk/Tec family kinases, LAT, SLP76, phospholipase C $\gamma 2$ (PLC $\gamma 2$), and PI3K isoforms (Figure 2)⁵⁴. As GPVI-deficient patients experience variable but mostly not severe bleeding episodes, this underscores the concept of a more prominent role of GPVI in arterial thrombosis than in haemostasis^{55,56}.

First studies using gel spots to identify phosphorylated signaling targets resulted in an only small sets of differentially regulated proteins linked to GPVI-induced platelet activation (Suppl. Table 1)^{57,58}. However, in a recent GPVI phosphoproteome paper, >3.0k phosphorylation events (>1.3k proteins) were identified by tandem mass tag (TMT) labelling and triple stage tandem mass spectrometry. With literature-guided causal inference tools, more than 0.3k site-specific signaling proteins could be obtained, among

which were key and emerging GPVI effectors (*i.e.*, FcR γ , Syk, PLC γ 2 and DAPP1)⁵⁹. Interesting is the phosphorylation identification, downstream of GPVI, of a wide panel of small GTP-binding proteins (Ras and Rab GTPases) and activities of MAPK pathways⁵⁹. The higher GPVI-induced platelet aggregation in patients with myocardial infarction was accompanied by increased phosphorylation of several of these signaling proteins⁶⁰. Similarly, ~0.2k basal phosphorylation sites were upregulated in platelets from obese patients, which were associated with augmented platelet adhesion to collagen⁶¹.

Proteomic studies also focussed on other post-translations modifications. Thus, a procedure to assess reversible protein acetylation found 0.6k acetyl-lysine residues (0.3k proteins) serving as substrates for lysine acetyltransferases, which seem to be regulated in response to GPVI activation and subsequent cytoskeletal changes⁶². Another study detected 0.8k extra-cytosolic N-linked glycosylation sites with some of these regulated by GPVI⁶³. This agrees with the finding that glycan glycosylation plays a role in platelet-collagen interaction⁶⁴. In GPVI-stimulated platelets it appeared that 0.9k out of 1.6k ubiquitinated peptides (corresponding to 0.7k proteins, including Syk, filamin and integrins) were upregulated, implicating a profound role of GPVI in the ubiquitin protein degradation pathway⁶⁵. To what extent proteins are degraded after GPVI stimulation is still unclear.

Lipidomic mass spectrometry of complexed phosphoinositides and bound proteins showed that upon PI3K activation, many proteins can interact with 3-phosphorylated phosphoinositides through their PH domains, among which is the new adaptor protein DAPP1⁶⁶. Membrane lipid rafts of GPVI-stimulated platelets were also analysed in detail⁶⁷. Oligophrenin as a small GTPase-binding protein regulator was furthermore recognised as a functional target of the GPVI-induced tyrosine kinase cascade⁶⁸. To which extent secondary mediators (ADP, TXA₂) contribute to the GPVI-induced proteome changes has not systematically been investigated.

Stimulation via GPVI - enforced by thrombin - is an exemplary condition to evoke platelet procoagulant activity^{69,70}. This response induced by a prolonged cytosolic Ca^{2+} elevation, ballooning and phosphatidylserine exposure allows the assembly and activation of coagulation factors on the platelet surface⁷¹. Proteomic studies have contributed to better understand these GPVI-mediated platelet responses. This held for platelets from a patient with Scott syndrome, *i.e.* a rare bleeding disorder with autosomal recessive mode of transmission. In the patient's platelets, lacking phosphatidylserine externalisation due to a mutation in the *ANO6* gene, the corresponding protein was found to be absent along with a reduction in calpain-like proteins²⁸. The latter observation could explain a reduced cytoskeleton cleavage and a prolonged agonist-induced phosphorylation pattern (1.6k phosphopeptides) in response to GPVI+PAR stimulation or ionomycin. Of the identified proteins, 6% were found to be up- or downregulated in the patient platelets, among which were several membrane glycoproteins (Table 2).

Signaling C-type lectin receptor 2 (CLEC-2)

The hem-ITAM linked receptor CLEC-2 triggers multiple platelet activation processes, with podoplanin as known ligand in the lymphatic system, but no clear ligand in the blood or healthy blood vessels. On the other hand, platelet CLEC-2 has been recognised as a key receptor in thrombo-inflammatory disorders⁷². Similarly to GPVI, activation of CLEC-2 triggers a tyrosine kinase cascade resulting in SFK and Syk activation via a hem-ITAM domain (Figure 2). Downstream signaling routes involve PLC γ 2, Tec and PI3K family members^{73,74}. A laboratory ligand of CLEC-2 is the snake venom rhodocytin.

Several platelet proteomic studies have helped to further resolve CLEC-2-induced signaling pathways. In rhodocytin-stimulated platelets, following gel separation and phosphoprotein enrichment, 0.1k proteins of the broad signalosome were identified next to the expected ones, including the novel adapters Dok2 and ADAP, the tyrosine kinase Fer and the phosphatase

Shp1⁷⁵. This study also revealed subtle differences between the CLEC-2 and GPVI signaling routes.

Another study of the protein composition of membrane lipid rafts found large similarities after platelet stimulation via CLEC-2 or GPVI⁶⁷. Intriguing is an observed loss of cytoskeletal proteins in the rafts from the activated platelets. Extended analysis of the rhodocytin-stimulated phosphoproteome revealed a large panel of 0.4k regulated phospho-tyrosine residues, among those multiple signaling and adaptor proteins, protein kinases and membrane-associated proteins²⁰. Similar to the GPVI-induced activation, platelet stimulation via CLEC-2 relies on autocrine feed forward processes via released ADP and thromboxane A₂^{20,21}. Exactly which (phospho)proteome changes are dependent on these second mediators is still unclear.

Thrombin and protease-activated receptors (PAR1, PAR4)

The serine protease thrombin cleaves coagulation factors, producing fibrin fibres from fibrinogen, and it also cleaves platelet protease-activated receptors (PARs)^{76,77}. On human platelets, thrombin cleaves and activates the Gαq-protein coupled receptors PAR1/4, while thrombin has an additional minor stimulatory role through its binding to the GPIIb-V-IX complex⁷⁸. PAR1 is the receptor operating at low thrombin concentrations, while PAR4 becomes activated at higher agonist concentrations⁷⁷. The classical Gαq pathway leads to activation of phospholipase Cβ (PLCβ), which like PLCγ2 hydrolyses phosphatidylinositol 4,5-bisphosphate into the second messengers inositol trisphosphate (IP₃) and diacylglycerol⁵. The formed IP₃ induces via IP₃ receptors the endoplasmic reticular release of Ca²⁺, while diacylglycerol stimulates protein kinase C (PKC) isoforms and the signaling mediator CalDAG-GEFI^{79,80}. Granule secretion and aggregation are important responses of thrombin receptor-stimulated platelets. In addition, PARs can couple to Gα13⁸¹, which leads to activation of RhoA and Rho kinase (ROCK) via small GTP-binding proteins, and mediates platelet shape change and low-

dose thrombin-induced aggregation⁸².

After activation or ageing, platelets lose part of their constituents to the environment in several ways, *i.e.* by granular secretion, extracellular vesicle (microparticle) formation and receptor shedding⁷⁷. Together the lost proteins are termed as the releasate proteome⁸³. Mass-spectrometric studies have examined the (granular) content of platelet releasates (Suppl. Table 1). For a set of 0.1k proteins, differences were reported between the PAR1- and GPVI-induced platelet releasates⁸⁴. Among a broader set of 0.7-0.9k proteins, ~10% seemed to be over- or under-represented in the platelet releasate from pregnant women^{85,86}. However, the studies report various limitations, including low sample numbers and unclear clinical relevance (Table 1).

Next to the released secretome, also the composition of PAR-induced extracellular vesicles (microparticles) was also analysed by mass spectrometry. For a set of 3.4k proteins (0.4k membrane proteins), it was found that thrombin induces the release of extracellular vesicles that are enriched in proteins sensitive to platelet activation, with an underrepresentation of granular proteins⁸⁷. Examination of the platelet-derived extracellular vesicles from obese individuals showed expression changes in mitophagy and antioxidant defence proteins, when compared to non-obese subjects⁸⁸.

A pioneering paper in 2004 identified 62 differentially regulated protein features in PAR1-stimulated platelets⁸⁹. A later report on a 3.4k platelet proteome mentioned abundance changes in >20% of the proteins after PAR stimulation¹⁸, a finding that will need further confirmation and explanation. In a focussed study, thrombin-induced Dab2 phosphorylation could be linked to platelet aggregation and ADP release⁹⁰. Another report showed inter-individual changes in the activated platelet proteome are related to miRNA levels⁹¹. This is one of the rare proteomic papers so far mentioning inter-individual variation.

Aspirin and thromboxane A₂

Several primary platelet agonists evoke release of the autocrine agent thromboxane A₂, which is formed from arachidonate in phospholipids and is converted by the cyclooxygenase 1 (COX1)-thromboxane synthase complex^{2,92}. Aspirin, the most common antithrombotic drug, irreversibly blocks the cyclooxygenase and hence the thromboxane synthesis. The platelet thromboxane receptor couples to the Gαq and Gα13 proteins, which results in PLCβ and ROCK activation, respectively⁹³. The latter mediates the RhoA-dependent platelet shape change.

Interesting proteomic observations have been made in this context (Suppl. Table 1). Using a label-free proteomic approach, platelets obtained from cord blood, which relatively poorly respond to thromboxane stimulation, express normal receptor levels, but are enriched in mitochondrial energy and metabolism proteins, including NDUFS1, NDUFA10, NDUFAS and NDUFY2⁹⁴. A perhaps accidental finding due to low sample size was that platelets from good and poor responders to aspirin treatment were differentiated in the level of carbonic anhydrase II⁹⁵.

Some reports have more extensively examined the aspirin effects on platelets, considering that this drug can N-acetylate not only the thromboxane synthase complex, but also other many proteins. In an iTRAQ labelling study of the platelet glycoproteome, a small subset of the 0.8k identified N-linked glycosylation sites was affected by aspirin treatment, among which the secretory protein TIMP1 (metallopeptidase inhibitor 1)⁶³. Furthermore, in a listing of 3.3k acetylated residues, 6% showed aspirin regulation, with a higher acetylation state in the platelets from diabetic patients⁹⁶. A pilot report stipulated that the lower aspirin effects on platelets from diabetics was linked to the glucose-suppressed glycation of in particular COX1⁹⁷.

ADP receptors and platelet inhibitors

ADP is another important secondary mediator that is released from granules after initial platelet activation, and ensures the formation of platelet aggregates and thrombi^{5,98}. ADP itself activates platelets through the G-protein coupled P2Y₁ and P2Y₁₂ receptors to trigger different downstream pathways. The P2Y₁ receptors support the first reversible phase of ADP-induced platelet aggregation, while the P2Y₁₂ counterparts function to consolidate this aggregation. The only lowly expressed P2Y₁ receptors evoke a Gα_q-mediated signaling route via PLCβ, cytosolic Ca²⁺ elevation and PKC, such as described for PAR1, but weaker in strength⁸⁰. The P2Y₁₂ receptors are Gα_i coupled, activate PI3K forms and prevent adenylate cyclase to synthesize cAMP⁹⁸.

An 'opposite' pathway leading to platelet inhibition is triggered by the endothelial-derived prostacyclin (prostaglandin I₂). Via a receptor on platelets, prostacyclin (or analogue iloprost) couples to Gα_s (*GNAS* gene), which activates adenylate cyclase and increases cAMP^{29,93}. The second messenger cAMP induces phosphorylation events by the broad-spectrum protein kinase A (PKA). In this way, prostacyclin can antagonise almost all platelet activation responses, including secretion, aggregation and procoagulant activity^{2,99,100}.

Proteomic-based studies were performed to better understand the antagonistic roles of ADP and prostacyclin (iloprost) by the analysis of (partly reversible) protein phosphorylations (Suppl. Table 1). Using a quantitative labelling method for analysis of time-resolved phosphorylation changes (13% of 2.7k phosphopeptides), it was concluded that platelet inhibition with iloprost is a multipronged process involving a broad spectrum of protein kinases and phosphatases, ubiquitinated proteins and many structural proteins¹⁰¹. Over 100 direct or indirect PKA targets were identified, revealing that platelets are inhibited by network-connected multiple signaling pathways¹⁰¹. Using the method of stable-isotope iTRAQ labelling (Figure 3), it was furthermore found that iloprost reverted 17% of the 0.4k regulated

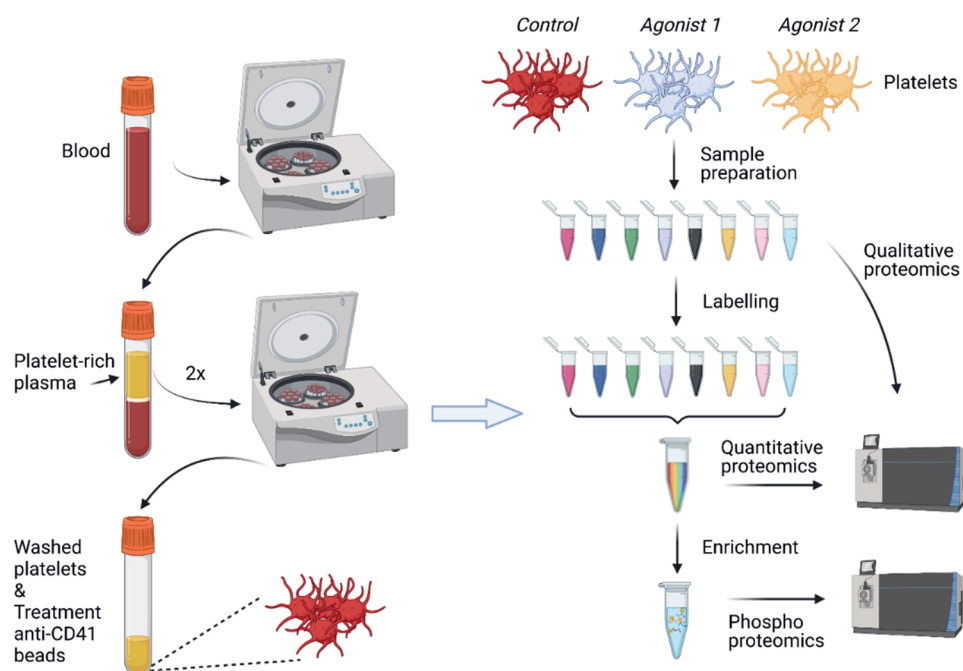


Figure 3. Global protocol of combined proteome analysis of (un)stimulated platelets. **A**, Human platelet isolation from freshly drawn blood. Platelet-rich plasma (PRP) is collected by centrifugation and then re-centrifuged twice to obtain double washed platelets. Removal of remaining leukocytes antibody-coated beads is advised. Platelet purity is determined by flow cytometry or microscopy. **B**, Isolated platelets are stimulated with agonists as required. After lysis, proteins are fragmented by trypsin under well-controlled conditions, in this case in the presence of unique stable isotope labels. Pooled, labelled samples are fractionated, and peptides are resolved by LC-MS/MS analysis. For quantitative proteome information, reference peptides can be added. In case of phosphoproteome analysis or other post-translational modifications, an enrichment step is included for improved detection. An example protocol is provided in Box 1. Figure created by Biorender.com.

phosphorylation sites (out of 3.6k phosphopeptides) of ADP-stimulated platelets¹⁰². Dual regulated phosphoproteins included signaling proteins and degranulation-regulating proteins, which in part were identified as targets of PKA or PKC.

Recently, such studies were extended to nitric oxide, another major endothelial-derived potent platelet inhibitor^{103,104}. Nitric oxide, as an unstable, membrane-permeable gas, increases platelet cGMP via guanylate cyclase, which produces protein kinase G (PKG)^{104,105}. The formation of nitric oxide by platelets themselves via nitric oxide synthase is not likely¹⁰¹. Via a battery of cAMP/cGMP-dependent phosphodiesterases, the two cyclic nucleotides - and hence PKA and PKG activities - are 'communicating'. The antagonism of platelet inhibitors (prostacyclin, nitric oxide) and platelets stimulators (ADP, thrombin, collagen) has led to phosphoproteomic analysis to identify protein phosphorylation events that determine the switch between inhibition and activation¹⁰⁶. Herein, cross-talk signaling mechanisms were discovered, such as a feedback regulation of Syk by PKC¹⁰⁷. It was also found that CLEC-2 activation triggers via ADP- and thromboxane the phosphorylation of a core set of signaling proteins (*e.g.*, Src, PLC γ 2)²⁰.

Platelet proteomics of patients with platelet defects or cardiovascular disease

Only limited proteomic studies have appeared on the changes in protein (modification) patterns of patients with platelet-related disorders (Suppl. Table 1). The few examples are patients with Glanzmann's thrombasthenia (lacking integrin α IIb β 3, mutated *ITGA2B*), Scott syndrome (mutated phospholipid scramblase *ANO6*), X-linked thrombocytopenia (*GATA1* mutation), pseudohypoparathyroidism type Ia (PHP Ia, mutated *GNAS* locus), and Gray platelet syndrome (mutated *NBEAL2*, α -granule deficiency).

Targeted mass spectrometry confirmed that, for platelets from patients with type I Glanzmann thrombasthenia (a severe bleeding disorder), the level of integrin α IIb was greatly reduced to <5% of control subjects¹⁰⁸. In addition, plasma proteins endocytosed by integrin α IIb β 3, such as fibrinogen, factor XIII, plasminogen, and carboxypeptidase 2B, appeared to be downregulated when compared to the control platelets. Upregulated was the immunoglobulin receptor Fc γ RIIA, and in one patient the tetraspanin CD63

after FcγRIIA crosslinking, while the granular proteins were normal. Extensive global, phospho- and N-terminal proteome analysis was performed on platelets from a Scott patient (a rare, mild bleeding disorder), characterised by failure to agonist-induced phosphatidylserine exposure and procoagulant activity¹⁰⁹. In the patient's platelets, quantitative proteomics revealed a spectrum of 134 (6%) up- or down-regulated proteins²⁸, including complete absence of the phospholipid scramblase anoctamin-6 and low calpain-1 protease (regulating platelet morphology changes) (Table 2). Interestingly, the cell volume-regulating protein aquaporin-1 was upregulated, putatively as a compensatory mechanism.

A mutation in exon 4 of the *GATA1* gene associates with X-linked thrombocytopenia with thalassemia (OMIM 314050), which is a severe bleeding disorder. Quantitative proteomics of the platelets from five male patients revealed 83 altered proteins³⁰. Among these were COX1 plus several cytoskeleton and proteasome proteins (Table 2). In comparison, in platelets with mutant GATA binding factor 1, more than 300 proteins were proposed to be differentially expressed in comparison to control subjects¹¹⁰.

In 5 out of 47 Gray platelet syndrome patients (a milder bleeding disorder) with new variants in *NBEAL2*, 123 platelet proteins were mostly downregulated, with the majority being α-granule-associated and cargo proteins at unaltered mRNA expression levels (Table 2)³¹. Markedly, plasma proteins related to immune responses and inflammation were upregulated, which suggested the presence of an immune defect in these patients as well. In the platelets from five patients with PHPla (Albright hereditary osteodystrophy, a disease of hormonal resistance and abnormal postures, no bleeding), quantitative phosphoproteomics revealed 0.5k iloprost-regulated phosphorylation sites²⁹. In agreement with a loss-of-function of Gαs in the patient's platelets, a panel of 51 phosphorylated proteins was identified that showed a consensus PKA phosphorylation site and that was altered in most of the patients (Table 2).

In addition to these rare congenital abnormalities, few proteomic studies

have examined platelets from patients with somatic mutations (cancer) or genetically less well-defined diseases. In a study on platelets from 12 patients with early-stage cancers (in comparison to healthy subjects), quantitative proteomic analysis indicated disease regulation of a wide variety of 85 (3%) proteins (Table 2), the majority of which normalised after surgical resection¹⁹. Some of the regulated proteins may be useful as biomarkers for such cancers. This area requires further attention.

Analysis of the platelet proteome of patients with progressive multiple sclerosis showed elevated levels of plasma proteins like fibrinogen and α_2 macroglobulin¹¹¹, pointing to increased endocytosis or stickiness of the patient platelets. In patients infected with dengue virus, platelet quantitative proteomics identified about 0.3k regulated proteins¹¹². With the aim to find a biomarker related to Alzheimer's disease, proteomic analysis of platelets from patients with mild and severe cognitive function revealed 360 differentially regulated proteins. Four of these (*PHB*, *UQCRH*, *GP1BA*, and *FINC*) were able to distinguish patients from healthy controls¹¹³. However, the link to disease is still unclear.

A few studies examined the platelets from patients with cardiovascular diseases (Suppl. Table 1). Differentially regulated proteins were identified in the platelets from two groups of patients with (acute) coronary syndrome; there were, in particular, signaling, glycolysis and cytoskeletal proteins^{114,115}. In patients experiencing ST-elevation myocardial infarction (STEMI), gel-based proteomics identified 16 altered proteins in platelets that were collected at the intracoronary culprit site, including integrin α IIb and thrombospondin-1, in comparison to the circulating platelets¹¹⁶. Additionally, in STEMI patients, platelet phosphoproteomic analysis revealed an increase in key tyrosine phosphorylations in response to GPVI stimulation, which raised the possibility of GPVI as an antithrombotic target in STEMI^{84,116}. Only few altered proteins were found in the platelet releasate of patients with stable angina pectoris¹¹⁷, and in whole platelets from patients with lupus anticoagulant related thrombosis¹¹⁸, along with evidence for increased

platelet activation. Additionally, in hyperlipidaemia, the platelet proteome was found to be markedly unchanged¹¹⁹. Semi-quantitative workflows were developed to find platelet-related protein biomarkers in cardiovascular disease¹²⁰.

Practical and technical considerations

Platelet preparation. In current platelet proteomic research, washed platelets are commonly used. As indicated in the Figure 3, the platelet isolation protocol is usually based on a series of centrifugation steps to separate platelets from other blood cells and plasma. In Box 1, we provide a validated protocol based on own experience. However, given the presence of an extended open canicular system in platelets in direct with the blood plasma, residual plasma proteins are invariably seen in most listed platelet proteomes¹¹. The reviewed papers show a wide variety of platelet purities, platelet concentrations and amounts of proteins used per analysed sample (Suppl. Table 1). Furthermore, the procedure to use platelets at a resting state is important; this can be evaluated by flow cytometry (*e.g.*, checking for integrin $\alpha\text{IIb}\beta 3$ activation and P-selectin expression) or by parallel-reaction monitoring (PRM) tests¹⁰². It is of no doubt that all these variables can influence the composition and size of an established platelet proteome, and that standardisation is therefore needed (Box 1). The agonists and ways to activate platelets are other matters of variation, as seen between papers, in that most agonists indirectly trigger secondary pathways via release of ADP, TXA₂ and other autocooids². This is very likely to affect (time courses) of phosphorylation outcomes¹⁰².

The complexity of platelet proteome analysis is increased by a wide variety of post-transcriptional protein modifications (protease processing, acetylation, acylation, phosphorylation and glycosylation)^{8,9}. In our experience, new mass spectrometry acquisition techniques such as data-independent acquisition make it easier to quantify low abundant (post-translated) protein forms.

Peptide sample preparation. At present, sample preparations for bottom-up proteomics analyses (no prior gel separation) is the most common. For the collection of trypsin-digested peptides, filter aided sample preparation, S-trap based digestion methods and ethanol precipitation are preferred^{121,122}. Novel proteomic approaches at the horizon are a nanodroplet processing platform for analysis of small cell numbers¹²³.

For higher throughput purposes, label-free analysis can be performed¹³, where unlimited sample numbers can be compared at the proteome level. Another ratioed method makes use of stable isotope sets, such as in iTRAQ- and TMT-based quantification, where to 16 (phosphopeptide) samples are pooled together^{29,63}. Prior enrichment methods for phosphopeptides relied on metal oxide affinity chromatography with titanium dioxide (TiO₂) beads^{24,28,102}. An alternative is provided by immobilized metal affinity chromatography (IMAC) with liquid handling systems, which allow phosphopeptide enrichment of up to 96 samples at the same time¹²⁴.

Data analysis. The mostly used strategy for proteomic data analysis is searching against established fragmentation spectra databases. A helpful overview of current bioinformatics methods for protein identification and quantification is given in¹²⁵. An important step in the analysis is data normalization, where corrections according to specific rules are applied to remove inconsistent data points, followed by statistical tests (checking for false discovery rates). Regarding phosphoproteomics, data normalization is also necessary because the apparent regulation of a phosphorylation site should not be caused by an altered protein abundance¹²⁶. Special algorithm have to be employed for assessing the phosphorylation position and the responsible kinase of a phosphorylated peptide²⁹.

Current limitations. Many of the publications indicated as a limitation the use and comparison of only few platelet samples (Table 1). This has made it difficult to draw conclusion on inter-subject variation, even when comparing healthy subjects with patients. Technical limitations include low peptide coverage linked to low protein abundance, complex spectral data analysis,

Box 1. Example workflow for bottom-up proteomic analysis of platelets.

- (i) *Platelet preparation.* Citrate-anticoagulated whole blood is centrifuged at 280 g for 10 minutes, to obtain platelet-rich plasma (PRP), the upper part of which is then centrifuged at 80 g for 10 minutes in the presence of anticoagulant medium²⁹ to pellet leukocytes. After pelleting the platelets (380 g for 10 minutes), the pellet is resuspended in buffer medium plus anticoagulant and apyrase. Another centrifugation step then gives washed platelets, which are resuspended in albumin-free buffer medium ($\geq 5 \times 10^8$ /mL, ≥ 1.0 mg protein/mL). Leukocytes are counted preferably by microscopy, and immune depletion is applied if needed. The platelet suspension is left standing for 15-30 minutes. Samples (50-200+ μ g protein) are stimulated by agonists as required, and stopped by addition of 4x concentrated lysis buffer (4% SDS, 150 mM NaCl, 50 mM Tris, pH 7.4, PhosStop added). Samples are frozen in liquid nitrogen and stored at -80°C.
- (ii) *Peptide sample preparation.* For in-solution digestion, the platelet proteins are reduced and alkylated in lysis buffer. Then, the lysis buffer is replaced by digestion buffer, and trypsin added to digest overnight. For relative quantification, isotopic reagents iTRAQ or TMT are used to label peptides. If needed, suitable enrichment methods are used, e.g. to concentrate phosphopeptides. RP-HPLC is commonly used to separate whole peptide mixtures, and hydrophilic interaction chromatography (HILIC) to separate phosphopeptides. Fractions are desalted to remove contaminants and detergents.

missing (hydrophobic) peptide sequences and unclear function of many discovered proteins⁸.

Future perspectives and challenges ahead

Over the last 20 years the field of platelet proteomics has evolved rapidly, from the early 2D gel electrophoresis studies to the more recent bottom-up-based ones. The evolution of recent generations of mass spectrometers has allowed protein quantitative studies and the elucidation of complex

phosphorylation patterns of proteins with often still unknown functions. Enrichment steps, for instance, to concentrate negatively charged peptides from trypsin-treated lysates, and advanced sample preparation protocols are now bypassing the earlier gel separation steps.

As shown in this review, the new proteomic methods have led to a gradual enlargement of the human molecular platelet (phospho)proteome, thus identifying so far up to 6k identified proteins (3.7k with copy numbers), which however are only partly linked to known platelet functions. The platelet phosphoproteome contains up to 5k phosphorylation sites with many sites altered upon platelet stimulation (via GPVI, PARs, CLEC-2, ADP) or platelet inhibition (with iloprost). The regulated Ser/Thr and Tyr phosphorylation sites included not only the known or expected signaling proteins, but also a multitude of poorly understood signaling, regulatory, structural and metabolic proteins. Diverse sets of previously known and new proteins were found to be altered in pathological situations, but the 'regulation' of these was mostly not confirmed in independent studies. As described above, advances in the proteomic field have also led to the identification of (novel) platelet proteins as potential biomarkers for disease.

Accordingly, proteomics has been developed as a fundamental tool for platelet research. On the other hand, it is time now to consider how to turn this field from the phase of discovery into the phase of biological and (pre)clinical application. The analysis of 70 papers in the present review has taught us that for this transition, a number of challenges are ahead. These can be grouped into the following eight points.

Despite the broad heterogeneity in mass spectrometry and spectral analysis methods, the precise composition of the 'normal' human platelet proteome is still unclear. While the theoretical proteome recently could be deduced from the genome-wide platelet transcriptome of 14.8k protein-encoding transcripts¹¹, published papers so far show only parts (up to 5k) of these proteins, with often limited overlap between the various lists. A coordinated multi-laboratory effort will be needed to demarcate the achievable human

platelet proteome. In this respect, also an update will be needed of the 2014 reported list of protein copy numbers per platelet²⁴.

The outcome of quantitative platelet proteomics greatly depends on the method and purity of sample preparation, including the platelet concentration, activation state and all sample processing. Even between recent papers, the described procedures highly deviate. The same holds for platelet 'products' such as the releasate, secretome and extracellular vesicles. We envision that inter-laboratory standardization is needed for better comparison of new study results. As a start, we provide an experience-based protocol (Box 1).

With the platelet proteomic field moving from protein discovery to assessment of protein composition, there is an urgent need for reliable and consistent quantification methods for (core sets of) platelet proteins. In only few published studies, the judgements on up- or downregulation of proteins were validated by independent means. Hence, in papers comparing subjects or patients, information is missing on the consistency and reproducibility of the found differences. As a solution, we propose duplicate or triplicate workflows on parallel platelet samples, and a consistent use of internal standards.

Analysis of the platelet phosphoproteome has revealed an unexpected wealth of time-dependent regulated protein phosphorylation sites. However, the precision and meaning of the changes in many proteins are unclear, even of stable isotope (iTRAQ, TMT) comparisons. On the other hand, the phosphorylation analysis of platelets from obese subjects and several genotyped patients does provide novel insight into the dysregulation of platelet functions in these disorders.

Several studies report on altered proteomes of stored platelets for transfusion and of released platelet products. The work mostly aims to provide new biomarkers for platelet product quality or the platelet activation state (*in vivo*). For many proteins with assumed biomarker role,

the physiological functions in platelets are unclear, which asks for a more sophisticated protein function analysis than the conventional pathway analyses (*e.g.*, by Gene Ontology). A recent classification system of all proteins presented or expected in platelets may help to achieve this goal¹¹. Once a biomarker is confirmed, at later the stage mass spectrometry can be replaced by cheaper, immune-based or flow-cytometry methods in larger (clinical) studies.

The published studies with patients so far all are limited by low sample sizes, so that common inter-subject variables such as blood cell traits, gender, age and health history are not examined. New high throughput analysis, using label-free quantification methods in combination with data-independent acquisition will allow to compare multiple platelet samples at the same time, which is conditional for these clinically related questions.

Application of platelet proteomics in the diagnostic laboratory is a challenge due to the expensive and complex requirements in terms of sample preparation and equipment. The additive value of clinical proteomics likely is highest for patients with complex disorders where genetic analysis fails, *e.g.* in case of not understood bleeding, or in metabolic or other systemic diseases. Additionally, otherwise, to understand the action mechanisms of new (antithrombotic) drugs.

In general, we propose that, for the field to move forward, common guidelines should be established that help to improve the inter-lab reproducibility of platelet preparation, proteomic sample processing and complex data analysis. This has also been acknowledged at the 2021 ISTH Congress.

Supplementary materials

Supplementary table with characteristics of all reviewed studies:
<https://www.mdpi.com/article/10.3390/ijms22189860/s1>.

Acknowledgements

J.H. is supported by the European Union's Horizon 2020 research and innovation program under the Marie Skłodowska-Curie grant agreement TAPAS No. 766118, and is enrolled in a joint PhD program of the Universities of Maastricht (The Netherlands) and Santiago de Compostela (Spain). P.Z. is supported by the European Union's Horizon 2020 research and innovation program under the Marie Skłodowska-Curie grant agreement TICARDIO No. 813409. P.Z. is enrolled in a joint PhD program of the Universities of Maastricht (The Netherlands) and Mainz (Germany).

Funding

Research support to A.S. and F.S. by the Ministerium für Innovation, Wissenschaft und Forschung from Nordrhein-Westfalen, by the German Federal Ministry of Education and Research (BMBF 01EO1503) and the Deutsche Forschungsgemeinschaft (ZA 639/4-1 and JU 2735/2-1). K.J. is supported by the German Federal Ministry of Education and Research (BMBF 01EO1503). A.G. is supported by the Spanish Ministry of Science and Innovation (grant No. PID2019-108727RB-I00), co-funded by the European Regional Development Fund (ERDF).

Conflicts of interest

The authors declare no relevant conflicts of interest.

References

1. Yau JW, Teoh H and Verma S. Endothelial cell control of thrombosis. *BMC Cardiovasc Disord.* 2015;15:130.

2. Van der Meijden PE and Heemskerk JW. Platelet biology and functions: new concepts and clinical perspectives. *Nat Rev Cardiol*. 2019;16:166-179.
3. Badimon L and Vilahur G. Thrombosis formation on atherosclerotic lesions and plaque rupture. *J Int Med*. 2014;276:618-632.
4. Boyanova D, Nilla S, Birschmann I, Dandekar T and Dittrich M. PlateletWeb: a systems biologic analysis of signaling networks in human platelets. *Blood*. 2012;119:e22-e34.
5. Versteeg HH, Heemskerk JW, Levi M and Reitsma PS. New fundamentals in hemostasis. *Physiol Rev*. 2013;93:327-358.
6. Weyrich AS, Schwertz H, Kraiss LW and Zimmerman GA. Protein synthesis by platelets: historical and new perspectives. *J Thromb Haemost*. 2009;7:241-246.
7. Bray PF, McKenzie SE, Edelstein LC, Nagalla S, Delgrosso K, Ertel A et al. The complex transcriptional landscape of the anucleate human platelet. *BMC Genomics*. 2013;14:1.
8. Loosse C, Swieringa F, Heemskerk JW, Sickmann A and Lorenz C. Platelet proteomics: from discovery to diagnosis. *Exp Rev Proteom*. 2018;15:467-476.
9. Mann M and Jensen ON. Proteomic analysis of post-translational modifications. *Nat Biotech*. 2003;21:255-261.
10. Rosenberger G, Koh CC, Guo TN, Rost HL, Kouvonen P, Collins B et al. A repository of assays to quantify 10,000 human proteins by SWATH-MS. *Sci Data*. 2014;1:140031.
11. Huang J, Swieringa F, Solari FA, Provenzale I, Grassi L, De Simone I et al. Assessment of a complete and classified platelet proteome from genome-wide transcripts of human platelets and megakaryocytes covering platelet functions. *Sci Rep*. 2021;11:12358.
12. Flores-Villalva S, Rogriguez-Hernandez E, Rubio-Venegas Y, Canto-Alarcon JG and Milian-Suazo F. What can proteomics tell us about tuberculosis? *J Microbiol Biotechnol*. 2015;25:1181-1194.
13. Rijkers M, Van den Eshof BL, Van der Meer PF, Van Alphen FP, de Korte D, Leebeek FW et al. Monitoring storage induced changes in the platelet proteome employing label free quantitative mass spectrometry. *Sci Rep*. 2017;7:11045.
14. Huang JN, Wang J, Li QQ, Zhang Y and Zhang XM. Enzyme and chemical assisted N-terminal blocked peptides analysis, ENCHANT, as a selective proteomics

- approach complementary to conventional shotgun approach. *J Proteome Res.* 2018;17:212-221.
15. Schmidt GJ, Reumiller CM, Ercan H, Resch U, Butt E, Heber S et al. Comparative proteomics reveals unexpected quantitative phosphorylation differences linked to platelet activation state. *Sci Rep.* 2019;9:19009.
 16. Tabb DL, Vega-Montoto L, Rudnick PA, Variyath AM, Ham AJL, Bunk DM et al. Repeatability and reproducibility in proteomic identifications by liquid chromatography-tandem mass spectrometry. *J Proteome Res.* 2010;9:761-776.
 17. Cremer SE, Catalfamo JL, Goggs R, Seemann SE, Kristensen AT and Brooks MB. Proteomic profiling of the thrombin-activated canine platelet secretome. *Plos One.* 2019;14:e0224891.
 18. Cimmino G, Tarallo R, Nassa G, De Filippo MR, Giurato G, Ravo M et al. Activating stimuli induce platelet microRNA modulation and proteome reorganisation. *Thromb Haemost.* 2015;114:96-108.
 19. Sabrkhanly S, Kuijpers MJ, Knol JC, Damink S, Dingemans AM, Verheul HM et al. Exploration of the platelet proteome in patients with early-stage cancer. *J Proteomics.* 2018;177:65-74.
 20. Izquierdo I, Barrachina MN, Hermida-Nogueira L, Casas V, Moran LA, Lacerenza S et al. A comprehensive tyrosine phosphoproteomic analysis reveals novel components of the platelet CLEC-2 signaling cascade. *Thromb Haemost.* 2020;120:262-276.
 21. Bye AP, Unsworth AJ and Gibbins JM. Platelet signaling: a complex interplay between inhibitory and activatory networks. *J Thromb Haemost.* 2016;14:918-930.
 22. Dowal L, Yang W, Freeman MR, Steen H and Flaumenhaft R. Proteomic analysis of palmitoylated platelet proteins. *Blood.* 2011;118:e62-e73.
 23. Lee H, Chae S, Park J, Bae J, Go E, Kim SJ et al. Comprehensive proteome profiling of platelet identified a protein profile predictive of responses to an antiplatelet agent sarpogrelate. *Mol Cell Proteomics.* 2016;15:3461-3472.
 24. Burkhardt JM, Vaudel M, Gambaryan S, Radau S, Walter U, Martens L et al. The first comprehensive and quantitative analysis of human platelet protein composition allows the comparative analysis of structural and functional pathways. *Blood.* 2012;120:e73-e82.
 25. Burkhardt JM, Gambaryan S, Watson SP, Jurk K, Walter U, Sickmann A et al. What can proteomics tell us about platelets? *Circ Res.* 2014;114:1204-1219.

26. Klockenbusch C, Walsh GM, Brown LM, Hoffman MD, Ignatchenko V, Kislinger T et al. Global proteome analysis identifies active immunoproteasome subunits in human platelets. *Mol Cell Proteomics*. 2014;13:3308-3319.
27. Handtke S, Steil L, Palankar R, Conrad J, Cauhan S, Kraus K et al. Role of platelet size revisited: function and protein composition of large and small platelets. *Thromb Haemost*. 2019;119:407-420.
28. Solari FA, Mattheij NJ, Burkhart JM, Swieringa F, Collins PW, Cosemans J et al. Combined quantification of the global proteome, phosphoproteome, and proteolytic cleavage to characterize altered platelet functions in the human Scott syndrome. *Mol Cell Proteomics*. 2016;15:3154-3169.
29. Swieringa F, Solari FA, Pagel O, Beck F, Huang J, Feijge MAH et al. Impaired iloprost-induced platelet inhibition and phosphoproteome changes in patients with confirmed pseudohypoparathyroidism type Ia, linked to genetic mutations in GNAS. *Sci Rep*. 2020;10:11389.
30. Bergemalm D, Ramström S, Kardeby C, Hultenby K, Eremo AG, Sihlbom C et al. Platelet proteome and function in X-linked thrombocytopenia with thalassemia and in silico comparisons with gray platelet syndrome. *Haematologica*. 2020.
31. Sims MC, Mayer L, Collins JH, Bariana TK, Megy K, Lavenu-Bombled C et al. Novel manifestations of immune dysregulation and granule defects in gray platelet syndrome. *Blood*. 2020;136:1956-1967.
32. Rocheleau AD, Melrose AR, Cunliffe JM, Klimek J, Babur O, Yunga ST et al. Identification, quantification, and system analysis of protein N-epsilon lysine methylation in anucleate blood platelets. *Proteomics*. 2019;19:e1900001.
33. Prudova A, Serrano K, Eckhard U, Fortelny N, Devine DV and Overall CM. TAILS N-terminomics of human platelets reveals pervasive metalloproteinase-dependent proteolytic processing in storage. *Blood*. 2014;124:e49-e60.
34. Schoenichen C, Bode C and Duerschmied D. Role of platelet serotonin in innate immune cell recruitment. *Front Biosci*. 2019;24:514-526.
35. Pang A, Cui Y, Chen Y, Cheng N, Delaney MK, Gu M et al. Shear-induced integrin signaling in platelet phosphatidylserine exposure, microvesicle release, and coagulation. *Blood*. 2018;132:533-543.
36. Zimmerman GA and Weyrich AS. Signal-dependent protein synthesis by activated platelets: new pathways to altered phenotype and function. *Arterioscler Thromb Vasc Biol*. 2008;28:s17-24.

37. Ng MS, Tung JP and Fraser JF. Platelet storage lesions: what more do we know now? *Transfus Med Rev.* 2018;2018:S0887-7963.
38. Thiele T, Braune J, Dhople V, Hammer E, Scharf C, Greinacher A et al. Proteomic profile of platelets during reconstitution of platelet counts after apheresis. *Proteomics Clin Appl.* 2016;10:831-838.
39. Prudent M, Crettaz D, Delobel J, Tissot JD and Lion N. Proteomic analysis of Intercept-treated platelets. *J Proteomics.* 2012;76:316-328.
40. Wang S, Jiang T, Fan Y and Zhao S. A proteomic approach reveals the variation in human platelet protein composition after storage at different temperatures. *Platelets.* 2019;30:403-412.
41. Wood B, Padula MP, Marks DC and Johnson L. Refrigerated storage of platelets initiates changes in platelet surface marker expression and localization of intracellular proteins. *Transfusion.* 2016;56:2548-2559.
42. Salunkhe V, De Cuyper IM, Papadopoulos P, Van der Meer PF, Daal BD, Villa-Fajardo M et al. A comprehensive proteomics study on platelet concentrates: platelet proteome, storage time and Mirasol pathogen reduction technology. *Platelets.* 2019;30:368-379.
43. Schubert P, Culibrk B, Karwal S, Goodrich RP and Devine DV. Protein translation occurs in platelet concentrates despite riboflavin/UV light pathogen inactivation treatment. *Proteomics Clin Appl.* 2016;10:839-850.
44. Sonogo G, Abonnenc M, Crettaz D, Lion N, Tissot JD and Prudent M. Irreversible oxidations of platelet proteins after riboflavin-UVB pathogen inactivation. *Transfus Clin Biol.* 2020;27:36-42.
45. Hermida-Nogueira L, Barrachina MN, Izquierdo I, García-Vence M, Lacerenza S, Bravo S et al. Proteomic analysis of extracellular vesicles derived from platelet concentrates treated with Mirasol identifies biomarkers of platelet storage lesion. *J Proteomics.* 2020;210:103529.
46. Aloui C, Barlier C, Claverol S, Fagan J, Awounou D, Tavernier E et al. Differential protein expression of blood platelet components associated with adverse transfusion reactions. *J Proteomics.* 2019;194:25-36.
47. Aloui C, Barlier C, Awounou D, Thiam S, Fagan J, Claverol S et al. Dysregulated pathways and differentially expressed proteins associated with adverse transfusion reactions in different types of platelet components. *J Proteomics.* 2020;218:103717.

48. Nieswandt B and Watson SP. Platelet-collagen interaction: is GPVI the central receptor? *Blood*. 2003;102:449-461.
49. Perrella G, Huang J, Provenzale I, Swieringa F, Heubel-Moenen FC, Farndale RW et al. Non-redundant roles of platelet glycoprotein VI and integrin $\alpha\text{IIb}\beta 3$ in fibrin-mediated microthrombus formation. *Arterioscler Thromb Vasc Biol*. 2021;41:e97-e111.
50. Nagy M, Van Geffen JP, Stegner D, Adams D, Braun A, de Witt SM et al. Comparative analysis of microfluidics thrombus formation in multiple genetically modified mice: link to thrombosis and hemostasis. *Front Cardiovasc Med*. 2019;6:99.
51. Baaten CC, Meacham S, de Witt SM, Feijge MA, Adams DJ, Akkerman JW et al. A synthesis approach of mouse studies to identify genes and proteins in arterial thrombosis and bleeding. *Blood*. 2018;132:e35-e46.
52. Konstantinides S, Ware J, Marchese P, Almus-Jacobs F, Loskutoff DJ and Ruggeri ZM. Distinct antithrombotic consequences of platelet glycoprotein $\text{Ib}\alpha$ and VI deficiency in a mouse model of arterial thrombosis. *J Thromb Haemost*. 2006;4:2014-2021.
53. Watson SP, Herbert JM and Pollitt AY. GPVI and CLEC-2 in hemostasis and vascular integrity. *J Thromb Haemost*. 2010;8:1457-1467.
54. Hughes CE, Finney BA, Koentgen F, Lowe KL and Watson SP. The N-terminal SH2 domain of Syk is required for (hem)ITAM, but not integrin, signaling in mouse platelets. *Blood*. 2015;125:144-154.
55. Matus V, Valenzuela G, Sáez CG, Hidalgo P, Lagos M, Aranda E et al. An adenine insertion in exon 6 of human GP6 generates a truncated protein associated with a bleeding disorder in four Chilean families. *J Thromb Haemost*. 2013;11:1751-1759.
56. Jandrot-Perrus M, Hermans C and Mezzano D. Platelet glycoprotein VI genetic quantitative and qualitative defects. *Platelets*. 2019;30:708-713.
57. Garcia A. Proteome analysis of signaling cascades in human platelets. *Blood Cells Mol Dis*. 2006;36:152-6.
58. Schulz C, Leuschen NV, Frohlich T, Lorenz M, Pfeiler S, Gleissner CA et al. Identification of novel downstream targets of platelet glycoprotein VI activation by differential proteome analysis: implications for thrombus formation. *Blood*. 2010;115:4102-4110.

59. Babur O, Melrose AR, Cunliffe JM, Klimek J, Pang J, Sepp AI et al. Phosphoproteomic quantitation and causal analysis reveal pathways in GPVI/ITAM-mediated platelet activation programs. *Blood*. 2020;136:2346-2358.
60. Velez P, Ocaranza-Sanchez R, Lopez-Otero D, Grigorian-Shamagian L, Rosa I, Guitian E et al. Alteration of platelet GPVI signaling in ST-elevation myocardial infarction patients demonstrated by a combination of proteomic, biochemical, and functional approaches. *Sci Rep*. 2016;6:39603.
61. Barrachina MN, Hermida-Nogueira L, Moran LA, Casas V, Hicks SM, Sueiro AM et al. Phosphoproteomic analysis of platelets in severe obesity uncovers platelet reactivity and signaling pathways alterations. *Arterioscler Thromb Vasc Biol*. 2021;41:478-490.
62. Aslan JE, Rigg RA, Nowak MS, Loren CP, Baker-Groberg SM, Pang J et al. Lysine acetyltransferase supports platelet function. *J Thromb Haemost*. 2015;13:1908-1917.
63. Shah P, Yang W, Sun S, Pasay J, Faraday N and Zhang H. Platelet glycoproteins associated with aspirin-treatment upon platelet activation. *Proteomics*. 2017;17:10.1002.
64. Toonstra C, Hu Y and Zhang H. Deciphering the roles of N-glycans on collagen-platelet interactions. *J Proteome Res*. 2019;18:2467-2477.
65. Unsworth AJ, Bombik I, Pinto-Fernandez A, McGouran JF, Konietzny R, Zahedi RP et al. Human platelet protein ubiquitylation and changes following GPVI activation. *Thromb Haemost*. 2019;119:104-116.
66. Durrant TN, Hutchinson JL, Heesom KJ, Anderson KE, Stephens LR, Hawkins PT et al. In-depth PtdIns(3,4,5)P₃ signalosome analysis identifies DAPP1 as a negative regulator of GPVI-driven platelet function. *Blood Adv*. 2017;1:918-932.
67. Izquierdo I, Barrachina MN, Hermida-Nogueira L, Casas V, Eble JE, Carrascal M et al. Platelet membrane lipid rafts protein composition varies following GPVI and CLEC-2 receptors activation. *J Proteomics*. 2019;195:88-97.
68. Bleijerveld OB, Van Holten TC, Preisinger C, Van der Smagt JJ, Farndale RW, Kleefstra T et al. Targeted phosphotyrosine profiling of glycoprotein VI signaling implicates oligophrenin-1 in platelet filopodia formation. *Arterioscler Thromb Vasc Biol*. 2013;33:1538-1543.

69. De Witt S, Verdoold R, Cosemans JMEM and Heemskerk JWM. Insights into platelet-based control of coagulation. *Thromb Res*. 2014;133:Suppl 2: S139-148.
70. Heemskerk JW, Cosemans JM and Van der Meijden PE. Platelets and coagulation. In: *Platelets in Thrombotic and Non-Thrombotic Disorders* (eds Gresele, P, Kleiman, N S, Lopez, J A, Page, C P). 2017;ISBN 978-3-319-47460-1:447-462.
71. Agbani EO, Van den Bosch MT, Brown E, Williams CM, Mattheij NJ, Cosemans JM et al. Coordinated membrane ballooning and procoagulant spreading in human platelets. *Circulation*. 2015;132:1414-1424.
72. Rayes J, Watson SP and Nieswandt B. Functional significance of the platelet immune receptors GPVI and CLEC-2. *J Clin Invest*. 2019;129:12-23.
73. Suzuki-Inoue K, Fuller GL, Garcia A, Eble JA, Pohlmann S, Inoue O et al. A novel Syk-dependent mechanism of platelet activation by the C-type lectin receptor CLEC-2. *Blood*. 2006;107:542-549.
74. Manne BK, Badolia R, Dangelmaier C, Eble JA, Ellmeier W, Kahn M et al. Distinct pathways regulate Syk protein activation downstream of immune tyrosine activation motif (ITAM) and hemITAM receptors in platelets. *J Biol Chem*. 2015;290:11557-11568.
75. Parguina AF, Alonso J, Rosa I, Velez P, Gonzalez-Lopez MJ, Guitian E et al. A detailed proteomic analysis of rhodocytin-activated platelets reveals novel clues on the CLEC-2 signalosome: implications for CLEC-2 signaling regulation. *Blood*. 2012;120:e117-e126.
76. Coughlin SR. Thrombin signaling and protease-activated receptors. *Nature*. 2000;407:258-264.
77. Wu J, Heemskerk JW and Baaten CC. Platelet membrane receptor proteolysis: implications for platelet function. *Front Cardiovasc Med*. 2020;7:608391.
78. Estevez B, Kim K, Delaney MK, Stojanovic-Terpo A, Shen B, Ruan CG et al. Signaling-mediated cooperativity between glycoprotein Ib-IX and protease-activated receptors in thrombin-induced platelet activation. *Blood*. 2016;127:626-636.
79. Mammadova-Bach E, Nagy M, Heemskerk JW, Nieswandt N and Braun A. Store-operated calcium entry in blood cells in thrombo-inflammation *Cell Calcium*. 2019;77:39-48.

80. Fernandez DI, Kuijpers MJ and Heemskerk JW. Platelet calcium signaling by G-protein coupled and ITAM-linked receptors regulating anoctamin-6 and procoagulant activity. *Platelets*. 2021; 32: 863-871.
81. Kim S, Foster C, Lecchi A, Quinton TM, Prosser DM, Jin JG et al. Protease-activated receptors 1 and 4 do not stimulate Gi signaling pathways in the absence of secreted ADP and cause human platelet aggregation independently of Gi signaling. *Blood*. 2002;99:3629-3636.
82. Moers A, Nieswandt B, Massberg S, Wettschureck N, Gruner S, Konrad I et al. G13 is an essential mediator of platelet activation in hemostasis and thrombosis. *Nat Med*. 2003;9:1418-1422.
83. Pagel O, Walter E, Jurk K and Zahedi RP. Taking the stock of granule cargo: Platelet releasate proteomics. *Platelets*. 2017;28:119-128.
84. Velez P, Izquierdo I, Rosa I and Garcia A. A 2D-DIGE-based proteomic analysis reveals differences in the platelet releasate composition when comparing thrombin and collagen stimulations. *Sci Rep*. 2015;5:8198.
85. Szklanna PB, Parsons ME, Wynne K, O'Connor H, Egan K, Allen S et al. The platelet releasate is altered in human pregnancy. *Proteomics Clin Appl*. 2019;13:e1800162.
86. Parsons ME, Szklanna PB, Guerrero JA, Wynne K, Dervin F, O'Connell K et al. Platelet releasate proteome profiling reveals a core set of proteins with low variance between healthy adults. *Proteomics*. 2018;18:e1800219.
87. Milioli M, Ibanez-Vea M, Sidoli S, Palmisano G, Careri M and Larsen MR. Quantitative proteomics analysis of platelet-derived microparticles reveals distinct protein signatures when stimulated by different physiological agonists. *J Proteomics*. 2015;121:55-66.
88. Grande R, Dovizio M, Marcone S, Szklanna PB, Bruno A, Ebhardt HA et al. Platelet-derived microparticles from obese individuals: characterization of number, size, proteomics, and crosstalk with cancer and endothelial cells. *Front Pharmacol*. 2019;10:7.
89. Garcia A, Prabhakar S, Hughan S, Anderson TW, Brock CJ, Pearce AC et al. Differential proteome analysis of TRAP-activated platelets: involvement of DOK-2 and phosphorylation of RGS proteins. *Blood*. 2004;103:2088-2095.
90. Tsai HJ, Chien KY, Liao HR, Shih MS, Lin YC, Chang YW et al. Functional links between disabled-2 Ser723 phosphorylation and thrombin signaling in human platelets. *J Thromb Haemost*. 2017;15:2029-2044.

91. Zufferey A, Ibberson M, Reny JL, Nolli S, Schwartz D, Docquier M et al. New molecular insights into modulation of platelet reactivity in aspirin-treated patients using a network-based approach. *Hum Genet.* 2016;135:403-414.
92. Fontana P, Zufferey A, Daali Y and Reny JL. Antiplatelet therapy: targeting the TXA₂ pathway. *J Cardiovasc Translat Res.* 2014;7:29-38.
93. Offermanns S. Activation of platelet function through G protein-coupled receptors. *Circ Res.* 2006;99:1293-1304.
94. Stokhuijzen E, Koornneef JM, Nota B, Van den Eshof BL, Van Alphen FP, Van den Biggelaar M et al. Differences between platelets derived from neonatal cord blood and adult peripheral blood assessed by mass spectrometry. *J Proteome Res.* 2017;16:3567-3575.
95. Jakubowski M, Debski J, Szahidewicz-Krupska E, Turek-Jakubowska A, Gawrys J, Gawrys K et al. Platelet carbonic anhydrase II, a forgotten enzyme, may be responsible for aspirin resistance. *Oxid Med Cell Longev.* 2017;2017:3132063.
96. Finamore F, Reny JL, Malacarne S, Fontana P and Sanchez JC. Shotgun proteomics data on the impact of hyperglycaemia on platelet protein acetylation by aspirin. *Data Brief.* 2018;21:2475-2481.
97. Finamore F, Reny JL, Malacarne S, Fontana P and Sanchez JC. A high glucose level is associated with decreased aspirin-mediated acetylation of platelet cyclooxygenase (COX)-1 at serine 529: a pilot study. *J Proteomics.* 2019;192:258-266.
98. Gachet C, Hechler B, Leon C, Vial C, Leray C, Ohlmann P et al. Activation of ADP receptors and platelet function. *Thromb Haemost.* 1997;78:271-275.
99. Monroe DM and Hoffman M. What does it take to make the perfect clot? *Arterioscler Thromb Vasc Biol.* 2006;26:41-48.
100. Rukoyatkina N, Walter U, Friebe A and Gambaryan S. Differentiation of cGMP-dependent and -independent nitric oxide effects on platelet apoptosis and reactive oxygen species production using platelets lacking soluble guanylyl cyclase. *Thromb Haemost.* 2011;106:922-933.
101. Beck F, Geiger J, Gambaryan S, Veit J, Vaudel M, Nollau P et al. Time-resolved characterization of cAMP/PKA-dependent signaling reveals that platelet inhibition is a concerted process involving multiple signaling pathways. *Blood.* 2014;123:e1-e10.

102. Beck F, Geiger J, Gambaryan S, Solari FA, Dell'Aica M, Lorocho S et al. Temporal quantitative phosphoproteomics of ADP stimulation reveals novel central nodes in platelet activation and inhibition. *Blood*. 2017;129:e1-e12.
103. Radomski MW, Palmer RM and Moncada S. Comparative pharmacology of endothelium-derived relaxinf factor, nitric oxide and prostacyclin in platelets. *Br J Pharmacol*. 1987;92:181-187.
104. Makhoul S, Walter E, Pagel O, Walter U, Sickmann A, Gambaryan S et al. Effects of the NO/soluble guanylate cyclase/cGMP system on the functions of human platelets. *Nitric Oxide*. 2018;76:71-80.
105. Dangel O, Mergia E, Karlisch K, Groneberg D, Koesling D and Friebe A. Nitric oxide-sensitive guanylyl cyclase is the only nitric oxide receptor mediating platelet inhibition. *J Thromb Haemost*. 2010;8:1343-1352.
106. Kumm EJ, Pagel O, Gambaryan S, Walter U, Zahedi RP, Smolenski A et al. The cell cycle checkpoint system MAST(L)-ENSA/ARPP19-PP2A is targeted by cAMP/PKA and cGMP/PKG in anucleate human platelets. *Cells*. 2020;9:472.
107. Makhoul S, Dorschel S, Gambaryan S, Walter U and Jurk K. Feedback regulation of Syk by protein kinase C in human platelets. *Int J Mol Sci*. 2019;21:176.
108. Lorocho S, Trabold K, Gambaryan S, Reiss C, Schwierczek K, Fleming I et al. Alterations of the platelet proteome in type I Glanzmann thrombasthenia caused by different homozygous delG frameshift mutations in ITGA2B. *Thromb Haemost*. 2017;117:556-569.
109. Van Kruchten R, Mattheij NJ, Saunders C, Feijge MA, Swieringa F, Wolfs JL et al. Both TMEM16F-dependent and TMEM16F-independent pathways contribute to phosphatidylserine exposure in platelet apoptosis and platelet activation. *Blood*. 2013;121:1850-1857.
110. Van Bergen MG, Marneth AE, Hoogendijk AJ, Van Alphen FP, Van den Akker E, Laros-Van Gorkom BA et al. Specific proteome changes in platelets from individuals with GATA1-, GFI1B-, and RUNX1-linked bleeding disorders. *Blood*. 2021;138:86-90.
111. Bijak M, Olejnik A, Rokita B, Morel A, Dziedzic A, Miller E et al. Increased level of fibrinogen chains in the proteome of blood platelets in secondary progressive multiple sclerosis patients. *J Cell Mol Med*. 2019;23:3476-3482.
112. Trugilho MR, Hottz ED, Brunoro GV, Teixeira-Ferreira A, Carvalho PC, Salazar GA et al. Platelet proteome reveals novel pathways of platelet activation and

- platelet-mediated immunoregulation in dengue. *Plos Pathogens*. 2017;13:e1006385.
113. Yu H, Liu Y, He B, He T, Chen C, He J et al. Platelet biomarkers for a descending cognitive function: a proteomic approach. *Aging Cell*. 2021;20:e13358.
 114. Parguina AF, Grigorian-Shamajian L, Agra RM, Teixeira-Fernandez E, Rosa I, Alonso J et al. Proteins involved in platelet signaling are differentially regulated in acute coronary syndrome: a proteomic study. *Plos One*. 2010;5:e13404.
 115. Lopez-Farré AJ, Zamorano-Leon JJ, Azcona L, Modrego J, Mateos-Caceres PJ, Gonzalez-Armengol J et al. Proteomic changes related to bewildered circulating platelets in the acute coronary syndrome. *Proteomics*. 2011;11:3335-48.
 116. Velez P, Ocaranza-Sanchez R, Lopez-Otero D, Grigorian-Shamagian L, Rosa I, Belen Bravo S. 2D-DIGE-based proteomic analysis of intracoronary versus peripheral arterial blood platelets from acute myocardial infarction patients: Upregulation of platelet activation biomarkers at the culprit site. *Proteomics Clin Appl*. 2016;10:851-858.
 117. Maguire PB, Parsons ME, Szklanna PB, Zdanyte M, Münzer P, Chatterjee M et al. Comparative platelet releasate proteomic profiling of acute coronary syndrome versus stable coronary artery disease. *Front Cardiovasc Med*. 2020;7:101.
 118. Hell L, Lurger K, Mauracher LM, Grilz E, Reumiller CM, Schmidt GJ et al. Altered platelet proteome in lupus anticoagulant-positive patients-protein disulfide isomerase and NETosis as new players in LA-related thrombosis. *Exp Mol Med*. 2020;52:66-78.
 119. Van Geffen JP, Swieringa F, Van Kuijk K, Tullemans BM, Solari FA, Peng B et al. Mild hyperlipidemia in mice aggravates platelet responsiveness in thrombus formation and exploration of platelet proteome and lipidome. *Sci Rep*. 2020;10:21407.
 120. Malchow S, Loosse C, Sickmann A and Lorenz C. Quantification of cardiovascular disease biomarkers in human platelets by targeted mass spectrometry. *Proteomes*. 2017;5:31.
 121. Zougman A, Selby PJ and Banks RE. Suspension trapping (STrap) sample preparation method for bottom-up proteomics analysis. *Proteomics*. 2014; 14:1006-1010

122. Ludwig KR, Schroll MM and Hummon AB. Comparison of in-solution, FASP, and S-trap based digestion methods for bottom-up proteomic studies. *J Proteome Res.* 2018;17:2480-2490.
123. Zhu Y, Piehowski PD, Zhao R, Chen J, Shen Y, Moore RJ et al. Nanodroplet processing platform for deep and quantitative proteome profiling of 10-100 mammalian cells. *Nat Commun.* 2018;9:882.
124. Ruprecht B, Koch H, Medard G, Mundt M, Kuster B and Lemeer S. Comprehensive and reproducible phosphopeptide enrichment using iron immobilized metal ion affinity chromatography (Fe-IMAC) columns. *Mol Cell Proteomics.* 2015;14:205-215.
125. Chen C, Hou J, Tanner JJ and Cheng J. Bioinformatics methods for mass spectrometry-based proteomics data analysis. *Int J Mol Sci.* 2020;21:2873.
126. Solari FA, Dell'Aica M, Sickmann A and Zahedi RP. Why phosphoproteomics is still a challenge. *Mol Biosyst.* 2015;11:1487-1493.

Chapter 3

Assessment of a complete and classified platelet proteome from genome-wide transcripts of human platelets and megakaryocytes covering platelet functions

Huang J, Swieringa F*, Solari FA*, Provenzale I, Grassi L, De Simone I, Baaten CCFMJ, Cavill R, Sickmann A*, Frontini M*, Heemskerk JWM*
(*equal contribution)

Sci. Rep. 2021;11:12358
Reprinted with permission

I designed research, analyzed and interpreted data and wrote the paper with M.F. and J.W.M.H. together, F.S., F.A.S., I.P. and I.D.S. analyzed and interpreted data and revised the manuscript; F.A.S., L.G., R.C., C.B., A.S., M.F. provided essential tools and revised the paper.

Abstract

Novel platelet and megakaryocyte transcriptome analysis allows prediction of the full or theoretical proteome of a representative human platelet. Here, we integrated the established platelet proteomes from six cohorts of healthy subjects, encompassing 5.2k proteins, with two novel genome-wide transcriptomes (57.8k mRNAs). For 14.8k protein-coding transcripts, we assigned the proteins to 21 UniProt-based classes, based on their preferential intracellular localization and presumed function. This classified transcriptome-proteome profile of platelets revealed: (i) Absence of 37.2k genome-wide transcripts. (ii) High quantitative similarity of platelet and megakaryocyte transcriptomes ($R=0.75$) for 14.8k protein-coding genes, but not for 3.8k RNA genes or 1.9k pseudogenes ($R=0.43-0.54$), suggesting redistribution of mRNAs upon platelet shedding from megakaryocytes. (iii) Copy numbers of 3.5k proteins that were restricted in size by the corresponding transcript levels. (iv) Near complete coverage of identified proteins in the relevant transcriptome ($\log_2\text{fpkm}>0.20$) except for plasma-derived secretory proteins, pointing to adhesion and uptake of such proteins. (v) Underrepresentation in the identified proteome of nuclear-related, membrane and signaling proteins, as well proteins with low-level transcripts. We then constructed a prediction model, based on protein function, transcript level and (peri)nuclear localization, and calculated the achievable proteome at ~10k proteins. Model validation identified 1.0k additional proteins in the predicted classes. Network and database analysis revealed the presence of 2.4k proteins with a possible role in thrombosis and hemostasis, and 138 proteins linked to platelet-related disorders. This genome-wide platelet transcriptome and (non)identified proteome database thus provides a scaffold for discovering the roles of unknown platelet proteins in health and disease.

Introduction

Platelets are generated in the bone marrow as cell fragments from hematopoietic stem cells that are differentiated into megakaryocytes. In the circulating, the mature platelets control many blood-related processes both in health and disease. These functions extend from blood vessel-lymph separation and maintenance of vascular integrity to allowing hemostasis, promoting arterial thrombosis, regulating inflammatory, immune and infection processes; and even facilitating tumor progression^{1,2}. The ultrastructure and the protein/RNA composition of a platelet, determined during their ontogenesis, allows the execution of all these functions. However, comparative studies of the molecular composition and structure of platelets in relation to their functions and megakaryocytic origin are still missing.

Although platelets do not contain a nucleus, they are equipped with mitochondria, several types of storage granules and multiple intracellular membrane structures, including endoplasmic reticulum (smooth and rough), a likely rudimentary Golgi apparatus, lysosomes, peroxisomes and endosomes³⁻⁵. Characteristic large invaginations, designated as open canicular or dense tubular system, make up ~1% of the cell volume and are filled with blood plasma components. A well-developed actin-myosin and tubulin cytoskeleton is required for proplatelet formation, micro-organization of the membrane structures, and mediates activation-dependent structural changes⁶⁻⁹. Whether the full repertoire of metabolic enzymes is present in platelets is still unclear, while the glucose metabolism is well-developed^{10,11}. Furthermore, the ribosomal mRNA translation machinery is retained as well as elements of protein processing and trafficking and a repertoire of proteolytic processes in the proteasome^{12,13}. Overviews point to a battery of receptors and channels, multiple adaptor molecules and small molecule GTP-binding proteins (G-proteins), and large protein kinase and phosphatase networks^{2,14}.

Human genetic studies supported by mouse models show that hundreds and

possibly thousands of platelet-expressed proteins contribute to thrombosis and hemostasis¹⁵. We reasoned that assembling the complete (quantitative) proteome and transcriptome of human platelets can provide a much better understanding of the molecules that determine platelet structure and functions in health and disease. As earlier platelet proteomes, reported in single articles, are limited in the numbers of identified proteins¹⁶⁻¹⁸, there is a need to integrate multiple proteomic studies based on the same methodology. While the number of genes detected in available transcriptomes of platelets and megakaryocytes are a magnitude higher¹⁹⁻²¹, these do not extend to the whole genome. Here, we combined multiple proteomes with the genome-wide RNA database of platelets and megakaryocytes generated by the Blueprint consortium^{22,23}, and integrated these into a platelet structure and function- based protein classification system, for defining the full platelet proteome. Detailed analysis of this database provided novel insights into the structure-function relations of platelets.

Methods

Subject cohorts and platelet samples

Washed, purified blood platelets were obtained in the same laboratories from six cohorts of healthy control donors, anonymized for medical-ethical reasons after informed consent. For each cohort, platelet samples were freshly isolated from anticoagulated blood by first collecting platelet-rich plasma, and removing plasma by a double wash step. Contamination was <0.02% for red blood cells and leukocytes, presence of plasma about 1 vol%. Raw proteomic data per cohort are provided in the following papers. Cohort 1 ($n=3$) in Burkhardt *et al.*²⁴, cohort 2 ($n=3$) in Beck *et al.*²⁵, cohort 3 ($n=3$) in Beck *et al.*²⁶, cohort 4 ($n=2$) in Solari *et al.*²⁷, cohort 5 ($n=8$) in Swieringa *et al.*²⁸, and cohort 6 ($n=3$) in Lewandrowski *et al.*²⁹. Platelets were always derived from anonymous healthy donors, due to ethics restrictions also not revealing age or sex. New experimental work was approved by the Ethics

Committee of Maastricht University and Maastricht University Medical Centre²⁸.

The genome-wide Blueprint gene expression data were generated from platelets obtained from venous blood ($n \geq 3$ per transcript, NHS Blood and Transplant healthy blood donors), and depleted from leukocytes^{23,31}. Primary data are public accessible via <https://blueprint.haem.cam.ac.uk/mRNA/> or <https://blueprint/haem.cam.ac.uk/bloodatlas/>³¹. Purity of platelets was checked by Sysmex, hemocytometer and from transcriptional signatures. Culturing of megakaryocytes ($n \geq 3$ per transcript) from cord blood, and check by flow cytometry (CD41 and CD42 double-positive) were as described¹⁹. Blood samples from healthy volunteers were obtained after full informed consent according to the Declaration of Helsinki.

Proteomes

In all reported studies, platelet lysates were analyzed according to a common bottom-up mass-spectrometry proteomics approach in the same laboratory. Experiments details are in the original papers²⁴⁻²⁹. Briefly, purified lysed platelets were subjected to a filter-aided sample preparation or ice-cold ethanol precipitation procedure. Isolated proteins were then trypsin-digested in guanidinium HCl or urea and (triethyl) ammonium bicarbonate (incubated over night at 37°C). For global proteome analysis, complex peptide mixtures were fractionated by high-pH reversed phase chromatography (pH 6 or 8). For detection and quantification of platelet phospho-peptides, an enrichment procedure was included using TiO₂ beads, followed by hydrophilic interaction liquid chromatography (HILIC) fractionation. Fractions of peptides or phosphopeptides were analyzed by nano-liquid chromatography (LC)-MS/MS using QExactive (QStar Elite) and Orbitrap Velos mass spectrometers. Raw data were processed with Proteome Discoverer, SearchGui and Peptide Shaker implemented with Mascot and Sequest and X!Tandem search algorithms. Spectra were searched against a human UniProt-KB database. For database versions, see

the original papers²⁴⁻²⁹. In all cases, a false discovery rate (FDR) of 1% was set.

Primary data deposits and links

Primary datasets were downloaded per proteome cohort via the website links of Table 1, also providing information on the deposited spectral datasets; the transcriptome data were obtained as fragments per kilobase of transcript per million fragments mapped (fpkm), and transformed to $\log_2(\text{fpkm}+1)$. For convenience, this was shortened to $\log_2\text{fpkm}$ (Table 1). In cohort one ($n=3$ subjects), relative protein abundance levels⁵² were determined in combination with a protein abundance estimate to give protein copy numbers per platelet⁵¹. In brief, protein copy numbers were assessed based on a normalized spectral abundance factor (NSAF) method. First, absolute quantification information was obtained from a set of 24 reference proteins (providing reference copy numbers), which then was used to correct NSAF indexes and was extrapolated to copy numbers of remaining proteins with known NSAF values.

In cohorts 2-5 ($n=3, 3, 2, 8$ subjects, respectively), additional proteins were obtained without copy numbers, obtained from either global proteome analysis and/or phosphoproteome analysis²⁵⁻²⁸. In cohort 6 ($n=3$ subjects), platelet membrane proteins were identified²⁹. Presence of individual proteins per cohort is indicated in Suppl. Datafile 2.

Proteome tabling construction

The summative identified proteins with or without copy numbers, derived from global proteome or sub-proteome/enrichment (phospho-proteins or membrane proteins) analysis, were all checked in UniProt-KD (consulted January 2019 - January 2020) and listed per corresponding gene (GeneCards). If no match between UniProt-KD assignment and gene name was found, additional gene databases were consulted (Biomart, Ensembl).

Transcriptomes

Genome-wide quantitative data of 57,849 transcripts assessed in human platelets and human megakaryocytes were established via a guided procedure by the Blueprint consortium^{23,31}. For link to sources, see Table 1. For establishing relevant transcription levels, we used an arbitrary, low expression cut-off of $\log_2\text{fpkm} \geq 0.20$, which included lowly abundant transcripts, to include all theoretical proteins presumably with very low levels (Suppl. Datafile 1).

Functional classification of protein-coding and other transcripts

The knowledge bases GeneCards (consulted January 2019 - January 2020) was used to primarily separate protein-coding genes, RNA genes and pseudogenes. GeneCards provides comprehensive information on the annotated and predicted human genes, integrating gene-centered data from ~150 web sources⁵³. Gene annotation was performed for all 20,425 gene transcripts (out of 57,849) with $\log_2\text{fpkm} \geq 0.20$ in platelets and/or megakaryocytes.

For all relevant transcripts of protein-coding genes ($\log_2\text{fpkm} \geq 0.20$), a supervised classification procedure was developed to combine the corresponding proteins into function classes. The classification was hierarchical, according to a yes/no decision tree (Figure 1), instructed by the EMBL UniProt-KB knowledgebase (visited January 2019 - January 2020)⁵⁴. UniProt-based decisions were based on the general description in Uniprot-KB of the (putative) protein's intracellular location and cellular function. Priority order of decision assignment was according to classical cell biology, *i.e.* from 'central' to 'peripheric': nucleus → mitochondria → endoplasmic reticulum and Golgi apparatus → cell → other cellular vesicles (lysosomes, peroxisomes, endosomes, secretory vesicles) → (plasma) membrane interactions → cytoskeleton structures → cytosolic protein types. When no relevant information was available, proteins were classified as 'Uncharacterized and other proteins'. Note that (assumed) extracellular

proteins were classified as secretory proteins, as these are considered to be released into the blood plasma by gland cells.

Area analysis of proteome-transcriptome space

For the matrix of 3,626 proteins with information on copy numbers and transcript levels in platelets ($\log_2\text{fpkm} \times 1000$), a rectangular triangle was obtained, in which five areas (I-V) were pre-defined as follows. Top right corner, I ($x = 100,000$, $y = 8$, $x\text{-radius} = 0.4$, $n = 58$ PLT); top left corner, II ($x = 1000$, $y = 8$, $x\text{-radius} = 0.3$, $n = 776$ PLT), bottom left corner, III ($x = 1000$, $y = 0.75$, $x\text{-radius} = 0.3$, $n = 137$ PLT); middle of triangle, IV ($x = 5000$, $y = 4$, $x\text{-radius} = 0.4$, $n = 928$ PLT), and all below the triangle, V ($x = 600\text{-}200,000$, $y = 0.6\text{-}10.2$, $n = 185$ PLT). For each dot (protein) in the matrix, using Matlab the distance (in log space) was determined to each of the predefined areas; and recordings were made as in/out. Subsequently, for the proteins per function class, p -values of over-representation in pre-defined areas were calculated, employing a native Matlab function.

Proteome prediction modelling

For prediction of the 'missing' (non-identified) part of the platelet proteome, we generated a model that was based on the definition, per protein class of three restraining factors: (i) low protein copy number, (ii) low mRNA level, and (iii) protein retainment in megakaryocytes upon proplatelet formation. Therefore, per function class, the fraction of non-identified proteins was calculated from all transcripts with $\log_2\text{fpkm} \geq 0.20$ in platelets and/or megakaryocytes, with an arbitrary setting of well-identified classes having <45% 'missing proteins'. Classes with low copy numbers were obtained from the proteome-transcriptome matrix (over-representation in areas II and III); or when no other explanation for low identification was present. Classes with low mRNA levels were also taken from the proteome-transcriptome space (over-representation in area V); or when the transcript fraction with $\log_2\text{fpkm} 0.20\text{-}1.00$ was >22.5% (arbitrary set at half of 45%). Classes with supposed protein retainment in megakaryocytes came from handbook

knowledge, i.e. the 'nuclear classes' C₁₃ and C₂₀; and furthermore C₃-cytoskeleton microtubule, given the retainment of mitotic spindle and centromere structures. Mean restraining factors were calculated from the averages of non-identified proteins in the corresponding classes. See further Suppl. Methods. Coverage of hemostatic pathways was checked in the Reactome database⁵⁵.

Model validation using extended novel proteome

To validate our model, platelet samples were collected as above from 30 healthy subjects, digested with trypsin, and analyzed by liquid chromatography-mass spectrometry. See further Suppl. Methods. Mass spectrometry proteomics data were deposited to the ProteomeXchange Consortium via the PRIDE partner repository⁵⁶ with the dataset identifier PXD022011 (username: reviewer_pxd022011@ebi.ac.uk; password: 7BeFQOxP).

Bioinformatics and statistics

Statistical comparison was by probability analysis in Excel (Mann–Whitney U-test or Student t-test for continuous variables). Distribution profiles were compared by a χ^2 test. Values of $p < 0.05$ were considered significant.

Results

Function-based classification of platelet proteins in merged proteome

Considering that the previously published (phospho)proteomics profiles of highly purified platelets from 22 healthy subjects in 6 cohorts were generated by the same analytical workflow²⁴⁻²⁹, we decided to integrate these datasets (Suppl. Figure 1A). Primary sources of these datasets are listed in Table 1. The resulting, merged human platelet proteome - one of the largest described so far - contained a total of 5,211 identified proteins, of which 80% were present in at least 2 cohorts (Suppl. Datafile 2). For 3,629 of these proteins, also copy numbers per platelet were present. In order to obtain a useful knowledgebase, we then categorized these proteins into 21

Table 1. Accessibility per proteome cohort of website link (a), used raw datasets (b) and deposited spectral data (c).

Cohort 1²⁴

- a. <https://ashpublications.org/blood/article/120/15/e73/30645/The-first-comprehensive-and-quantitative-analysis>
- b. Supplemental Table S2 and S3: identified phosphopeptides and proteins.
- c. Pride repository (<http://www.ebi.ac.uk/pride/>), accessions 22201-22203, 22206.

Cohort 2²⁵

- a. <https://ashpublications.org/blood/article/123/5/e1/32883/Time-resolved-characterization-of-cAMP-PKA>
- b. Supplemental Table S3 and S4: identified phosphopeptides and proteins.
- c. ProteomeXchange repositories PXD002883 and 10.6019/PXD002883.

Cohort 3²⁶

- a. <https://ashpublications.org/blood/article/129/2/e1/36101/Temporal-quantitative-phosphoproteomics-of-ADP>
- b. Supplemental Table 1 and 2: identified phosphopeptides and proteins.
- c. ProteomeXchange repository PXD001189.

Cohort 4²⁷

- a. <https://www.ncbi.nlm.nih.gov/pmc/articles/PMC5054341/>
- b. Supplemental Table 1 and 2: identified phosphopeptides and proteins.
- c. ProteomeXchange repositories PXD002883 and 10.6019/PXD002883.

Cohort 5²⁸

- a. <https://www.nature.com/articles/s41598-020-68379-3#Sec25>
- b. Datafile S1 and Datafile S2: identified phosphopeptides and proteins.
- c. ProteomeXchange repository PXD016534.

Cohort 6²⁹

- a. <https://ashpublications.org/blood/article/114/1/e10/26099/Platelet-membrane-proteomics-a-novel-repository>
- b. Table S4: list of proteins and peptides.
- c. Pride repository (<http://www.ebi.ac.uk/pride/init.do>), accessions 8127-8129.

PLT and MGK transcriptomes

- a. <https://doi.org/10.3324/haematol.2019.238147>
 - b. Transcript levels: <https://blueprint.haem.cam.ac.uk/mRNA/>
 - c. Deposited at BioRxiv <https://doi.org/10.1101/764613>
-

classes, based on intracellular localization and function (Figure 1A). For an objective classification, we used a dichotomous decision scheme together with human UniProt-KB assignments regarding the supposed primary location and/or function of that protein (Figure 1B). Highest fractions of identified proteins were seen in the following classes (Suppl. Figure 1B): C₂₀ (transcription & translation, $n=488$ proteins), C₁₂ (other metabolism, $n=475$), C₁₈ (signaling & adaptor proteins, $n=471$), C₁₁ (mitochondrial proteins, $n=455$), and C₁₀ (membrane receptors & channels, $n=327$). Distribution profiles of the 3,629 proteins with copy numbers (Suppl. Figure 1C) showed highest abundance and gene expression levels of the classes: C₀₁ (cytoskeleton actin- myosin), C₀₇ (glucose metabolism) and C₀₄ (cytoskeleton receptor-linked). This clustering analysis hence underscored the importance in platelets of signaling, mitochondrial and cytoskeletal proteins².

Relevant genome-wide transcriptomes of platelets and megakaryocytes

Based on well-purified human platelet and megakaryocyte preparations, the Blueprint consortium^{30,31} has recently generated one of the largest databases with genome-wide, quantitative information on a total of 57.8k transcripts in either cell type (Figure 2, for source see Table 1). Examination of the distribution pattern of all gene-linked transcripts indicated that 37.2k of these were essentially absent ($\log_2\text{fpkm } 0.02\text{-}0.03 \pm 0.03$, mean \pm SD) in platelets (Figure 3A) and megakaryocytes (Figure 3B). The residual presence of ~20k expressed transcripts supports earlier analyses of the comparative transcriptomes of blood cells¹⁹. We then combined these Blueprint datasets with the combined proteome data to come to a draft full platelet proteome.

Based on a low threshold of $\log_2\text{fpkm} \geq 0.20$ for relevant expression levels (see below), we obtained a defined set of 20.4k transcripts, which was taken to assemble the relevant transcriptomes for platelets (17.6k) and megakaryocytes (16.8k). Comparison between cell types gave a same distribution pattern ($p > 0.10$, χ^2) for platelets and megakaryocytes (Figure 3C, D). Filtering for transcripts of the 5.2k identified platelet proteins, again resulted in similar distribution patterns (Figure 3E, F). In either cell type, the

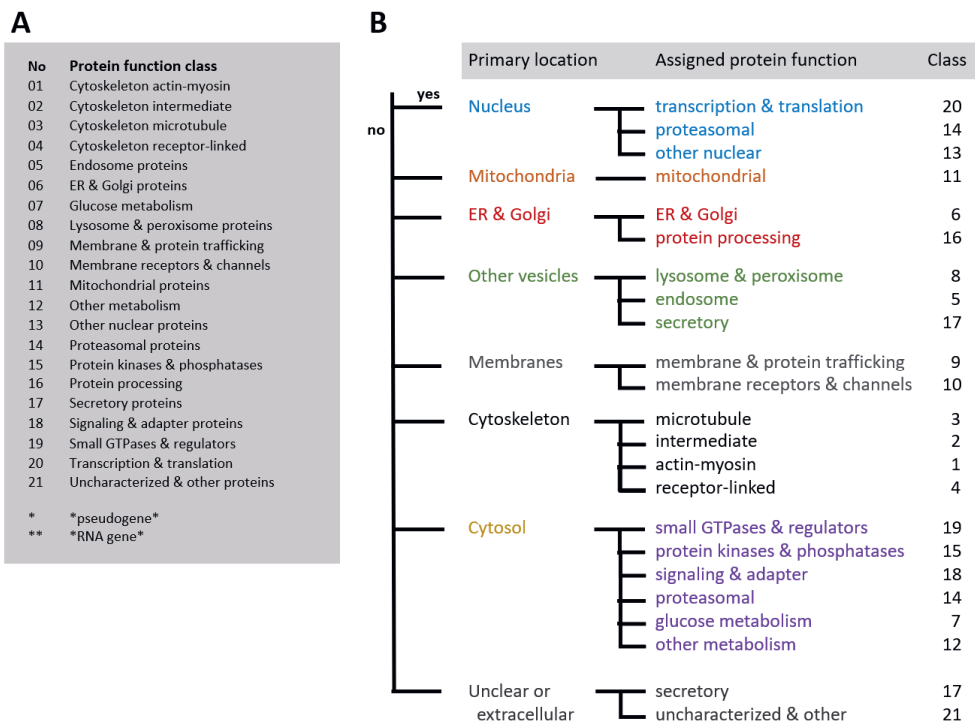


Figure 1. Classification scheme and decision tree for gene and protein assignment to 21 function classes. Assignment was based on primary subcellular localization of the protein and its assumed function according to UniProt-KB. **A**, Class numbering in alphabetical order. **B**, Hierarchical decision tree.

lower level transcripts ($\log_2\text{fpkm} < 1.00$) were under-represented in comparison to the unfiltered genome-wide distribution ($p=0.049$, χ^2).

Correlational analysis learned that the platelet and megakaryocyte transcriptomes were highly correlated; this was the case for both the 57.3k genome-wide transcripts ($\log_2\text{fpkm} \geq 0.00$, $R=0.85$, $\beta > 0.99$) and the 20.4k transcripts with relevant expression levels in either/both cell types ($\log_2\text{fpkm} \geq 0.20$, $R=0.75$, $\beta > 0.99$; Suppl. Figure 2A, B). This markedly revealed high similarity of the RNA species composition in human platelets and megakaryocytes. Concerning different RNA biotypes, this correlation remained high, when extracting only the protein-coding genes (14.8k,

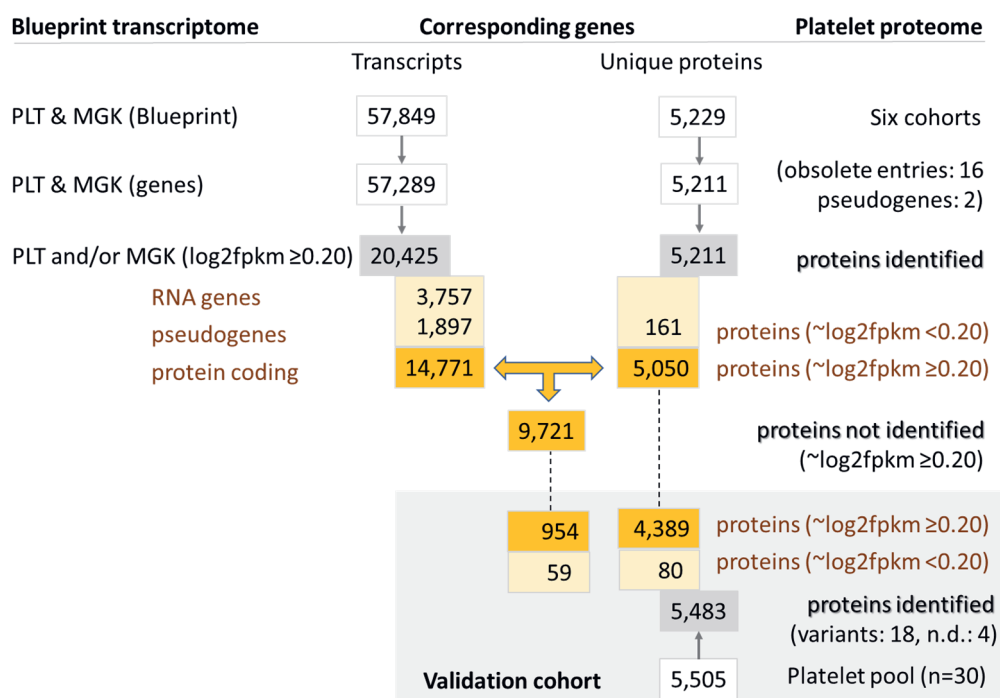


Figure 2. Dataflow of numbers of transcripts of proteome proteins. Relevant transcripts were defined as those of $\log_2\text{fpm} \geq 0.20$. Identified proteins refer to proteins present in the combined proteome from six cohorts. Non-identified proteins refer to proteins with relevant transcript levels in the combined PLT and MGK transcriptome. Data from validation cohort are also indicated.

$R=0.75$, $\beta>0.99$), but it reduced for the 3.8k RNA genes and 1.9k pseudogenes ($R=0.43-0.54$) (Suppl. Figure 2C-E).

For justification of the relevant transcript threshold for protein expression, we reduced this further from $\log_2\text{fpm}$ 0.20 to 0.15; this resulted in inclusion of no more than 8 extra proteins from the combined proteome, half of it being plasma-derived proteins and the other half with minimal copy numbers. This indicated that $\log_2\text{fpm}$ of 0.20, although arbitrary, provides a reasonable cutoff value for transcripts resulting in measurable proteins.

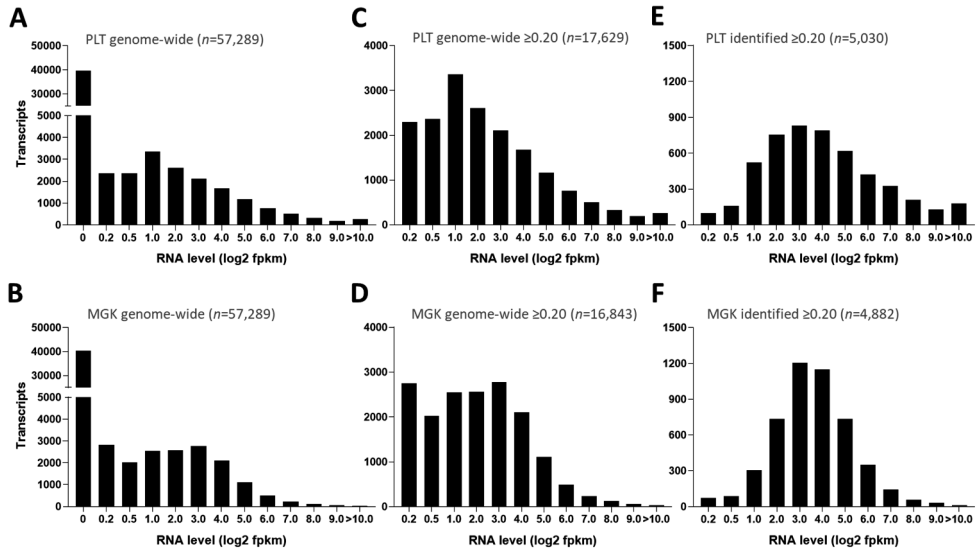


Figure 3. Histograms of RNA levels in transcriptome of platelets (PLT) or megakaryocytes (MGK). **A, B,** Distribution of all 57,289 genome-wide transcripts. **C, D,** Distribution of all relevant transcripts ($\log_2\text{fpkm} \geq 0.20$) for PLT (n=17,629) or MGK (n=16,843). **E, F,** Distribution of protein-coding transcripts, as identified in the proteome, for PLT (n=5,030) or MGK (n=4,882). Levels of RNA expression ($\log_2\text{fpkm}$) were binned as <0.20, 0.20-0.50, 0.50-1.00, 1.00-2.00, etc. For flow of numbers of transcripts and proteins, see Figure 2.

Using the combined knowledgebase of platelets and megakaryocytes, we assessed which of the 20.4k expressed transcripts ($\log_2\text{fpkm} \geq 0.20$) were also present in the 5.2k platelet proteome (Figure 2). It appeared that the majority of proteins had relevant transcription levels. In 19 of the 21 protein function classes only 1.6% of the protein transcripts were below the cut-off (77/4,907 with $\log_2\text{fpkm} 0.04 \pm 0.05$, mean \pm SD, n=19) (Table 2). However, in the classes C₀₂ (cytoskeleton intermediate) and C₁₇ (secretory proteins), percentages of below cut-off were much higher, amounting to 58% and 24%, respectively.

Given the analysis above, we considered that the combined platelet and megakaryocyte transcriptome (either $\log_2\text{fpkm} \geq 0.20$) provides the most extensive list of mRNAs that can be translated into proteins. To evaluate this,

we performed the same analysis as above for the platelet-only transcriptome. This resulted in a number of 'false' assignments of 181 (Table 2). For the megakaryocyte-only transcriptome data, this number increased to 329. Accordingly, the combined list of relevant platelet and megakaryocyte transcripts appeared to provide the best overlap with the proteomics dataset. By confining to proteins with relevant mRNA expression, the identified platelet proteome was therefore set at 5,050 proteins.

Comparison of (non-)identified parts of the platelet proteome

We then reasoned that starting from the genome-wide transcriptome of platelets and megakaryocytes ($\log_2\text{fpkm} \geq 0.20$), it was possible to construct a 'full' theoretical platelet proteome and compare this with the identified platelet proteins. By thus comparing the identified proteins with the transcripts of protein-coding genes, we could calculate the remaining, non-identified part of the proteome at 9,721 proteins, *i.e.* 66% of all mRNA transcripts (Suppl. Figure 3A). Based on this analysis, the majority of the 14.8k proteins in the theoretical proteome was still absent in the current platelet proteomes. A similar number of 14.3k was obtained when only including the relevant transcripts of platelets (Suppl. Figure 3B, C).

Detailed examination of the genes for which no protein products were detected revealed marked differences between function classes (Figure 4A, B). Highest numbers and percentages of transcripts of the 'missing' proteins were obtained for: C₂₀ (transcription & translation, $n=1,795$), C₂₁ (uncharacterized and other proteins, $n=1,683$), C₁₃ (other nuclear proteins, $n=1,269$), C₁₀ (membrane receptors & channels, $n=1,112$), C₁₇ (secretory proteins, $n=583$), and C₁₈ (signaling & adapter proteins, $n=561$). This prompted us to investigate the reasons for these inter-class differences in coverage of the identified proteome.

Restraining factors for a complete platelet proteome

Acknowledging current mass-spectrometry limitations (see Suppl. Methods), we hypothesized that absence of mRNA products can be explained by three

Table 2. See next page. Identified proteins in proteome in comparison to relevant transcriptome of platelets (PLT) and/or megakaryocytes (MGK). Indicated per function class are numbers of proteins with relevant ($\log_2\text{fpkm} \geq 0.20$) or no relevant ($\log_2\text{fpkm} < 0.20$) mRNA expression. Analyzed were the combined PLT/MGK transcriptome **(A)** as well as the separate PLT **(B)** and MGK **(C)** transcriptomes. For the total of 5,232 identified proteins in the proteome, 2 appeared to be encoded by pseudogenes, and 16 were designated as obsolete entries in UniProt-KB. Also given are percentages of proteins without relevant expression level (% false). **D**, Total numbers of assigned proteins per class independent of transcript level.

A	PLT and/or MGK	Proteins in transcriptome			% False	B			C			D
		yes ≥0.20	no <0.20			PLT	yes ≥0.20	no <0.20	MGK	yes ≥0.20	no <0.20	Total
	C01 Cytoskeleton actin-myosin	132	9	6.4		C01	132	9	C01	125	16	141
	C02 Cytoskeleton intermediate	8	11	57.9		C02	8	11	C02	6	13	19
	C03 Cytoskeleton microtubule	140	6	4.1		C03	139	7	C03	133	13	146
	C04 Cytoskeleton receptor-linked	51	0	-		C04	51	0	C04	48	3	51
	C05 Endosome proteins	52	0	-		C05	52	0	C05	52	0	52
	C06 ER & Golgi proteins	190	1	0.5		C06	190	1	C06	190	1	191
	C07 Glucose metabolism	46	1	2.1		C07	46	1	C07	45	2	47
	C08 Lysosome & peroxisome proteins	74	1	1.3		C08	74	1	C08	74	1	75
	C09 Membrane & protein trafficking	243	4	1.6		C09	242	5	C09	240	7	247
	C10 Membrane receptors & channels	318	9	2.8		C10	315	12	C10	300	27	327
	C11 Mitochondrial proteins	454	1	0.2		C11	454	1	C11	454	1	455
	C12 Other metabolism	469	6	1.3		C12	467	8	C12	463	12	475
	C13 Other nuclear proteins	200	3	1.5		C13	200	3	C13	196	7	203
	C14 Proteasomal proteins	311	1	0.3		C14	310	2	C14	311	1	312
	C15 Protein kinases & phosphatases	266	2	0.7		C15	266	2	C15	264	4	268
	C16 Protein processing	199	1	0.5		C16	197	3	C16	198	2	200
	C17 Secretory proteins	228	73	24.3		C17	223	78	C17	155	146	301
	C18 Signaling & adapter proteins	463	8	1.7		C18	462	9	C18	446	25	471
	C19 Small GTPases & regulators	284	3	1.0		C19	284	3	C19	281	6	287
	C20 Transcription & translation	485	3	0.6		C20	484	4	C20	482	6	488
	C21 Uncharacterized & other proteins	437	18	4.0		C21	434	21	C21	419	36	455
Total identified proteins		5050	161				5030	181		4882	329	
Pseudogenes		2	0				2	0		2	0	
Obsolete entries		0	16				0	16		0	16	
Together		5052	177	5229			5032	197		4884	345	

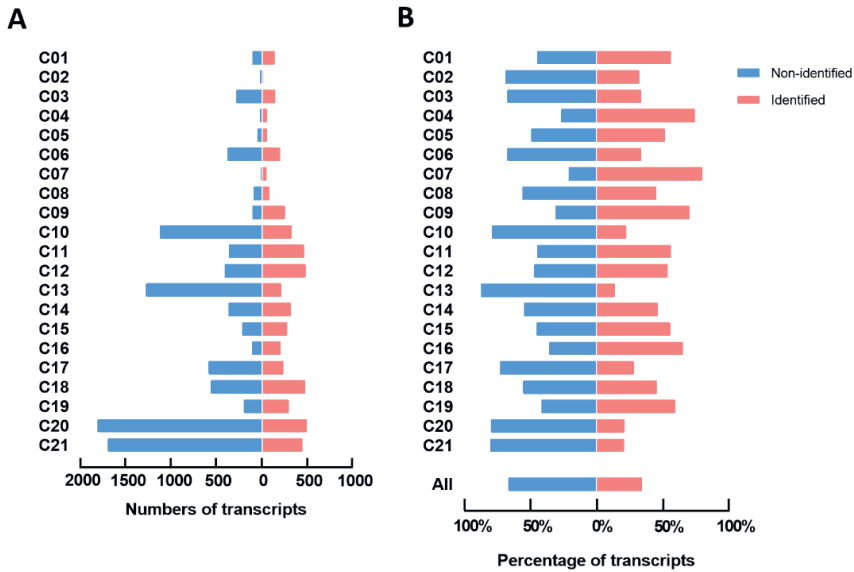


Figure 4. Transcript distribution of identified and not identified proteins in the platelet proteome per function class. Examined were all relevant protein-coding transcripts ($\log_2\text{fpm} \geq 0.20$) of the combined relevant PLT/MGK transcriptome, with separation of identified proteins ($n=5,050$) and not identified proteins ($n=9,721$). For full data, see Suppl. Figure 3. **A**, Numbers of transcripts numbers per function class. **B**, Percentage distribution of transcripts per function class.

restraining factors: (i) low protein copy number, (ii) low mRNA level, and/or (iii) retaining of a protein in the megakaryocyte perinuclear region. The annotated platelet and megakaryocyte transcriptome knowledgebase allowed us to estimate these restraining factors.

The relation between platelet copy numbers and transcript levels is still unclear^{32,33}. To reassess this issue, we compared the relevant Blueprint transcriptome ($\log_2\text{fpm} \geq 0.20$) with the 3.5k proteins with known copy numbers. Correlative scatter plots showed a marked triangular pattern (Figure 5A, B). This pattern indicated that the abundance of a protein was restricted by, but was not otherwise dependent of the transcript level. Given the high similarity of the platelet and megakaryocyte transcriptomes, this implied that the megakaryocytic mRNA levels in fact maximized the extent of protein expression in platelets.

To examine this further, we defined five regions in the proteome-transcriptome space, labeled as areas I-V (Figure 5C). For each of 3.5k quantified proteins, we performed a modeling analysis per function class in Matlab. This modelling revealed that - regardless of the use of platelet or megakaryocyte plots - several classes were significantly over-represented ($p=10^{-2}$ to 10^{-10}) in some of these areas (Suppl. Table 1). As illustrated in Figure 5D, for area I (high copy number and high mRNA), four classes were over-represented (*i.e.*, cytoskeletal and glucose- metabolism proteins, $p<10^{-2}$). For the areas II and III with low copy numbers ('low translation'), six and three classes were over-represented, respectively (*e.g.*, signaling-related, proteasomal, transcriptional and mitochondrial proteins). Thus, the classes accumulating in areas II-III appeared to be enriched in proteins with low copy numbers, irrespective of their corresponding transcript levels. Area V (low transcript levels) was enriched in keratin-like and secretory proteins (classes C₀₂ and C₁₇); and area IV of medium mRNA levels contained most of the remaining classes.

To categorize the low-level mRNAs, we examined the transcript level distributions per class, in which we separated the identified and non-identified parts of the theoretical proteome. Overall, the majority of the identified proteins showed relatively high corresponding transcript levels, regardless of their function class (Figure 6A). On the other hand, the low-level mRNAs (log2fpkm 0.20-1.00) were enriched in the non-identified proteome (median $P=0.0005$) (Figure 6B). This held for 12 out of 21 classes, where transcripts of non-identified proteins appeared to be of a lower level.

To examine the low-level transcripts in these 12 classes, we searched for common elements ($n\geq 10$) in protein names. Examples are: for C₀₁: 'actin' or 'myosin'; for C₀₃: 'centromere', 'centrosomal' or 'dynein'; for C₀₆: 'AP1-3 complex subunit', 'Golgi' or 'trafficking protein particle' (Table 3). Close examination showed that, for all 12 classes with >20% low-level mRNAs, the same >20% also applied for elements of the non-identified proteome (Suppl. Table 2). As apparent from the listed most abundant transcripts of elements

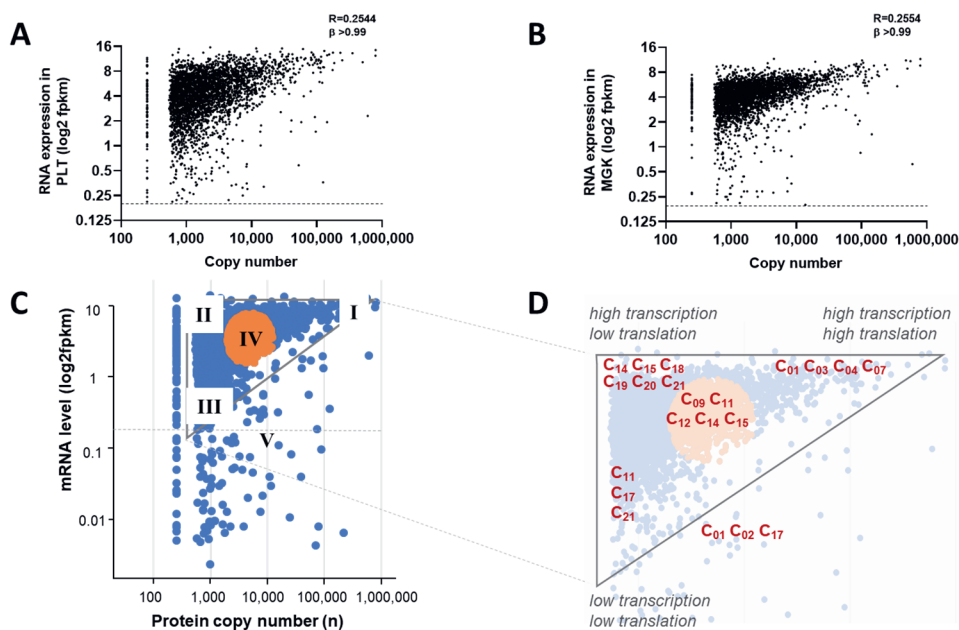


Figure 5. Comparison of protein copy numbers with mRNA levels and class-based analysis. **A, B,** Protein copy numbers compared per gene to transcript levels (log2fpkm) for datasets of platelets (PLT, $n=3,519$) (**A**) or megakaryocytes (MGK, $n=3,442$) (**B**). Note triangular space, with low-abundance proteins (<500 copies/platelet) were normalized to 150 copies. **C, D,** Over-representation of protein function classes in quantitative proteome-transcriptome space per predefined area (I-V). Area I is considered to represent a condition of high translation (high mRNA level) and high transcription (high copy number); area II of high translation and low transcription; area III of low translation and transcription, and area IV an intermediate condition. Area V represents proteins without relevant transcript levels in PLT. Transcriptome-proteome triangle with analyzed areas (**C**). Enlarged space indicating function classes (C_{01} - C_{21}) with significant over-representation per area. Statistics in Suppl. Table 1.

in almost all classes, the non-identified protein segments contained multiple isoforms or subunits of complexes that were also present in the identified segments, although the former had lower-level mRNAs (Table 3). Furthermore, sets of proteins seemed to be missing in almost all elements.

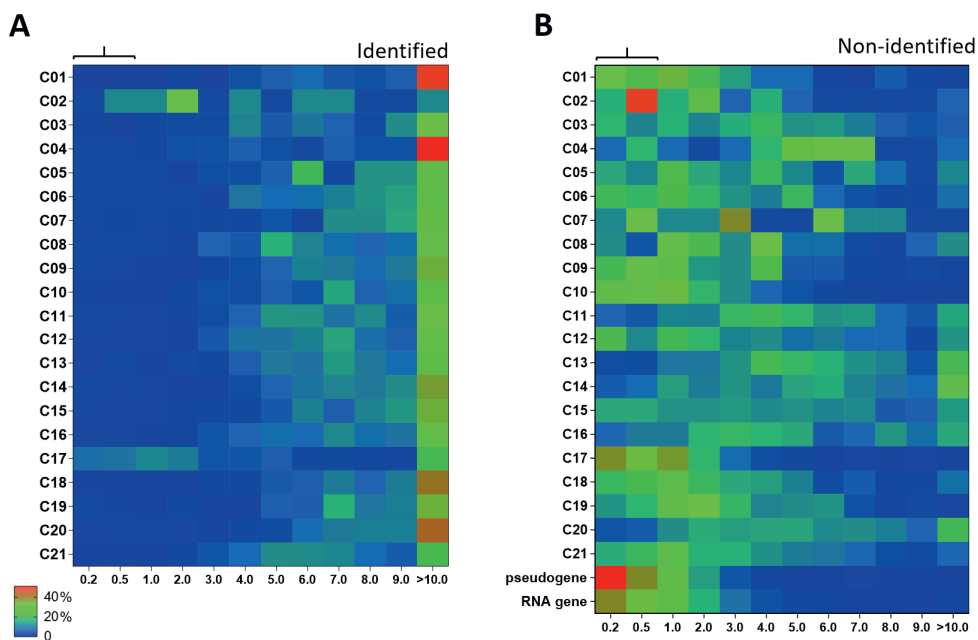


Figure 6. Distribution profile of relevant transcripts of per protein function class. For the relevant platelet transcriptome ($n=17,629$), heatmaps were constructed of percentual distribution of transcript levels per function class (rainbow colors; blue = low, red = high). **A**, Heatmap for transcripts of identified proteins ($n=5,030$). **B**, Heatmap for transcripts of non-identified proteins ($n=9,267$); furthermore RNA genes ($n=2,480$) and pseudogenes ($n=852$). Expression levels ($\log_2\text{fpkm}$) were binned as 0.20-0.50, 0.50-1.00, 1.00-2.00, etc. For numbers of transcripts, see Suppl. Figure 3.

As a third restraining factor, we examined protein retainment in the megakaryocyte, by reasoning that in particular (peri)nuclear proteins will not move into a shedding proplatelet. This applied for the classes C₂₀ (transcription & translation), C₁₃ (other nuclear proteins) and C₀₃ (cytoskeleton microtubule), containing multiple centromere/mitotic spindle proteins (Figure 6A). Hence, these three classes were listed as providing additional explanation for low identification in the proteome (Suppl. Table 2).

Table 3. See next page. Subgroup analysis of non-identified proteins (n=9,721) of the relevant PLT/MGK transcriptome. Per function class (C₀₁-C₂₁), the transcriptome database was searched for common elements in protein names ('actin', 'myosin'), and frequency was recorded as identified in the proteome, or not identified with a separation into high mRNA (log2fpkm >1.00) or low mRNA (log2fpkm 0.20-1.00). Top-4 of most abundant transcripts were listed per element. Further indicated per element: numbers of all transcripts (Sum all), and numbers of transcripts not identified in proteome (Sum NI).

Protein function class (n, log2(pkm≥0.20))			Identified in proteome (log2(pkm ≥0.20))			Not identified in proteome (high mRNA)			Not identified in proteome (low mRNA)			Sum all			Sum NI			Low mRNA		
UniProt-KB: in protein name (n≥10)			(n)	Examples (top 4 genes)	(n)	Examples (top 4 genes)	(n)	Examples (top 4 genes)	(n)	Examples (top 4 genes)	(n)	(n)	(n)	(n)	(n)	(n)	(n)	(n)	(n)	(n)
C01 Cytoskeleton actin-myosin																				
Actin	31	ACTB, ACTG1, ABUM3, ABLIM1	3	FAM107A, AFAP1L1, IPP	2	ACTL10, ACTRT3	36	5	40%											
	25	MYL6, MYL12A, MYL9, MYH9	9	MYLPF, MYO19, MYO1E, MYO10	11	MYO7B, MYO5C, MYO15A, MYBPC1	45	20	55%											
C02 Cytoskeleton intermediate																				
Keratin	5	KRT8, KRT1, KRT10, KRT73	3	KRT18, TCHP, KRT23	4	KRT7, KRTAP29-1, KRTCAP3, KRTAP10-6	12	7	57%											
C03 Cytoskeleton microtubule																				
Centromere	2	ZW10, CENPF	11	CENPI, CENPH, CENPI, INCENP	3	CENPO, CENPM, CENPP	16	14	21%											
	9	CEP162, CEP44, CEP128, CEP41	24	CEP70, CEP57L1, CEP350, CEP57	3	CEP126, CEP55, CEP295	36	27	11%											
Centrosomal	16	DYNLRB1, DYNLL1, DNMA3, DCTN2	15	DNMH14, EFCAB2, DYNLT1, DNHAH2	10	CCDC65, DNAAF1, DNAAH6, IQCA1	41	25	40%											
	11	KIF2A, KIFC3, KIF5B, KLC4	17	KIF28P, KIF3C, KIF22, KNL1	10	KIF21A, KIF25, KIF24, KLC3	38	27	37%											
Kinesin	4	MZT2B, NUNMA1, MZT1, HAL56	7	SKA2, SKA3, HAUS2, HAUS7	2	MAD2L1, SKA1	13	9	22%											
	40	TUBB1, TUBA4A, TUBA8, TUBB4B	24	TUBA1B, MAP1LC3A, AKNA, TTL17	10	MAP10, C16orf59, TRPP2, MAP9	74	34	29%											
C04 Cytoskeleton receptor-linked																				
LIM / Wiskott	7	LIMS1, PDLIM1, LASP1, WASF3	2	PDLIM2, WHAMMP3	1	FBLIM1	10	3	33%											
C05 Endosome proteins																				
Multivesicular body	9	CHMP3, CHMP4B, CHMP5, CHMP2A	2	MVB12A, CHMP4C	0	-	11	2	0%											
	6	WASHC3, WASHC2C, WASHC4, WASHC1	5	WASHBP, WASP3P, WASH2P, WASH4P	0	-	11	5	0%											
C06 ER & Golgi proteins																				
AP-1/3 complex subunit	15	AP1S1, AP2S1, AP2B1, AP3S1	3	AP1M2, AP3M2, AP1S3	1	AP3B2	19	4	25%											
	20	EMC3, KDELR2, EMC2, ERP29	9	KDELR1, EDEM3, HERPUD1, ERWARD	5	HPD9, SERP2, HRC, ERP27	34	14	36%											
ER membrane / lumen protein	31	TGOLN2, GOLGA7, GOLGA2, GOSR1	12	BIZF1, GOLGA8N, GOLGA8A, TVP23C	16	TVP23C-CDR14, GOLGA8M, GOLGA7B, GOLGA8R	59	28	57%											
	12	TRAPPC1, TRAPPC6B, TRAPPC5, TRAPPC9	4	TRAPPC2, TRAPPC3L, TRAPPC6A,	0	-	16	4	0%											
Trafficking protein particle	4	MGST3, MGST2, GFTP1, ACAT2	50	CSGALNACT2, LFNG, STB3A4, CHST2	41	FUT1, UBIAD1, UGT2B11, GCNT2, PIGA	95	91	45%											
C07 Glucose metabolism																				
Glucose	12	GPI, G6PD, SLC37A1, PRKCSH	5	NUDT22, GANC, G6PC3, TGDS	1	G6PC2	18	6	17%											
	7	ALDOA, GFTPT1, PKFM, PFKP	3	PFKFB4, TIGAR, FBP1	1	PFKFB1	11	4	25%											
C08 Lysosome & peroxisome proteins																				
Lysosome / lysosomal	10	CTSA, LIPA, LAMP1, LAMP2	10	LAPTM5, LAPTM4B, LMBRD1, LAMP5	1	LAMP3	21	11	9%											
	17	HSD17B4, ACOX1, ACAA1, PEX19	14	PXMP4, ACOX1, PEX2, PHFY, PEX26	6	TYSDN1, PEX12, PEX11A, ACOX2	37	20	30%											
Peroxisomal / peroxisomal	12	ATP6V1E1, ATP6V1F, ATP6V1G1, ATP6V1D	3	ATP6VOC, ATP6V0E1, ATP6V0B	2	ATP6VIG2, ATP6V1B1	17	5	40%											

Table 3. (to next page)

C09 Membrane & protein trafficking	9	EXOC5, EXO6B, EXOC4, EXOC6	0	-	1	EXOC3L1	10	1	<div><div></div></div> 100%
	10	SEC31A, SEC6B, SEC6B, SEC23A	1	SEC31B	0	-	11	1	<div><div></div></div> 0%
	17	SNX3, SNX6, SNX1, SNX5	6	SNX3, SNX19, SNX20, SNX10	0	-	27	10	<div><div></div></div> 40%
	5	SNAP23, ESYT2, SYTL1, SNAP29	6	SYTL1, SYTL3, SYTL11, SNAP47	8	SYTL7, SYTL5, SYTL1, SYNGR2	19	14	<div><div></div></div> 57%
	36	STXB2, STX7, STXB3, STX11	4	STX3, STXB4, STXB6, STX1B	0	-	20	4	<div><div></div></div> 0%
	26	VPS28, VPS37A, VPS41, VPS37B	0	-	0	-	26	0	<div><div></div></div> 0%
C10 Membrane receptors & channels									
C10 Membrane receptors & channels	9	ORA2, ORA1, SLC8A3, ITPR2	15	SLC24A3, ORA3, CACNB1, CALHM6	18	CACRL, KCNMA1, CACNA1D, CACNA1A	42	33	<div><div></div></div> 55%
	3	IL6ST, CXCR4, CCR4, IL17RA	6	IL7R, IL10RA, IL18R, CXCR2	9	CCR7, IL1R1, IL18R1, CXCR3	18	15	<div><div></div></div> 60%
	1	CLEC1B	8	CLEC7A, CLEC2D, CLEC12A, CLEC10A	3	CLEC7A, CLEC12B, CLEC5A, CLEC17A	19	18	<div><div></div></div> 56%
	8	GPIIb/IIIa, GP9, GP1BA, CD36	15	CD28, CD3E, CD8A, CD3G	30	CD1E, CD1C, KEL, MCAM	32	24	<div><div></div></div> 38%
	1	ADGRG1	14	ADGRE1, ADGRE2, GRP97, GRP183	3	GPCR3B, GPR135, GPR162, ADGR14	45	44	<div><div></div></div> 68%
	13	ITGB1, ITGB3, ITGB2, ITGB5	7	ITGAM, ITGAX, ITGAE, ITGAL	10	ITGA7, ITGB4, ITGA3, ITGB11	30	17	<div><div></div></div> 59%
	0	-	4	OR2W3, OR2L13, OR2I8, OR2B6	24	OR2L2, OR2ALP, OR2M4, OR52N4	28	28	<div><div></div></div> 88%
	3	P2RY12, P2RX1, P2RY11	7	P2RY10, P2RX5, P2RX4, P2RX7	7	P2RY11, P2RY14, P2RX6, P2RY6	14	11	<div><div></div></div> 36%
	52	SLC40A1, SLC2A3, SLC44A2, SLC3E1	51	SLC38A2, SLC35F5, SLC11A1, SLC2A11	43	SLC12A7, SLC6A9, SLC16A6, SLC24A4	146	94	<div><div></div></div> 46%
	6	VDAC3, KCNA3, VDAC2, VDAC1	12	KCNE3, KCND3, HVCN1, KCNQ1	20	KCNH3, KCNC3, KCNQ5, KCNA2	38	32	<div><div></div></div> 63%
	17	MT-ATP6, MT-ATP8, ATP5MPL, ATP5L	5	ATP5MC3, ATP5MC1, ATP5CKMT, ATPAF2	1	ATP5MGL	23	6	<div><div></div></div> 17%
	31	MT-CO2, UQCRL, COX6B1, UQCRL1	14	MT-CO3, MT-CO1, MT-CYB, COX17	4	UQCCL3, COX4I2, COA7, UQCRLH	49	18	<div><div></div></div> 22%
C11 Mitochondrial proteins	21	TOMM6, TOMM5, TOMM20, TIMM19	6	TIMM17B, TIMM10B, TIMM23, TIMM17A	0	-	27	6	<div><div></div></div> 0%
	32	NDUFA6, NDUFA5, NDUFB4, NDUFS5	5	NDUFA3, NDUFA1, NDUFC1, NDUFAF6	2	NDUFAF4, NDUFA4L2	39	7	<div><div></div></div> 29%
	47	MRPL41, MRPL35, MRPS28, MRPS23	37	MRPL28, MRPL47, MRPL30, MRPL34	0	-	84	37	<div><div></div></div> 0%
	19	CARS2, FARS2, RARS2, MRPL58	11	GATB, TRMT6B, TRMT6T, GATC	1	VARS2	31	12	<div><div></div></div> 8%
	44	CMPK1, GUK1, GK, DGKD	15	PANK3, ETKN1, TK1, RBKS	10	ETNK2, PANK1, TK1, RBKS	69	25	<div><div></div></div> 40%
	30	INP5K, PFKFB3, ACYP1, FIG4	15	CTDNBP1, PI3P5, IMPA2, PHOSPHO1	8	NUDT15, INP5E, PAH, PHOSPHO2	53	23	<div><div></div></div> 35%
C12 Other metabolism	31	CYB5R3, GMBR, CYB5R1, MRSB3	20	PI3R2, SHRS3, WWOX, PAR2	8	PI3R1, AKR1C2, TXNRD3, AKR1C4	49	18	<div><div></div></div> 44%
	29	GLUL, SER52, SMS, PAPSS1	20	MTR, FDF1, MTRR, DHS	8	CARN51, ADSL1, GYS2	57	28	<div><div></div></div> 29%
	76	AGPAT1, MBOAT2, GSTO1, UGP2	49	SAT1, PCMTD1, NAT8B, SGM51	37	HSEST1, GSTA4, PRMT10, TGM1	162	86	<div><div></div></div> 43%
	6	GALM, RPE, GALE, GNE	1	DSE	1	DSE	8	2	<div><div></div></div> 50%
	4	CMPK1, GUK1, GK, DGKD	15	PANK3, ETKN1, TK1, RBKS	10	ETNK2, PANK1, TK1, RBKS	69	25	<div><div></div></div> 40%
	30	INP5K, PFKFB3, ACYP1, FIG4	15	CTDNBP1, PI3P5, IMPA2, PHOSPHO1	8	NUDT15, INP5E, PAH, PHOSPHO2	53	23	<div><div></div></div> 35%
C13 Other nuclear proteins	31	CYB5R3, GMBR, CYB5R1, MRSB3	20	PI3R2, SHRS3, WWOX, PAR2	8	PI3R1, AKR1C2, TXNRD3, AKR1C4	49	18	<div><div></div></div> 44%
	29	GLUL, SER52, SMS, PAPSS1	20	MTR, FDF1, MTRR, DHS	8	CARN51, ADSL1, GYS2	57	28	<div><div></div></div> 29%
	76	AGPAT1, MBOAT2, GSTO1, UGP2	49	SAT1, PCMTD1, NAT8B, SGM51	37	HSEST1, GSTA4, PRMT10, TGM1	162	86	<div><div></div></div> 43%
	6	GALM, RPE, GALE, GNE	1	DSE	1	DSE	8	2	<div><div></div></div> 50%
C13 Other nuclear proteins	4	SMARCA5, CHRA1, ACIN1	12	HP1BP3, BAP18, MEAF6, PDSSA	1	CHAF1B	17	13	<div><div></div></div> 8%
	16	H1-2, H2AC11, H1-4, KMT2C	121	H2AC6, H3-3A, H2BC4, H3C10	13	-	150	134	<div><div></div></div> 10%
	6	NUP54, NUP58, NUP88, NUP214	19	NUP54, NUP58, NUP35, NUP98	9	NIPB2, NIP47, NUP210L, NIP43	34	28	<div><div></div></div> 32%
	4	PARP14, PARP9, PARP10, PARP12	24	POLD4, POLR2J3, POLR1D, POLE3	0	-	28	24	<div><div></div></div> 0%
	4	MRE11, RAD50, MMS19, MSH6	22	MLH3, SPIDR, SWI5, RAD21	3	XRC3, RAD51, ERCC6L	29	25	<div><div></div></div> 12%
	9	COP59, COP53, COP54, COP58	1	COP59	0	-	10	1	<div><div></div></div> 0%
C14 Proteasomal proteins	55	RBX1, MARCKS, TRIM58, RNFI3	104	MARCH5, MKRN1, RBBP6, SIAH2	21	RNF43, PEU3, TRIM32, SNURF	180	125	<div><div></div></div> 17%
	0	-	14	KULH18, KULH8, KULH2, KULH7	6	KULH15, KULH3, KBTBD8, KULH17	20	20	<div><div></div></div> 30%
	12	UBE2F, NEDD8, NAE1, UBA3	2	NDP1, WWP1	1	NDP1P2	15	3	<div><div></div></div> 33%
	37	PSMB9, PSMB8, PSME1, PSMF1	7	SEMI, POMP, PSME3, PSME2	1	C1orf105	45	8	<div><div></div></div> 13%
	15	UBE2D3, UBE2E3, UBE2H, UBE2K	15	UBE2Q2, UBE2D2, UBE2C, UBE2D	2	UBE2Q7, UBE2Q2L	32	17	<div><div></div></div> 12%
	15	UBE2D3, UBE2E3, UBE2H, UBE2K	15	UBE2Q2, UBE2D2, UBE2C, UBE2D	2	UBE2Q7, UBE2Q2L	32	17	<div><div></div></div> 12%

Table 3. (to next page)

C15 Protein kinases & phosphatases	Mitogen-activated protein kinase	23	MAP2K3, MAPKAPK2, MAPK1, MAP4K5	12	MAPK6, MAP2K5, MAPK8, MAP3K3	6	MAPK11, MAPK12, MAP3K12, MAP3K21	41	18	<div><div></div></div>	33%
	Serine/threonine-protein kinase	83	RIOK3, TLK1, STK24, AKT3	40	STK40, PRKD3, TLK2, MNK2, UHMK1	21	STK31, PRKY, NEK8, PLK1	144	61	<div><div></div></div>	34%
	Serine/threonine-protein phosphatase	25	ANKRD28, PPP1C8, PPP6C, PPP6R1	11	PPP4C, PPP1R3D, PPP4R2, PPP4R3A	4	PPP4R4, PPP2R3A, PPEF1, PPEF2	40	15	<div><div></div></div>	27%
	Tyrosine (protein) phosphatase	16	PTPN18, PTPN12, PTP4A2, PTPRA	7	PTPN18, PTPN12, PTPN4, PTPN22	7	PTPRB, PTPN13, PTPN20B, PTPN20A	29	13	<div><div></div></div>	54%
	Tyrosine-protein kinase	19	LYN, FYN, BTK, CSK	7	TYK, HCK, LCK, ZAP70	3	STYK1, BMX, TNK1	29	10	<div><div></div></div>	30%
C16 Protein processing	DoI / dolichol	14	DAD1, STT3B, DPM3, STT3A	2	DPM2, ALG6	0	-	16	2	<div><div></div></div>	0%
	Galactosyltransferase (C12)	5	CIGALT1, B4GALT1, B4GALT6, COIGALT1	4	B4GALT6, B3GALT4, B4GALT3, B4GALT5	2	B4GALT7, CIGALTIC1	11	5	<div><div></div></div>	40%
	Glucosyl / glycosyltransferase	14	ALG6, RPN2, UGGT1, RPN1	3	ALG6, ALG10B, OST4	0	-	17	3	<div><div></div></div>	0%
	Methyltransferase	5	PRMT2, PRMT1, PRMT3, PRMT5	8	EEF1AKMT1, DPH7, PRMT7, NTMT1	0	-	13	8	<div><div></div></div>	0%
	Palmitoyl / snailtransferase	1	ST3GAL6	4	ST3GAL3, SPFS3A, ST3GAL4, ST3GAL1	5	PORCN, ZDHHC23, ZDHHC9, SPFS5B	20	19	<div><div></div></div>	26%
C17 Secretory proteins	Pept / peptidyl	37	PPIA, FKBP1A, FKBP8, XPNPPEP1	9	PII3, XPNPPE3, PGPEP1, FKBP9	4	CPA3, FKBP10, CPA1, FOLH1	50	13	<div><div></div></div>	31%
	Collagen	9	COL4A3BP, COL6A3, COL4A2, COL6A1	7	COL24A1, COL10A1, COL18A1, COL25A1	17	COL4A1, COL9A3, COL15A1, COL17A1	33	24	<div><div></div></div>	71%
	Growth factor	14	TGFB1, EGF, HGF, PDGFA	8	VEGFB, FGF2, IGF1BP4, VEGFA	14	LTBP2, TGF α , FGF12, TGF β 3	36	22	<div><div></div></div>	64%
	Interleukin / chemokine	7	CCL5, CXCL5, CXCL3, IL16	16	IL32, CXCL8, CK1F, CXCL16	18	IL33, IL6, CCLF1, CCL7	41	34	<div><div></div></div>	53%
	Metalloproteinase	5	TIMP1, ADAM8, TIMP2, TIMP3	9	ADAMTS6, MMP25, ADAM15, MMP28	14	TIMP4, ADAMTS9, MMP11, ADAMTS10	28	23	<div><div></div></div>	61%
C18 Signaling & adaptor proteins	Protease	4	SPINT2, SERPING1, MASP1, SERPINA5	7	PRSS27, PRSS53, CTRL, PRADCL	10	KAZALD1, HTRA3, HPN, PRSS57	21	17	<div><div></div></div>	59%
	14-3-3 / S100 protein	11	YWHAZ, YWHAE, YWHAH, S100A8	2	S100A10, S100P	2	S100A2, S100A1	15	4	<div><div></div></div>	50%
	Adaptor / adaptor protein	13	GRAP2, SLA2, FAM89B, SH2B3	13	STRAD8, PRAM1, SH2B1, GRAP	9	TICAM2, GULP1, STAP2, SHF	35	22	<div><div></div></div>	41%
	Bcl / Bax	9	BNIP2, BNIP3L, BCL2L1, BAD, BAK1	5	TNFRSF6, BCL2B, BME, BCL9, BCL2	4	BNIP1, BIK, BCL2L14	18	9	<div><div></div></div>	48%
	Calcium / calpain	15	CAPN3, CAPN1, ATP2A3, CAPN2	11	CALM3, CALM2, CABP5, CAPN11	12	CADPS2, SLC24A1, CABP4, PDE1B	38	23	<div><div></div></div>	52%
C19 Small GTPases & regulators	cAMP / A-kinase	8	Zor1B8, AKAP13, AKAP2, ADCY3	14	PKIG, PDE4D, AKAP7, AKIP1	12	ADCY4, PDE4C, ARPP21, AKAP3	34	26	<div><div></div></div>	46%
	Caspase	11	CARD19, CARD8, CASP4, CASP2	7	CARD16, CASP1, CARD11, CASP10	1	CARD14	19	8	<div><div></div></div>	13%
	cGMP / G-kinase	7	PDE5A, GUCY1B3, GUCY1A3, GMP5	7	GKAP1, PDE6D, PDE6H, PDE6B	3	PDE9A, GUCY2D, GUCY1B2	17	10	<div><div></div></div>	30%
	Guanine nucleotide / G-protein	25	RGS18, RGS10, GNAS, GNG11	6	RGS3, GNG2, RGS9, GNGT2	12	RGS5, RGS22, RGS17, GNG12	43	18	<div><div></div></div>	67%
	Phosphatidyl / phosphoinositide	41	PIK4R2, DAPPI1, TMEM55A, PIK3C3	20	PIK3R5, PLCD4, PIK3CD, PIK3R3	5	PLCZ1, PIP5K11, NYP42, PREX1	66	25	<div><div></div></div>	20%
C20 Transcription & translation	Arf-GAP	7	ACAP2, GIT2, ACAP1, GIT1	8	AGAP4, ADAP1, ARAP3, ADAP2	3	AGAP8, AGAP6, AGAP7	18	11	<div><div></div></div>	27%
	Rab	63	RABGAP1L, RAB11A, RAB27B, RAB31	11	RABL2A, RAB11FIP1, RGP1, RIN2	4	RAB44, RAB39B, RAB26, RAB36	78	15	<div><div></div></div>	27%
	Rel	8	RALB, RALBP1, RALGAPA1, RALGAPB	2	RALGDS, RALGPS1	2	RGL1, RGL3	12	4	<div><div></div></div>	50%
	Rap	9	RAP1B, RAP1A, RAP1GDS1, RAP1GAP2	7	RAPGEF1, RAP1GAP, RAPGEF3, RAPGEF5	1	GARNL3	17	8	<div><div></div></div>	13%
	Ras (non RAB, Raf, Rap)	6	RSU1, RASGRP2, RASA3, RASA1	7	RASGEF5, RASGEF2, RASA4, RASGRP4	7	RASEF, IQGAP3, RASGEF1A, RASAL1	20	14	<div><div></div></div>	50%
C21 Signaling & regulators	Rho	38	ARHGAP18, RHOA, ARHGAP18, ARHGAP21	28	ARHGAP30, RHOQ, ARHGAP26, TAGAP	22	ARHGAP22, ARHGAP25, ARHGFE5, SYDE1	88	50	<div><div></div></div>	48%
	Nuclear	42	NCOR1, TIA1, NCOA7, NFAT5	82	NCOA4, HNRNPUL1, NCOA2, NFYC	3	NPIPB15, NFATC4, NARF	127	85	<div><div></div></div>	4%
	Ribosomal protein	34	RP520, RPLP1, RPS11, RPS18	60	RPL41, RPS27, RPS29, RPL3	2	RPL17, RPS6K11	96	62	<div><div></div></div>	3%
	Transcription	40	SLTM, BTF3, FLU1, NFE2	48	ATF4, CAMTA1, SUPT4H1, RUNX1	215	YAP1, TEAD4, E2F5, POU6F1	303	263	<div><div></div></div>	82%
	Translation	44	EIF1, TMA7, EIF4G2, EIF4G3	31	EIF2AK1, EIF1B, EIF4A3, EIF4E3	1	EIF3CL	56	12	<div><div></div></div>	8%
C22 Translation & translation	tRNA	31	RARS, WARS, NARS, DARS	31	ADAT1, TRIT1, DUS1L, CKA11	9	METTL2A, TRMT10A, TRMT6A, CTU1	71	40	<div><div></div></div>	23%
	Zinc finger	9	ZC3H7A, HELZ, ZC3HAV1, ZBTB7A	409	GF1B, ZEB2, ZNF664, ZNF271	161	ZNF483, ZNF588, IKZF4, ZNF563	579	570	<div><div></div></div>	28%

Table 3. (to next page)

C21 Uncharacterized & other proteins									
Coiled-coil	15	CCDC92, CCDC98, CCDC25, CCDC9	55	CCDC7, CCDC126, CCDC175, CCDC180	21	CCDC157, CCDC136, CCDC121, CCDC81	91	76	28%
FAM	58	FAM110A, FAM122B, FAM177A1, FAM114A2	118	FAM138, FAM81B, FAM228B, FAM193B	79	FAM13C, FAM209A, FAM71F2, FAM161B	255	197	40%
Leucine-rich repeat	6	LRCH3, LRCH4, LRRC47, C10orf11	12	LRRC28, LRRC37A3, LRRC23, LRRC37B	18	LRRC61, LRFN4, LRIG2, LRRC1	36	30	60%
Putative	10	INAFM2, UOCRFSP1, SNX29P2, HSPA7	49	PLEKHA8P1, NBPf8, C15orf54, NSHG12	31	ALG1L2, CCDC144Cp, ZNF815, C22orf34	90	80	39%
Transmembrane	40	TMEM50A, CMTM5, CMTM6, TM6SF1	56	TMEM91, TMAM158, TMEM185A, TMEM248	37	TMEM268, TMEM267, TMEM185B, TMEM273	133	93	40%
Uncharacterized	19	C1orf198, KIAA0513, C1orf43, KIAA2013	119	C4orf3, C12orf76, C6orf62, LOC100287036	111	ZSWIM9, ENS00000173366, C16orf74, C3orf80	249	230	48%

Prediction model of the total platelet proteome

We then established a matrix for determining the three restraining factors per class (Figure 7A). This matrix was then used to calculate weighted mean values of the fractions of identified proteins grouped per factor. The fractions of identified proteins for (i) low copy number, (ii) low mRNA >20%, and (iii) retainment in megakaryocytes, amounted to 43%, 45% and 20%, respectively. For all other classes, the average fraction of identified proteins was 65% (Figure 7A). By ratioing, this resulted in correction factors (0.66, 0.69 and 0.31, respectively) for class predictions of the likeliness that additional proteins would appear in an enlarged proteome (Figure 7B).

Summarizing, the prediction model indicated a greatly enlarged size of the platelet proteome up to 10k proteins at a 1- or twofold higher detection efficacy. Markedly, apart from a consistent underrepresentation of classes of (peri)nuclear proteins (C₀₃, C₁₃, C₂₀), the model also predicted that a poor detection of proteins in the classes: C₁₀ (membrane receptors & channels), C₁₇ (secretory proteins), and C₂₁ (uncharacterized & other proteins).

Proteome model validation

For validation of the model, we performed a new proteomic analysis with pooled platelets from 30 healthy subjects and the newest mass spectrometers. The obtained proteome included 4,389 of the previously identified proteins with relevant transcripts, as well as 954 previously not identified proteins (Figure 2; details in Suppl. Datafile 3). Of additional 139 proteins without relevant transcript levels ($\log_2\text{fpkm} < 0.20$), the majority of 70% again appeared in C₀₂ (intermediate cytoskeleton, $n=15$, 11%) and C₁₇ (secretory proteins, $n=81$, 58%). This underscored the earlier observation that keratins and plasma proteins are present in the proteome of platelet samples.

Concerning the 954 novel obtained proteins, only small fraction of 3.8% showed low transcript levels with $\log_2\text{fpkm} 0.20-1.00$. Heatmap showed a similar distribution profile for all classes (Suppl. Figure 4).

A	Class (n)	Identified fraction	Well identified ID	Low copy number II, III	Low mRNA LM, V	Retained in MGK nuclear
	C01 Cytoskeleton actin-myosin (237)	0.56	X		X	
	C02 Cytoskeleton intermediate (27)	0.30			X	
	C03 Cytoskeleton microtubule (420)	0.33				X
	C04 Cytoskeleton receptor-linked (69)	0.74	X			
	C05 Endosome proteins (101)	0.51		X		
	C06 ER & Golgi proteins (568)	0.33			X	
	C07 Glucose metabolism (58)	0.79	X		X	
	C08 Lysosome & peroxisome proteins (168)	0.44			X	
	C09 Membrane & protein trafficking (349)	0.70	X		X	
	C10 Membrane receptors & channels (1430)	0.22			X	
	C11 Mitochondrial proteins (814)	0.56	X	X		
	C12 Other metabolism (877)	0.53			X	
	C13 Other nuclear proteins (1469)	0.14				X
	C14 Proteasomal proteins (677)	0.46		X		
	C15 Protein kinases & phosphatases (481)	0.55		X	X	
	C16 Protein processing (308)	0.65	X			
	C17 Secretory proteins (811)	0.28		X	X	
	C18 Signaling & adapter proteins (1024)	0.45		X	X	
	C19 Small GTPases & regulators (483)	0.59	X	X	X	
	C20 Transcription & translation (2280)	0.21		X		X
	C21 Uncharacterized & other proteins (2120)	0.21		X	X	
				Restraining factor		
Mean of classes (weighted)			0.65	0.43	0.45	0.20
Correction factor			1.00	0.66	0.69	0.31

B		Identified (n)	Estimated fraction at higher detection											C validated
			now	+20%	+40%	+60%	+80%	+100%	+120%	+140%	+160%	+180%	+200%	
C01	132	0.56	0.65	0.75	0.84	0.93	1.00	1.00	1.00	1.00	1.00	1.00	1.00	0.65
C02	8	0.30	0.34	0.38	0.42	0.46	0.50	0.54	0.58	0.62	0.67	0.71	0.71	0.37
C03	140	0.33	0.37	0.40	0.43	0.47	0.50	0.53	0.57	0.60	0.63	0.67	0.67	0.40
C04	51	0.74	0.89	1.00	1.00	1.00	1.00	1.00	1.00	1.00	1.00	1.00	1.00	0.75
C05	52	0.51	0.59	0.66	0.73	0.80	0.87	0.94	1.01	1.00	1.00	1.00	1.00	0.61
C06	190	0.33	0.38	0.42	0.47	0.51	0.56	0.60	0.65	0.69	0.74	0.79	0.79	0.44
C07	46	0.79	0.95	1.00	1.00	1.00	1.00	1.00	1.00	1.00	1.00	1.00	1.00	0.84
C08	74	0.44	0.50	0.56	0.62	0.68	0.75	0.81	0.87	0.93	0.99	1.05	1.05	0.56
C09	243	0.70	0.84	0.97	1.00	1.00	1.00	1.00	1.00	1.00	1.00	1.00	1.00	0.72
C10	318	0.22	0.25	0.28	0.31	0.34	0.37	0.40	0.43	0.46	0.49	0.52	0.52	0.26
C11	454	0.56	0.65	0.74	0.83	0.93	1.00	1.00	1.00	1.00	1.00	1.00	1.00	0.68
C12	469	0.53	0.61	0.68	0.76	0.83	0.90	0.98	1.05	1.00	1.00	1.00	1.00	0.62
C13	200	0.14	0.14	0.15	0.16	0.17	0.18	0.19	0.20	0.20	0.21	0.22	0.22	0.22
C14	311	0.46	0.52	0.58	0.64	0.70	0.76	0.82	0.88	0.94	1.00	1.00	1.00	0.53
C15	266	0.55	0.63	0.70	0.78	0.85	0.93	1.00	1.00	1.00	1.00	1.00	1.00	0.62
C16	199	0.65	0.78	0.90	1.00	1.00	1.00	1.00	1.00	1.00	1.00	1.00	1.00	0.71
C17	228	0.28	0.32	0.36	0.39	0.43	0.47	0.51	0.55	0.58	0.62	0.66	0.66	0.33
C18	463	0.45	0.51	0.57	0.63	0.70	0.76	0.82	0.88	0.94	1.00	1.00	1.00	0.50
C19	284	0.59	0.67	0.75	0.83	0.90	0.98	1.00	1.00	1.00	1.00	1.00	1.00	0.65
C20	485	0.21	0.23	0.25	0.27	0.30	0.32	0.34	0.36	0.38	0.40	0.42	0.42	0.27
C21	437	0.21	0.23	0.26	0.29	0.32	0.34	0.37	0.40	0.43	0.46	0.48	0.48	0.25
Total (n)		5050	5747	6436	7064	7654	8190	8683	9101	9399	9745	9987	5341	

Figure 7. See upper page. Restraining factors per function class and prediction model of full platelet proteome. Analysis of non-identified proteins (n=9,721) from the relevant, combined PLT/MGK transcriptome per function class. Full dataset is provided in Suppl. Table 2. **A**, Fraction of identified proteins in green. Well-identified classes with fractions >0.55 labeled as ID. Indicated in red are each of three restraining factors per class: (i) over- represented low copy number (areas II-III in Figure 5D), (ii) low mRNA level (area V, LM = low mRNA >45%); (iii) retainment in megakaryocyte (peri)nucleus upon platelet shedding. Bottom: means of identified fractions (weighted for the presence of multiple factors); and correction factor in comparison to 'well-identified'. **B**, Based on identified proteins (n=5,050), modelled prediction of increased identification of missing proteins per class at higher proteomic detection. Shown per class are fractions of total relevant transcripts (heatmapped), and total expected proteins (bottom line). **C**, Validation of prediction model based on novel proteome with 5,341 identified proteins.

Markedly, inclusion of the novel proteins agreed with the prediction model for the majority of classes (Figure 7C). Interestingly, higher than expected were the novel proteins for C₂₀ (transcription & translation, additional 139

proteins) and C₁₃ (other nuclear proteins $n=+121$); lower were those of C₀₉ (membrane proteins, $n=+7$).

Coverage of genes associated with hemostasis and thrombosis

To further establish the clinical relevance of these datasets, we incorporated the identified proteome set into a Reactome-based protein-protein interaction network (267 core proteins and 2,679 new nodes) that was constructed to identify the roles of platelet and coagulation proteins in thrombosis and hemostasis¹⁵. As shown in Figure 8, this network incorporated 1.3k of the identified proteins (median protein copies 2,200, median transcript level log2fpkm 4.97), as well as a set of 1.1k proteins/transcripts (median log2fpkm 1.97) not present in the combined proteome (Figure 8A, B). Importantly, of the latter set, 172 proteins were obtained in the proteome of the validation cohort.

To further establish the coverage for platelet-related disorders, we extracted the databases Online Mendelian Inheritance in Man (OMIM)³⁴ and Bloodomics²³ in combination with a recent overview paper³⁵ for genes associated with bleeding, thrombocythemia or thrombophilia. This resulted in 138 genes, of which 9 were absent in the platelet transcriptome but present in the proteome (coagulation factor and other plasma proteins), and 5 were absent in both (Table 4). For the remaining set of 124 genes, transcript levels (log2fpkm 4.58 ± 3.70 , mean \pm SD) and copy numbers ($22.8 \pm 73.0k$) in platelets were relatively high. Markedly, the majority of these 124 genes encoded for proteins in the classes C₁₀ (membrane receptors and channels, $n=22$), C₁₇ (secretory proteins, $n=19$), C₂₀ (transcription & translation, $n=12$), C₁₈ (signaling & adapter proteins, $n=10$), with a lower presence in the other classes. In accordance with the network analysis, it is likely that many still unknown gene products link to a platelet quantitative or qualitative traits, and hence to bleeding or thrombosis. The near complete coverage of the theoretical platelet proteome for known hemostatic pathways was also checked in the Reactome database (not shown).

Table 4. Platelet-expressed proteins in whole-genome transcriptome implicated in hemostasis and thrombosis. Listed are per platelet function class genes expressed in the (non)identified platelet proteome, which according to recent OMIM, Bloodomics and overviews^{23,34,35} in man contribute to bleeding, thrombocytopenia or thrombophilia. Coding as follows. **Bold:** identified in platelet proteome; **green:** bleeding or thrombocytopenia; **red:** thrombophilia; **black:** either reported.

Class	Genes/proteins
C01 Cytoskeleton actin-myosin (7/237)	ANKRD26 , ACBT , ACTN1 , ARPC1B , FLNA , MYH9 , TPM4 , WIPF1
C03 Cytoskeleton microtubule (1/420)	TUBB1
C04 Cytoskeleton receptor-linked (1/69)	FERMT3
C05 Endosome proteins (1/101)	LYST
C06 ER & Golgi proteins (9/568)	AP3B1 , AP3D1 , CISD2 , COG6 , HPS1 , HPS4 , LIMAN1 , MCFD2 , SLC35A1
C08 Lysosome & peroxisome proteins (3/168)	ABCD4 , GBA , HPS6
C09 Membrane & protein trafficking (7/349)	DTBBP1 , HPS3 , HPS5 , BLOC1S3 , BLOC1S5 , BLOC1S6 , NBEAL2
C10 Membrane receptors & channels (23/1430)	ACVRL1 , ANO6 , CD36 , CD40LG , CD55 , CD81 , CLCN7 , ENG , FCGR2A , FCGR2C , GP1BA , GP1BB , GP6 , GP9 , ITG2A , ITG2B , ITGA2B , ITGB3 , MPL , ORAI1 , P2RY12 , TBXA2R , THBD , TRPM7
C11 Mitochondrial proteins (5/814)	AGK , CYCS , DGUOK , DHFR , GPX4
C12 Other metabolism (5/877)	ADA , ADA2 , DGKE , GALE , KDSR
C13 Other nuclear proteins (3/1469)	ACD , CTC1 , CDRE1C
C15 Protein kinases & phosphatases (6/481)	MASTL , MPIG6B , NBEA , PTPN11 , PTPRJ , SRC
C16 Protein processing (7/308)	ACP5 , ALG8 , CHST14 , GGCX , GNE , HLC5 , VKORC1
C17 Secretory proteins (19/811)	A2M , ADAMTS13 , C2 , C3 , CFH , ELANE , F13A1 , F5 , F8 , FCGR2B , KLKB1 , PLAT , PLAU , PLG , PROC , PROS1 , SERPINE1 , SERPINF2 , VWF
C18 Signaling & adapter proteins (11/1024)	CALR , DIAPH1 , FYB , GDF2 , GNAS , PLA2G4A , PTGS1 , SH2B3 , SMAD4 , STIM1 , TBXAS1
C19 Small GTPases & regulators (3/483)	CDC42 , RASGRP2 , WAS
C20 Transcription & translation (13/2280)	DKC1 , DNAJC21 , ETV6 , FLI1 , FOXP3 , GATA1 , GATA2 , GF11B , IKZF5 , MECOM , RBM8A , RUNX1 , SLFN14
Absent in transcriptome (C17)	F13B , F2 , FGA , FGB , FGG , HABP2 , HRG , SERPINC1 , SERPIND1
Absent in transcriptome and proteome	ABCG5 , ABCG8 , EPHB2 , HOXA11 , PRKACG

Discussion

In this paper, we integrated in a functional way the human platelet proteome, using data from six cohorts established in the same institute, with the recently composed genome-wide, >57k platelet and megakaryocyte transcriptomes from the Blueprint consortium³⁰. By UniProt-aided categorization of all relevant transcripts (set at log2fpkm ≥0.20) into 21 protein function classes, we were able to generate a first full proteomic map of the sub-cellular, metabolic and signaling molecules in an average human platelet. Importantly, this analysis also provides a reference list of 37.2k transcripts according to our lists are not or hardly expressed in platelets.

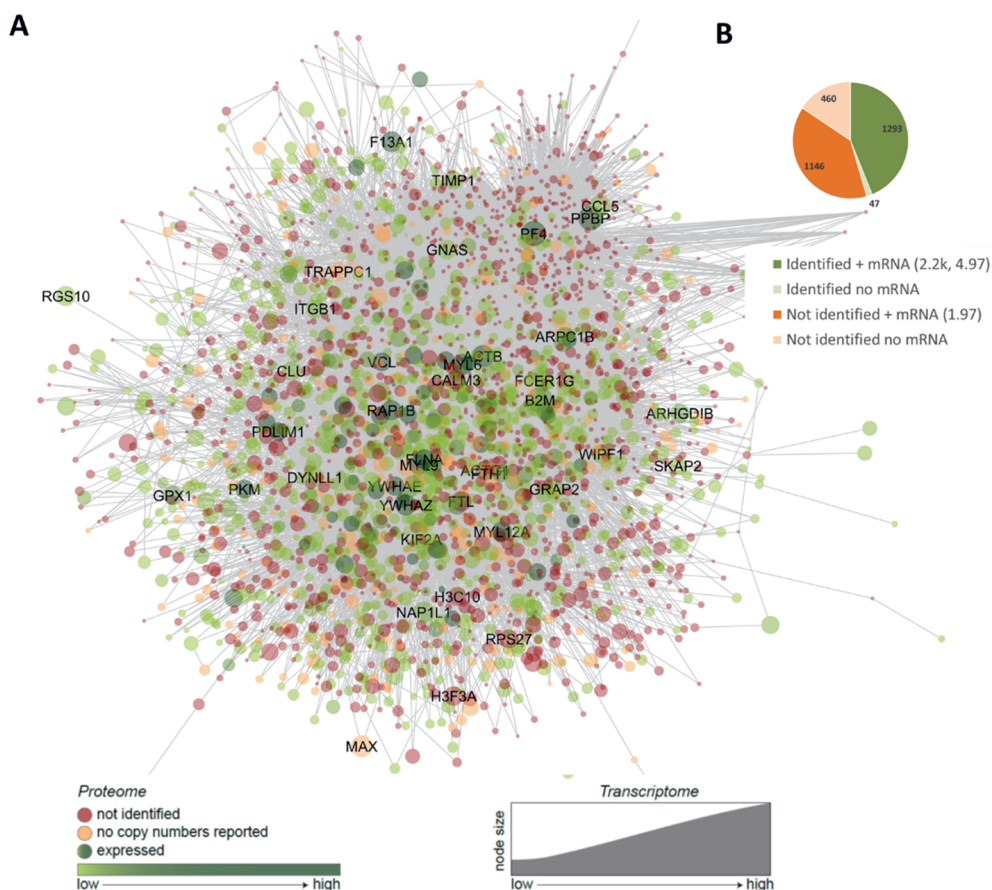


Figure 8. Network-based potential roles of (non)identified proteins in platelet proteome in arterial thrombosis and hemostasis. Using a published meta-analysis of mouse genes in thrombosis and bleeding, the network was built in Cytoscape, containing 267 core genes (bait nodes), 2,679 new nodes, connected by 19.7k interactions¹⁵. **A**, Redrawn network visualization with color-coded proteins identified (green) or not identified (red) in the platelet proteome, with relevant transcript levels (node size, log2fpm). Names are listed of 40 proteins with highest mRNA expression levels. **B**, Distribution profile of (non)identified proteins with transcript levels (median copy numbers, median log2fpm). No mRNA = below relevant threshold. Attribute lists are given in Suppl. Datafile 4.

Overall, the manuscript covers six major novel aspects: (i) for the first time we established the full or theoretical platelet proteome based on a state-of-the-art genome-wide platelet and megakaryocyte transcriptome; (ii) using >57k transcripts we identified an unexpected high similarity of the quantitative platelet and megakaryocyte transcriptomes (including RNA gene transcripts), in spite of a weak correlation between the protein and transcript levels, providing insight into the distribution of RNA species upon platelet shedding; (iii) based on the systematic protein classification, the collected data provide molecular understanding of the complexity of platelet structures and functions; (iv) based on the established theoretical proteome, we developed and also validated a prediction model for identifying missing proteins in the current proteome sample sets; (v) the combined datasets offer better understanding of protein adhesion and uptake of plasma proteins by platelets; (vi) the combination of quantitative transcriptomes and (partly) quantitative proteomes completes our knowledge of the roles of >100 genes and proteins in diseases not limited to thrombosis and hemostasis.

Correlational analysis of the 20k expressed transcripts in platelets and/or megakaryocytes indicated an overall high similarity between the transcriptomes of the two cell types. This particularly held for the 14.8k transcripts of protein-coding genes ($R=0.75$), while the correlation was lower for the 3.8k RNA genes and 1.9k pseudogenes ($R=0.43-0.54$). Although inter-individual differences are expected, our findings indicate that the majority of mRNA species evenly spread from megakaryocytes to the formed proplatelets, with limited degradation during platelet ageing. The aberrant transcript profiles of pseudogenes and RNA genes, which in general were more abundant in megakaryocytes, may be due to retention or to enhanced degradation of such shorter RNA forms³⁶. In agreement with our findings, also other authors presenting smaller-size and not genome-wide datasets (3.5k proteins and 5.5k mRNAs), have reported a low correlation between platelet protein and transcript levels^{37,38}. This lack of correlation however

does exclude a role of altered mRNA and protein levels in platelet-related diseases²¹.

Based on the composition of the genome-wide transcriptomes of platelets and megakaryocytes, we calculated that the current proteome of 5,050 expressed proteins misses approximately 66% of the expected translation products. Highest percentages of missing proteins were seen in the classes C₂₀ (transcription & translation 79%), C₂₁ (uncharacterized proteins 79%), C₁₃ (other nuclear proteins 86%), C₁₀ (membrane receptors & channels 78%), C₁₇ (secretory proteins 72%), and C₁₈ (signaling & adapter proteins 55%). Especially low-level mRNAs (log2fpkm 0.20-1.00) appeared to be missing in the identified proteome, likely giving rise to only low copy numbers of proteins.

Proteomic technologies have been well developed, since the publication of the first draft human proteome, which revealed 17.3k gene products and 4.1k protein N-termini³⁹. Accordingly, the present set of 5.0k identified platelet proteins is higher than earlier published proteomes, *e.g.* of mouse platelets of 4.4k proteins with copy numbers⁴⁰, or of the semi-quantitative 3.5-4.8k proteins in human platelets^{38,41}. Smaller size published platelet sub-proteomes are a 0.1k secretome⁴², and a 1.0k sheddome⁴³. Regarding platelet transcriptomes, which are more uniformly to construct, other authors have published a similar 20k size with 16k transcripts at >0.3 fpkm⁴⁴.

As a check of the present concept - starting from genome-wide platelet and megakaryocyte transcriptomes to determine the theoretical proteome - we evaluated the proteomes reported in three papers, using the current GeneCards gene designations. The proteomes of platelets from Dengue patients⁴⁵ or from platelet concentrates⁴⁶ were found to contain 93.1% (1,769/1,901) and 98.4% (2,466/2,505) proteins that were present in our protein database. Proteins without relevant transcripts were quite low, 2.1% and 0.1%, respectively. A paper analyzing the proteomes from cord blood and adult peripheral blood platelets⁴⁷ showed lower overlap of 79.9% (3,950/4,941) with the current proteome, supplemented with 16.4%

proteins with relevant transcripts and 3.7% (183/4,941) without relevant transcripts in dataset. For the last fraction, it is unclear if residual presence of neonatal transcripts contributes to this higher percentage.

In platelet proteomics, the detection of proteins from blood plasma or other blood cells is a continuous point of attention. Our analysis based on highly purified, washed platelet preparations indicated the invariable present presence of plasma proteins. This can be explained by the fact that platelets exhibit an extensive open canicular system (estimated at 1 vol%) in open contact with the plasma, and furthermore also endocytose plasma proteins. The list includes 73 proteins classified as C₁₇ (secretory proteins) without corresponding mRNAs, of which at least fibrinogen and β 2-glycoprotein 1 are known to be taken up by platelets⁴⁸. Of note, fibrinogen levels are greatly reduced in the proteome of patients with Glanzmann's thrombasthenia, lacking integrin α IIb β 3. At the other hand, we find that multiple 'plasma proteins' can also be expressed by platelets themselves. Hence, even with the development of quality checks of 'plasma contamination', it may be difficult to rate many secretory proteins as platelet or non-platelet.

Apart from the inevitable presence of plasma proteins in platelet preparations, also other conditions may influence the obtained platelet protein composition. One relevant condition is that of macrothrombocytopenia (*e.g.*, Bernard-Soulier syndrome), often resulting in more fragile platelets, where obtaining of the high quality platelet preparation is a challenge. Another factor is emperipoiesis, such as engulfment of hematopoietic cells by megakaryocytes in malign disorders, also affecting the platelet proteome.

To explain the missing of proteins in the identified proteome, we considered three restraining factors: (i) low protein copy number, (ii) low mRNA level, and (iii) protein retainment in the megakaryocyte perinuclear region. By estimating these restraining factors per protein function class, we calculated the technically achievable proteome of ~10k proteins. The assumption is

that improved technical developments will generate larger size proteomes (Suppl. Methods).

For validation of the function class-based prediction model of the remaining part of the proteome, we generated an additional proteomic set, which revealed 1.0k new proteins in the predicted classes, of which 97% with relevant transcript levels. Interestingly, nuclear-related proteins were more frequently present than was predicted, thus pointing to a more prominent incorporation of (peri)nuclear proteins in megakaryocyte-shed platelets than was anticipated.

The function class-based analysis of (non)identified platelet proteome, based on relevant transcript levels ($\log_2\text{fpkm} \geq 0.20$) as well as the listing of 37.2k genome-wide not expressed transcripts provides novel and detailed information on the presence of protein isoforms, subunits of complexes and metabolic, protein processing and signaling pathways (see Table 3). For instance, regarding the apoptosis-related Bcl/Bax proteins (C_{18}) involved in platelet clearance⁴⁹, the isoforms BNIP2, BCL2L1 (BCL-XL or BIM), BAD and BAK1 are present in the current proteome, while also the transcripts of BLC7B, BCL9 and BCL2 are highly expressed. As another example, regarding the glycosyl transferases (C_{16}) and epimerases (C_{12}) implicated in the surface glycosylation pattern and thereby in platelet survival time⁵⁰, prominently present in the proteome (transcriptome) are GALM, GALE, GNE, C1GALT1 and B4GALT1/3/4/5/6, while C1GALT1C1 (COSMC) is only lowly transcribed.

In this Covid-19 era, our list also provides information on ACE2, BSG and TMPRSS2. In platelets and megakaryocytes, ACE2 expression levels appear to be very low ($\log_2\text{fpkm}$ 0.00-0.03), similar to the levels in other blood cells (<https://blueprint.haem.cam.ac.uk/bloodatlas>). On the other hand, BSG (basigin) with high transcript levels is present in the platelet proteome, but not the marginally expressed TMPRSS2.

Both network analysis and OMIM-based evaluation of the genes/proteins known to contribute to platelet count, hemostasis and thrombosis showed

high coverage by the current platelet proteome and transcriptome dataset. Since still little is known of many of the proteins, the list of 20k transcripts reveals a wealth of novel information on proteins that will influence platelet structure and function. Knowledge for understanding disease processes is still limited, as prior work from our and other labs describe only small-size alteration in platelet (phospho)proteomes of patients with Scott (*ANO6*)²⁷ or Glanzmann (*ITGA2B*)⁴⁸ disorders or with pseudohypoparathyroidism (*GNAS*)²⁸. Altogether, this underscores that our approach to define a complete platelet proteome provides a valuable scaffold for further exploring and understanding platelet traits in and beyond thrombosis and hemostasis.

The current approach to define a classified full or theoretical platelet proteome from transcriptomes of platelets and megakaryocytes offers new insights into platelet composition and function, but also has limitations. As discussed above, platelets and megakaryocytes can bind and incorporate proteins from plasma, extracellular matrix or other cells, where the corresponding transcripts can be missing. In case of low transcript levels, copy numbers of proteins in platelets can be too low to be detected by mass spectrometric techniques (for detailed discussion on technical limitations, see supplementary methods). Furthermore, the source (individual healthy, diseased subject) and purification method of platelets and megakaryocytes can influence the specific composition of proteome and transcriptome, especially regarding the more rare molecules. It is noted here, that a subset of proteins expressed at very low copy numbers may be relevant for platelet ontogenesis, but have limited impact on platelet functions.

Earlier analyses indicated that the platelet proteome from healthy subjects is quite stable with <15% of changes⁵¹. Similarly, the global platelet proteomes from the few patients, extensively studied so far - such as Albright hereditary osteodystrophy, Glanzmann or Scott syndrome patients - showed only minor changes compared to that of control subjects^{27,28,48}. The technical abilities to study this in the future is made in the revised discussion

(page 16). In the near future, with the use of robotics techniques allowing higher throughput analysis of large sample sets and with the application of stable isotope markers¹⁷, we expect to know more on the variable part of the platelet proteome in health and disease.

Supplementary materials

Supplementary files: <https://doi.org/10.1038/s41598-021-91661-x>

Datafile 1 Genome-wide transcriptome and identified proteome of PLT and MGK.

Datafile 2. Identified proteins in cohorts 1-6.

Datafile 3. Validation proteome and newly identified proteins.

Datafile 4. Nodes of protein interaction network of T&H.

Acknowledgments

JH, IP and IDS are supported by the European Union's Horizon 2020 research and innovation program under the Marie Skłodowska-Curie grant agreement TAPAS No. 766118. JH is enrolled in a joint PhD program of the Universities of Maastricht and Santiago de Compostela (Spain); IP and IDS are enrolled in a joint PhD program of the Universities of Maastricht and Reading (UK). MF is supported by the British Heart Foundation (FS/18/53/22863). Research support by the Ministerium für Innovation, Wissenschaft und Forschung from Nordrhein-Westfalen, the Cardiovascular Centre (HVC) of Maastricht University Medical Centre+, the Centre for Molecular Translational Medicine (INCOAG, MICRO-BAT), the German Federal Ministry of Education and Research (BMBF 01EO1503) and the Deutsche Forschungsgemeinschaft (ZA 639/4-1 and JU 2735/2-1).

Competing interests

The authors declare to have no competing interests.

References

1. Versteeg HH, Heemskerk JW, Levi M and Reitsma PS. New fundamentals in hemostasis. *Physiol Rev.* 2013;93:327-358.
2. Van der Meijden PE and Heemskerk JW. Platelet biology and functions: new concepts and clinical perspectives. *Nat Rev Cardiol.* 2018;16:166-179.
3. Werner G and Morgenstern E. Three-dimensional reconstruction of human blood platelets using serial sections. *Eur J Cell Biol.* 1980;20:276-282.
4. Van Nispen tot pannerden H, de Haas F, Geerts W, Posthuma G, Van Dijk S and Heijnen HF. The platelet interior revisited: electron tomography reveals tubular alpha-granule subtypes. *Blood.* 2010;116:1147-1156.
5. Thon JN and Italiano JE. Platelets: production, morphology and ultrastructure. *Handbook Exp Pharmacol.* 2012;210:3-22.
6. Pertuy F, Eckly A, Weber J, Proamer F, Rinckel JY, Lanza F et al. Myosin IIA is critical for organelle distribution and F-actin organization in megakaryocytes and platelets. *Blood.* 2014;123:1261-1269.
7. Poulter NS and Thomas SG. Cytoskeletal regulation of platelet formation: Coordination of F-actin and microtubules. *Int J Biochem Cell Biol.* 2015;66:69-74.
8. Bender M, Giannini S, Grozovsky R, Jönsson T, Christensen H, Pluthero FG et al. Dynamin 2-dependent endocytosis is required for normal megakaryocyte development in mice. *Blood.* 2015;125:1014-1024.
9. Becker IC, Scheller I, Wackerbarth LM, Beck S, Heib T, Aurbach K et al. Actin/microtubule crosstalk during platelet biogenesis in mice is critically regulated by twinfilin1 and cofilin1. *Blood Adv.* 2020;26:2124-2134.
10. Akkerman JW. Regulation of carbohydrate metabolism in platelets: a review. *Thromb Haemost.* 1978;39:712-722.
11. Kramer PA, Ravi S, Chacko B, Johnson MS and Darley-Usmar VM. A review of the mitochondrial and glycolytic metabolism in human platelets and leukocytes: implications for their use as bioenergetic biomarkers. *Redox Biol.* 2014;2:206-210.
12. Nayak MK, Kulkarni PP and Dash D. Regulatory role of proteasome in determination of platelet life span. *J Biol Chem.* 2013;288:6826-6834.

13. Colberg L, Cammann C, Greinacher A and Seifert U. Structure and function of the ubiquitin-proteasome system in platelets. *J Thromb Haemost.* 2020;18:771-778.
14. Boyanova D, Nilla S, Birschmann I, Dandekar T and Dittrich M. PlateletWeb: a systems biologic analysis of signaling networks in human platelets. *Blood.* 2012;119:e22-34.
15. Baaten CC, Meacham S, de Witt SM, Feijge MA, Adams DJ, Akkerman JW et al. A synthesis approach of mouse studies to identify genes and proteins in arterial thrombosis and bleeding. *Blood.* 2018;132:e35-e46.
16. Burkhart JM, Gambaryan S, Watson SP, Jurk K, Walter U, Sickmann A et al. What can proteomics tell us about platelets? *Circ Res.* 2014;114:1204-1219.
17. Loosse C, Swieringa F, Heemskerk JW, Sickmann A and Lorenz C. Platelet proteomics: from discovery to diagnosis. *Exp Rev Proteomics.* 2018;15:467-476.
18. Van der Meijden PE and Heemskerk JW. Platelet protein shake as playmaker. *Blood.* 2012;120:2931-2942.
19. Chen L, Kostadima M, Martens JH, Canu G, Garcia SP, Turro E et al. Transcriptional diversity during lineage commitment of human blood progenitors. *Science.* 2014;345:6204.
20. Wright JR, Amisten S, Goodall AH and Mahaut-Smith MP. Transcriptomic analysis of the ion channelome of human platelets and megakaryocytic cell lines. *Thromb Haemost.* 2016;116:272-284.
21. Davizon-Castillo P, Rowley JW and Rondina MT. Megakaryocyte and platelet transcriptomics for discoveries in human health and disease. *Arterioscler Thromb Vasc Biol.* 2020;40:1432-1440.
22. Astle WJ, Elding H, Jiang T, Allen D, Ruklisa D, Mann AL et al. The allelic landscape of human blood cell trait variation and links to common complex disease. *Cell.* 2016;167:1415-1429.
23. Petersen R, Lambourne JJ, Javierre BM, Grassi L, Kreuzhuber R, Ruklisa D et al. Platelet function is modified by common sequence variation in megakaryocyte super enhancer. *Nat Commun.* 2017;8:16058.
24. Burkhart JM, Schumbrutzki C, Wortelkamp S, Sickmann A and Zahedi RP. Systematic and quantitative comparison of digest efficiency and specificity reveals the impact of trypsin quality on MS-based proteomics. *J Proteomics.* 2012;75:1454-1462.

25. Beck F, Geiger J, Gambaryan S, Veit J, Vaudel M, Nollau P et al. Time-resolved characterization of cAMP/PKA-dependent signaling reveals that platelet inhibition is a concerted process involving multiple signaling pathways. *Blood*. 2014;123:e1-e10.
26. Beck F, Geiger J, Gambaryan S, Solari FA, Dell'Aica M, Lorocho S et al. Temporal quantitative phosphoproteomics of ADP stimulation reveals novel central nodes in platelet activation and inhibition. *Blood*. 2017;129:e1-e12.
27. Solari FA, Mattheij NJ, Burkhart JM, Swieringa F, Collins PW, Cosemans JM et al. Combined quantification of the global proteome, phosphoproteome, and proteolytic cleavage to characterize altered platelet functions in the human Scott syndrome. *Mol Cell Proteomics*. 2016;15:3154-3169.
28. Swieringa F, Solari FA, Pagel O, Beck F, Huang J, Feijge MAH et al. Impaired iloprost-induced platelet inhibition and phosphoproteome changes in patients with confirmed pseudohypoparathyroidism type Ia, linked to genetic mutations in GNAS. *Sci Rep*. 2020;10:11389.
29. Lewandrowski U, Wortelkamp S, Lohrig K, Zahedi RP, Wolters DA, Walter U et al. Platelet membrane proteomics: a novel repository for functional research. *Blood*. 2009;114:e10-e19.
30. Stunnenberg HG, The International Human Epigenome Consortium and Hirst M. The International Human Epigenome Consortium: a Blueprint for scientific collaboration and discovery. *Cell*. 2016;167:1145-1149.
31. Grassi L, Izuogu OG, Jorge NA, Seyres D, Bustamante M, Burden F et al. Cell type specific novel lncRNAs and circRNAs in the Blueprint haematopoietic transcriptomes atlas. *Haematologica*. 2021; 106: 2613-2623
32. Geiger J, Burkhart JM, Gambaryan S, Walter U, Sickmann A and Zahedi RP. Response: platelet transcriptome and proteome: relation rather than correlation. *Blood*. 2013;121:5257-5258.
33. Rowley JW and Weyrich AS. Coordinate expression of transcripts and proteins in platelets. *Blood*. 2013;121:5255-5256.
34. Online Mendelian Inheritance in Man (OMIM): an online catalog of human genes and genetic disorders. <https://omim.org>. 2020.
35. Palma-Barqueros V, Revilla N, Sánchez A, Zamora Cánovas A, Rodríguez-Alén A, Marín-Quílez A et al. Inherited platelet disorders: an updated overview. *Int J Mol Sci*. 2021;22:4521.

36. Schubert S, Weyrich AS and Rowley JW. A tour through the transcriptional landscape of platelets. *Blood*. 2014;124:493-502.
37. Frobel J, Cadeddu RP, Hartwig S, Bruns I, Wilk CM, Kundgen A et al. Platelet proteome analysis reveals integrin-dependent aggregation defects in patients with myelodysplastic syndromes. *Mol Cell Proteomics*. 2013;12:1272-1280.
38. Londin ER, Hatzimichael E, Loher P, Edelstein L, Shaw C, Delgrosso K et al. The human platelet: strong transcriptome correlations among individuals associate weakly with the platelet proteome. *Biol Direct*. 2014;9:3.
39. Kim MS, Pinto SM, Getnet D, Nirujogi RS, Manda SS, Chaerkady R et al. A draft map of the human proteome. *Nature*. 2014;509:575-581.
40. Zeiler M, Moser M and Mann M. Copy number analysis of the murine platelet proteome spanning the complete abundance range. *Mol Cell Proteomics*. 2014;13:3435-3445.
41. Sabrkhanly S, Kuijpers MJ, Knol JC, Olde Damink SW, Dingemans AC, Verheul HM. Exploration of the platelet proteome in patients with early-stage cancer. *J Proteomics*. 2018;177:65-74.
42. Van Holten TC, Bleijerveld OB, Wijten P, de Groot PG, Heck AJ, Barendrecht AD. Quantitative proteomics analysis reveals similar release profiles following specific PAR-1 or PAR-4 stimulation of platelets. *Cardiovasc Res*. 2014;103:140-146.
43. Fong KP, Barry C, Tran AN, Traxler EA, Wannemacher KM, Tang HY et al. Deciphering the human platelet sheddome. *Blood*. 2011;117:e15-e26.
44. Middleton E, Rowley JW, Campbell RA, Grissom CK, Brown SM, Beesley SJ et al. Sepsis alters the transcriptional and translational landscape of human and murine platelets. *Blood*. 2019;134:911-923.
45. Trugilho MR, Hottz ED, Brunoro GV, Teixeira-Ferreira A, Carvalho PC, Salazar GA et al. Platelet proteome reveals novel pathways of platelet activation and platelet-mediated immunoregulation in dengue. *Plos Pathog*. 2017;13:e1006385.
46. Salunkhe V, De Cuyper IM, Papadopoulos P, Van der Meer PF, Daal BB, Villa-Fajardo M et al. A comprehensive proteomics study on platelet concentrates: Platelet proteome, storage time and Mirasol pathogen reduction technology. *Platelets*. 2019;30:368-379.
47. Stokhuijzen E, Koornneef JM, Nota B, Van den Eshof BL, Van Alphen FP, Van den Biggelaar M et al. Differences between platelets derived from neonatal

- cord blood and adult peripheral blood assessed by mass spectrometry. *J Proteome Res.* 2017;16:3567-3575.
48. Loroach S, Trabold K, Gambaryan S, Reiss C, Schwierczek K, Fleming I et al. Alterations of the platelet proteome in type I Glanzmann thrombasthenia caused by different homozygous delG frameshift mutations in ITGA2B. *Thromb Haemost.* 2017;117:556-569.
 49. Quach ME, Chen W and Li R. Mechanisms of platelet clearance and translation to improve platelet storage. *Blood.* 2018;131:1512-1521.
 50. Lee-Sundlov MM, Stowell SR and Hoffmeister KM. Multifaceted role of glycosylation in transfusion medicine, platelets, and red blood cells. *J Thromb Haemost.* 2020;18:1535-1547.
 51. Burkhart JM, Vaudel M, Gambaryan S, Radau S, Walter U, Martens L et al. The first comprehensive and quantitative analysis of human platelet protein composition allows the comparative analysis of structural and functional pathways. *Blood.* 2012;120:e73-82.
 52. Colaert N, Gevaert K and Martens L. RIBAR and xRIBAR: methods for reproducible relative MS/MS-based label-free protein quantification. *J Proteome Res.* 2011;10:3183-3189.
 53. Stelzer G, Rosen N, Plaschkes I, Zimmerman S, Twik M, Fishilevich S et al. The GeneCards suite: from gene data mining to disease genome sequence analyses www.genecards.org. *Curr Protoc Bioinformatics.* 2016;54:1.30.1-33.
 54. Dogan T, MacDougall A, Saidi R, Poggioli D, Bateman A, O'Donovan C et al. UniProt-DAAC: domain architecture alignment and classification, a new method for automatic functional annotation in UniProtKB. *Bioinformatics.* 2016;32:2264-2271.
 55. Jassal B, Matthews L, Viteri G, Gong C, Lorente P, Fabregat A et al. The reactome pathway knowledgebase. *Nucleic Acids Res.* 2020;48:D498-D503.
 56. Perez-Riverol Y, Csordas A, Bai J, Bernal-Llinares M, Hewapathirana S, J. KD et al. The PRIDE database and related tools and resources in 2019: improving support for quantification data. *Nucleic Acids Res.* 2019;47:D442-D450.

Supplementary materials of Chapter 3

Methods

Novel combined proteome analysis for validation

Well-purified platelet samples were obtained from 30 healthy subjects, and digested with trypsin using filter aided sample preparation, as described in the methods section. After digestion, 2 µg of peptide mixture from each sample were pooled. The pooled sample was desalted using a SpecVarian C₁₈ cartridge, according to manufacturer instructions (Agilent, Santa Clara, California). 50 µg of the pooled sample was fractionated by high pH-reversed phase chromatography (C₁₈ column; BioBasic-18, 0.5 mm ID x 15 cm, 5 µm particle size, 300 Å pore size, (Thermo Scientific) using a linear gradient ranging from 5-38% of solvent B (mobile phase A: 10 mM ammonium formate, pH 8.0, B: 10 mM ammonium formate 84% acetonitrile, pH 8.0) for 90 minutes. Thirty fractions were collected every minute in a concatenated mode and dried under vacuum. Each fraction was analyzed on a Q Exactive HF mass spectrometer on line coupled to a U3000 RSLCnano (both from Thermo Scientific). Separate peptides fractions were loaded onto a trap column (Acclaim PepMap100 C₁₈ trap column; 100 µm x 2 cm) with 0.1% trifluoroacetic acid at a flow rate of 20 µL/minute, followed by separation of peptides on the main column (PepMap100 C18; 75 µm x 50 cm), using a non-linear gradient ranging from 7-24-38% of solvent B (84% acetonitrile, 0.1% formic acid) for 150 minutes. On the Q Exactive HF, a 90 minutes acquisition time was used, where survey scans were acquired at resolution of 30,000 using an automatic gain control (AGC) target value of 3×10^6 . MS/MS spectra of the top 15 most intense ions were acquired with a resolution of 15,000 an isolation width of 1.2 m/z , a normalized collision energy of 27%, an AGC target value of 5×10^4 ions, a maximum injection time of 200 ms. Raw data were searched in Proteome Discoverer (Thermo Scientific) using Uniprot-KD (Human Uniprot 23/07/2018), with trypsin as an enzyme, carbamidomethylation as fixed modification, and oxidation of methionine as variable

modification. For MS spectra, the mass tolerance was set to 10 ppm, and for MS/MS spectra, the mass tolerance was set to 0.02 Da. Obtained in the validation cohort were 5,505 unique proteins, which were separated into previously identified and newly identified, and were compared per corresponding gene with transcriptome data (Suppl. Datafile 2).

Technical limitations for obtaining the full platelet proteome

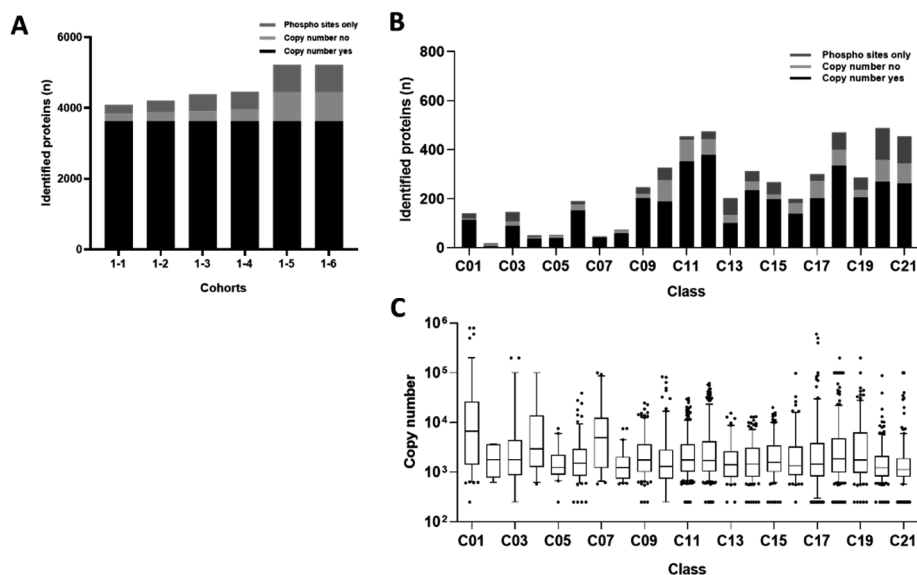
Integral membrane proteins (C₁₀ and vesicular protein classes) with low relative abundance and high hydrophobicity are usually under-represented^{1,2}. Use of specific enrichment steps can help here³. Second, while trypsin is the common choice as a digesting enzyme (cleaving at lysine and arginine residues), it is less efficient for domains rich in negatively charged amino acids⁴. This can be overcome by the use of other proteases or by changing digestion conditions. Third, loss of peptides is unavoidable in digested samples during sample preparation (FASP, precipitation, enrichment, desalting, elution)⁵, and by the choice of protein denaturation agent. Fourth, data-dependent acquisition (DDA) is the most common procedure to obtain mass spectrometric data, however due to the TopN method used in DDA experiments, some precursors could be under-represented due to the defined threshold. Alternatively, in the data-independent acquisition (DIA) all precursors detected within a defined mass window are selected for MS/MS fragmentation and acquisition. This window is stepped across the entire mass range to collect MS/MS data from all detected precursors⁶. Furthermore, partial post-translational modifications (N-terminal acetylation, serine/threonine phosphorylation) can complicate the data analysis^{7,8}. Concerning mass spectra analysis, current algorithms search for peptide-spectrum matches with 1% false discovery rate, estimated by a target-decoy search strategy⁹⁻¹¹, but this threshold may be less reliable for large data sets^{12,13}. From our own data, we calculated that (with the exception of classes C₀₂, C₁₇, C₂₁).

References

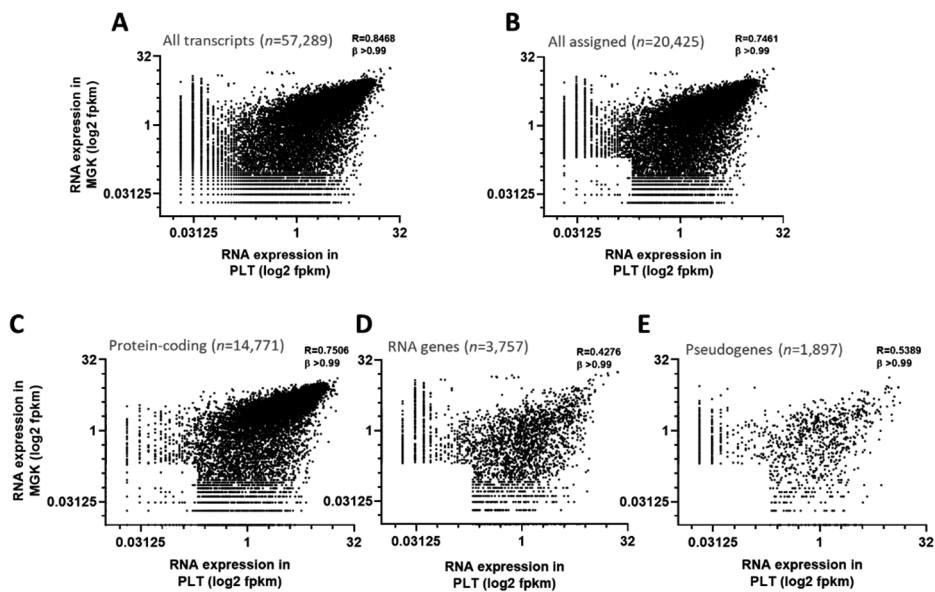
1. Vuckovic D, Dagley LF, Purcell AW and Emili A. Membrane proteomics by high performance liquid chromatography-tandem mass spectrometry: analytical approaches and challenges. *Proteomics*. 2013;13:404-423.
2. Vit O and Petrak J. Integral membrane proteins in proteomics. How to break open the black box? *J Proteomics*. 2017;153:8-20.
3. Lewandrowski U, Wortelkamp S, Lohrig K, Zahedi RP, Wolters DA, Walter U et al. Platelet membrane proteomics: a novel repository for functional research. *Blood*. 2009;114:e10-e19.
4. Giansanti P, Tsiatsiani L, Low TY and Heck AJ. Six alternative proteases for mass spectrometry-based proteomics beyond trypsin. *Nat Protocols*. 2016;11:993-1006.
5. Mendes Maia T, Staes A, Plasma K, Pauwels J, Boucher K, Argentini A et al. Simple peptide quantification approach for MS-based proteomics quality control. *ACS Omega*. 2020;17:6754-6762.
6. Kalli A, Smith GT, Sweredoski MJ and Hess S. Evaluation and optimization of mass spectrometric settings during data-dependent acquisition mode: focus on LTQ-Orbitrap mass analyzers. *J Proteome Res*. 2013;12:3071-3086.
7. Zhang X, Ye J, Engholm-Keller K and Hojrup P. A proteome-scale study on in vivo protein N α -acetylation using an optimized method. *Proteomics*. 2011;11:81-93.
8. Hu A, Noble WS and Wolf-Yadlin A. Technical advances in proteomics: new developments in data-independent acquisition. *F1000 Res*. 2016;4:419.
9. Reiter L, Claassen M, Schrimpf SP, Jovanovic M, Schmidt A, Buhmann JM et al. Protein identification false discovery rates for very large proteomics data sets generated by tandem mass spectrometry. *Mol Cell Proteomics*. 2009;8:2405-2417.
10. Elias JE and Gygi SP. Target-decoy search strategy for increased confidence in large-scale protein identifications by mass spectrometry. *Nat Methods*. 2007;4:207-214.
11. Jeong K, Kim S and Bandeira N. False discovery rates in spectral identification. *BMC Bioinformatics*. 2012;13:Suppl. 16, S2.

12. Savitski MM, Wilhelm M, Hahne H, Kuster B and Bantscheff M. A scalable approach for protein false discovery rate estimation in large proteomic data sets. *Mol Cell Proteomics*. 2015;14:2394-2404.
13. Zhang Y, Xu T, Shan B, Hart J, Aslanian A, Han X et al. ProteinInferencer: confident protein identification and multiple experiment comparison for large scale proteomics projects. *J Proteomics*. 2015;129:25-32.

Supplementary figures and tables of Chapter 3



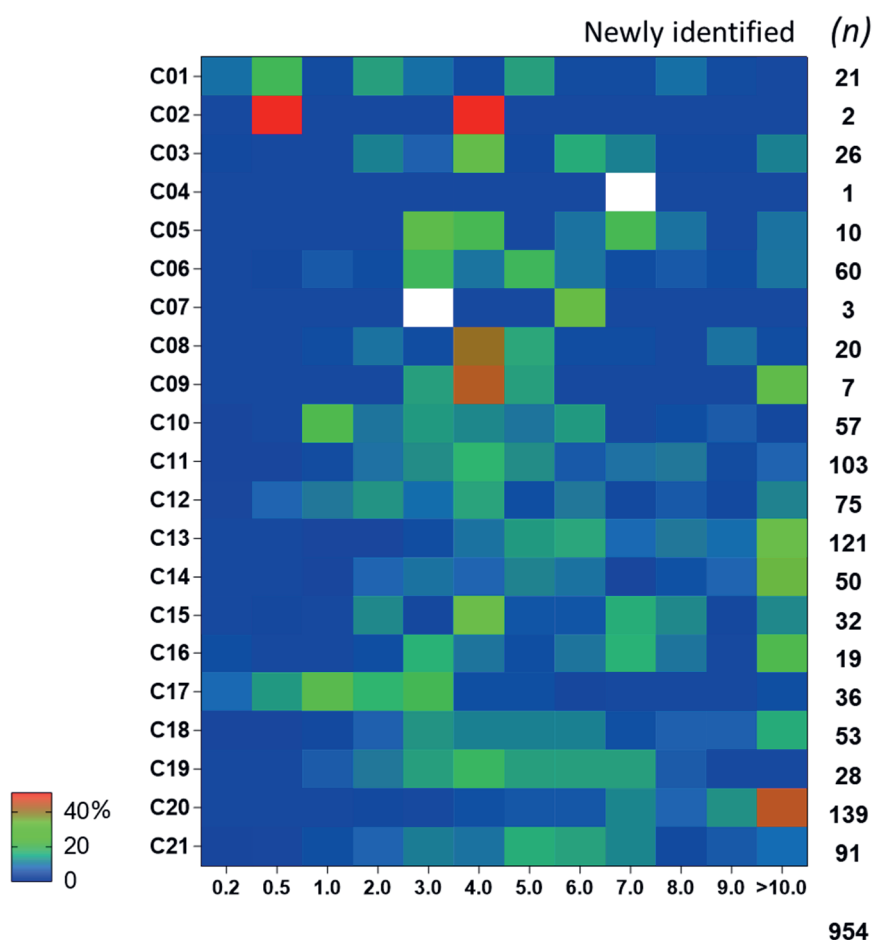
Suppl. Figure 1. Buildup of identified human platelet proteome. **A**, Progressive buildup of platelet proteome, obtained in six cohort studies (numbered 1 to 6) with healthy subjects. Black = 3,629 proteins with copy numbers; light gray = additional protein without copy numbers; dark gray = additional proteins by TiO_2 enrichment of phosphoproteome. **B**, Assignment of 5,211 identified proteins (all 6 cohorts) to 21 function classes (see Figure 1). **C**, Ranges of copy numbers per function class.



Suppl. Figure 2. Correlation of platelet (PLT) and megakaryocyte (MGK) transcriptomes. **A**, Correlation of all transcript levels in PLT vs. MGK genome-wide. **B**, Correlation of relevant transcripts ($\log_2\text{fpkm} \geq 0.20$) in PLT and MGK. **C-E**, Correlation of relevant transcripts separated out between protein-coding genes (**C**), RNA genes (**D**) and pseudogenes (**E**).

A					B					C				
Transcripts with proteins					Transcripts with proteins					Transcripts with proteins				
PLT and/or MGK	total >0.20	yes >0.20	no >0.20	yes <0.20	PLT	total >0.20	yes >0.20	no >0.20	yes <0.20	MGK	total >0.20	yes >0.20	no >0.20	yes <0.20
C01 Cytoskeleton actin-myosin	237	132	105	9	C01	230	132	98	9	C01	186	125	61	16
C02 Cytoskeleton intermediate	27	8	19	11	C02	26	8	18	11	C02	20	6	14	13
C03 Cytoskeleton microtubule	420	140	280	6	C03	416	139	277	7	C03	355	133	222	13
C04 Cytoskeleton receptor-linked	69	51	18	0	C04	69	51	18	0	C04	64	48	16	3
C05 Endosome proteins	101	52	49	0	C05	98	52	46	0	C05	88	52	36	0
C06 ER & Golgi proteins	568	190	378	1	C06	549	190	359	1	C06	478	190	288	1
C07 Glucose metabolism	58	46	12	1	C07	58	46	12	1	C07	52	45	7	2
C08 Lysosome & peroxisome proteins	168	74	94	1	C08	164	74	90	1	C08	152	74	78	1
C09 Membrane & protein trafficking	349	243	106	4	C09	344	242	102	5	C09	313	240	73	7
C10 Membrane receptors & channels	1430	318	1112	9	C10	1344	315	1029	12	C10	914	300	614	27
C11 Mitochondrial proteins	814	454	360	1	C11	805	454	351	1	C11	783	454	329	1
C12 Other metabolism	877	469	408	6	C12	855	467	388	8	C12	781	463	318	12
C13 Other nuclear proteins	1469	200	1269	3	C13	1442	200	1242	3	C13	1378	196	1182	7
C14 Proteasomal proteins	677	311	366	1	C14	665	310	355	2	C14	638	311	327	1
C15 Protein kinases & phosphatases	481	266	215	2	C15	477	266	211	2	C15	432	264	168	4
C16 Protein processing	308	199	109	1	C16	301	197	104	3	C16	289	198	91	2
C17 Secretory proteins	811	228	583	73	C17	756	223	533	78	C17	429	155	274	146
C18 Signaling & adapter proteins	1024	463	561	8	C18	1008	462	546	9	C18	829	446	383	25
C19 Small GTPases & regulators	483	284	199	3	C19	478	284	194	3	C19	432	281	151	6
C20 Transcription & translation	2280	485	1795	3	C20	2230	484	1746	4	C20	2111	482	1629	6
C21 Uncharacterized & other proteins	2120	437	1683	18	C21	1982	434	1548	21	C21	1772	419	1353	36
Protein coding	14771	5050	9721	161		14297	5030	9267	181		12496	4882	7614	329
RNA genes	3757	0	3757	0		2480	0	2480	0		2783	0	2783	0
Pseudogenes	1897	0	1897	0		852	0	852	0		1564	0	1564	0
Total transcripts	20425	5050	15375	161		17629	5030	12599	181		16843	4882	11961	329

Suppl. Figure 3. See upper page. Comparison of relevant transcripts with or without identified platelet proteins. A, C, Listing per function class of numbers of relevant transcripts ($\log_2\text{fpkm} \geq 0.20$) that were yes/no identified in the platelet proteome. Transcriptomes were combined from platelets (PLT) and megakaryocytes (MGK), or used from PLT or MGK only. Indicated in gray are proteins without relevant mRNA expression ($\log_2\text{fpkm} < 0.20$). Transcripts were summed as protein coding, RNA genes and pseudogenes. Data are shown for: **A, Combined PLT/MGK transcriptome; **B**, PLT transcriptome; **C**, MGK transcriptome.**



Suppl. Figure 4. Distribution profile of transcripts of newly identified proteins per protein function class. Heatmap of percentual distribution of transcript levels per function class (rainbow colors; blue = low, red = high) for 954 newly identified proteins in validation cohort. Numbers per class are indicated in right column.

Suppl. Table 1. See next page. Clustering of proteins per class in quantitative proteome-transcriptome space. P-values are given, representing significance of over-representation of protein in defined areas I-V of proteome-transcriptome matrix, based on transcript levels in platelets (PLT) or megakaryocytes (MGK). For visualization of areas I-V, see Figure 4C, D. Modelling was as described in the methods section. Statistical significance increasing with red coloring.

Protein function class	High transl. high transl.			High transl. low transl.			Low transl. low transl.			Mid transl. mid transl.			Unrelevant transl.			Protein count		
	Area I			Area II			Area III			Area IV			Area V			Area I-V		
	PLT	MGK		PLT	MGK		PLT	MGK		PLT	MGK		PLT	MGK		PLT	MGK	Total
01 Cytoskeleton actin-myosin	1.31E-09	1.10E-10		9.92E-01	9.99E-01	6.32E-01	8.82E-02	9.92E-01	9.74E-01	1.71E-03	4.22E-04		1.71E-03	4.22E-04		66	66	114
02 Cytoskeleton intermediate	1.00E+00	1.00E+00		8.15E-01	1.00E+00	1.00E+00	9.98E-02	1.00E+00	9.13E-01	3.99E-03	2.76E-04		3.99E-03	2.76E-04		4	6	7
03 Cytoskeleton microtubule	5.27E-04	3.00E-03		5.93E-01	4.17E-01	6.76E-01	7.49E-01	5.69E-01	5.24E-01	9.06E-02	1.27E-01		9.06E-02	1.27E-01		60	56	91
04 Cytoskeleton receptor-linked	2.90E-03	2.90E-03		7.36E-01	9.97E-01	7.70E-01	4.36E-01	6.67E-01	8.33E-01	8.65E-01	8.86E-01		8.65E-01	8.86E-01		22	16	38
05 Endosome proteins	1.00E+00	1.00E+00		1.30E-01	1.99E-01	7.88E-01	1.00E+00	7.30E-01	7.85E-01	8.78E-01	1.00E+00		8.78E-01	1.00E+00		23	18	40
06 ER & Golgi proteins	1.00E+00	1.00E+00		1.17E-01	3.41E-02	3.51E-01	6.69E-01	6.00E-01	7.24E-01	1.00E+00	1.00E+00		1.00E+00	1.00E+00		85	74	152
07 Glucose metabolism	4.57E-03	4.57E-03		9.69E-01	9.56E-01	7.73E-02	1.00E+00	2.93E-01	1.01E-01	6.53E-01	9.14E-01		6.53E-01	9.14E-01		28	25	43
08 Lysosome & peroxisome proteins	1.00E+00	1.00E+00		1.98E-01	6.34E-01	3.97E-01	1.00E+00	9.65E-01	9.34E-01	9.58E-01	9.68E-01		9.58E-01	9.68E-01		30	22	60
09 Membrane & protein trafficking	1.00E+00	1.00E+00		4.10E-01	8.06E-01	9.85E-01	8.13E-01	3.27E-03	9.77E-03	9.81E-01	9.99E-01		9.81E-01	9.99E-01		122	105	202
10 Membrane receptors & channels	2.20E-01	2.20E-01		1.03E-01	3.73E-02	9.53E-01	3.55E-01	1.00E+00	9.93E-01	5.88E-01	5.65E-01		5.88E-01	5.65E-01		98	103	202
11 Mitochondrial proteins	1.00E+00	1.00E+00		1.00E+00	1.00E+00	5.49E-04	4.31E-01	1.31E-04	1.24E-04	1.00E+00	1.00E+00		1.00E+00	1.00E+00		187	170	353
12 Other metabolism	7.40E-01	8.71E-01		1.00E+00	9.64E-01	1.19E-01	6.80E-01	2.90E-01	4.05E-02	9.96E-01	1.00E+00		9.96E-01	1.00E+00		203	186	379
13 Other nuclear proteins	1.00E+00	1.00E+00		6.03E-01	4.69E-01	7.43E-01	1.00E+00	6.16E-01	7.64E-01	9.69E-01	9.25E-01		9.69E-01	9.25E-01		51	45	101
14 Proteasomal proteins	1.00E+00	1.00E+00		3.58E-01	1.84E-02	9.82E-01	6.90E-01	6.62E-03	1.32E-02	1.00E+00	1.00E+00		1.00E+00	1.00E+00		136	134	235
15 Protein kinases & phosphatases	1.00E+00	1.00E+00		1.77E-02	4.60E-01	9.83E-01	5.73E-01	1.74E-02	3.55E-03	9.93E-01	9.96E-01		9.93E-01	9.96E-01		126	112	198
16 Protein processing	8.98E-01	8.98E-01		8.16E-01	3.14E-02	7.78E-02	6.20E-01	3.47E-01	7.43E-01	5.71E-01	1.00E+00		5.71E-01	1.00E+00		81	70	139
17 Secretory proteins	8.43E-01	8.43E-01		1.00E+00	1.00E+00	8.38E-03	2.78E-05	1.00E+00	1.00E+00	1.43E-52	2.78E-18		1.43E-52	2.78E-18		141	155	202
18 Signaling & adaptor proteins	8.09E-02	3.67E-02		3.70E-02	8.74E-01	9.90E-01	7.47E-01	2.53E-01	2.79E-03	1.00E+00	2.53E-81		1.00E+00	2.53E-81		196	177	334
19 Small GTPases & regulators	2.34E-01	2.34E-01		7.83E-02	5.65E-01	1.00E+00	1.00E+00	3.97E-01	3.46E-01	9.95E-01	1.00E+00		9.95E-01	1.00E+00		121	102	207
20 Transcription & translation	9.89E-01	9.89E-01		2.78E-08	3.35E-11	9.98E-01	1.00E+00	9.95E-01	9.96E-01	9.99E-01	9.98E-01		9.99E-01	9.98E-01		156	146	268
21 Uncharacterized & other proteins	9.87E-01	9.87E-01		7.64E-02	4.61E-01	8.46E-03	5.52E-01	1.00E+00	1.00E+00	1.75E-01	9.98E-01		1.75E-01	9.98E-01		148	108	261

All classes 2084 1896 3626

Suppl. Table 2. Restraining factors per function class and prediction model of full platelet proteome. Analysis of non-identified proteins (n=9,721) from the relevant, combined PLT/MGK transcriptome per function class. Indicated in **blue** are fractions transcripts present in the identified proteome, and fractions with low mRNA (arbitrarily set at log2fpkm <1.00). Indicated in **green** (ID) are well-identified classes with fractions >0.55 identified. Indicated in **red** is indication of one or more restraining factors per class: (i) over-representation of low copy number (areas II-III in Figure 4D), (ii) low mRNA level (area V, LM = low mRNA >45%); (iii) retainment in megakaryocyte (peri)nucleus upon platelet shedding (RET).

Protein function class (n)	Fraction not identified		Mostly identified	Explanation for low identification		
	(fraction)	(fraction)		Low copy number (II, III)	Low mRNA (>20%, V)	Retained in MGK
UniProt-KB: in protein name (n≥10)			>55%			
C01 Cytoskeleton actin-myosin (237)	0.44	0.30	ID		LM, V	
Actin (36)	0.14	0.40				
Myosin (45)	0.44	0.55				
C02 Cytoskeleton intermediate (27)	0.70	0.42	NID		LM, V	
Keratin (12)	0.58	0.57				
C03 Cytoskeleton microtubule (420)	0.67	0.19	NID			RET
Centromere (16)	0.88	0.21				
Centrosomal (36)	0.75	0.11				
Dynein (41)	0.61	0.40				
Kinesin (38)	0.71	0.37				
Mitotic spindle / HAUS (13)	0.69	0.22				
Tubulin (74)	0.46	0.29				
C04 Cytoskeleton receptor-linked (69)	0.26	0.17	ID			
LIM / Wiskott (10)	0.30	0.33				
C05 Endosome proteins (101)	0.49	0.18	NID	?		
Multivesicular body (11)	0.18	0.00				
WAS / WASH (11)	0.45	0.00				
C06 ER & Golgi proteins (568)	0.67	0.24	NID		LM	
AP-1/3 complex subunit (19)	0.21	0.25				
ER membrane / lumen protein (34)	0.41	0.36				
Golgi (59)	0.47	0.57				
Trafficking protein particle (16)	0.25	0.00				
Transferase (95)	0.96	0.45				
C07 Glucose metabolism (58)	0.21	0.25	ID		LM	
Glucose (18)	0.33	0.17				
Fructose (11)	0.35	0.25				
C08 Lysosome & peroxisome proteins (168)	0.56	0.13	NID		LM	
Lysosome / lysosomal (21)	0.52	0.09				
Peroxisome / peroxisomal (37)	0.54	0.30				
V-type proton ATPase (17)	0.29	0.40				
C09 Membrane & protein trafficking (349)	0.30	0.31	ID		LM	
Exocyst complex (10)	0.10	1.00				
Protein transport (11)	0.09	0.00				
Sorting nexin (27)	0.37	0.40				
Synapto (19)	0.74	0.57				
Syntaxin (20)	0.20	0.00				
Vacuolar protein sorting-associated (26)	-	-				

Suppl. Table 2. (to next page)

Protein function class (n)	Fraction not identified		Fraction low mRNA	Mostly identified	Explanation for low identification			
	(fraction)				(fraction)	>55%	Low copy number (II, III)	Low mRNA (>20%, V)
UniProt-KB: in protein name (n≥10)	(fraction)		(fraction)	>55%				
C10 Membrane receptors & channels (1430)	0.78		0.39	NID		LM		
Calcium / Cal (42)	0.79		0.55					
Chemokine/Interleukin receptor (18)	0.83		0.60					
C-type lectin domain family (19)	0.95		0.56					
Glycoprotein (32)	0.75		0.38					
G-protein coupled (45)	0.98		0.68					
Integrin (30)	0.57		0.59					
Olfactory receptor (28)	1.00		0.86					
Purinoreceptor (14)	0.79		0.36					
Solute carrier family / SLC (146)	0.64		0.46					
Voltage-dependent/gated (38)	0.84		0.63					
C11 Mitochondrial proteins (814)	0.44		0.10	ID	III			
ATP synthase (23)	0.26		0.17					
Cytochrome b/c (49)	0.37		0.22					
Import (27)	0.22		0.00					
NADH dehydrogenase (39)	0.18		0.29					
Ribosomal protein (84)	0.44		0.00					
tRNA (31)	0.39		0.08					
C12 Other metabolism (877)	0.47		0.22	NID		LM		
(Metabolite) kinase (69)	0.36		0.40					
(Metabolite) phosphatase (53)	0.43		0.35					
(Metabolite) reductase (49)	0.37		0.44					
(Metabolite) synthase (57)	0.49		0.29					
(Metabolite) transferase (162)	0.53		0.43					
C13 Other nuclear proteins (1469)	0.86		0.07	NID			RET	
Chromatin (17)	0.76		0.08					
Histone (150)	0.89		0.10					
Nuclear pore complex (34)	0.82		0.32					
Polymerase (28)	0.86		0.00					
Repair protein (29)	0.86		0.12					
C14 Proteasomal proteins (677)	0.54		0.11	NID	II			
COP9 signalosome (10)	0.10		0.00					
E3 ubiquitin-protein ligase (180)	0.69		0.17					
Kelch-like (20)	1.00		0.30					
NEDD (15)	0.20		0.33					
Proteasome/ proteasomal (45)	0.18		0.13					
Ubiquitin-conjugating (32)	0.53		0.12					
C15 Protein kinases & phosphatases (481)	0.45		0.20	NID	II	LM		
Mitogen-activated protein kinase (41)	0.44		0.33					
Serine/threonine-protein kinase (144)	0.42		0.34					
Serine/threonine-protein phosphatase (40)	0.38		0.27					
Tyrosine (-protein) phosphatase (29)	0.45		0.54					
Tyrosine-protein kinase (29)	0.34		0.30					

Suppl. Table 2. (to next page)

Protein function class (n)	Fraction not identified	Fraction low mRNA	Mostly identified >55%	Explanation for low identification		
	(fraction)	(fraction)		Low copy number (II, III)	Low mRNA (>20%, V)	Retained in MGK
C16 Protein processing (308)	0.35	0.13	ID			
Dol / dolichol (16)	0.00	-				
Glucosyl / glycosyltransferase (17)	0.18	0.00				
Methyltransferase (13)	0.62	0.00				
Palmitoyl / sialyl (20)	0.95	0.26				
Pept/ peptidyl (50)	0.26	0.31				
C17 Secretory proteins (811)	0.72	0.47	NID	III	LM, V	
Collagen (33)	0.73	0.71				
Growth factor (36)	0.61	0.64				
Interleukin / chemokine (41)	0.83	0.53				
Metalloproteinase (28)	0.82	0.61				
Protease (21)	0.81	0.59				
C18 Signaling & adapter proteins (1024)	0.55	0.26	NID	II	LM	
14-3-3 / S100 protein (15)	0.27	0.50				
Adapter / adaptor protein (35)	0.63	0.41				
Bcl / Bax (18)	0.50	0.44				
Calcium / calpain (38)	0.61	0.52				
cAMP / A-kinase (34)	0.76	0.46				
Caspase (19)	0.42	0.13				
cGMP / G kinase (17)	0.59	0.30				
Guanine nucleotide / G-protein (43)	0.42	0.67				
Phosphatidyl / phosphoinositide (66)	0.38	0.20				
C19 Small GTPases & regulators (483)	0.41	0.20	ID	II	LM	
Arf-GAP (18)	0.61	0.27				
Rab (78)	0.19	0.27				
Ral (12)	0.33	0.50				
Rap (17)	0.47	0.13				
Ras (<i>non RAb, Ral, Rap</i>) (20)	0.70	0.50				
Rho (88)	0.57	0.44				
C20 Transcription & translation (2280)	0.79	0.09	NID	II		RET
Nuclear (127)	0.67	0.04				
Ribosomal protein (96)	0.65	0.03				
Transcription (303)	0.87	0.82				
Translation (56)	0.21	0.08				
tRNA (71)	0.56	0.23				
Zinc finger (579)	0.98	0.28				
C21 Uncharacterized & other proteins (2120)	0.79	0.23	NID	III	LM	
Coiled-coil (91)	0.84	0.28				
FAM (255)	0.77	0.40				
Leucine-rich repeat (36)	0.83	0.60				
Putative (90)	0.89	0.39				
Transmembrane (133)	0.70	0.40				
Uncharacterized (249)	0.92	0.48				

Chapter 4

A classified reference genome wide transcriptome and proteome of human and mouse platelets revealing high qualitative similarity

Huang J, Swieringa F, Solari FA, Provenzano I, Grassi L, De Simone I, Baaten CCFMJ, Cavill R, Middleton E, Sickmann A, Rondina MT, Frontini M, Heemskerk JWM

To be submitted

I designed research, analyzed and interpreted data and wrote the paper with M.T.R., M.F. and J.W.M.H. together. F.S., I.P., I.D.S. and E.A.M. analyzed and interpreted data and revised the manuscript; F.A.S., L.G., R.C., C.B. and A.S. provided essential tools and revised the paper.

Chapter 5

Impaired iloprost-induced platelet inhibition and phosphoproteome changes in patients with confirmed pseudohypoparathyroidism type Ia, linked to genetic mutations in GNAS

Swieringa F, Solari FA*, Pagel O*, Beck F, Huang J, Feijge MAH, Jurk K, Körver-Keularts IMLW, Mattheij NJA, Faber J, Pohlenz J, Russo A, Stumpel CTRM, Schrande DE, Zieger B, van der Meijden PEJ, Zahedi RP, Sickmann A, Heemskerk JWM
(*equal contribution)

Sci. Rep. 2020;10:11389.
Reprinted with permission

I performed analytical work with F.B., F.S., F.A.S., M.A.H.F., N.J.A.M. and O.P. F.S., F.A.S., J.W.M.H. and R.P.Z. were the principal investigators and take primary responsibility for the paper; A.R., B.Z., C.T.R.M.S., D.E.S., I.M.L.W.K.K., J.F., J.P. and K.J. recruited the patients; A.S., F.A.S., F.S., R.P.Z. and J.W.M.H. coordinated the research; A.S., F.A.S., F.S., R.P.Z. and J.W.M.H. wrote the paper.

Abstract

Patients diagnosed with pseudohypoparathyroidism type Ia (PHP Ia) suffer from hormonal resistance and abnormal postural features, in a condition classified as Albright hereditary osteodystrophy (AHO) syndrome. This syndrome is linked to a maternally inherited mutation in the *GNAS* complex locus, encoding for the GTPase subunit $G\alpha_s$. Here, we investigated how platelet phenotype and omics analysis can assist in the often difficult diagnosis. By coupling to the IP receptor, $G\alpha_s$ induces platelet inhibition via adenylyl cyclase and cAMP-dependent protein kinase A (PKA). In platelets from seven patients with suspected AHO, one of the largest cohorts examined, we studied the PKA-induced phenotypic changes. Five patients with a confirmed *GNAS* mutation, displayed impairments in $G\alpha_s$ -dependent VASP phosphorylation, aggregation, and microfluidic thrombus formation. Analysis of the platelet phosphoproteome revealed 2,516 phosphorylation sites, of which 453 were regulated by $G\alpha_s$ -PKA. Common changes in the patients were: (1) a joint panel of upregulated and downregulated phosphopeptides; (2) overall PKA dependency of the upregulated phosphopeptides; (3) links to key platelet function pathways. In one patient with *GNAS* mutation, diagnosed as non-AHO, the changes in platelet phosphoproteome were reversed. This combined approach thus revealed multiple phenotypic and molecular biomarkers to assist in the diagnosis of suspected PHP Ia.

Introduction

Pseudohypoparathyroidism (PHP) characterises a heterogeneous group of disorders, of which the common feature is an end-organ resistance to parathyroid hormone. Patients diagnosed with pseudohypoparathyroidism type Ia (PHP Ia, OMIM: #103580) or with the related disorder PHP Ic also exhibit resistance to other hormones and show a variable set of clinical features, including as short stature, obesity, round face, subcutaneous ossification, brachydactyly, and other skeletal anomalies. Some patients also have mental retardation. Jointly these characteristics are classified as Albright hereditary osteodystrophy (AHO) syndrome. This infrequent and serious syndrome occurs with an estimated prevalence of 1:250,000, but it is likely underdiagnosed because of variation in the presentation and severity of the disease. In the past, PHP was also deduced from a defective activity of the erythrocyte $G_{\alpha s}$ protein, but the suitability of this test has been questioned¹.

Consistent among patients with established PHP (including AHO) is impairment in the $G_{\alpha s}$ -mediated signaling effects of tissues in response to multiple hormones². This impairment is linked to dysfunctional mutations in the *GNAS* complex locus, encoding for the $G_{\alpha s}$ protein. The imprinted gene complex locus *GNAS* is located on chromosome 20q13.2-13.3^{3,4}. Importantly, genetic variation in this locus can also link to an altered regulation of blood pressure and an increased risk of cardiovascular disease⁵. In case of AHO, the syndrome characteristics are inherited from the mother, implicating that the affected tissues may preferentially express the maternal *GNAS* allele⁶. However, the disease can also be due to epigenetic variation⁶, in which case *GNAS* methylation studies are needed for a proper diagnosis of PHP patients⁷. On the other hand, paternal transmission of the mutated *GNAS* allele is not accompanied by hormone resistance, and is then classified as pseudopseudohypoparathyroidism (PPHP).

In platelets like in other cells, the stimulation of G protein-coupled receptors (GPCR), interacting with the $G_{\alpha s}$ β/γ complex, causes activation of adenylyl

cyclase (AC), which enzyme produces the second messenger cAMP⁸. Elevation in cAMP triggers intracellular signaling events via the broad-spectrum, cAMP-dependent protein kinase A (PKA)⁹. The platelet G α s-AC-PKA pathway is by far most strongly triggered via the IP receptor (*PTGIR*)¹⁰, which cause global inhibition of platelet adhesion, shape change, cytoskeletal changes, secretion, aggregation and procoagulant activity^{11,12}. The endothelium-derived prostaglandin I₂ (prostacyclin, stable mimetic iloprost) provides the main high-affinity trigger of IP receptors, along with the stable prostanoid prostaglandin E₁ (PGE₁) showing a somewhat lower affinity¹³. The other high-affinity receptor for prostacyclin, EP1, is not expressed on platelets¹⁴. Accordingly, both iloprost and PGE₁ elevate platelet cAMP levels via G α s, activate PKA and cause suppression of key signaling events including Ca²⁺ fluxes and integrin α IIb β 3 activation^{15,16}. Earlier studies describe that in patients with PHP Ia (AHO) the G α s functional defect is indeed linked to lower platelet responses to both iloprost and PGE₁¹⁷.

In our previous work, we have used protein mass spectrometry techniques for quantitative analysis of the global platelet proteome¹⁸ and of the iloprost-induced platelet phosphoproteome¹⁹. In the platelets from healthy individuals, the (phospho)proteome appeared to be markedly stable. This offers the possibility to exploit the platelet proteome to find abnormalities on the protein level in patients with a congenital deficiency or other pathologies^{20,21}.

Here, we studied seven rare patients of four families with confirmed or suspected PHP Ia, which is the largest cohort examined so far for this rare syndrome. In the platelets from these patients, we determined altered responses of the G α s-AC-PKA pathway using various multiparameter function tests, and compared these with quantitative changes in the PKA-dependent (phospho)proteome. These proteome changes were: (1) linked to a defective G α s and PKA activity, (2) related to changes in platelet function, and (3) evaluated for the potential of discriminating between AHO and non-

AHO.

Materials and Methods

Materials

Iloprost was obtained from Bayer Schering Pharma (Leverkusen, Germany), and PGE₁ from Fluka-Sigma Aldrich (Buchs, Switzerland). Horm type I collagen was purchased from Nycomed (Munich, Germany). Fluorescein isothiocyanate (FITC)-labelled antibody against phosphorylated vasodilator-stimulated phosphoprotein (P-VASP, phospho-Ser239) was from nanoTools (Teningen, Germany), Alexa Fluor (AF)647-labelled fibrinogen from Invitrogen Life Technologies (Bleiswijk, The Netherlands), FITC-labelled anti-CD62P mAb against P-selectin from Beckman Coulter (Marseille, France), and FITC-labelled PAC1 mAb against activated α IIb β 3 integrin from Becton Dickinson (San Jose CA, USA). The membrane probe DiOC₆ came from Anaspec (Reeuwijk, The Netherlands). Other materials were obtained from sources, as described before³⁵.

Patients and control subjects

Blood was obtained from healthy controls and indicated patients, after full informed consent and in accordance with the Declaration of Helsinki. Experiments were approved by the Ethics Committee of Maastricht University & Maastricht University Medical Centre. Blood samples from patients (P1-7) were freshly taken, and always analysed in parallel with blood samples of unrelated day-control subjects (C1-12). The numbering of individual patients and control subjects in this paper is unchanged for all assays. Platelet samples for proteomics assays were stored at an internal biobank, until assayed for this purpose on a later time point, such in accordance with the European data protection law.

Patients from four families were investigated with diagnosed or suspected PHP Ia (Table 1). based on elevated parathyroid hormone levels. All families showed typical symptoms associated with AHO, such as short stature and

brachydactyly, while the degree of mental retardation was variable. Family I consisted of a mother (P1), who similarly to a son (not included), carried a heterozygous single nucleotide substitution in exon 1 (c.1A→G) of the *GNAS* complex locus, resulting in a truncated G α s protein³⁶. This mutation is known to be linked to an impaired expression of functional G α s, thus reducing the G α s bioactivity in blood cells³⁷. Family II consisted of a mother (P2) and affected two sons (P3, P4), all of whom carried a heterozygous single nucleotide substitution in exon 338 (c.1G→C), encoding for a dysfunctional G α s protein, with an estimated reduction of 46%, 49% and 51% in G α s activity in the erythrocyte membranes³⁸. Family III consisted of two related subjects, a mother (P5) with an unremarkable phenotype; and an affected daughter (P6) with PHP diagnosis, of whom no mutation in the *GNAS* locus could be detected (epigenetic imprinting analysis not performed). In family IV, patient P7 obtained a diagnosis, not differentiating between PHP and POH (progressive osseous heteroplasia), while genetic analysis revealed a heterozygous deletion in the *GNAS* locus (c.565_568del), linked to nonsense-mediated decay of mRNA (unpublished). Both parents did not allow examinations. In all 7 patients, blood platelet counts were within the normal range (Table 1). Patients and day control subjects had not used antiplatelet or anticoagulant medication for at least two weeks.

Blood collection and platelet isolation

For whole blood perfusion experiments, blood samples were collected into 0.1 volume of saline containing D-phenylalanyl-prolyl-arginyl chloromethyl ketone (PPACK, 40 μ M) and fragmin (40 U/mL)³⁹. For light transmission aggregometry, blood was collected into 0.1 volume of 129 mM trisodium citrate. Platelet-rich plasma (PRP) was prepared by centrifuging blood samples at 240 *g* for 15 minutes. Platelet counts were determined with a thrombocounter (Coulter Electronics; Woerden, The Netherlands).

For measurements with washed platelets, including proteomics analyses, blood was collected into 0.1 volume of acid-citrate glucose solution (ACD, 52 mM citric acid, 80 mM trisodium citrate, 180 mM D-glucose)³⁵. PRP was then

obtained by centrifuging as above. After the addition of 0.066 volume of ACD, the platelets were pelleted by centrifugation at 870 *g* for 15 minutes. Pellets were resuspended in Hepes buffer pH 6.6 (136 mM NaCl, 2.7 mM KCl, 10 mM Hepes, 2 mM MgCl₂ and 0.1% D-glucose), while carefully excluding any bottom layer of red cells. The suspended platelets were then transferred to a clean Eppendorf tube. After the addition of 0.066 volume ACD and apyrase (1 U/mL), collected platelets were washed by centrifugation at 2,000 *g* for 5 minutes. Final resuspension then was in Hepes buffer pH 7.45 (136 mM NaCl, 2.7 mM KCl, 10 mM Hepes, 2 mM MgCl₂, 0.1% D-glucose), once more by excluding any residual erythrocytes, followed by transfer to a clean Eppendorf tube. Purity of the final platelet preparations ($1-2 \times 10^8$ /mL) for proteomics analyses was assessed by a thrombocounter and microscopic analysis. Contamination of platelets with red blood cells was <1:15,000 and with leukocytes <1:20,000.

Flow cytometry

For analysis of VASP phosphorylation as a measure of G α s-PKA activity, samples of purified platelet suspensions (2×10^8 /mL) were incubated with vehicle or iloprost (0.5-10 nM) for 1 minute, after which reactions were stopped with 2% formaldehyde (in filtered phosphate-buffered saline with 0.2% bovine serum albumin). Fixed samples were centrifuged at 2,000 *g* for 2 minutes, and pellets were washed twice with phosphate-buffered saline. The pelleted platelets were then resuspended in phosphate-buffered saline containing 0.1% saponin, to allow membrane permeabilization during 15 minutes. After addition of FITC-labelled anti-P-VASP mAb against phospho-Ser-239 (1:1,000), samples were incubated for 30 minutes, and analysed by flow cytometry (10,000 events/sample), using a BD Accuri C6 flow cytometer (San Jose CA, USA).

Light transmission aggregometry

Aggregation of platelets in plasma (normalised to 3×10^8 platelets/mL) was measured with an automated Chronolog aggregometer (Havertown PA,

USA). The platelets were preincubated with vehicle (ethanol), PGE₁ or iloprost for 4 minutes, and then activated with collagen (5 µg/mL) at 37°C. Platelet aggregation rate was determined from the slopes of curves (% transmission change per minute). In earlier functional experiments PGE₁ was used, which was later replaced by iloprost because of the meanwhile published iloprost phosphoproteome¹⁹. Cyclic AMP measurements in washed platelets were performed, as before⁴⁰.

Microfluidic thrombus formation and platelet activation under flow

To measure whole blood thrombus formation, glass coverslips were coated with type I collagen and mounted into a Maastricht flow chamber, as described⁴¹. Samples of PPACK-anticoagulated blood, preincubated for 4 minutes with vehicle (ethanol), PGE₁ (100 nM) or iloprost (5 or 10 nM), were perfused over the collagen surface at a wall shear rate of 1,000 s⁻¹ for 4.0 minutes. Thrombi on coverslips were post-stained with FITC-labelled anti-P-selectin mAb (25 µg/mL)²⁵. Brightfield differential interference contrast and confocal fluorescence images were taken from the collagen surface, as described⁴². Microscopic images were analysed for five variables (V1-5) using Image J (version 1.48g, US NIH; Bethesda MD, USA)²⁵. Deposited platelets (V1) and P-selectin staining (V2) were quantified as percentage of surface-area-coverage (%SAC); integrated feature size of aggregated platelets (V3) was expressed as µm²; thrombus multilayer score (V4) was scaled 0-3, depending on the presence of multilayered thrombi; and thrombus morphological score (V5) was scaled 0-5, ranging from no or single platelet adhesion to full thrombus formation²⁴.

Sample preparation for proteome analysis

Well-purified washed platelets (5 × 10⁸/mL) in Hepes buffer pH 7.45 were incubated with vehicle or iloprost (1-10 nM) for 1.0 minute at 37 °C. Reactions were stopped by addition of 50% lysis buffer (50 mM Tris, 150 mM NaCl, 1% SDS, 1 tablet Roche PhosStop/7 mL buffer, pH 7.8, f.c.), and incubated on ice. Directly after lysis, the samples were snap-frozen, and then

stored at -80°C until use. The following sample sets were simultaneously analysed (Suppl. Table 1). *Set I*: four samples from patient P1 and four samples from control subject C1 (*i.e.* resting, 1, 2 or 10 nM iloprost). *Set II*: four samples from patient P7 and four samples from control subject C4 (resting, 2, 5 or 10 nM iloprost). *Set III*: three samples for patient P2, three samples for patient P6, three samples for control subject C2 (resting, 2 or 10 nM iloprost), and a calibration sample. *Set IV*: three samples for patient P3, three samples for patient P4, three samples for control subject C3, (resting, 2 or 10 nM iloprost) and a calibration sample. In parallel, platelet samples were analysed for VASP-P determination. Platelets from asymptomatic patient P5 were not available for this analysis.

Protein digestion and stable isotope labelling for proteomic analysis

Sample preparation, proteolytic digestion and iTRAQ/TMT labelling were based on previously described methods^{18,27,43,44}. The TMT labelling was performed according to the manufacturer's instructions. Quality control of all samples was as before¹⁹. Lysed samples of the purified platelets (5×10^8 /mL) were diluted to the same protein concentration (checked with a bicinchoninic acid protein assay kit; Pierce, Thermo-Fisher Scientific, Bremen, Germany). Cysteines were reduced (30 minutes, 56°C) and free sulfhydryl groups were alkylated (30 minutes, room temperature, in darkness) with 10 mM dithiothreitol and 30 mM iodoacetamide, respectively. Samples of sets I-IV were handled in equivalent manners, as described below.

For sets I and II, aliquots containing 100 µg of protein were diluted 10-fold with ice-cold ethanol and incubated for 1 hour at -40 °C. The mixtures were centrifuged for 30 minutes at 4°C and 18,000 *g*, and supernatants were carefully removed. The precipitates were washed using 50 µL of ice-cold acetone, followed by a 15 minutes centrifugation. This step was repeated once. Precipitated proteins were re-solubilised into 6 M guanidine hydrochloride, and digested in-solution with trypsin (Sequence grade modified, Promega, Madison WI, USA) at a 1:20 enzyme: protein ratio, with a final concentration of 0.2 M guanidine hydrochloride, 2 mM CaCl₂ and 50

mM triethylammonium bicarbonate (14 hours, 37°C). Digestion controls were performed, using a monolithic-RP HPLC system, as before⁴⁵. Digests were individually labelled with iTRAQ 8-plex labels (113-119, 121). After drying in vacuum, the samples were dissolved in iTRAQ 8-plex dissolution buffer (AB Sciex; Dreieich, Germany), and labelled according to the manufacturer's protocol. Samples per set were pooled at 1:1 ratios, were desalted by C₁₈ solid phase extraction (SPEC C₁₈ AR, 4 mg bed; Agilent Technologies, Brussels, Belgium) and dried under vacuum.

For sets III and IV, 150 µg protein per sample was loaded onto a 30 kDa molecular weight cut off spin filter to perform filter-aided sample preparation, as described elsewhere^{46,47}, with slight modifications. Proteins were digested (14 hours, overnight) in 50 mM triethylammonium bicarbonate, 0.2 M guanidine hydrochloride, 2 mM CaCl₂, pH 8.5 with trypsin (w/w 1:25, sequencing grade, Promega, USA)¹⁹. The peptides were collected by centrifugation at 14,000 g for 20 minutes. To increase peptide yield, filters were additionally washed with 50 µL 50 mM triethylammonium bicarbonate, and subsequently with 50 µL water. Digestion performance and peptide yield was controlled, as previous⁴⁸. Digests were individually labelled with TMT 10-plex labels (126, 127N, 127C, 128N, 128C, 129N, 129C, 130N, 130C, 131, from Thermo Scientific). Equal peptide amounts of vacuum dried samples were reconstituted in 100 µL 100 mM triethylammonium bicarbonate, and labelled with 0.8 mg reagent according to the manufacturer's protocol. Samples were then pooled at 1:1 ratios, and further treated similar to sets I+II.

The multiplexed iTRAQ or TMT pools were used to quantify the global proteomes and the phosphoproteomes of the individual samples. For global proteome analysis, 10% (iTRAQ) or 3.5% (TMT) of a pooled mixture was pre-fractionated on a U3000 HPLC (Thermo Scientific) by high pH reversed-phase chromatography (C₁₈ column; BioBasic-18, 0.5 mm ID x 15 cm, 5 µm particle size, 300 Å pore size, Thermo Scientific) using a linear gradient. For iTRAQ pools, this gradient was ranging from 3-50% solvent B (mobile phase A: 10

mM ammonium acetate, pH 6.0, *B*: 10 mM ammonium acetate, 84% acetonitrile, pH 6.0, 75 minutes). For TMT pools, a linear gradient ranged from 3-50% solvent *B* (mobile phase *A*: 10 mM ammonium formate pH 8.0, *B*: 10 mM ammonium formate, 84% acetonitrile, pH 8.0, 75 minutes) to obtain 20 concatenated fractions for LC-MS analysis.

For phosphopeptide analysis, the remaining of the pooled iTRAQ or TMT samples were subjected to a TiO₂-based phosphopeptide enrichment protocol, as described elsewhere with slight modifications⁴³. Briefly, samples were resuspended in TiO₂ loading buffer (80% acetonitrile, 5% trifluoroacetic acid, 1 M glycolic acid), and incubated twice with TiO₂ beads for 10 minutes. Incubations first had a peptide to bead ratio of 1:6, and then a ratio of 1:3. For set III or IV, an additional incubation at 1:1.5 ratio was performed. Subsequently, the beads of all incubation steps were combined in one Eppendorf tube, and washed and eluted, as previously⁴⁹. In short, 80% acetonitrile, 1% trifluoroacetic acid was used for washing step 1, and 10% acetonitrile, 0.1% trifluoroacetic acid for washing step 2. The phosphopeptides were eluted by incubation with 1% NH₄OH for 10 minutes. The eluates were acidified using formic acid (pH < 2). To obtain better phosphopeptide recovery, the enrichment procedure was repeated once with a slight variation, *i.e.* a loading buffer of 70% acetonitrile, 2% trifluoroacetic acid, and a washing buffer of 50% acetonitrile, 0.1% trifluoroacetic acid. Phosphopeptides were eluted as described above and then acidified.

The acidified phosphopeptides were desalted using Oligo R3 micro-columns⁵⁰, and fractionated on a U3000 RSLC system in hydrophilic interaction liquid chromatography (HILIC) mode (Polar phase TSKgel Amide-80; 150 µm ID × 15 cm length; 5 µm particle size; 80 Å pore size, Tosoh Bioscience, Tessenderlo, Belgium), using a binary gradient ranging from 10-35% solvent *B* (solvent *A*: 98% acetonitrile, 0.1% trifluoroacetic acid; solvent *B*: 0.1% trifluoroacetic acid) in 40 minutes (flow rate: 4 µL/ minutes). A total of 9 fractions per set were collected for subsequent LC-MS analysis.

Global proteome and phosphoproteome analysis by iTRAQ or TMT labelling

Sets I and II (*in italic sets III and IV, if different*): RP and HILIC fractions were individually analysed by nano-LC/MS-MS, using a Ultimate 3,000 RSLC-nano system online-coupled to a Q-Exactive Plus (iTRAQ) or a Q-Exactive HF (TMT) mass spectrometer (both Thermo Scientific). Individual fractions were loaded onto a trap column (Acclaim PepMap100 C₁₈ trap column; 100 µm x 2 cm) with 0.1% trifluoroacetic acid; flow rate: 20 µL/ minutes. This was followed by separation of peptides on the main column (PepMap100 C₁₈; 75 µm x 50 cm), using a binary gradient ranging from 3-42% (3-35%) solvent B [84% acetonitrile, 0.1% formic acid] in 145 minutes (*60 minutes*). In the Q-Exactive, survey scans were acquired at resolution of 70,000 (*60,000*) using an automatic gain control (AGC) target value of 3×10^6 (1×10^6). MS/MS spectra of the top 15 most intense ions were acquired with a resolution of 17,500 (*60,000*), an isolation width of 2.0 (*0.8*) m/z , a normalised collision energy of 35% (*33%*), an AGC target value of $1 (2) \times 10^5$ ions, a maximum injection time of 250 (*200*) ms and a dynamic exclusion of 12 (*30*) s with and underfill ratio of 10%. The first fixed mass was set to 105 (*100*) m/z . In order to compensate for the iTRAQ-induced increase of peptide charge states, reaction tubes with 10% ammonium water were placed in front of the ion source as described elsewhere⁵¹. For TMT samples, to compensate for a higher complexity of the global proteome fractions, the isolation width was reduced to 0.4 m/z to reduce the potential precursor co-isolation.

Raw data were processed with Proteome Discoverer 1.4 (Thermo-Fisher Scientific). Data were searched against the Uniprot human database (August 2012; 20,232 target sequences) using Mascot and Sequest with the following settings: (1) trypsin as enzyme allowing two missed cleavages, (2) iTRAQ 8-plex (*TMT 10-plex*) at N-termini and lysines of +304.2053 (*+229.163*) Da and carbamidomethylation of Cys +57.0214 Da as fixed modifications, (3) oxidation of Met +15.9949 Da as variable modification, (4) mass tolerances of 10 ppm and to 0.02 Da for MS and MS/MS, respectively. For HILIC

fractions, phosphorylation of Ser/Thr/Tyr (+79.9663 Da) was selected as additional variable modification. False discovery rate (FDR) estimation on the level of peptide spectrum matches (PSM) was performed using the peptide validator node, filtering for high confidence 1% FDR. The reporter ion quantifier node was used for iTRAQ (*TMT*) reporter quantification.

For global proteome quantification (RP fractions) only unique proteins quantified with at least 2 unique peptides were considered. For phosphoproteome quantification (HILIC fractions), phosphorylation site localisation was determined using phospho-RS⁵², and only phosphopeptides with phospho-RS site probabilities >90% were considered as confident. Sorting and evaluation of the exported data as well as calculations were done in Microsoft Excel.

Data analysis of platelet global proteomes and phosphoproteomes

Sets I+II (*sets III+IV*): As Proteome Discoverer only provided 7 (9) ratios for the 8 (10) samples, an artificial 113/113 (126/126) ratio was created and set to 1.0 per protein and all ratios were log2 transformed. Per channel, the median ratio over all proteins was calculated, from which the median of all eight (*ten*) values was determined to define normalisation factors per iTRAQ (*TMT*) channel. These factors compensated for systematic errors (*i.e.*, unequal sample amounts derived from pipetting errors or inaccurate protein determination results) and allowed to obtain normalised ratios per protein. The normalised ratios were divided by the median (log2 transformed) over all eight (*ten*) values to obtain scaled normalised abundance values (NAVs) for all proteins and channels. The NAVs (log2 transformed) allowed determination of inter-sample ratios for platelets from the patients and control subjects for each condition.

Inter-individual variation for the global proteome was estimated by separate analysis of the samples from all subjects (combined sets) in comparison to averaged control values (C1-4). Differences from average control values were thresholded based on altered ratios log2 transformed ($\geq 25\%$ up or

downregulation: range of -0.322 to +0.322).

For determination of confident phosphorylation sites at the peptide level, a ready-to-use Excel macro provided by Mechtler lab (<http://ms.imp.ac.at/?goto=phosphors>) was used. Data were normalised as described above. NAVs were calculated per phospho-site, as described for the global proteome. Average NAVs were calculated per iTRAQ or TMT channel, after grouping per phosphopeptide sequence, phosphorylation site and protein. Phosphopeptides present in ≥ 3 control samples were used to assess average control values, after normalisation per data set, and were log2 transformed. Treatment effects were estimated based on an arbitrary cut-off of $\geq 25\%$ up- or downregulation (log2 range of -0.322 to +0.322). Thresholds for relevant changes in patient samples were more strictly set at $2 \times (-0.322 \text{ to } +0.322)$; comparisons were made to mean control NAVs, for up- or downregulation per phosphopeptide.

Reference values of phosphoproteomes and determination of PKA phosphorylation sites

Phosphorylation data were compared with a reference dataset of iloprost-induced changes in protein phosphorylation of healthy control platelets (2,700 phosphopeptides, of which 299 regulated by iloprost), as published^{19,32}. Iloprost-regulated phosphopeptides were defined as those responsive to 1 minute treatment with 2 or 10 nM iloprost. A three-point scale was used (1 = upregulated, 0 = unchanged, -1 = downregulated). Consensus sites for PKA-induced phosphorylation were as before¹⁹, using the GPS2.1 algorithm for kinase consensus sequence prediction⁵³. Classification of proteins was as before²⁷.

Reactome pathway analysis

Lists of protein identifiers (gene names, Uniprot) were introduced in the Reactome pathway database (reactome.org), and analysed on biological pathways with $n > 4$ entities and false discovery rates of > 0.82 . Lists contained phosphorylated proteins regulated by 2 and/or 10 nM iloprost: 196

upregulated and 159 downregulated. Weight factors were included, presenting the numbers of regulated phosphorylation sites per protein.

Experimental design and rationale

Inclusion of the quite rare patients with suspected PHP Ia (expected prevalence of 1/250,000, but underdiagnosed) occurred over the years 2014-2017. As required for diagnostic platelet function analyses, blood samples from the 8 patients were directly compared with samples from a healthy day-control subject (in total 12 controls). The common rationale in diagnostic laboratories is that the (isolated) platelets from all healthy subjects make up a normal pool (with defined normal ranges of test outcomes) that, however, needs to be validated day-by-day to check for the quality of blood drawing and sample preparation. At a first visit, blood from patients and day controls was analysed for platelet functions with Gαs-stimulating agents (platelet aggregation, microfluidics, flow cytometry). In addition, platelet samples were made for proteomics analysis (both global proteome and phospho-proteome). If possible and required, at a second visit, blood from patients (*e.g.*, children) and controls was used for additional functional assays. Note that flow cytometry of VASP phosphorylation was performed with all samples. The total number of included controls was 12.

Given the earlier established high stability of the platelet proteome and phosphoproteome among healthy subjects^{18,19} and to retain an affordable work-flow, for the proteomic assays, for omics analyses we compared patient samples with the means of respective day-control samples. Sets I-II of platelet and control samples, obtained in 2014-2015, were analysed in 8-plex using iTRAQ labelling. Set III-IV samples, obtained in 2017, were analysed in 10-plex using TMT labelling

Statistics

Functional and proteomics data of control subjects are represented as medians ± interquartile ranges; data from patients are indicated individually. Differences of individual patients were considered to be statistically

significant, when outside the normal ranges (defined by 95% confidence intervals). Effect sizes were calculated from the Cohen's d , *i.e.* $(M_1 - M_2) / SD_{M_1 + M_2}$, in which M_1 refers for means of patients and M_2 to means of controls). For medium effect size, we used a $d \geq 0.5$. Cohen's d calculates a standardised difference between both groups that are not affected by sample size. Heatmaps were created using the R package version 3.5.1. Unsupervised hierarchical clustering of datasets from patients and controls was also performed in R.

Results

Impairment of G α s-dependent responses in platelets from patients with suspected PHP Ia

In order to assess abnormalities of the G α s-AC-PKA pathway, we analysed the platelets from seven rare patients (four families) with confirmed or suspected PHP Ia (Table 1). Family I patient (mother P1) had a heterozygous, deleterious mutation in exon 1 of *GNAS*. Family II (mother P2 and two children P3-4) had a heterozygous, dysfunctional mutation of *GNAS* in exon 3. Family III with unaffected mother P5 included a child (P6), showing all physical characteristics of PHP Ia, while no genetic mutation was found so far. Family IV consisted of a child (P7) with a heterozygous deleterious mutation in the *GNAS* locus and a differential diagnosis including PHP. On the days of measurement, blood samples were also obtained from healthy control subjects (C1-12). Throughout this paper, the numbering of individual patients and controls has been kept the same.

Isolated platelets from all seven patients (P1-7) and 12 control subjects (C1-12) were used for the assessment of iloprost-induced VASP phosphorylation at Ser-239, which is a golden standard method to establish affected PKA-dependent phosphorylation events²². For this purpose, platelets were treated with a range of iloprost concentrations (0.5-10 nM) for 1 minute, *i.e.* a time point reflecting the early phosphorylation activity of PKA. In the cells from control subjects, VASP phosphorylation increased dose-dependently

Table 1. Investigated families and patients with symptomatic or suspected PHP Ia. Listed are patients with (suspected) PHP Ia (OMIM: 103,580), confirmed mutations and whole blood platelet counts. Limited blood was obtained from P7 (young child).^aParents did not allow further examination.

	Patient	Diagnosis	Mutation in <i>GNAS</i> locus	Platelet count L ⁻¹
Family I	P1	PHP type Ia	c.1A>G (p.Met1Val)	226 x 10 ⁹
	P2 (mother P3,4)	PHP type Ia	c.338G>C (p.Lys338Asn)	215 x 10 ⁹
	P3	PHP type Ia	c.338G>C (p.Lys338Asn)	173 x 10 ⁹
Family II	P4	PHP type Ia	c.338G>C (p.Lys338Asn)	244 x 10 ⁹
	P5 (mother P6)	(asymptomatic)	not found	255 x 10 ⁹
Family III	P6	PHP type Ia	not found	214 x 10 ⁹
Family IV*	P7	PHP suspected	c.565_568del	278 x 10 ⁹

with limited inter-individual variation (Figure 1A, B). In the platelets from patients P1-4,6 (families I-III), VASP phosphorylation was impaired at a variable degree, in that higher doses of iloprost were needed to reach the phosphorylation level seen in platelets from the control group. Exceptions were the platelets from the unaffected patient P5 and the atypical patient P7, which showed a normal dose response of iloprost-induced VASP phosphorylation.

In the diagnostics laboratory, light transmission aggregometry (LTA) is commonly used to monitor platelet function abnormalities, requiring the use of day control samples²³. The LTA method can reveal defects in G α s signaling activity, by establishing the inhibitory effects of IP receptor agonists iloprost or PGE₁ on collagen-induced platelet aggregation¹⁷.

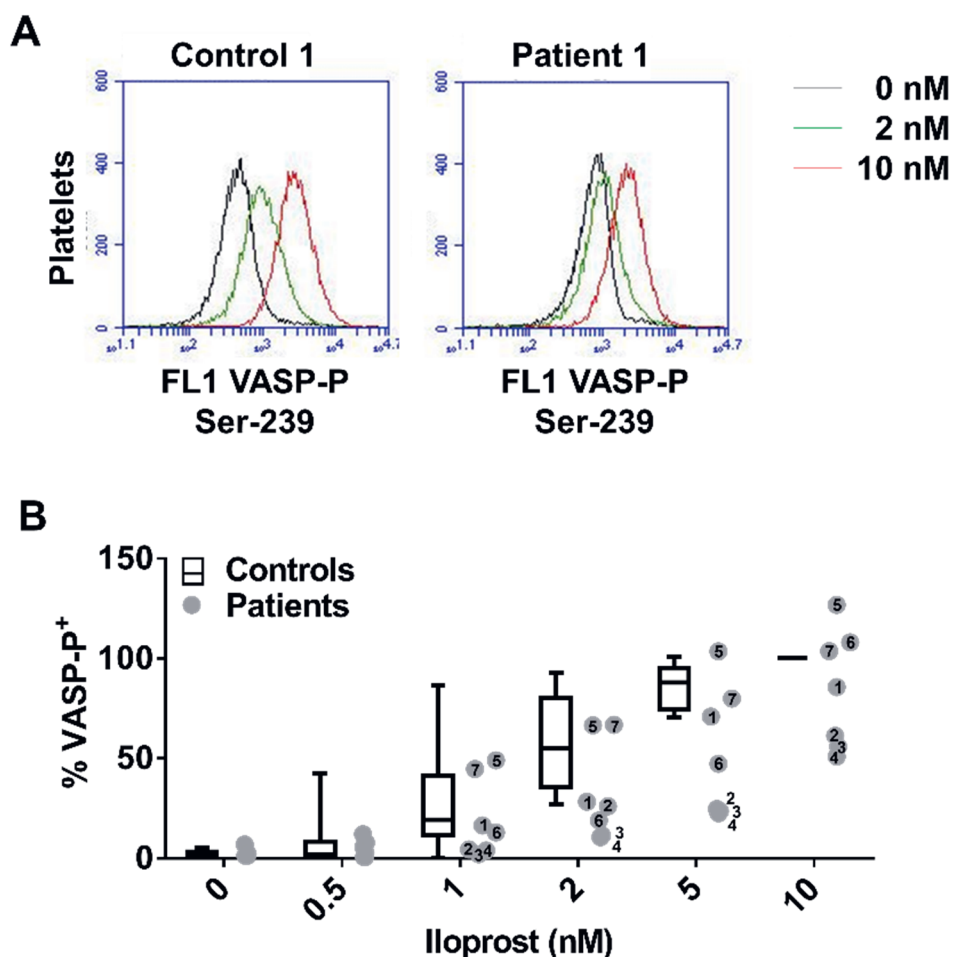


Figure 1. Changes in Gas-mediated VASP phosphorylation in platelets from patients with suspected PHP Ia. Isolated, washed platelets were preincubated with iloprost (0-10 nM), fixed, permeabilised and stained with FITC anti-P-VASP mAb. **A**, Representative flow cytometric histograms of VASP phosphorylation after iloprost treatment of platelets from control subject C1 and patient P1. **B**, Quantified VASP phosphorylation results from control subjects (C1-12) and patients (P1-7). Box plots indicate medians \pm interquartile ranges (whiskers represent 2.5-97.5th percentiles, $n = 12$).

From four patients, sufficient blood could be obtained to measure platelet aggregation responses. In the platelets from the day-control subjects, collagen-induced aggregation was fully inhibited by 100 nM PGE₁ (Suppl. Figure 1A). In the platelets from patient P1 (family I), PGE₁ was less inhibitory; in that 300 nM still caused appreciable aggregate formation. A similar defective response to PGE₁ was seen in response to platelet aggregation with stable ADP, PAR1 agonist or convulxin (Suppl. Figure 1B). For the other patients, the platelets from P2 (family I) and P5 (family III) showed a similar impairment, again requiring an increased dose of PGE₁ to abrogate collagen-induced aggregation (Suppl. Figure 1C). In contrast, the platelets from P5 responded similarly as the control platelets. For patient P1, sufficient platelets were isolated to confirm low inhibition of aggregation also with iloprost (Suppl. Figure 1D), and to establish an impairment in G α s-dependent elevation in cytosolic cAMP (Suppl. Figure 1E, F). Taken together, these data indicate that the platelets from patients P1-4 and P6 (but not the asymptomatic P5) show a variably impaired response to PGE₁ and iloprost in terms of cAMP-dependent VASP phosphorylation and aggregation inhibition.

Impairment of G α s-mediated thrombus formation in whole blood from patients with suspected PHP Ia

Microfluidic assessment of collagen-dependent thrombus formation in flowing whole blood provides an overall assessment of platelet functions²⁴. To determine a role of G α s in this assay, whole blood samples from patients and control subjects were preincubated with vehicle or PGE₁, and then flowed at defined wall shear rate²⁵. The thrombi formed on collagen were analysed for variables, indicative of the platelet activation state: platelet adhesion (V1), P-selectin expression (V2), platelet aggregation as integrated feature size (V3), a thrombus multilayer score (V4), and a thrombus morphological score (V5). Blood samples from control subjects indicated that 100 nM PGE₁ was sufficient to cause an ~50% overall reduction in thrombus formation. Hence, this PGE₁ concentration produced smaller-sized thrombi (V3,4), which was accompanied by lower platelet adhesion (V1) and

platelet secretion (V2) (Figure 2). The other G α s-stimulating agent iloprost induced similar effects as PGE₁ (Suppl. Figure 2).

Application of the flow assay with blood samples from patients P1-6 and consecutive control subjects (C1-8) resulted in a reducing effect of PGE₁ for all variables, although we noted some differences between the patients. This was illustrated in a heatmap (Figure 2A), constructed of the normalised variables (range 0-10) per patient, in comparison to the averaged data from control subjects, using an earlier used procedure²⁶. This assessment of PGE₁ effects on thrombus formation pointed to largest deviations for patients P2,3,6, when compared to normal ranges (C1-8) (Figure 2B). Visualisation in a heatmap thus showed the effects of PGE₁ per variable and patient, in comparison to the average control data after applying a statistical filter of $p < 0.05$ (Figure 2C, D). These flow data revealed that the inhibitory effect of PGE₁ is reduced for most thrombus variables in patients P3,6, and for two/three variables in patients P1,2,4. In contrast, values for P5 were largely within the normal ranges. Taken together, these findings pointed to a consistent impairment in PGE₁-mediated suppression of whole blood thrombus formation for patients P1-4,6, but not for the asymptomatic patient P5.

Minor changes in global proteome of patient platelets

By combined analysis of the proteome and phosphoproteome²⁷, we examined the protein composition of available platelets from all patients with suspected PHP Ia (P1-4,6,7), again in comparison to the day control subjects (C1-4). Directly after isolation, the purified platelets were incubated with 0, 2 or 10 nM iloprost for 1 minute at 37°C, *i.e.* a condition known to identify the iloprost/PKA phosphoproteome¹⁹.

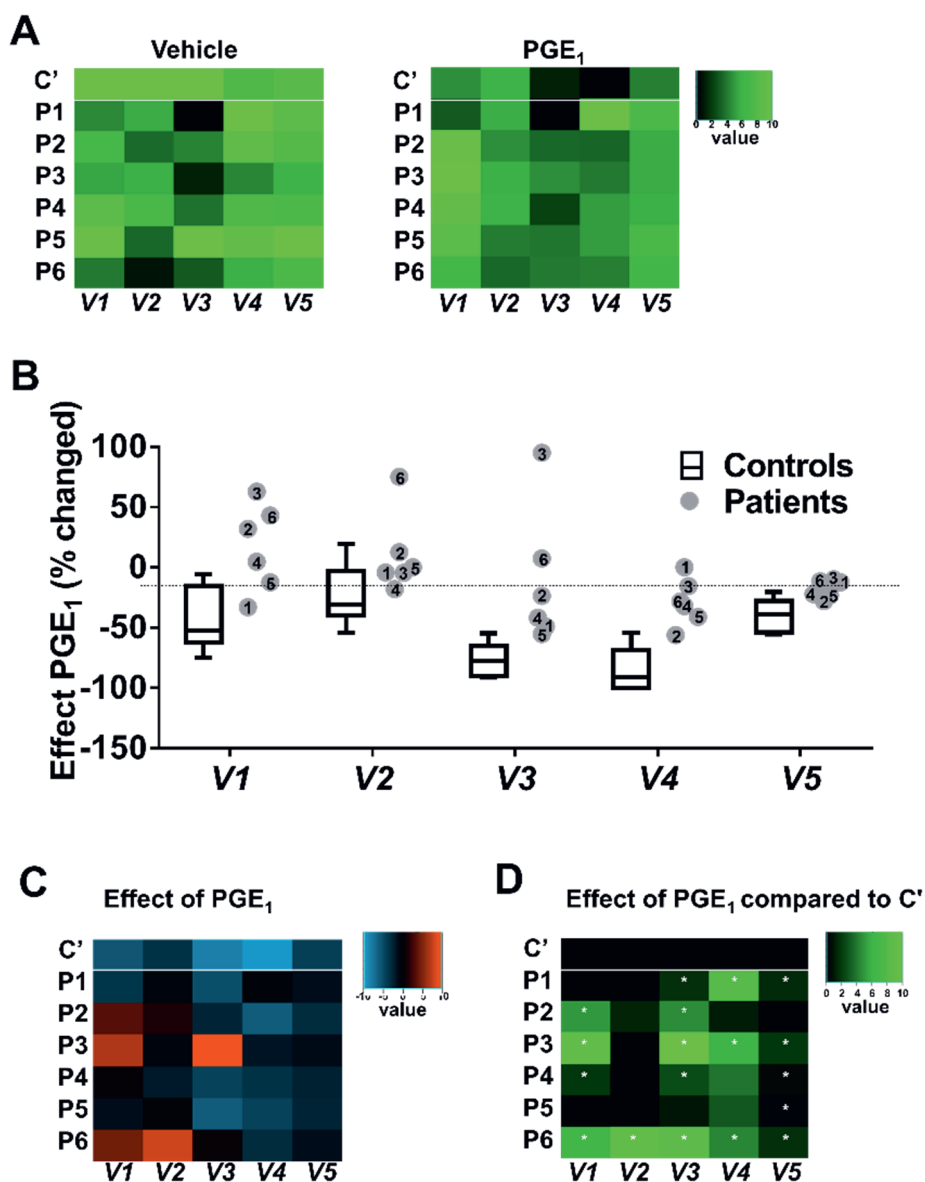


Figure 2. Changes in Gas-mediated inhibition of thrombus formation in blood from patients with suspected PHP Ia. Whole blood from control subjects (C1-8) and patients (P1-6) was perfused over collagen at wall shear rate of 1000 s^{-1} for 4

minutes. Thrombi formed were evaluated from brightfield microscopic images and fluorescence images (staining with FITC anti-P-selectin mAb). Blood samples were preincubated with vehicle or PGE₁ (100 nM), as indicated. **A**, Unit variance normalised parameters of thrombus formation (0-10): platelet adhesion (V1); P-selectin expression (V2); aggregate integrated feature size (V3); thrombus multilayer score (V4); and thrombus morphological score (V5). Heatmaps show median values for all control subjects (C1-8, C') and values for individual patients (P1-6) of blood flow runs in the presence of vehicle (left) or PGE₁ (right). **B**, Quantified effect of PGE₁ on thrombus parameters; data for control subjects indicated as medians \pm interquartile ranges (whiskers represent 2.5-97.5th percentiles, $n = 8$). **C**, Heatmap of normalised effects of PGE₁ per parameter and patient. **D**, Subtraction heatmap of PGE₁ effects in comparison to means of control platelets, * $P < 0.05$ (one-way ANOVA).

Because of the use of iTRAQ or TMT labels, proteome analysis of the platelets was performed in four sets in 8-plex or 10-plex measurements, respectively (Suppl. Table 1). Mass spectrometry of the trypsin-treated platelet lysates provided quantitative information on 1,651 (C1, P1), 3,917 (C2, P2,6), 3,859 (C3, P3,4), and 1,957 (C4, P7) unique proteins (Suppl. Datafile S1). To assess for relevant differences in protein abundance between platelet preparations, we applied cut-off ratios outside the range of -0.322 to 0.322 (log₂ transformed), representing $\geq 25\%$ up- or downregulation. Mean normalised abundance values (NAVs) for all proteins, analysed per set of samples, were grossly within normal ranges for all patients (Figure 3A). Importantly, for the individual control subjects, small proportions of about 1-3% of the identified proteins showed $\geq 25\%$ down- or upregulation (Figure 3B). This small variation of the platelet proteome of healthy subjects is well in-line with our previous papers. For the individual patients P2,3,4,6 these percentages increased up to 4-5%. We hence concluded that the analysed global platelet proteomes of controls and patients were comparable.

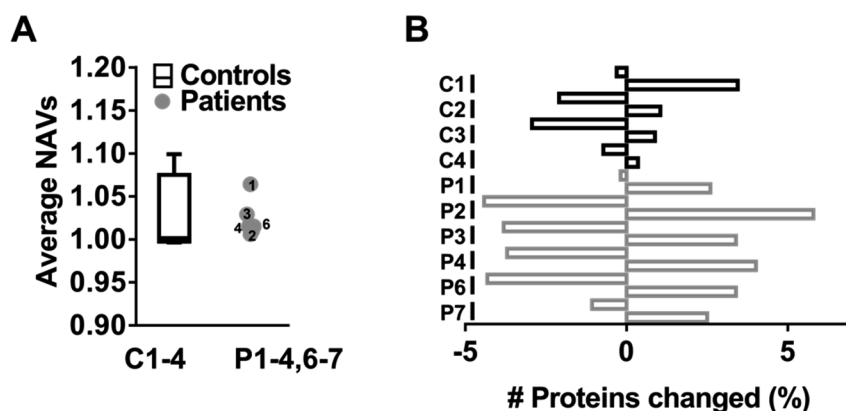


Figure 3. Minor alterations in global platelet proteome in patients with suspected PHP Ia. Global proteomics analysis of platelets from day control subjects (C1-4) and patients P1-4,6,7, providing quantitative information on 1,651-3,917 unique proteins. **A**, Averaged normalised abundance ratios over all identified proteins per control subject, presented as medians \pm interquartile ranges (whiskers indicate 2.5-97.5th percentiles). **B**, Percentage fractions of altered proteins per subject in comparison to mean of controls, C'; defined as values outside range of \log_2 -0.322 to +0.322.

Assessment of iloprost-induced, Gas-dependent phosphoproteome in control platelets

Phosphoproteomics analysis of the iTRAQ- or TMT-labelled lysates from resting and iloprost-treated (2 or 10 nM) platelets was performed after TiO_2 enrichment. The total numbers of phosphopeptides quantified were 3,457 (C1, P1), 4,845 (C2, P2,6), 5,540 (C3, P3,4), and 3,812 (C4, P7) (Suppl. Datafile S1). This corresponded per sample set to 1,164, 1,599, 1,676 and 1,361 unique proteins, respectively.

To establish the relevant iloprost-induced changes, we first listed the phosphopeptides that were present in multiple, ≥ 3 control samples (C1-4). For the found 2,516 phosphopeptides, the same cut-off was used as above, in order to define relevant changes induced by 2 nM iloprost (in brackets 10 nM iloprost), *i.e.* with $\geq 25\%$ up- or downregulation. This provided an overall

list of 453 regulated phosphopeptides, of which 146 (263) were upregulated and 192 (190) were downregulated (Suppl. Datafile S2). This represents a 50% increase in comparison to the earlier reported 299 iloprost-regulated phosphopeptides¹⁹.

By ordering the regulated phosphopeptides according to mean changes in (10 nM stimulated) control platelets, we importantly obtained highly similar patterns of iloprost-induced changes for the individual control subjects (Figure 4A). Raising the iloprost dose from 2 to 10 nM resulted in more upregulated phosphopeptides, as expected (Figure 4B). At either iloprost concentration, the majority of upregulated phosphopeptides (68-70%) were found to contain a consensus PKA phosphorylation site, whereas only few of the downregulated phosphopeptides (16-18%) contained such sites (Figure 4C). The Venn diagrams of Figure 4D illustrate this by showing a larger overlap of the upregulated than of downregulated phosphoproteins with PKA consensus site.

Assignment of the 453 phosphopeptides (regulated by 2-10 nM iloprost) to platelet function classes indicated a similar pattern for the up- and downregulated sites (Table 2). In general, the higher dose of 10 nM iloprost gave an expected higher number of upregulated (not downregulated) phosphopeptides. Those function classes that comprised (phospho)proteins that were most frequently modified included: signaling & adapter proteins (13.0-19.0%), cytoskeleton actin-myosin (9.5-13.7%), protein kinases & phosphatases (9.1-14.6%), and small GTPases & regulators (8.9-14.4%).

To further assess the signaling mechanisms altered by iloprost, we performed a Reactome pathway analysis. Taking as input the iloprost-regulated proteins, this again showed a high similarity in pathways that were covered by upregulated or downregulated proteins. Reactome thus identified pathways of signal transduction, haemostasis, cell-cell interactions, and platelet activation (Suppl. Table 2). As an alternative approach, we furthermore performed pathway analysis using the Gene

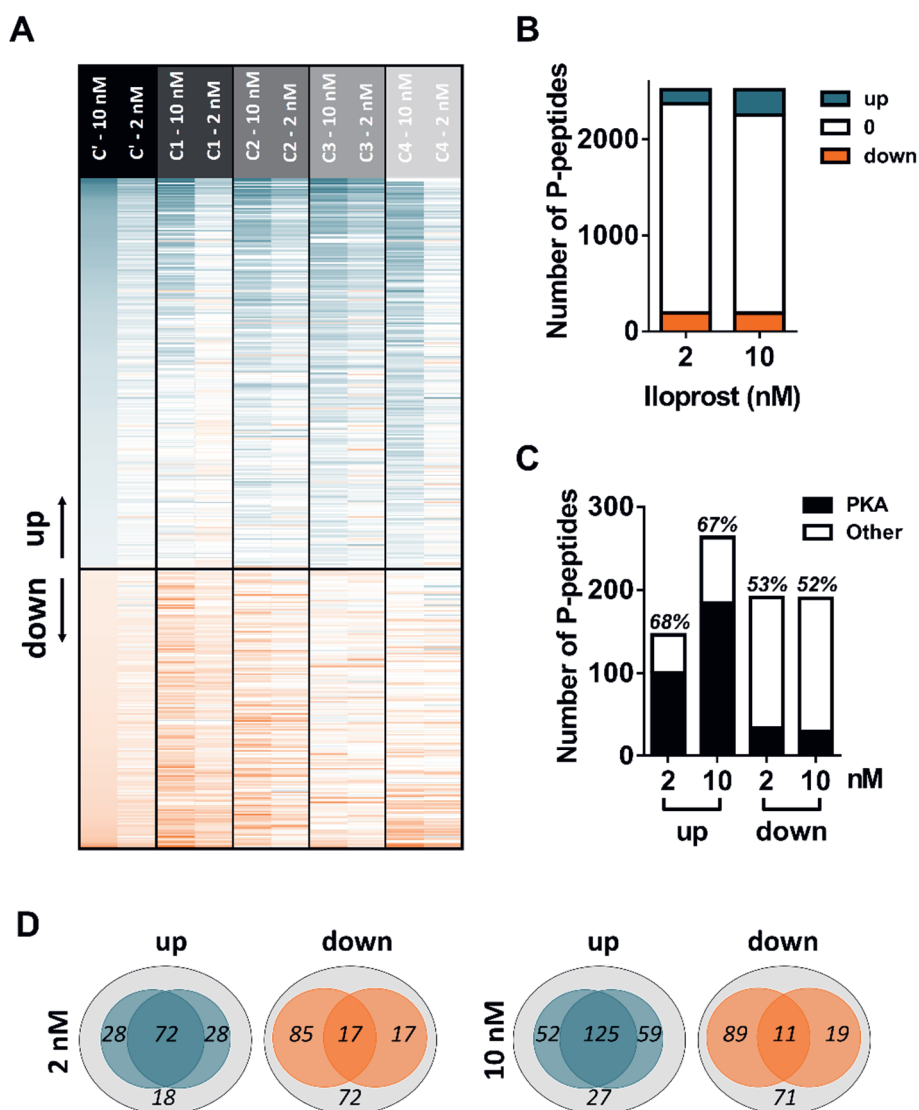


Figure 4. Iloprost-induced and PKA-mediated changes in phosphoproteome of control platelets. **A**, Heatmap of 453 phosphopeptides assigned as upregulated (blue) or downregulated (orange) by 10 or 2 nM iloprost in control platelets (C1-4). Left lanes: mean effects in platelets from the control subjects (C'). Phosphopeptides were ordered according to mean effect size by 10 nM iloprost. Next lanes: iloprost effects for the control subjects. Relevant regulated changes were arbitrarily

thresholded for outside range of log2 -0.322 to +0.322. B, Numbers of phosphopeptides identified as up- or downregulated by iloprost in ≥ 3 control subjects. C, Fractions of phosphopeptides identified as up- or downregulated with a PKA consensus site; percentages refer to overlap with previous identification¹⁹. D, Venn diagrams presenting relevant up- and downregulated proteins by 2 or 10 nM iloprost. Left circles: previously identified, right circles: positive PKA consensus site.

Ontology resource. Again, the most abundant specific pathways were those of: response to stimulus, signal transduction, cytoskeleton organization, regulation of phosphorylation and haemostasis (Suppl. Table 3). These pathway analyses thus support a coordinated mechanism of iloprost-induced platelet inhibition via G α s-AC-PKA signaling to modulate a wide range of platelet haemostatic responses.

Overall phosphoproteome changes by iloprost in patient platelets

In the peptide panels of platelets from all patients, stimulated or not with iloprost, we then searched for consistent changes in phosphorylation patterns, in comparison to the means of control platelets. For the 453 regulated phosphopeptides, this resulted in a heatmap of ratio differences per patient (Figure 5A). After filtering for relevant changes (outside normal range of 2x -0.322 to +0.322; log2 values), we identified a list of iloprost-modulated peptides, which were consistently reduced in the platelets from P1,2,4,6 (Figure 5B). However, these peptides were less deviant in P3 and were changed in the opposite way in P7. Calculation of the mean differences in the top-100 up- and down-regulated phosphopeptides between controls and patients P1,2,4,6 showed a consistent decrease in iloprost-upregulated phosphopeptides and a converse increase in iloprost-downregulated phosphopeptides in the patients' platelets (Figure 5C). Counting the numbers of phosphopeptides with relevant changes in comparison to control subjects, resulted in an order of P1,6 > P2,4 > P3 > P7 (Table 3). Typically, for patient P7, the numbers of phosphopeptides with increased phosphorylation exceeded those with decreased phosphorylation.

Table 2. Iloprost-induced changes in phosphoproteome and platelet functions. All 2,516 phosphopeptides of the iloprost phosphoproteome, identified in control platelets, were assigned to 22 platelet function classes, according to Uniprot. Indicated per class are the fractions of phosphopeptides identified as up- or downregulated by 2 or 10 nM iloprost, in platelets from ≥ 3 control subjects (C1-4). Note that cut-off levels were used per column to define downregulation or upregulation, as for Figure 4. Indicated also are numbers (n) of altered phosphopeptides per function class.

All phosphopeptides			Regulated phosphopeptides						
Platelet function class		2 nM				10 nM			
(Uniprot)	(n)	down %	(n)	up %	(n)	down %	(n)	up %	(n)
1 Cytoskeleton actin-myosin	(278)	10.9	(21)	9.5	(18)	13.7	(26)	10.6	(28)
2 Cytoskeleton intermediate	(2)	0.5	(1)	0.7	(1)	0.0	-	0.0	-
3 Cytoskeleton microtubule	(111)	2.1	(4)	5.5	(8)	3.7	(7)	6.8	(18)
4 Cytoskeleton receptor-linked	(123)	5.2	(10)	8.2	(12)	7.4	(14)	6.1	(16)
5 Endosome proteins	(22)	0.0	-	2.1	(3)	0.0	-	1.9	(5)
6 ER & Golgi proteins	(61)	1.0	(2)	0.7	(1)	1.6	(3)	1.5	(4)
7 Glucose metabolism	(28)	1.0	(2)	0.7	(1)	0.5	(1)	1.1	(3)
8 Lysosome & peroxisome proteins	(6)	0.0	-	0.7	(1)	0.0	-	0.4	(1)
9 Membrane & protein trafficking	(96)	2.6	(5)	4.1	(6)	4.7	(9)	3.4	(9)
10 Membrane receptors & channels	(171)	10.4	(20)	4.1	(6)	8.9	(17)	4.9	(13)
11 Mitochondrial proteins	(26)	0.5	(1)	0.7	(1)	0.5	(1)	0.8	(2)
12 Other metabolism	(70)	3.0	(6)	2.7	(4)	1.6	(3)	3.4	(9)
13 Other nuclear proteins	(64)	1.6	(3)	0.7	(1)	1.1	(2)	1.5	(4)
14 Proteasome	(89)	3.1	(6)	2.7	(4)	4.2	(8)	3.4	(9)
15 Protein kinases & phosphatases	(255)	14.6	(28)	13	(19)	10.5	(20)	9.1	(24)
16 Protein processing	(19)	0.5	(1)	0.0	-	0.5	(1)	0.4	(1)
17 Secretory proteins	(22)	1.6	(3)	0.0	-	1.1	(2)	0.0	-
18 Signalling & adapter proteins	(411)	15.6	(30)	13	(19)	14.2	(27)	19.0	(50)
19 Small GTPases & regulators	(290)	8.9	(17)	14.4	(21)	11.1	(21)	11.4	(30)
20 Transcription & translation	(151)	5.2	(10)	6.2	(9)	4.2	(8)	5.7	(15)
21 Unknown & other platelet proteins	(199)	8.9	(17)	9.6	(14)	10.0	(19)	8.4	(22)
22 Extracellular plasma proteins	(22)	2.6	(5)	0.7	(1)	0.5	(1)	0.0	-
Total	(2,516)	100	(192)	100	(146)	100	(190)	100	(263)

As further confirmation we evaluated how many of altered phosphopeptides contained a PKA consensus site. Histograms indicated a highly significant increase in mean NAVs after stimulation with 2 or 10 nM iloprost ($P < 0.0001$) for those phosphopeptides with PKA consensus site *versus* no such site (Suppl. Figure 3A). When comparing control and patient platelets, we found a moderate to strong reduction in altered proteins with PKA consensus site for patients P1,2,4,6 (Suppl. Figure 3B). Again, platelets from P7 were deviant in showing an *increase* in peptides with PKA consensus site. Taken together, these data indicated that the platelets from P1,2,4,6 and to a lesser

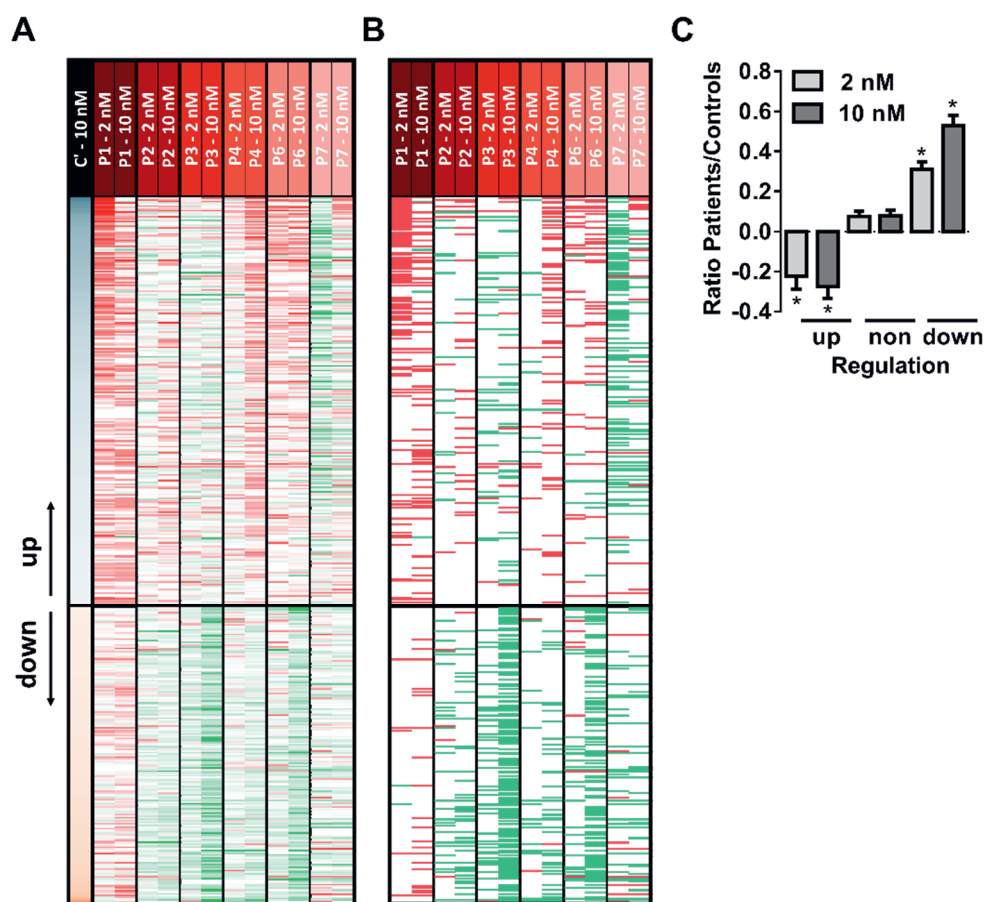


Figure 5. Iloprost-induced changes in phosphoproteome of platelets from patients with suspected PHP Ia. **A**, Heatmap of 453 platelet phosphopeptides identified as increased (green) or decreased (red) at indicated iloprost concentration per patient in comparison to mean effect in 3 or 4 control subjects (C1-4, C'). Left lane: mean effect of 10 nM iloprost in control platelets (see Figure 4A). **B**, Heatmap as in panel A, but restricted to relevant differences, filtered for outside control range of log₂ 2x (-0.322 to +0.322). **C**, Average ratios of iloprost effects in platelets from selected patients (P1-4,6) versus control subjects (C1-4) regarding top-100 up-, non-, and downregulated phosphopeptides. *P < 0.05 vs. controls (2-sided t-test).

Table 3. Relevant changes in iloprost upregulated phosphopeptides in platelets from individual patients. Phosphopeptides classified as upregulated by 2 nM (146) or 10 nM (263) iloprost, and compared per patient (P1-4,6,7) versus mean values of controls (C', C1-4). As relevant changes were considered all ratios outside the normal range of log2 2x (-0.322 to +0.322). Listed per patient are numbers of phosphopeptides lower or higher than normal ranges. Colour code of upregulated phosphopeptides: red, decreased compared to controls; white, unchanged; green, increased.

	Iloprost upregulated					
	Lower than C'		Higher than C'		Net difference	
	2 nM	10 nM	2 nM	10 nM	2 nM	10 nM
P1	96	64	0	4	96	60
P2	7	27	17	3	-10	24
P3	5	12	29	35	-24	-23
P4	6	55	8	2	-2	53
P6	25	34	4	8	21	26
P7	5	19	103	40	-98	-21

extent from P3, responded different in iloprost-induced phosphorylation response, when compared to control platelets.

Defining patterns of phosphoproteome changes by iloprost

To find specific patterns of phosphorylation changes, we listed those phosphopeptides with PKA consensus site that were most consistently changed in the patient platelets (see Table 4). Here, most pronounced phosphorylation defects were seen for patients P1,2,4,6 and lesser changes for P3. In contrast, multiple phosphopeptides were increased in patient P7, when compared to control platelets.

Table 4. Overview of altered $G_{s\alpha}$ -dependent changes in platelet function and proteome of investigated patients. Indicated are altered responses to iloprost or PGE_1 per patient (P1-7), in comparison to control subjects on: (1) VASP Ser293 phosphorylation; (2) platelet aggregation by collagen-induced LTA; (3) microfluidic whole-blood thrombus formation; (4) global platelet proteome; (5) platelet phosphoproteome; (6) PKA phosphorylation sites. Colour code: red, decreased in comparison to controls; yellow, unchanged; green, increased; white, not determined. Last columns show clinical diagnosis regarding AHO and confirmed mutation in GNAS.

	Platelet function			Platelet proteome			Patient characteristics	
	VASP-P	LTA	Thrombus	Global	Phospho	PKA	PHP	Mutation
P1	-	-	-	o	--	--	PHP Ia (AHO)	Met1Val
P2	-		-	o	-	-	PHP Ia (AHO)	Lys338Asn
P3	-		-	o	o	-	PHP Ia (AHO)	Lys338Asn
P4	-		-	o	--	-	PHP Ia (AHO)	Lys338Asn
P5	o	o	o				(asymptomatic)	not found
P6	-	-	--	o	--	--	PHP Ia (AHO)	not found
P7	o			o	+	+	suspected (non-AHO)	deletion

Discussion

This paper reveals a set of dysfunctional $G_{s\alpha}$ -mediated responses in platelets from seven rare patients with established or suspected PHP Ia (Albright hereditary osteodystrophy, AHO), *i.e.* VASP phosphorylation, aggregation, and microfluidic thrombus formation. In all cases, the patient platelets were compared with day-control platelets from healthy control donors. These functional defects of platelets to $G_{s\alpha}$ stimuli (iloprost, PGE_1) appeared to be accompanied by a consistent set of changes in the platelet protein phosphorylation pattern. Table 4 compares our findings for the five patients with confirmed PHP Ia (AHO), the asymptomatic family member P5 and the atypical patient P7.

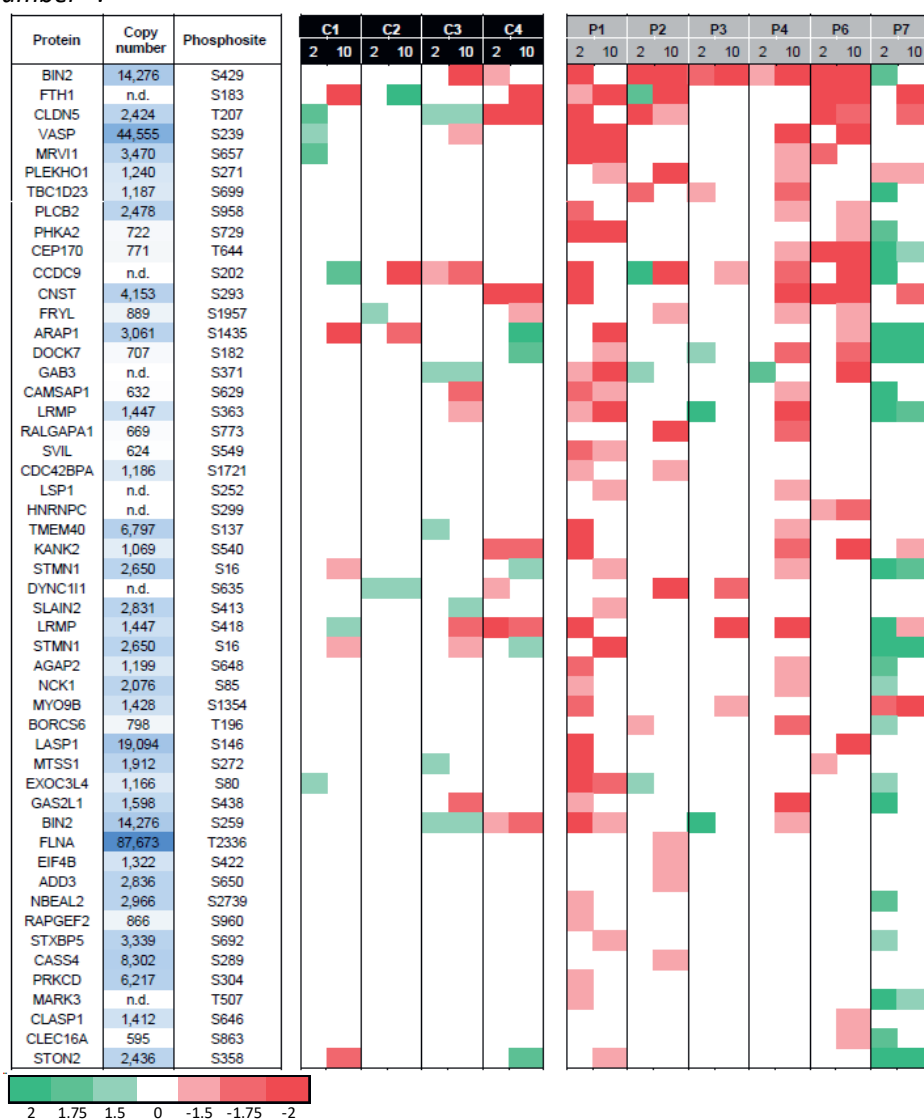
Patients with PHP-related disorders present with characteristic phenotypic

features, such as a short stature and brachydactyly, but diagnosis only by physical examination is notoriously difficult. Genetic screening is usually performed to confirm a maternally inherited mutation in the *GNAS* complex locus or to find a possible epigenetic defect²⁸. If positive, the molecular characterisation PHP Ia is made, matching the clinical phenotype of AHO (OMIM: #103580). On the other hand, in the related disorder pseudopseudohypoparathyroidism (PPHP), mutations in the *GNAS* locus occur, which are usually paternally inherited and are designated as non-AHO. Molecular diagnosis of these syndromes is further complicated, as an AHO phenotype can also be accompanied by normal or hyper-activity of the G α s protein²⁹. Because of this complexity, platelet phenotyping for aberrant G α s activity may assist in diagnosis.

In platelets, the G α s-AC-PKA pathway, induced by endothelial prostacyclin (prostaglandin I₂), is a main mechanism by which the vessel wall prevents activation^{11,12}. Accordingly, iloprost or PGE₁ addition to platelets - similarly to PKA inhibition - potently suppresses agonist-induced responses including Ca²⁺ fluxes, integrin activation, adhesion, secretion, aggregation and thrombus formation^{15,30}. Since the early recognition that the platelet inactivation is controlled by PKA-dependent phosphorylation³¹, extensive analyses have been performed to characterize the iloprost-induced phosphoproteome^{19,32}. The present paper provides a first report to extend this work to patients with suspected G α s defects, in order to explore how this technology can aid in new biomarker finding and diagnosis^{20,21}.

As indicated in overview Table 4, the investigated patients P1-4 (families I and II), with typical characteristics and maternal inheritance of a mutation in the *GNAS* locus, were all diagnosed as AHO. In family III, unlike the unaffected mother patient P5, patient P6 (child) with typical characteristics also obtained the ad-hoc diagnosis of AHO, although no mutation in *GNAS* was found (epigenetic analysis not yet performed). Patient P7 (family IV) was originally suspected for PHP Ia, as genetic screening revealed a heterozygous deletion mutation in *GNAS*. However, paternal inheritance is suspected, but

Table 5. Shortlist of major PKA-dependent changes in iloprost-upregulated phosphoproteome in platelets from individual patients. Identified iloprost-upregulated phosphopeptides with PKA consensus site and altered in platelets from indicated patients, in comparison to mean of controls (C'), with medium to strong effect size (Cohen's $d > 0.5$). Colour bar: phosphopeptides that are fold decreased (red) or increased (green) compared to C', for individual control subjects (C1-4) and patients (P1-4,6,7). Per phospho-site are indicated gene name and protein copy number¹⁸.



not proven, which has led to a diagnosis of non-AHO. Markedly, our platelet phosphoproteome analysis is in accordance with a non-AHO phenotype.

Table 4 furthermore indicates overall consistency of impairments in the various G α s-dependent platelet function tests, with respect to the blood samples from patients P1-4 and P6, when compared to day-control subjects. In the patient platelets, we noted an overall dysfunctional iloprost-induced VASP phosphorylation on Ser²³⁹, as a standard assay to check for G α s-AC-PKA signaling^{33, 34}. Furthermore, for the same patients P1-4,6, we detected a dysfunctional response to PGE₁ and iloprost, in terms of parameters of thrombus formation. Of note, due to the limited available blood samples, LTA could only be performed for two patients as a confirmation of this dysfunction. On the other hand, for patient P5 (unremarkably phenotype, mother of P6) and patient P7 (concluded as non-AHO), the performed platelet function tests were within normal ranges.

For platelets from six of the patients (P1-4,6-7) we measured the iloprost-induced phosphoproteome as an alternative way to detect abnormalities in the G α s-AC-PKA pathway. Therefore, we aimed to quantify per patient: (1) the overall changes in iloprost-induced protein phosphorylation patterns in patients versus controls; (2) the changes that can be linked to PKA dependent phosphorylation; and (3) shortlist of consistently changed phosphoproteins.

In the five patients with established AHO (P1,2-4,6), we noticed a dose-dependent increase in upregulated, but not in downregulated phosphopeptides in response to iloprost (Table 5). Shortlisting these events to phosphopeptides with a PKA consensus site, we found that the platelets from four patients (P1,2,4,6) had a relatively large impairment in G α s-AC-PKA dependent phosphorylation. In the platelets from P3, the aberrations were limited, while in the platelets from (non-AHO) P7 an increased, rather than decreased phosphorylation pattern was seen. This corroborated the findings on platelet functions. An unanswered question is why the platelets from P3 showed more subtle differences in G α s-dependent phosphorylation

than the platelets from family members P2,4 (all carrying the same *GNAS* mutation). This may be due to different thresholds in dose and time for $G\alpha s$ -AC-PKA stimulation in the platelets from P3.

Reactome pathway analysis pointed to similar iloprost-induced changes in platelet functions, when evaluating the upregulated or the downregulated phosphoproteins. In either case, identified (sub)pathways were those of signal transduction, haemostasis, cell-cell interactions, and platelet activation. Jointly, this supports the presence of a coordinated mechanism of iloprost-induced platelet inhibition: directly mediated via PKA, and indirectly via a network of protein kinases as well as protein phosphatases³². Regarding the identified altered PKA-dependent phosphorylation events in confirmed AHO patients, several of the regulated proteins are of key importance for platelet signaling. These include the phospholipase C- $\beta 2$ isoform (PLC $\beta 2$); vasodilator-stimulated phosphoprotein (VASP) and the inositol-phosphate receptor regulator MRVI1³⁴. In addition, phosphorylated proteins were listed that control platelet shape change, including a myosin isoform (MYO9B) and the tight junction protein claudin-5 (CLDN5). Differentially regulated also were the regulatory subunit RII β (PRKAR2B) of the PKA-II holoenzyme, as well as BIN2, a protein with unknown function, but previously recognised as one of the most strongly regulated proteins in PKA signaling¹⁹.

The current data are in support of the use of platelet phosphoproteomics in the diagnosis of AHO and related diseases, for instance by checking a panel of biomarker phosphorylation sites as in Table 5. However, it should also be mentioned that the mass spectrometric technique is expensive and requires trained personnel. On the other hand, the consistent, but still variable changes in the phosphoproteomes of multiple patients argues for a more extensive set of biomarker tests than only an anti-phospho VASP antibody.

Altogether, this work demonstrates an overall similarity in $G\alpha s$ -AC-PKA mediated aberrations between functional responses and quantitative phosphoproteomics of platelets from patients with confirmed PHP Ia (AHO).

The findings of aberrant upregulated as well as downregulated phosphopeptides in patients point to a change in the network of key protein kinases (starting from PKA) and phosphatases, which regulate multiple platelet functional properties.

Acknowledgements

This research was supported by the Ministerium für Innovation, Wissenschaft und Forschung from Nordrhein-Westfalen, the Cardiovascular Centre (HVC) of Maastricht University Medical Centre⁺, the Centre for Molecular Translational Medicine (INCOAG, MICRO-BAT), the German Federal Ministry of Education and Research (BMBF 01EO1503) and the Deutsche Forschungsgemeinschaft (ZA 639/4-1 and JU 2735/2-1). FS was supported by the Alexander von Humboldt Foundation. This work also received funding from the European Union's Horizon 2020 research and innovation program under Marie Skłodowska-Curie grant agreement TAPAS No. 766118. JH is enrolled in a joint doctoral program of the universities of Maastricht (The Netherlands) and Santiago de Compostela (Spain).

Conflict of interest

JWMH is co-founder and shareholder of FlowChamber. Other authors declare no conflicts of interest.

Supplementary information

Supplementary information is available for this paper at <https://doi.org/10.1038/s41598-020-68379-3>.

ProteomeXchange repository PXD016534.

References

1. Mantovani G. Pseudohypoparathyroidism: diagnosis and treatment. *J Clin Endocrinol Metab.* 2011;96:3020-3030.

2. Mantovani G, Bastepe M, Monk D, de Sanctis L, Thiele S, Usardi A et al. Diagnosis and management of pseudohypoparathyroidism and related disorders: first international Consensus Statement. *Nat Rev Endocrinol*. 2018;14:476-500.
3. Kozasa T, Itoh H, Tsukamoto T and Kaziro Y. Isolation and characterization of the human Gs alpha gene. *Proc Natl Acad Sci USA*. 1988;85:2081-2085.
4. Peters J and Williamson CM. Control of imprinting at the Gnas cluster. *Epigenetics*. 2007;4:207-213.
5. International Consortium for Blood Pressure Genome-Wide Association Studies, Ehret GB, Munroe PB, Rice KM, Bochud M, Johnson AD et al. Genetic variants in novel pathways influence blood pressure and cardiovascular disease risk. *Nature*. 2011;478:103-109.
6. Hayward BE, Barlier A, Korbonits M, Grossman AB, Jacquet P, Enjalbert A et al. Imprinting of the Gsa gene GNAS1 in the pathogenesis of acromegaly. *J Clin Invest*. 2001;107:R21-R36.
7. Rochtus A, Martin-Trujillo A, Izzi B, Elli F, Garin I, Linglart A et al. Genome-wide DNA methylation analysis of pseudohypoparathyroidism patients with GNAS imprinting defects. *Clin Epigenetics*. 2016;8:e10.
8. Wettschureck N and Offermanns S. Mammalian G proteins and their cell type specific functions. *Physiol Rev*. 2005;85:1159-1204.
9. Tasken K and Aandahl EM. Localized effects of cAMP mediated by distinct routes of protein kinase A. *Physiol Rev*. 2004;84:137-167.
10. Rex S and Freedman JE. Inhibition of platelet function by the endothelium. In: *Platelets* (Ed A D Michelson, Elsevier, Amsterdam, The Netherlands). 2007:pp. 251-279.
11. Versteeg HH, Heemskerk JW, Levi M and Reitsma PS. New fundamentals in hemostasis. *Physiol Rev*. 2013;93:327-358.
12. Van der Meijden PE and Heemskerk JW. Platelet biology and functions: new concepts and future clinical perspectives. *Nat Rev Cardiol*. 2019;16:166-179.
13. Whittle BJ, Silverstein AM, Mottola DM and Clapp LH. Binding and activity of the prostacyclin receptor (IP) agonists, treprostinil and iloprost, at human prostanoid receptors: treprostinil is a potent DP1 and EP2 agonist. *Biochem Pharmacol*. 2012;84:68-75.

14. Swieringa F, Kuijpers MJ, Heemskerk JW and Van der Meijden PE. Targeting platelet receptor function in thrombus formation: the risk of bleeding. *Blood Rev.* 2014;28:9-21.
15. Feijge MA, Ansink K, Vanschoonbeek K and Heemskerk JW. Control of platelet activation by cyclic AMP turnover and cyclic nucleotide phosphodiesterase type-3. *Biochem Pharmacol.* 2004;67:1559-1567.
16. Vanschoonbeek K, Feijge MA, Van Kampen RJ, Kenis H, Hemker HC, Giesen PL et al. Initiating and potentiating role of platelets in tissue factor-induced thrombin generation in the presence of plasma: subject-dependent variation in thrombogram characteristics. *J Thromb Haemost.* 2004;2:476-484.
17. Freson K, Izzi B, Labarque V, Van Helvoirt M, Thys C, Wittevrongel C et al. GNAS defects identified by stimulatory G protein alpha-subunit signaling studies in platelets. *J Clin Endocrinol Metab.* 2008;93:4851-4859.
18. Burkhardt JM, Vaudel M, Gambaryan S, Radau S, Walter U, Martens L et al. The first comprehensive and quantitative analysis of human platelet protein composition allows the comparative analysis of structural and functional pathways. *Blood.* 2012;120:e73-e82.
19. Beck F, Geiger J, Gambaryan S, Veit J, Vaudel M, Nollau P et al. Time-resolved characterization of cAMP/PKA-dependent signaling reveals that platelet inhibition is a concerted process involving multiple signaling pathways. *Blood.* 2014;123:e1-e10.
20. Burkhardt JM, Gambaryan S, Watson SP, Jurk K, Walter U, Sickmann A et al. What can proteomics tell us about platelets? *Circ Res.* 2014;114:1204-1219.
21. Loosse C, Swieringa F, Heemskerk JW and Sickmann A. Platelet proteomics: from discovery to diagnosis. *Exp Rev Proteomics.* 2018;15:467-476.
22. Schwarz UR, Geiger J, Walter U and Eigenthaler M. Flow cytometry analysis of intracellular VASP phosphorylation for the assessment of activating and inhibitory signal transduction pathways in human platelets: definition and detection of ticlopidine/clopidogrel effects. *Thromb Haemost.* 1999;82:1145-1152.
23. Dawood BB, Lowe GC, Lordkipanidze M, Bern D, Daly ME, Makris M et al. Evaluation of participants with suspected heritable platelet function disorders including recommendation and validation of a streamlined agonist panel. *Blood.* 2012;120:5041-5049.

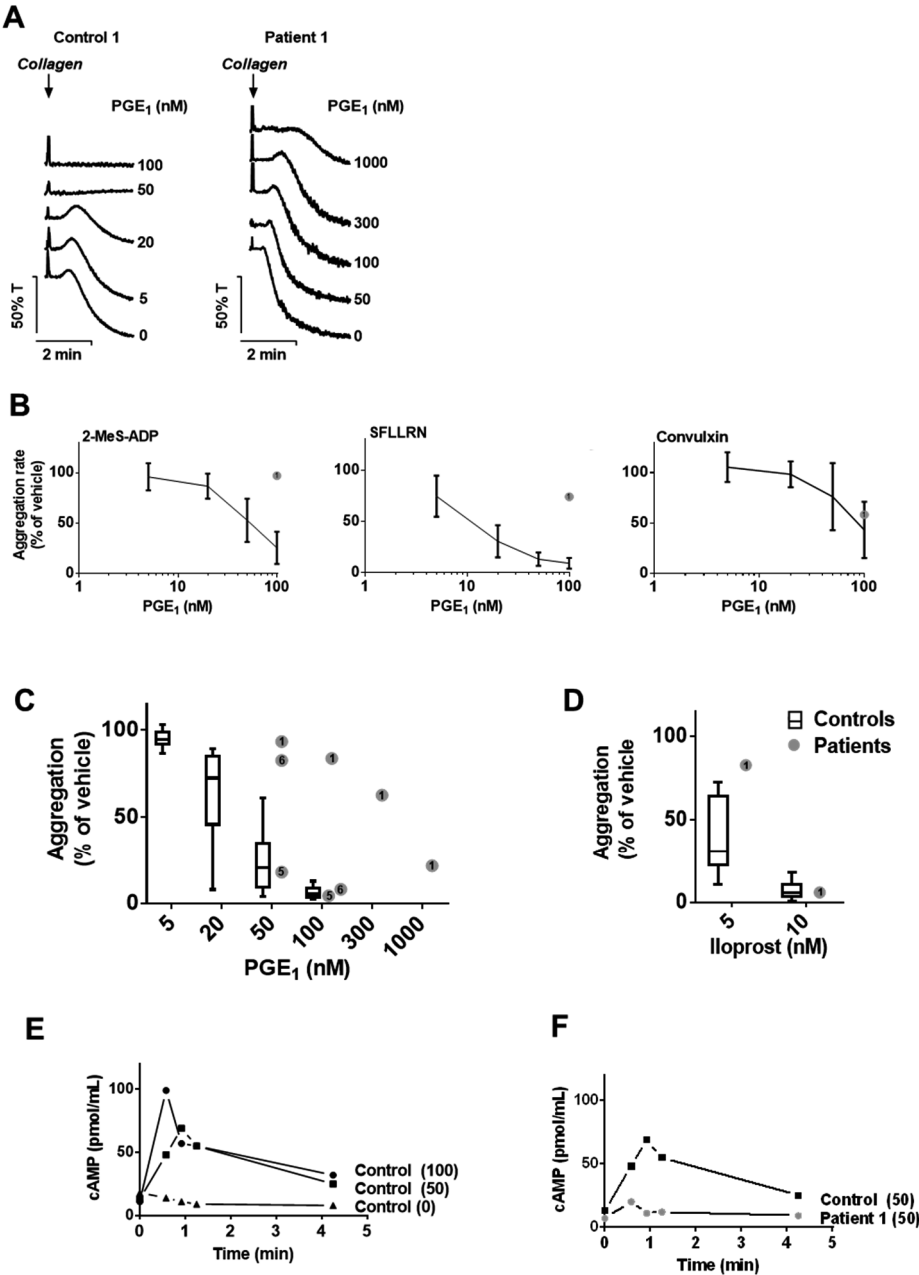
24. Van Geffen JP, Brouns S, Batista J, McKinney H, C. K, Sivapalaratnam S et al. High-throughput elucidation of thrombus formation reveals sources of platelet function variability. *Haematologica*. 2019;104:1256-1267.
25. De Witt SM, Swieringa F, Cavill R, Lamers MM, Van Kruchten R, Mastenbroek T et al. Identification of platelet function defects by multi-parameter assessment of thrombus formation. *Nat Commun*. 2014;5:#4257.
26. Nagy M, Mastenbroek TG, Mattheij NJ, de Witt S, Clemetson KJ, Kirschner J et al. Variable impairment of platelet functions in patients with severe, genetically linked immune deficiencies. *Haematologica*. 2018;103:540-549.
27. Solari FA, Mattheij NJ, Burkhart JM, Swieringa F, Collins PW, Cosemans JM et al. Combined quantification of the global proteome, phosphoproteome, and proteolytic cleavage to characterize altered platelet functions in the human Scott syndrome. *Mol Cell Proteomics*. 2016;15:3154-3169.
28. Elli FM, de Sanctis L, Bollati V, Tarantini L, Filopanti M, Barbieri AM et al. Quantitative analysis of methylation defects and correlation with clinical characteristics in patients with pseudohypoparathyroidism type I and GNAS epigenetic alterations. *J. Clin. Endocrinol. Metab*. 2014;99:e508-e517.
29. Izzi B, de Zegher F, Francois I, del Favero J, Goossens D, Wittevrongel C et al. No evidence for GNAS copy number variants in patients with features of Albright's hereditary osteodystrophy and abnormal platelet Gs activity. *J Hum Genet*. 2012;57:277-9.
30. Aburima A, Wraith KS, Raslan Z, Law R, Magwenzi S and Naseem KM. cAMP signaling regulates platelet myosin-light chain (MLC) phosphorylation and shape change through targeting the Rho-A-Rho kinase-MLC phosphatase signaling pathway. *Blood*. 2013;122:3533-3545.
31. Siess W and Lapetina EG. Functional relationship between cyclic AMP-dependent protein phosphorylation and platelet inhibition. *Biochem J*. 1990;271:815-819.
32. Beck F, Geiger J, Gambaryan S, Solari FA, Dell'Aica M, Loroch S et al. Temporal quantitative phosphoproteomics of ADP stimulation reveals novel central nodes in platelet activation and inhibition. *Blood*. 2017;129:e1-e12.
33. Gambaryan S, Kobsar A, Rukoyatkina N, Herterich S, Geiger J, Smolenski A et al. Thrombin and collagen induce a feedback inhibitory signaling pathway in platelets involving dissociation of the catalytic subunit of protein kinase A from an NFkappaB-IkappaB complex. *J Biol Chem*. 2010;285 18352-18363.

34. Smolenski A. Novel roles of cAMP/cGMP-dependent signaling in platelets. *J Thromb Haemost.* 2012;10:167-176.
35. Gilio K, Munnix IC, Mangin P, Cosemans JM, Feijge MA, Van der Meijden PE et al. Non-redundant roles of phosphoinositide 3-kinase isoforms alpha and beta in glycoprotein VI-induced platelet signaling and thrombus formation. *J Biol Chem.* 2009;284:33750-33762.
36. Klaassens M, Blom EW, Schrander JJ, Ris-Stalpers C, Nieuwenhuijzen Kruseman AC, van Steensel MA et al. Unique skin changes in a case of Albright hereditary osteodystrophy caused by a rare GNAS1 mutation. *Br. J Dermatol.* 2010;162:690-694.
37. Patten JL, Johns DR, Valle D, Eil C, Gruppuso PA, Steele G et al. Mutation in the gene encoding the stimulatory G protein of adenylate cyclase in Albright's hereditary osteodystrophy. *N. Engl. J. Med.* 1990;322:1412-1419.
38. Pohlenz J, Ahrens W and Hiort O. A new heterozygous mutation (L338N) in the human Gsalpha (GNAS1) gene as a cause for congenital hypothyroidism in Albright's hereditary osteodystrophy. *Eur J Endocrinol.* 2003;148:463-468.
39. Gilio K, Van Kruchten R, Braun A, Berna-Erro A, Feijge MAH, Stegner D et al. Roles of STIM1 and Orai1 in glycoprotein VI- and thrombin-dependent procoagulant activity and thrombus formation. *J Biol Chem.* 2010;285:23629-23638.
40. Keularts IM, Van Gorp RM, Feijge MA, Vuist MW and Heemskerk JW. α_2A -Adrenergic receptor stimulation potentiates calcium release in platelets by modulating cAMP levels. *J Biol Chem.* 2000;275:1763-1772.
41. Van Kruchten R, Cosemans JM and Heemskerk JW. Measurement of whole blood thrombus formation using parallel-plate flow chambers: a practical guide. *Platelets.* 2012;23:229-242.
42. Swieringa F, Kuijpers MJ, Lamers MM, Van der Meijden PE and Heemskerk JW. Rate-limiting roles of tenase complex of factors VIII and IX in platelet procoagulant activity and formation of platelet-fibrin thrombi under flow. *Haematologica.* 2015;100:748-756.
43. Engholm-Keller K, Birck P, Storling J, Pociot F, Mandrup-Poulsen T and Larsen MR. TiSH: a robust and sensitive global phosphoproteomics strategy employing a combination of TiO₂, SIMAC, and HILIC. *J Proteomics.* 2012;75:5749-5761.

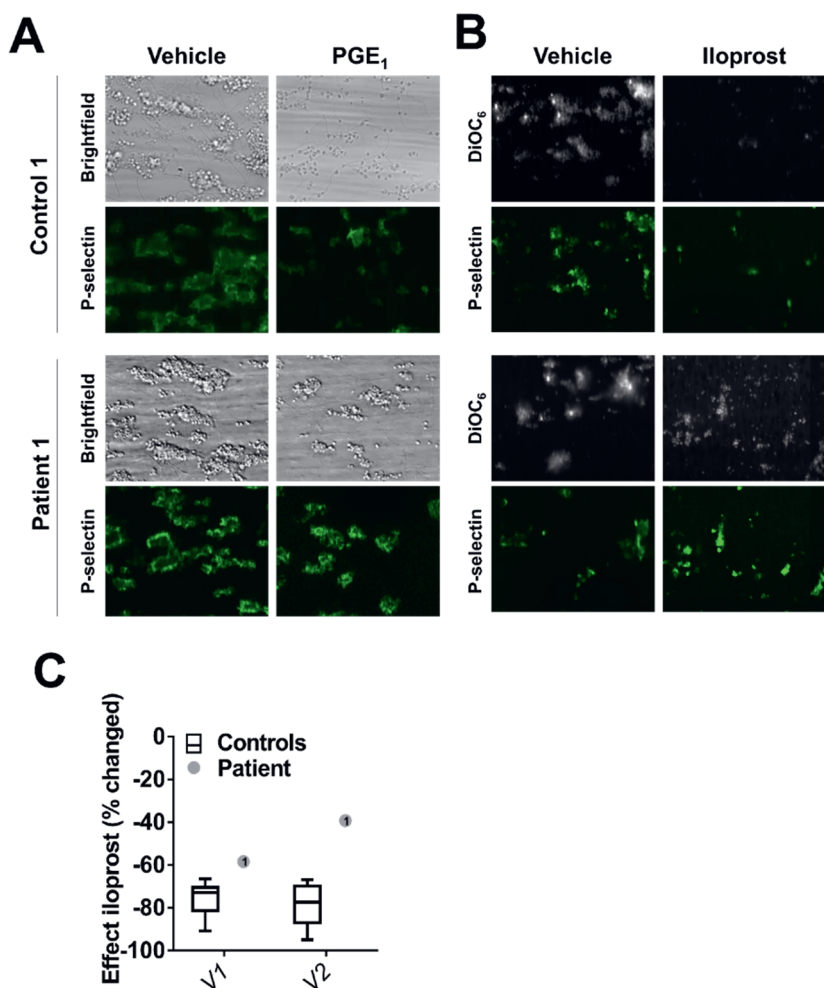
44. Vaudel M, Burkhardt JM, Radau S, Zahedi RP, Martens L and Sickmann A. Integral quantification accuracy estimation for reporter ion-based quantitative proteomics (iQuARI). *J Proteome Res.* 2012;11:5072-5080.
45. Burkhardt JM, Schumbrutski C, Wortelkamp S, Sickmann A and Zahedi RP. Systematic and quantitative comparison of digest efficiency and specificity reveals the impact of trypsin quality on MS-based proteomic. *J Proteomics.* 2012;75:1454-1562.
46. Manza LL, Stamer SL, Ham AJ, Codreanu SG and Liebler DC. Sample preparation and digestion for proteomic analyses using spin filters. *Proteomics.* 2005;5:1742-1745.
47. Wisniewski JR, Zougman A and Mann M. Combination of FASP and StageTip-based fractionation allows in-depth analysis of the hippocampal membrane proteome. *J Proteome Res.* 2009;8:5674-5678.
48. Burkhardt JM, Schumbrutski C, Wortelkamp S, Sickmann A and Zahedi RP. Systematic and quantitative comparison of digest efficiency and specificity reveals the impact of trypsin quality on MS-based proteomics. *J Proteomics.* 2012;75:1454-1462.
49. Dickhut C, Radau S and Zahedi RP. Fast, efficient, and quality-controlled phosphopeptide enrichment from minute sample amounts using titanium dioxide. *Methods Mol. Biol.* 2014;1156:417-30.
50. Larsen MR, Graham ME, Robinson PJ and Roepstorff P. Improved detection of hydrophilic phosphopeptides using graphite powder microcolumns and mass spectrometry: evidence for in vivo doubly phosphorylated dynamin I and dynamin III. *Mol Cell Proteomics.* 2004;3:456-465.
51. Thingholm TE, Palmisano G, Kjeldsen F and Larsen MR. Undesirable charge-enhancement of isobaric tagged phosphopeptides leads to reduced identification efficiency. *J Proteome Res.* 2010;9:4045-4052.
52. Taus T, Kocher T, Pichler P, Paschke C, Schmidt A, Henrich C et al. Universal and confident phosphorylation site localization using phosphoRS. *J Proteome Res.* 2011;10:5354-5362.
53. Xue Y, Ren J, Gao X, Jin C, Wen L and Yao X. GPS 2.0, a tool to predict kinase-specific phosphorylation sites in hierarchy. *Mol Cell Proteomics.* 2008;7:1598-1608.

Supplementary materials of Chapter 5

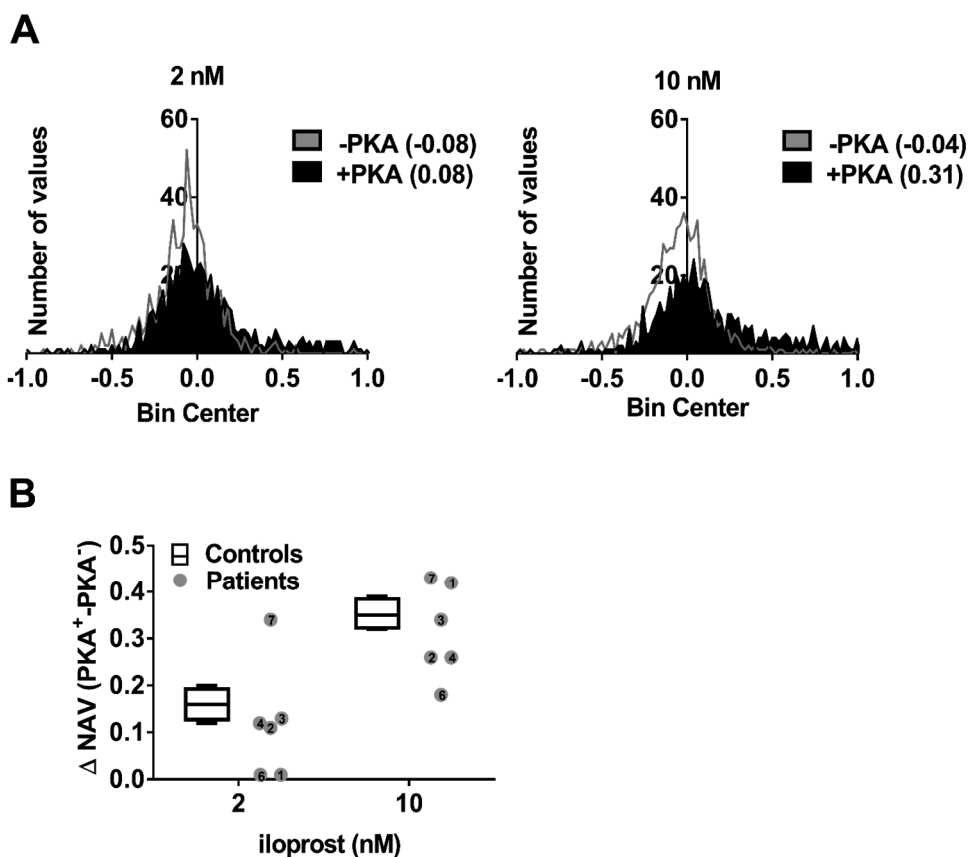
Supplementary figures and tables of Chapter 5



Suppl. Figure 1. See upper page. Impaired Gas-mediated inhibition of aggregation and cAMP rise in platelets from patients with PHP Ia. Platelet-rich plasma was preincubated with vehicle or indicated concentration of PGE₁ or iloprost (in nM) for 4 min. **A**, Representative aggregation traces of platelets from day control subject C1 and patient P1. **B**, Effect for of PGE₁ on aggregation rate with Me-ADP (5 μM), SFLLRN (15 μM) or convulxin (10 ng/mL). Data from C1-10 and P1. **C**, **D**, Dose-dependent effect of PGE₁ (**C**) or iloprost (**D**) on platelet aggregation rate for controls C1-10 and patients P1,5,6. Box plots indicate medians ± interquartile ranges (whiskers represent 2.5-97.5th percentiles, n = 10). **E**, **F**, Transient effect of PGE₁ (nM) on cAMP level in washed platelets from control C1 (**E**) and patient P1 (**F**).



Suppl. Figure 2. Impaired Gas-mediated inhibition of thrombus formation in patient P1. Blood samples from control subject (C1) and patient (P1) were perfused over collagen, and brightfield or fluorescence microscopic images were captured, as in Figure 2. Samples were preincubated with vehicle, PGE₁ (100 nM) or iloprost (10 nM), as indicated. **A, B,** Representative brightfield and fluorescence images (FITC anti-P-selectin mAb, DiOC₆-labelled platelets), illustrating effects of PGE₁ and iloprost. **C,** Quantitative effect of iloprost on parameters V1 (platelet adhesion) and V2 (P-selectin expression) for all control subjects (C1-8) and patient (P1). Medians \pm interquartile ranges (whiskers represent 2.5-97.5th percentiles, $n = 8$).



Suppl. Figure 3. Altered iloprost effect on PKA-mediated phosphorylation in patient platelets. **A**, Histograms of normalised abundance values (NAVs) for all phosphopeptides identified in control platelets (C', C1-4), illustrating the effects of 2 or 10 nM iloprost. Phosphopeptides were separated according to the absence (PKA⁻) or presence (PKA⁺) of PKA consensus site. **B**, Mean difference of NAVs for PKA⁺ and PKA⁻ phosphopeptides, shown for platelets from controls (medians \pm interquartile ranges) and from patients P1-4,6,7.

Suppl. Table 1. Sample sets for patients and corresponding day controls used for (phospho)proteome analysis. Sets of platelet samples from controls (C) and patients (P) simultaneously assessed. Indicated samples were combined per set I-IV for iTRAQ labelling (8-plex) or TMT labelling (10-plex). Platelets from P5 were not available for this analysis.

Set	Subjects	Conditions	Label	Calibration	# Samples
I	C1, P1	0, 1, 2, 10 nM iloprost	iTRAQ	no	2 x 4
II	C4, P7	0, 2, 5, 10 nM iloprost	iTRAQ	no	2 x 4
III	C2, P2, P6	0, 2, 10 nM iloprost	TMT	yes	3 x 3 + 1
IV	C3, P3, P4	0, 2, 10 nM iloprost	TMT	yes	3 x 3 + 1

Suppl. Table 2. Reactome pathway analysis of 196 iloprost-upregulated (up) and 159 iloprost-downregulated (down) phosphoproteins (entities). Indicated are Reactome pathway identifiers; pathway names; entities identified as up- or downregulated; total numbers of entities in pathway; numbers of identified interactors per pathway; mean false discovery rate (FDR) based on null hypothesis of unchanged; numbers of reactions in Reactome; and mean numbers of phosphosites (weight) per pathway. Shown are top 62 pathways (Σ entities + interactors) with FDR<0.16. Pathways in bold are relevant for platelet activation and inhibition.

Pathway identifier	Pathway name	#Entities found up	#Entities found down	#Entities total	#Interactors found up	#Interactors found down	Entities FDR u/d	#Reactions found up	#Reactions found down	#Weight u/d
R-HSA-162582	Signal Transduction	51	44	3303	113	83	0.01	652	453	1.4
R-HSA-168256	Immune System	46	36	2822	60	79	0.01	381	305	1.3
R-HSA-1280215	Cytokine Signaling in Immune system	19	17	1261	67	20	0.01	192	23	1.3
R-HSA-1266738	Developmental Biology	17	21	1207	47	38	0.01	132	142	1.3
R-HSA-1643685	Disease	11	14	1552	52	46	0.01	148	153	1.3
R-HSA-392499	Metabolism of proteins	10	16	2354	47	39	0.01	95	103	1.2
R-HSA-449147	Signaling by Interleukins	11	8	639	58	29	0.01	134	59	1.3
R-HSA-168249	Innate Immune System	23	19	1328	28	33	0.01	130	151	1.2
R-HSA-74160	Gene expression (Transcription)	7	3	1822	51	38	0.01	110	85	1.4
R-HSA-73857	RNA Polymerase II Transcription	7	3	1664	51	37	0.01	107	83	1.4
R-HSA-9006934	Signaling by Receptor Tyrosine Kinases	16	8	553	39	34	0.01	281	135	1.4
R-HSA-422475	Axon guidance	16	19	584	36	25	0.11	111	101	1.3
R-HSA-212436	Generic Transcription Pathway	7	3	1525	50	35	0.01	101	80	1.4
R-HSA-109582	Hemostasis	22	2	821	34	33	0.11	82	78	1.3
R-HSA-1430728	Metabolism	24	4	3636	30	25	0.01	102	86	1.3
R-HSA-597592	Post-translational protein modification	7	9	1592	35	32	0.01	71	63	1.1
R-HSA-372790	Signaling by GPCR	13	13	1484	30	26	0.01	66	56	1.3
R-HSA-5653656	Vesicle-mediated transport	18	20	824	19	25	0.13	83	82	1.2
R-HSA-1280218	Adaptive Immune System	14	11	999	28	27	0.01	64	65	1.3
R-HSA-199991	Membrane Trafficking	17	19	665	19	25	0.13	79	80	1.2
R-HSA-388396	GPCR downstream signalling	13	13	1358	26	21	0.01	59	47	1.2
R-HSA-76002	Platelet signaling and aggregation	10	10	293	25	22	0.15	46	47	1.4
R-HSA-5663202	Diseases of signal transduction	10	8	484	25	19	0.02	92	82	1.4
R-HSA-73887	Death Receptor Signalling	6	4	157	20	20	0.01	23	23	1.2
R-HSA-556833	Metabolism of lipids	8	2	1445	19	19	0.01	56	65	1.3
R-HSA-5663205	Infectious disease	1	7	540	21	17	0.01	40	54	1.1
R-HSA-2682334	EPH-Ephrin signaling	4	7	101	19	15	0.11	46	44	1.3
R-HSA-4420097	VEGFA-VEGFR2 Pathway	5	4	126	18	17	0.1	48	28	1.2
R-HSA-9006925	Intracellular signaling by second messenger	8	3	362	14	17	0.01	39	17	1.3
R-HSA-354192	Integrin alphaIIb beta3 signaling	5	2	39	14	19	0.15	21	21	1.4
R-HSA-9006921	Integrin signaling	5	2	39	19	14	0.15	21	21	1.4
R-HSA-1640170	Cell Cycle	8	4	682	19	8	0.01	82	68	1.2
R-HSA-373752	Netrin-1 signaling	4	3	59	14	17	0.12	16	10	1.4
R-HSA-166520	Signaling by NTRKs	5	0	118	15	16	0.02	40	14	1.3
R-HSA-109581	Apoptosis	4	5	189	15	11	0.02	22	18	1.2

Suppl. Table2. (to next page)

R-HSA-8953897	Cellular responses to external stimuli	9	7	586	15	4	0.01	51	25	1.2
R-HSA-5357801	Programmed Cell Death	4	5	197	15	11	0.02	22	18	1.1
R-HSA-418594	G alpha (i) signalling events	5	5	566	14	10	0.01	26	16	1.4
R-HSA-3700989	Transcriptional Regulation by TP53	4	1	486	19	10	0.01	34	15	1.3
R-HSA-382551	Transport of small molecules	9	7	965	10	8	0.01	21	25	1.2
R-HSA-202733	Cell surface interactions at the vascular wa	5	5	257	14	8	0.13	21	11	1.2
R-HSA-162906	HIV Infection	0	5	262	16	10	0.01	20	31	1.1
R-HSA-2454202	Fc epsilon receptor (FCERI) signaling	4	4	235	12	10	0.05	31	26	1.3
R-HSA-112316	Neuronal System	6	5	499	12	6	0.01	24	28	1.3
R-HSA-75153	Apoptotic execution phase	4	4	54	12	8	0.15	13	10	1.1
R-HSA-69278	Cell Cycle, Mitotic	8	4	570	12	4	0.01	69	53	1.2
R-HSA-186763	Downstream signal transduction	4	0	37	14	10	0.12	12	5	1.4
R-HSA-983231	Megakaryocytes and platelet production	8	4	194	6	4	0.15	11	8	1.4
R-HSA-381119	Unfolded Protein Response (UPR)	2	5	155	11	4	0.01	9	11	1.7
R-HSA-1483249	Inositol phosphate metabolism	5	9	90	4	3	0.15	6	3	1.7
R-HSA-446203	Asparagine N-linked glycosylation	3	5	421	4	8	0.05	16	22	1.2
R-HSA-500792	GPCR ligand binding	1	4	652	6	5	0.01	7	9	1.3
R-HSA-397014	Muscle contraction	3	6	256	6	0	0.15	10	12	1.6
R-HSA-948021	Transport to the Golgi and modification	3	5	219	4	3	0.12	16	17	1.2
R-HSA-2559583	Cellular Senescence	4	3	198	6	1	0.01	9	7	1.3
R-HSA-2428924	IGF1R signaling cascade	4	0	72	5	5	0.13	11	3	1.8
R-HSA-2428928	IRS-related events triggered by IGF1R	4	0	69	5	5	0.13	9	3	1.8
R-HSA-68886	M Phase	6	4	390	3	1	0.15	25	20	1.3
R-HSA-373755	Semaphorin interactions	1	6	70	2	5	0.11	7	11	1.6
R-HSA-2404192	Signaling by Type 1 IGF1R	4	0	73	5	5	0.13	11	3	1.8
R-HSA-71387	Metabolism of carbohydrates	9	0	456	1	1	0.08	13	1	1
R-HSA-418346	Platelet homeostasis	1	4	123	2	0	0.03	5	5	1.5

Suppl. Table 3. Gene Ontology resource analysis (geneontology.org) of 196 iloprost-upregulated phosphoproteins according to GO biological processes. Shown are main discriminative processes, ranked according to numbers of items covered, fold enrichment and false discovery rates (FDR).

GO biological process (main)	Items	Fold enrichment	FDR
Response to stimulus	173	1.37	1.98E-5
Signal transduction	127	1.69	5.17E-8
Regulation of signaling	104	1.95	2.00E-9
Cytoskeleton organization	68	4.18	1.34E-19
Cell surface receptor signaling	63	1.75	8.40E-4
Regulation of phosphorylation	52	2.19	2.10E-5
Regulation of kinase activity	40	3.08	1.89E-7
Regulation of GTPase activity	39	6.43	4.58E-16
Haemostasis	21	4.76	2.18E-6
Platelet activation	17	8.35	4.16E-8

Chapter 6

Non-redundant roles of platelet glycoprotein VI and integrin $\alpha\text{IIb}\beta\text{3}$ in fibrin-mediated microthrombus formation

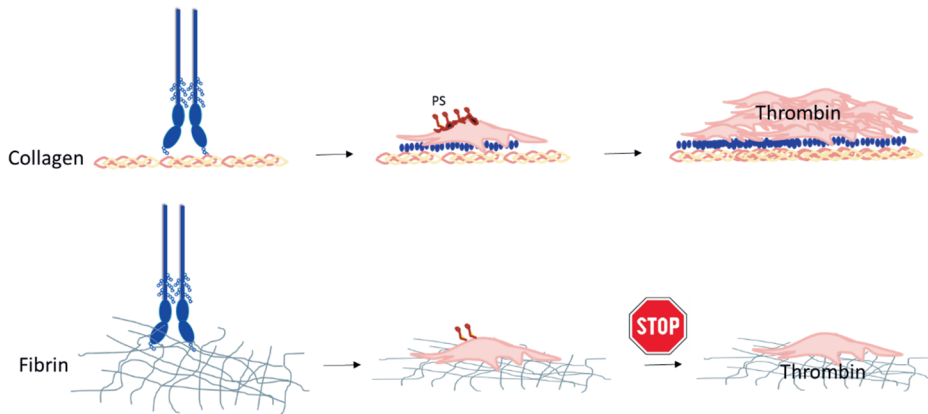
Perrella G, Huang J, Provenzale I, Swieringa F, Heubel-Moenen FCJ, Farndale RW, Roest M, van der Meijden PEJ, Thomas M, Ariëns RAS, Jandrot-Perrus M, Watson SP, Heemskerk JWM

This is a non-final version of an article published in final form in
Arterioscler. Thromb. Vasc. Biol. 2021; 41: e97-e111.

Reprinted with permission

I performed experiments and co-wrote the article; G.P. designed and performed experiments, analyzed and interpreted data, and wrote the article; I.P. and F.S. edited the article; R.A.S.A. and M.J-P. provided reagents and edited the article; S.P.W. edited the article. J.W.M.H. designed experiments, supervised research, interpreted data, and wrote the article.

Visual abstract



Highlights

- Platelet adhesion to a fibrin layer under flow elicits only moderate glycoprotein VI activation.
- The interaction with glycoprotein GPVI (glycoprotein VI) interaction relies on $\alpha IIb\beta 3$ and forms small, bilayered thrombi.
- This consolidated thrombus formation is restricted by thrombin binding to fibrin.

Abstract

Objective: Fibrin is considered to strengthen thrombus formation via integrin $\alpha\text{IIb}\beta 3$, but recent findings indicate that fibrin can also act as ligand for platelet glycoprotein VI.

Approach and Results: To investigate the thrombus-forming potential of fibrin and the roles of platelet receptors herein, we generated a range of immobilized fibrin surfaces, some of which were cross-linked with factor XIIIa and contained VWF-BP (von Willebrand factor-binding peptide). Multicolor microfluidics assays with whole-blood flowed at high shear rate (1000 s^{-1}) indicated that the fibrin surfaces, regardless of the presence of factor XIIIa or VWF-BP, supported platelet adhesion and activation (P-selectin expression), but only microthrombi were formed consisting of bilayers of platelets. Fibrinogen surfaces produced similar microthrombi. Markedly, triggering of coagulation with tissue factor or blocking of thrombin no more than moderately affected the fibrin-induced microthrombus formation. Absence of $\alpha\text{IIb}\beta 3$ in Glanzmann thrombasthenia annulled platelet adhesion. Blocking of glycoprotein VI with Fab 9O12 substantially, but incompletely reduced platelet secretion, Ca^{2+} signaling and aggregation, while inhibition of Syk further reduced these responses. In platelet suspension, glycoprotein VI blockage or Syk inhibition prevented fibrin-induced platelet aggregation. Microthrombi on fibrin surfaces triggered only minimal thrombin generation, in spite of thrombin binding to the fibrin fibers.

Conclusions: Together, these results indicate that fibrin fibers, regardless of their way of formation, act as a consolidating surface in microthrombus formation via nonredundant roles of platelet glycoprotein VI and integrin $\alpha\text{IIb}\beta 3$ through signaling via Syk and low-level cytosolic Ca^{2+} rises.

Introduction

GP (glycoprotein) VI is a platelet immunoglobulin (Ig) receptor, expressed at 3,000 to 4,000 copies per platelet, and known to be involved in the onset of thrombus formation^{1,2}. Common concept is that GPVI mediates the initial activation of platelets in contact with exposed collagen in the vasculature, assisted by platelet integrins and by GPIb-V-IX which interacts with collagen-bound VWF (von Willebrand factor)³⁻⁵. In the platelet membrane, GPVI is constitutively associated with the Fc receptor γ -chain, containing an intracellular immunoreceptor tyrosine-based activation motif. Ligand binding induces clustering of GPVI and ensuing phosphorylation of the immunoreceptor tyrosine-based activation motif via Src-family kinases⁶. This leads to activation of the tyrosine kinase Syk through its tandem SH2 (Src homology2) domain, culminating in activated phospholipase $Cy2$ and ensuing Ca^{2+} mobilization^{2,6}.

Since 2015, it has been recognized that GPVI can also act as a receptor for fibrin and fibrinogen⁷⁻⁹. Relevance of this finding comes from the earlier observation that fibrin formation can be both an initial and propagating process in vaso-occlusive thrombus formation upon vascular damage¹⁰⁻¹². In this setting, the role of GPVI as a functional receptor for fibrin implies a crucial contribution of this receptor interaction in thrombus growth and in the propagation of coagulation. This idea is supported by the observations that (1) GPVI binding to fibrin can trigger platelet procoagulant activity and ensuing thrombin generation⁸ and (2) fibrin binds to procoagulant platelets via the cross-linking transglutaminase FXIIIa (factor XIIIa)¹³. However, some authors have questioned the role of GPVI as a fibrin receptor in blood¹⁴.

Integrin $\alpha IIb\beta 3$ is known as the conventional platelet receptor for fibrinogen and fibrin, being expressed at 50,000 to 80,000 copies per platelet¹⁵⁻¹⁷. Similarly to GPVI, integrin $\alpha IIb\beta 3$ promotes platelet adhesion and activation via outside-in signaling through Src-family and Syk protein tyrosine kinases^{6,18}. Questions then arising are (1) what are the roles of GPVI and $\alpha IIb\beta 3$ in fibrin-dependent platelet activation; (2) how do these receptor

interactions contribute to thrombus formation; (3) how can they prevent endless growth of the platelet-fibrin thrombus; and (4) which is the role of blood flow and shear in this process.

In the present article, we aimed to answer these questions and resolving the dispute on the role of GPVI. We studied the relative contribution of GPVI and integrin $\alpha\text{IIb}\beta 3$ in fibrin-dependent platelet activation and thrombus formation under defined flow conditions. Since fibrin is known to bind VWF¹⁹, we also explored the contribution herein of the VWF receptor, GPIb-V-IX. Our results show that GPVI provides a weakly activating signal that relies on $\alpha\text{IIb}\beta 3$ -dependent platelet adhesion and Syk activation to form small-sized thrombi. Markedly, our data also indicate that the platelet-activating role of thrombin is dampened on fibrin surfaces.

Materials and methods

The authors declare that materials and data are available upon reasonable request from the authors. An extended version of Materials and Methods is available in the supplement.

Major resources

Please see the Major Resources Table in the supplement.

Blood withdrawal and platelet preparation

Blood was obtained by venepuncture from healthy volunteers (male and female), who had not received antiplatelet or anticoagulant medication for at least 2 weeks. Informed consent was obtained according in compliance with the ethical principles of the Declaration of Helsinki, and studies were approved by the local Medical Ethics Committee (METC 10-30-023, Maastricht University). Blood samples were collected into 3.2% trisodium citrate (Vacuette tubes, Greiner Bio-One, Alphen a/d Rijn, the Netherlands). Blood samples were also obtained from 2 patients with diagnosed Glanzmann thrombasthenia, that is, one homozygous patient lacking expression of integrin $\alpha\text{IIb}\beta 3$ on platelets, and one heterozygous patient

with 50% of normal $\alpha\text{IIb}\beta\text{3}$ expression. PRP (platelet-rich plasma) was obtained from the citrated blood by centrifugation at 200 g for 15 minutes²⁰. After addition of 1:10 vol/vol acid-citrate-dextrose (80 mM trisodium citrate, 183 mM glucose, 52 mM citric acid), the PRP was centrifuged at 2360 g for 2 minutes. Platelet pellets were resuspended into Hepes buffer pH 6.6 (10 mM Hepes, 136 mM NaCl, 2.7 mM KCl, 2 mM MgCl_2 , 5.5 mM glucose, and 0.1% BSA). After addition of apyrase (1 U/mL) and 1:15 vol/vol acid-citrate-dextrose, another centrifugation step was performed to obtain washed platelets. The platelet pellet was resuspended into Hepes buffer pH 7.45 (10 mM Hepes, 136 mM NaCl, 2.7 mM KCl, 2 mM MgCl_2 , 5.5 mM glucose, and 0.1% BSA)²⁰.

Microfluidic flow experiments

Glass coverslips were coated for 1 hour with two 1.5 mm diameter spots, each 3 mm apart, which contained the indicated type of fibrin or fibrinogen (upstream) and, when indicated, collagen type III (50 $\mu\text{g/mL}$) as a reference spot (downstream), and collagen type I (50 $\mu\text{g/mL}$). This microspot coating procedure eliminates cross-talk of thrombus formation between the adjacent surfaces²¹. For fibrin spots, fibrinogen (1 mg/mL, 0.5 μL) was applied for 30 minutes, after which α -thrombin (20 nM, 1 μL) was supplemented for additional 30 minutes. Where indicated, mixtures (1 μL) of α -thrombin (2 U/mL), FXIIIa (0.7 $\mu\text{g/mL}$), and CaCl_2 (10 mM) were applied on top of the fibrinogen. Residual FXIIIa activity of the fibrinogen preparation used was determined as 6% in comparison to plasma. Indicated spots were postcoated with the peptide VWF-BP (von Willebrand factor-binding peptide; 100 $\mu\text{g/mL}$, 1 μL). After the completion of coating, coverslips were blocked with 1% BSA in Hepes buffer pH 7.45 for 30 minutes.

As a standard, whole blood was flowed over the coated spots using a microfluidics chamber under conditions allowing coagulation¹². In brief, 1.0 mL samples of citrated blood were co-perfused with recalcification medium using 2 pulse-free micro-pumps (Model 11 Plus, 70-2212, Harvard Apparatus), and a y-shaped mixing tubing. The recalcification medium (in a

second 1 mL syringe) consisted of 32 mM MgCl₂ and 63 mM CaCl₂ in Hepes buffer pH 7.45. Complete mixing was achieved at a volume ratio of 10 (blood) to 1 (recalcification medium)²². Flow rates were adjusted to give a total wall-shear rate of 1000 or 100 s⁻¹.

Fluorescent labels added per blood sample were DiOC₆ (platelet staining), AF568-annexin A5 (phosphatidylserine, exposure), and Alexa Fluor 647-anti-CD62P mAb (P-selectin expression), as described²³. When appropriate, samples were preincubated for 10 minutes with vehicle, inhibitor PRT-060318 (10 μM, in 0.4 μg/mL pluronic plus 0.5% DMSO) and Fab 9012 (50 μg/mL, in saline). Inhibition of GPVI was achieved with Fab 9012 (50 μg/mL), which has previously been shown to interfere in the interaction of GPVI and fibrin⁸. Brightfield and multicolor fluorescence images were recorded per spot over time²⁴. Per donor, all control and intervention conditions were repeated at least in duplicates. Collected time series of brightfield and fluorescence microscopic images were analyzed by using predefined scripts²⁵, formatted in the open-source package Fiji²⁶.

Scanning electron microscopy

For electron microscopy, fibrin-coated spots were prepared as for flow studies and coated on a Sefar matrix (sieve mesh, pores: 170 μm; Sefar Pharma) using 96-wells plates²⁷. Samples were fixed with 4% paraformaldehyde for 1 hour. After wash with PBS, the samples were dehydrated by a 5-step gradient of ethanol (30–100%), and then dried by 10-minutes treatment with hexamethyl disilizane/ethanol (1:1) and 1 hour exposure to air. Dried samples were mounted onto aluminium pin studs with 12 mm carbon conductive tabs (Ted Pella, Redding, CA, USA), were sputter coated with gold (Quorum Technologies, Ashford, United Kingdom; vacuum pump: Edwards, Crawley, United Kingdom) on carbon tabs, and imaged. Table-top electron microscopy was performed, as before²⁷.

Fibrin suspension preparation

Fibrinogen (1 mg/mL) was mixed with CaCl_2 (10 mM), FXIIIa (0.7 $\mu\text{g/mL}$), and thrombin (1 U/mL) and was left to polymerize for 1 hour. Subsequently, D-Phe-Pro-Arg chloromethyl ketone (PPACK; 20 μM) was added to inactivate the thrombin, the clot mixture was agitated until it turned liquid, and it was left for 15 minutes. The gel solution was then ultrasonicated at 20 kHz and amplitude of 80 to 100 μm until clear; this was followed by a centrifugation step at 1000 g for 5 minutes. The obtained pellet was homogeneously resuspended into Hepes buffer pH 7.45.

Platelet aggregometry

Platelet aggregation was monitored by light transmission aggregometry using an automated Chronolog aggregometer (Havertown, PA, USA) at 37°C with stirring at 1200 rpm. Platelet suspensions ($2 \times 10^8/\text{mL}$) were incubated at 37°C for 2 minutes, antagonists were added for 10 minutes, followed by agonists sonicated fibrin, collagen-I (5 $\mu\text{g/mL}$), or α -thrombin (0.1 U/mL).

Cytosolic Ca^{2+} measurements

Washed human platelets ($2 \times 10^8/\text{mL}$) were loaded with Fluo-4 acetoxymethyl ester (8 $\mu\text{mol/L}$) and pluronic (0.4 mg/mL) by a 40 minutes incubation in the presence of apyrase (1 U/mL)²⁸. After centrifugation step in the presence of acid-citrate-dextrose, the Fluo-4-loaded platelets were resuspended into Hepes buffer pH 7.45. Blood samples were supplemented with 10% of autologous Fluo-4-loaded platelets; inhibitors were added after 5 minutes. Changes in cytosolic $[\text{Ca}^{2+}]_i$ during flow-dependent adhesion of labeled platelets were recorded for 5 minutes, using a Zeiss LSM 510 confocal microscope, essentially as described before²⁹. Time series of fluorescence images were analyzed for changes in fluorescence intensity and for platelet adhesion, using Fiji/Image J software.

Data handling and statistics

Data are represented as means \pm SD. Statistical analysis was performed using GraphPad Prism v8 software (San Diego, CA, USA). Significance was

determined using a 2-way ANOVA (Dunnett and Sidak multiple comparison test) or a 1-way ANOVA (Dunnett multiple comparison test); differences with $P<0.05$ were considered as significant.

Heatmaps were generated with the program R. For the heatmap representation, all parameters were univariate scaled to 0 to 10^{21} . According to earlier procedures³⁰, thrombus values of duplicate or triplicate flow runs from one blood donor were averaged to obtain one parameter set per spot. Mean values of control and inhibitor runs were then compared per blood sample. For subtraction heatmaps, a conventional filter of $P<0.05$ (1-way ANOVA) was applied to determine relevant effects, as described before^{25,30}.

Results

Fibrin microstructure of coated spots

To assess the suitability of fibrin-coatings for flow chamber studies, we prepared a series of spotted fibrinogen surfaces which were treated with a thrombin mixture in the presence or absence of the cross-linking transglutaminase, FXIIIa, and a peptide (VWF-BP) capable to capture free VWF from blood³¹. Ultrastructural observation of the different preparations by scanning electron microscopy showed that in all conditions multiple layers of fibrin were formed, which presented as microstructures with both thicker and thinner fibers (Figure 1, arrows). The addition of VWF-BP did not alter the overall fiber structure. However, addition of FXIIIa resulted in fibrin fibers that appeared to be less densely packed with an overall thicker size. The latter observation may be due to the local high transglutaminase concentration upon the fibrin formation. For comparison, also fibrinogen-only spots were examined with or without VWF-BP. Electron microscopy did not reveal any fibrous structures in this case (Figure 1, Appendix Figure 1).

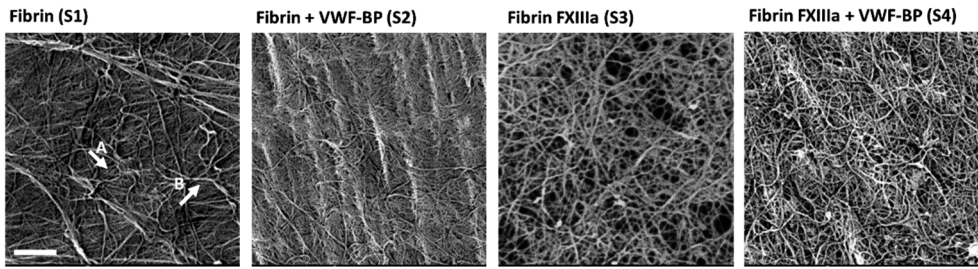


Figure 1. Fibrillar microstructure of immobilized fibrin surfaces. Representative scanning electron microscopy (SEM) images of immobilized fibrin spots, produced from fibrinogen coatings with or without FXIIIa (factor XIIIa) and VWF-BP (von Willebrand factor-binding peptide). Mixtures were allowed to generate fibrin fibers on a SEFAR (Sefar Pharma) filter for 30 minutes. Representative images are shown; scale bar 2 μm . Arrow A points to a thin fiber, arrow B indicates a thick fiber.

Formation of only small-sized microthrombi on fibrin surfaces under flow

We examined how the different types of fibrin(ogen) spots formed with or without FXIIIa and VWF-BP (coded as S1-S6, see Table 1) were able to support thrombus formation under flow in microfluidics chambers. Therefore, citrated whole blood (labeled with DiOC₆, AF568-annexin A5, and Alexa Fluor 647-anti-CD62P mAb) was flowed over sets of 2 spots at defined conditions, in coagulating condition (absence of PPACK)²². After 10 minutes of flow at arterial shear rate (1000 s⁻¹), on all fibrin(ogen) surfaces, platelets adhered and formed small aggregates, not extending 2 or 3 cell layers, which we characterized as bilayer aggregates or microthrombi (Figure 2A; representative images of all 6 spots in Suppl. Figure 1). In contrast, simultaneous flow experiments using collagen-I spots produced larger thrombi composed of multi-layered platelet aggregates (see below), such as reported before³². No platelets adhered to coverslip areas in between the coated spots²¹.

Capturing of multicolor fluorescence microscopic images at time points of 2, 4, 6, 8, and 10 minutes allowed to assess the kinetics of the process, in terms of 6 parameters. These were DiOC₆ platelet adhesion (P1), thrombus morphological score (P2), thrombus contraction score (P3), bi- or multi-layer

score (P4), bi- or multilayer size (P5), P-selectin expression (P6), and phosphatidylserine exposure (P7)²⁵. End stage brightfield and triple-colored microscopic images from fibrin-FXIIIa spots (S3) are shown in Figure 2A. To compare the time-dependent parameter increases per type of fibrin spots (S1–S4) and fibrinogen spots (S5–S6), we scaled all values per parameter across surfaces (scale 0–10) and represented the results in a practical heatmap format (Figure 2B).

Overall, the heatmap analysis pointed to similar parameter increases over time for all types of fibrin spots (S1–S4), although rates of platelet adhesion (P1) were slightly higher in spots containing VWF-BP (S2, S4). The latter observation pointed to a moderate enhancement of platelet adhesion but not to bilayer microthrombus formation, by plasma-bound VWF. On all fibrin spots, the adhered platelets gradually increased in P-selectin expression (P6), but remained low in phosphatidylserine exposure (P7), thus indicating an only moderate platelet activation state². Addition of FXIIIa during fibrin formation (S3, S4) slightly increased the formation of platelet aggregates, when compared with no added FXIIIa (S1, S2). Furthermore, the 2 spots with fibrinogen (S5, S6) were even less active in supporting platelet adhesion, bilayer aggregate formation and platelet activation (P-selectin expression) in comparison to the fibrin surfaces (Figure 2A, B).

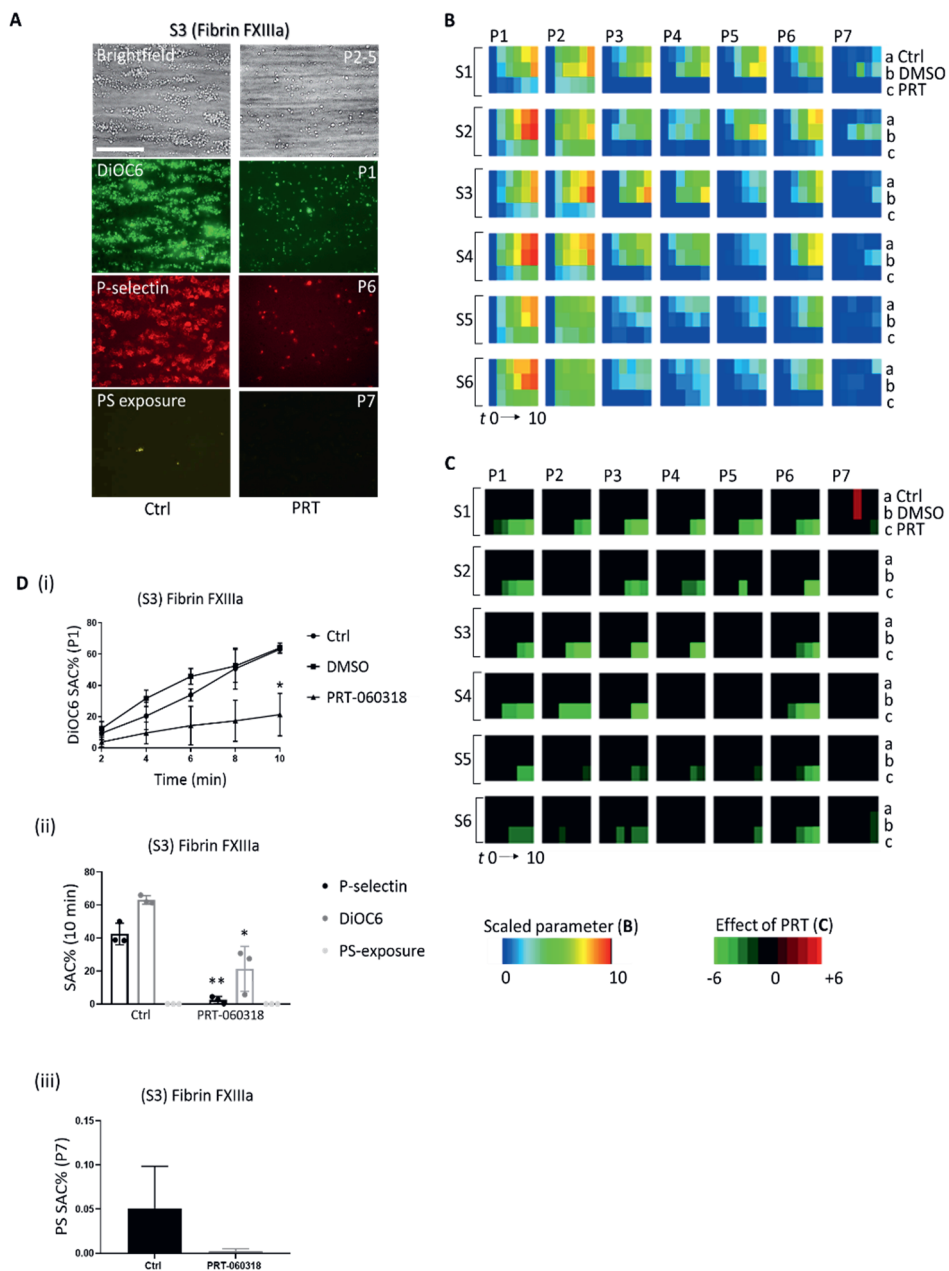
Given the presence of 6% residual FXIIIa in the fibrinogen preparation used for the coating, we checked if transglutaminase contributed to platelet-activating effects by generating spots of fibrin (S1) and fibrin-FXIIIa (S3) in the presence of the FXIIIa inhibitor T101. However, after 10 minutes of whole-blood flow, both end stage images (Suppl. Figure 2 A) and scaled time-dependent parameters P1,5-7 did not show significant effects of this inhibitor (Suppl. Figure 2 B, C). Together, these results pointed to a no more than modest role of FXIIIa-induced cross-linking in fibrin-dependent microthrombus formation.

Table 1. Coding of spots (*S*) and parameters (*P*) in whole-blood thrombus formation.

S	Microspot coating	Adhesive receptors	
<i>S1</i>	Fibrin	GPVI, α IIb β 3	
<i>S2</i>	Fibrin + VWF-BP	GPIb, VI, α IIb β 3	
<i>S3</i>	Fibrin FXIIIa	GPVI, α IIb β 3	
<i>S4</i>	Fibrin FXIIIa + VWF	GPIb, VI, α IIb β 3	
<i>S5</i>	Fibrinogen	GPVI, α IIb β 3	
<i>S6</i>	Fibrinogen + VWF-BP	GPIb, VI, α IIb β 3	
<i>S7</i>	Collagen III	GPIb, VI, α 2 β 1	
P	Image type	Description	Unit or scaling
<i>Platelet parameters</i>			
<i>P1</i>	DiOC ₆	platelet adhesion	%SAC
<i>P6</i>	AF647 α -P-selectin	platelet activation	%SAC
<i>P7</i>	AF568 annexin A5	platelet PS exposure	%SAC
<i>Thrombus parameters</i>			
<i>P2</i>	brightfield	thrombus morphology	score 1-5
<i>P3</i>	brightfield	thrombus aggregation	score 1-3
<i>P4</i>	brightfield	thrombus contraction	score 1-3
<i>P5</i>	brightfield	thrombus multilayer coverage	%SAC

Major role of Syk kinase in microthrombus formation on fibrin independently of coagulant strength

To assess tyrosine kinase-dependent signaling, blood samples were preincubated with the selective Syk kinase inhibitor PRT-060318, known to completely abolish the thrombus formation on collagen-like surfaces³⁰. This inhibitor lowered platelet adhesion and abolished the bilayer aggregate formation and P-selectin expression on all prepared fibrin and fibrinogen spots (Figure 2A, B). Subtraction heatmaps of the scaled treatment effects over time showed for essentially all parameters a relevant reduction with PRT-060318, but not with DMSO vehicle (Figure 2C). For instance, on fibrin-FXIIIa spots, PRT-060318 gradually suppressed platelet adhesion parameters *P1* to *P2* (Figure 2D i-ii) and even tended to suppress the low phosphatidylserine exposure (Figure 2D iii).



Surfaces were imaged (brightfield and fluorescence) at time points $t = 0, 2, 4, 6, 8, 10$ minutes to obtain parameters P1 (DiOC₆ platelet adhesion), P2 (thrombus morphological score), P3 (contraction score), P4 (bi- or multi-layer score), P5 (bi- or multi-layer size), P6 (P-selectin expression), and P7 (phosphatidylserine [PS] exposure). Effects of PRT were assessed per blood sample, surface, and parameter. **A**, Representative brightfield and fluorescence images of microthrombi on fibrin-FXIIIa (factor XIIIa) spots (S3) after 10 minutes. Scale bar, 50 μm . **B**, Mean parameter values from 3–4 blood samples over time, univariate scaled to 0–10 per parameter. Heatmap of the scaled parameters, demonstrating effects of PRT. Rainbow color code indicates scaled values from 0 (blue) to 10 (red). **C**, Subtraction heatmap representing effects of PRT, filtered for relevant differences ($n=3-4$, $P<0.05$, 2-way ANOVA). Color code showing relevant decrease (green) or increase (red) in comparison to control runs. **D**, Time-dependent increase in platelet adhesion (P1) in the presence or absence of PRT (**D, i**). Mean effects of PRT on platelet adhesion (P1) and platelet activation (P6) after 10 minutes (**D, ii**); mean effects of PRT on platelet PS exposure (P7) after 10 minutes (**D, iii**). SAC indicates surface-area-coverage. Data are means \pm SD ($n=3-4$), * $P<0.01$, ** $P<0.001$ (2-way ANOVA).

Subsequent flow experiments were performed with fibrin-FXIIIa (S3) spots, which were used as a standard. We first examined how the formation of microthrombi relied on the extent of coagulation, that is, thrombin generation. Therefore, blood samples were incubated either with the thrombin inactivator PPACK, or with 5 or 10 pM tissue factor to trigger the extrinsic coagulation pathway. During 10 minutes of flow at 1000 s^{-1} , microscopic images again were captured and analyzed for DiOC₆ platelet adhesion (P1), multilayer score (P5), P-selectin expression (P6), and phosphatidylserine exposure (P7). Markedly, the presence of either PPACK and tissue factor did not significantly change platelet adhesion, size of microthrombi or the P-selectin expression at fibrin-FXIIIa spots, when compared with control runs (Suppl.Figure 3A). In addition, Syk inhibition with PRT-060318 had a similar lowering effect on all parameters, regardless of the presence of PPACK or tissue factor (Suppl.Figure 3B).

A marked finding was that, for all variable coagulation conditions, the extent of phosphatidylserine exposure remained low for fibrin-FXIIIa spots (0.1–0.4 SAC%). On the contrary, parallel flow experiments on collagen-I spots caused formation of large-sized platelet thrombi, with high staining for DiOC₆ and high phosphatidylserine exposure, with or without tissue factor (Suppl. Figure IV). Hence, the low level of phosphatidylserine exposure observed on fibrin-FXIIIa spots was not due to limitations of the flow set-up, in agreement with earlier findings²².

To further assess the apparently limited role of thrombin in the microthrombus formation on fibrin spots, we compared the effects of PPACK with the thrombin receptor antagonist atopaxar and the thrombin inhibitor lepirudin. When added to the blood, neither end stage images nor (subtraction) heatmaps of scaled parameters P1,5-7 indicated any effect of these interventions (Suppl. Figure 5A, B). In addition, we measured the ability of thrombi formed on fibrin-FXIIIa and collagen-I spots to support (phosphatidylserine-dependent) thrombin generation, using an earlier described procedure based on the thrombin-induced cleavage of substrate Z-GGR-ACM (Z-Gly-Gly-Arg aminomethyl coumarine)³³. The observed no more than minimal thrombin generation on fibrin-FXIIIa spots supported the conclusion that the procoagulant activity of the fibrin surface is low in comparison to the collagen-I surface (Suppl. Figure 5C, D). Together, these results indicated that the low thrombogenic effect of fibrin surfaces relies on Syk kinase signaling, which is relatively independent of coagulation triggering.

Shear-dependent contribution of integrin α Ib β 3 in microthrombus formation on fibrin

Considering that also integrin α Ib β 3 interaction with fibrin(ogen) can trigger Syk activation^{6,34}, we went on to determine the role of this integrin in the microthrombus formation. Therefore, blood samples from 2 patients with Glanzmann thrombasthenia were obtained and flowed over fibrin-FXIIIa spots (S3) at arterial (1000 s⁻¹) or venous (100 s⁻¹) shear rate. Markedly, with

blood from the homozygous patient, completely lacking platelet surface expression of $\alpha\text{IIb}\beta 3$, the platelets failed to adhere to fibrin, regardless of the shear rate (Figure 3A, B). Control experiments indicated that VWF was present on the S3 (fibrin-FXIIIa) surfaces (see below). With blood from the heterozygous patient, presenting with reduced platelet $\alpha\text{IIb}\beta 3$ expression, the platelets again did not adhere at the high shear rate. However, there was substantial platelet adhesion (P1) at the low shear rate. In the latter case, the normal P-selectin expression (P6) pointed to residual platelet activation. Taken together, these results pointed to a crucial, shear-dependent role of the $\alpha\text{IIb}\beta 3$ integrin in the flow-dependent platelet interaction with fibrin.

Complementary roles of GPVI, $\alpha\text{IIb}\beta 3$, and GPIb-V-IX in microthrombus formation on fibrin

Subsequent flow experiments were performed with spots of fibrin-FXIIIa (S3) in combination with downstream collagen-III (S7), which was considered as a reference platelet-activating surface. The comparative analysis of fibrin-FXIII and collagen-III surfaces showed that the microthrombi on fibrin were less contracted and activated than those on the collagen-III (Figure 4A, B). Considering that both GPVI and integrin $\alpha\text{IIb}\beta 3$ can activate Syk kinase, in this setting we established the role of GPVI in the thrombus-forming process at both surfaces. Whole-blood samples were treated with anti-GPVI Fab 9012 and flowed over the spots for 10 minutes at high shear rate of 1000 s^{-1} . Microscopic images, captured from these surfaces over time, were analyzed for the same parameters as before (P1,5-7). The results showed that, for fibrin-FXIIIa (S3), GPVI inhibition caused significant decreases of platelet adhesion, bilayered aggregation, and P-selectin expression (Figure 4A, B). The effects of Fab 9012 on platelet adhesion and activation were similar for fibrin-FXIIIa and collagen-III spots. However, these were lower in comparison to Syk inhibition (compare Figures 2C and 4C). This notion agrees with a complementary activation pathway of Syk kinase, involving integrin $\alpha\text{IIb}\beta 3$.

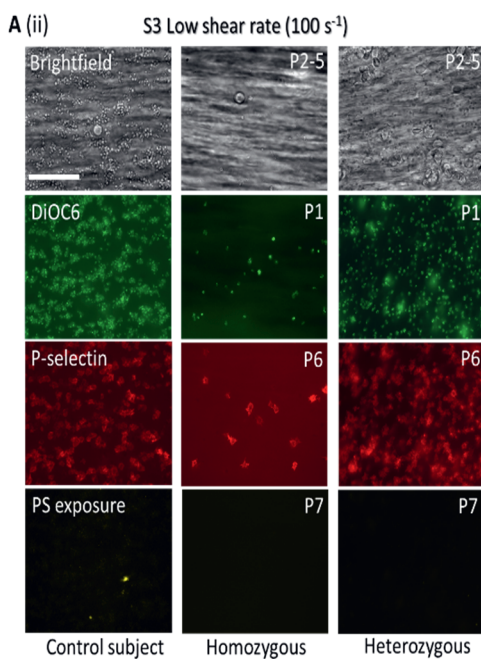
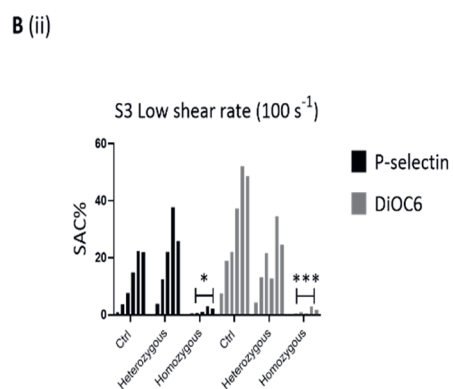
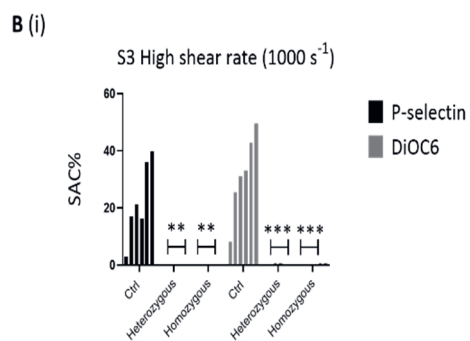
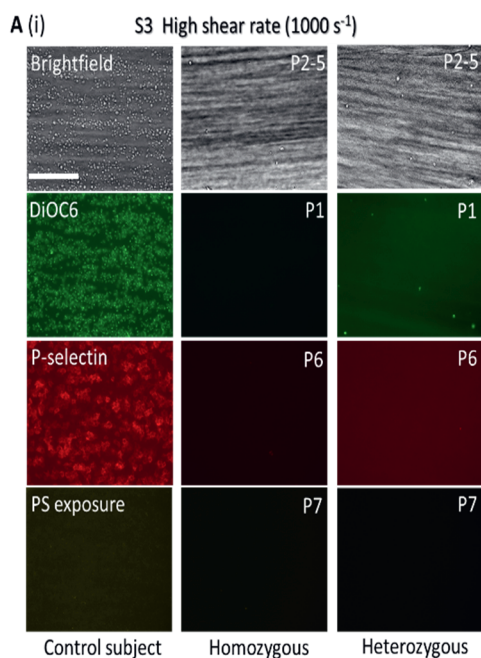


Figure 3. See upper page. Abolished microthrombus formation on fibrin in Glanzmann thrombasthenia. A, Representative brightfield and fluorescence images from microthrombi after flow of blood from control subjects or 2 Glanzmann patients over spots of fibrin-FXIIIa (factor XIIIa; 10 minutes). Flow perfusion was at arterial shear rate of 1000 s^{-1} (A, i) or at venous shear rate of 100 s^{-1} (A, ii). Scale bars $50\text{ }\mu\text{m}$. B, Time-dependent increases in platelet activation (P-selectin expression, P6) and platelet adhesion (DiOC₆, P1) for controls (Ctrl, n=4), heterozygous and homozygous patients at time points t=0, 2, 4, 6, 8, and 10 minutes. Graphs at shear rates of 1000 s^{-1} (B, i) and 100 s^{-1} (B, ii). SAC indicates surface-area-coverage. Mean \pm SD (n=4 for controls), **P<0.001, ***P<0.0001 (2-way ANOVA).

Fibrin has previously been shown to bind to VWF¹⁹. For the fibrin-FXIIIa spots exposed to flowing blood, we could confirm the binding of plasma-derived VWF by staining with a fluorescein isothiocyanate-labeled anti-VWF antibody (Figure 5A). The presence of VWF was yet lower than on the reference spot, collagen-III. To determine contribution of the VWF-GPIb-V-IX axis to the microthrombus, we used an established blocking anti-GPIb α antibody, RAG35.³⁵ For both spots S3 (fibrin-FXIIIa) and S7 (collagen-III), the addition of RAG35 antibody resulted in a marked reduction in platelet adhesion, bilayer formation, and P-selectin expression, already observable from the first minutes of flow (Figure 5B, C). Subtraction heatmaps, however, pointed to larger effect for collagen-III than for fibrin-FXIIIa spots (Figure 5D).

Role of Syk and GPVI in fibrin-induced platelet aggregation

To further confirm the moderate signaling via Syk kinase and GPVI in fibrin-induced platelet activation, we examined the aggregation response of platelets upon stimulation with a sonicated, homogeneous fibrin suspension. This suspension was treated with PPACK to remove thrombin traces. Similar to the results of microthrombus formation, pretreatment of platelets with Syk inhibitor PRT-060318 abrogated the fibrin-induced aggregation (Figure 6A, B). Similarly, the GPVI blocking Fab 9O12 suppressed fibrin-induced aggregation, but a residual shape change and aggregation remained. In comparison, both inhibitors also antagonized the platelet aggregation induced by collagen-I, but not by thrombin (Figure 6). As expected,

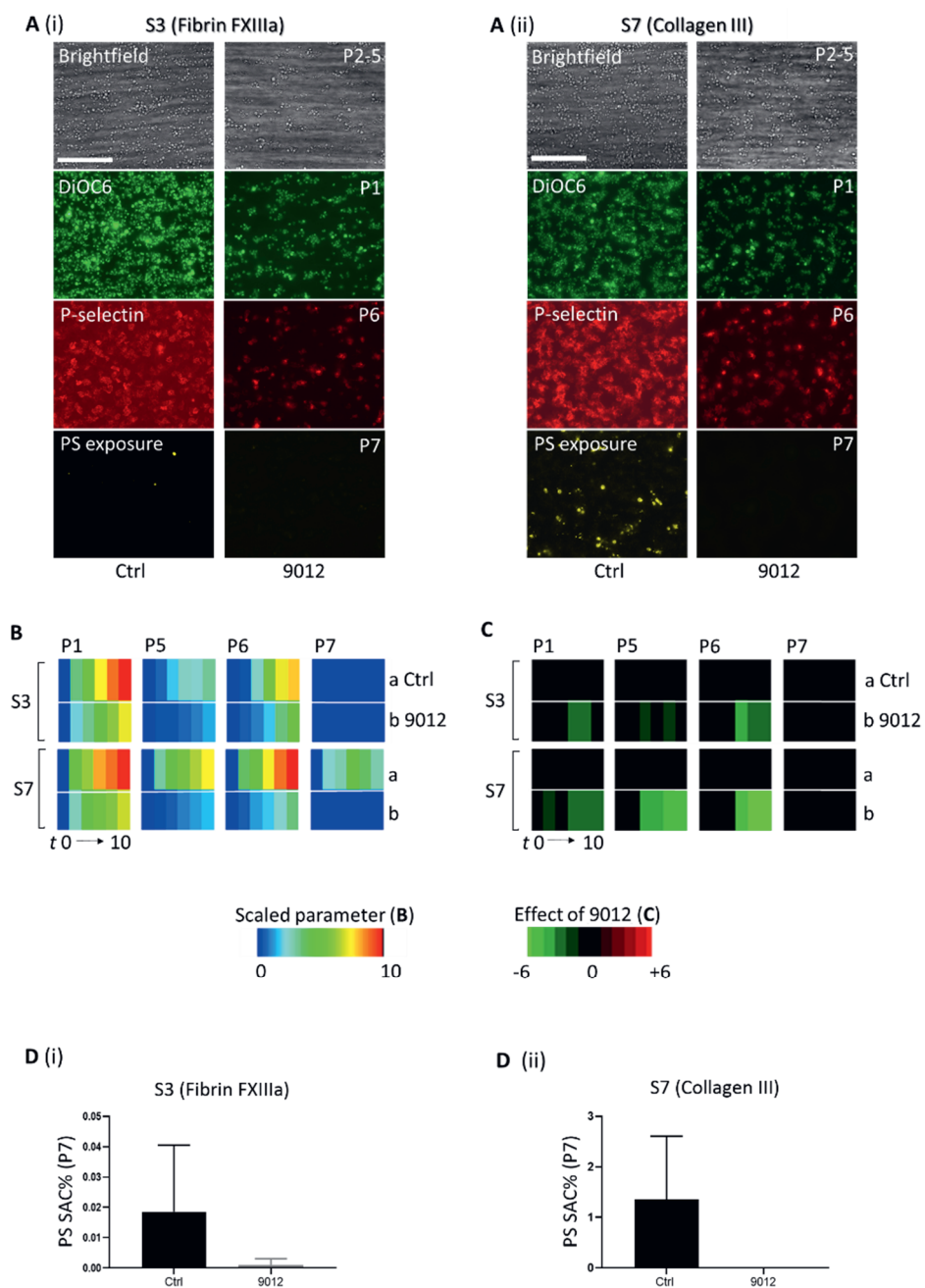


Figure 4. Effect of GPVI (glycoprotein VI) inhibition on parameters of microthrombus formation on immobilized fibrin-FXIIIa (factor XIIIa) or collagen-

III. Blood samples preincubated with vehicle (Ctrl) or GPVI blocking agent (9O12 Fab, 50 $\mu\text{g/mL}$) were flowed over spots S3 (fibrin-FXIIIa, upstream) and S7 (collagen-III, downstream) for 10 minutes at 1000 s^{-1} . Microthrombi formed were imaged to obtain parameters P1 (DiOC₆ platelet adhesion), P5 (bi- or multilayer size), P6 (P-selectin expression), and P7 (PS exposure). **A**, Representative brightfield and fluorescence images from fibrin-FXIIIa (**A, i**) and collagen-III spots (**A, ii**) at 10 minutes. **B**, Heatmap of scaled parameters, demonstrating mean effects of GPVI inhibition on thrombus formation per spot. Effects of GPVI inhibition were assessed per blood sample, surface, and parameter. Mean values from individual blood samples were univariate scaled to 0–10 per parameter. Rainbow color code indicates scaled values between 0 (blue) and 10 (red). **C**, Subtraction heatmaps representing scaled effects of GPVI inhibition, filtered for relevant changes ($P < 0.05$, 2-way ANOVA per surface and parameter). Color code represents decrease (green) or increase (red) in comparison to control runs. Scale bar 50 μm . **D**, Graphs representing PS exposure (P7) for fibrin-FXIIIa (**D, i**) and collagen-III (**D, ii**) at 10 min. SAC indicates surface-area-coverage. Data are means \pm SD ($n=7$), $*P < 0.05$ (2-way ANOVA).

treatment with the integrin antagonist tirofiban blocked the fibrin-induced aggregation response by >80% (Figure 2, Appendix Figure 2).

Fibrin-induced platelet Ca^{2+} signaling under flow

In collagen-induced platelet activation, GPVI adhesion under flow is known to induce a prolonged and high Ca^{2+} signal, leading to massive P-selectin expression and phosphatidylserine exposure^{21,36}. To investigate the Ca^{2+} signal of platelets flowed over fibrin-FXIIIa, blood samples were supplemented with autologous Fluo-4-loaded platelets, and fluorescent $[\text{Ca}^{2+}]_i$ rises were measured in real time by confocal microscopy. The results show a consistent, moderate increase in Fluo-4 fluorescence in fibrin-adhered platelets, which was suppressed by Fab 9O12 (Figure 7A). A near complete major reduction in fluorescence increase was observed upon Syk inhibition with PRT-060318. The effects on Fluo-4 fluorescence increases paralleled effects on platelet adhesion (Figure 7B). However, detailed analysis of traces from single adhered platelets confirmed suppression of

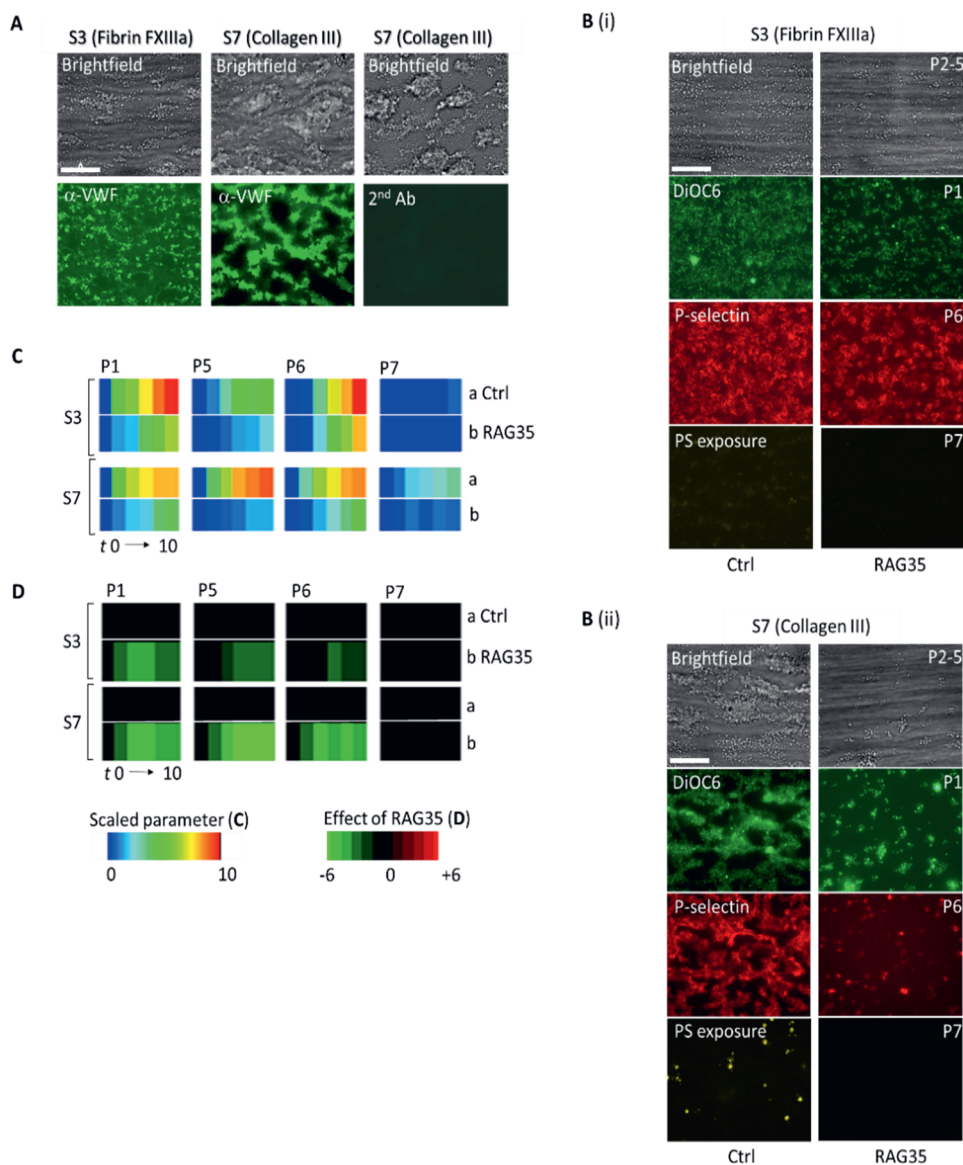


Figure 5. Roles of VWF (von Willebrand factor) and GPIb-V-IX (glycoprotein Ib-V-IX) in microthrombus formation on immobilized fibrin-FXIIIa or on collagen-III. Blood samples preincubated with vehicle (Ctrl) or GPIb blocking antibody RAG35 (20 $\mu\text{g}/\text{mL}$) were flowed at 1000 s^{-1} over spots S3 (fibrin-FXIIIa, upstream) and S7 (collagen-III, downstream). After 10 minutes, microthrombi formed were imaged to obtain parameters P1 (DiOC₆ platelet adhesion), P5 (bi- or multilayer size), P6 (P-

selectin expression), P7 (phosphatidylserine [PS] exposure). **A**, Staining of microthrombi formed on S3 and S7 spots after 10 min for VWF using fluorescein isothiocyanate-labeled anti-VWF antibody (green) or irrelevant control antibody. **B–E**, Effects of RAG35 antibody on thrombus parameters were assessed over time per blood sample for S3 and S7 surfaces. Scale bar 50 μ m. Shown are representative end stage brightfield and fluorescence images for fibrin-FXIIIa (**B, i**) and collagen-III (**B, ii**). Furthermore, heatmap of univariate scaled parameters (0–10), indicating increased build-up of microthrombi over time in the absence or presence of RAG35 antibody (**C**). Rainbow color code shows scaled values between 0 (blue) and 10 (red). In addition, subtraction heatmap representing scaled effects of GPIIb blocking (**D**). Filtering was applied for relevant changes ($n=6$, $P<0.05$, 2-way ANOVA per surface and parameter). Colour code represents decrease (green) or increase (red) in comparison to control runs. Means \pm SD ($n=6$), $P<0.05$ (2-way ANOVA).

transient, spiking Ca^{2+} signal generation in the presence of Fab 9O12 or PRT-060318 (Suppl. Figure 6A, C). Of note, no platelet adhesion could be observed in the presence of integrin inhibitor, tirofiban. Taken together, these results confirm that fibrin interaction activates platelets via Syk kinase and GPVI.

Fibrin in consolidating microthrombus formation

We explored why the fibrin-adhered platelet were insensitive to thrombin, for instance in flow with tissue factor. As a first approach, we adapted an earlier protocol, where single immobilized platelets in a flow chamber were triggered to generate star-like fibrin fibers³⁷. These fibrin-forming platelets were postperfused for up to 10 minutes with blood samples, again containing labels for platelets (DiOC₆), and P-selectin and phosphatidylserine exposure. Recording of brightfield and tri-colour fluorescence images from the same microscopic fields after blood flow showed considerable overlap between the staining (Suppl. Figure 7A). Detailed analysis showed that the stainings concentrated around the immobilized platelets, rather than at the extending fibrin fibers (Suppl. Figure 7B). Thus, the DiOC₆-labeled microaggregates showed high overlap with the P-selectin exposing prior immobilized platelets, which was confirmed by measuring the overlap

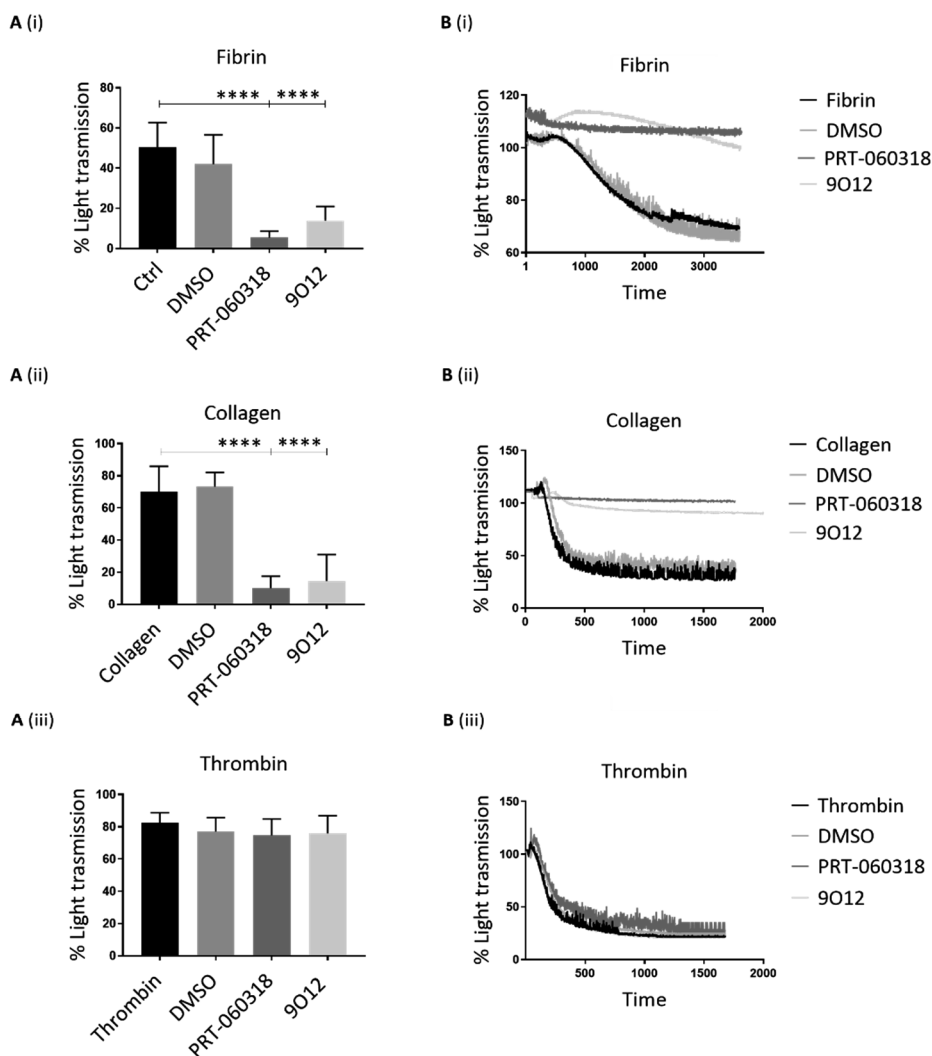
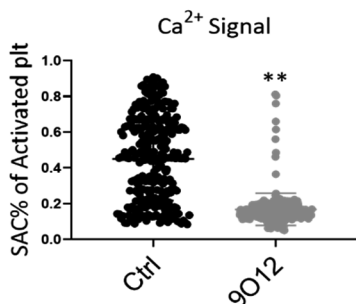
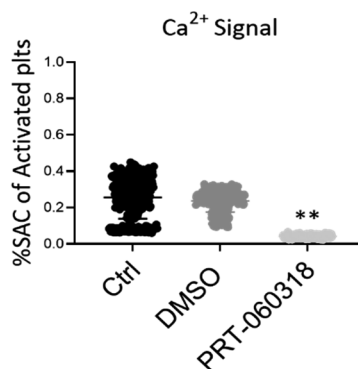


Figure 6. Comparative effects of GPVI (glycoprotein VI) or Syk inhibition on fibrin-mediated platelet aggregation. Platelets in suspension were treated with Syk inhibitor PRT-060318 (10 μ M) or GPVI-inhibitor 9O12 (50 μ g/mL) for 10 minutes, before agonist addition. Platelet aggregation was monitored by conventional light transmission aggregometry. **A**, Quantitation of maximal aggregation upon stimulation with fibrin, collagen, or thrombin. **B**, Representative aggregation traces upon stimulation with indicated agonist. Mean \pm SD ($n=5$), **** $P<0.0001$ (1-way ANOVA).

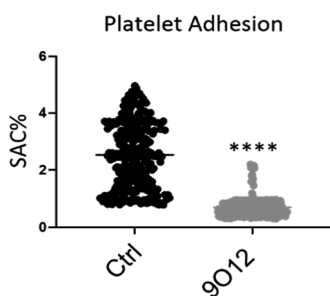
A (i)



A (ii)



B (i)



B (ii)

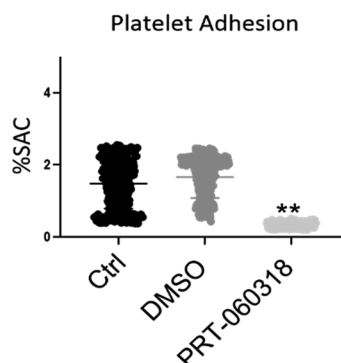


Figure 7. Effects of glycoprotein VI (GPVI) or Syk inhibition on Ca²⁺ signaling in fibrin-adhered platelets under flow. Blood samples containing autologous Fluo-4-loaded platelets were preincubated with vehicle (Ctrl), GPVI blocking agent 9012 Fab (50 µg/mL) or Syk inhibitor PRT-060318 (10 µM), and flowed over S3 spots (fibrin-FXIIIa), as for Figure 2. Fluorescence changes in cytosolic [Ca²⁺]_i of adhered platelets were recorded by confocal microscopy for 5 minutes. Time series of fluorescence images were analyzed for threshold increases in fluorescence intensity representing platelet activation (**A, i and ii**), and for fluorescence coverage as a measure of platelet adhesion (**B, i and ii**). Parts present data from parallel flow runs; dots represent values from analyzed images. SAC indicates surface-area-coverage. Bars are means (n=3 experiments), **P<0.001, ****P<0.0001 (1-way ANOVA).

coefficients R (Suppl. Figure 7C). This overlap was further increased by blood flow in the presence of integrin $\alpha\text{IIb}\beta 3$ antagonist tirofiban.

In an earlier study, we observed high binding of Oregon Green 488-labeled thrombin to fibrin-containing thrombi¹¹. This could be confirmed using the present coagulant flow conditions for fibrin-FXIIIa and collagen-I spots (Suppl. Figure 8A, B). As a control, blocking of the coagulation process with PPACK suppressed cleavage of the Oregon Green 488-labeled prothrombin probe, with as a consequence binding to phosphatidyl-serine-exposing platelets only (Suppl. Figure 8A ii and 8B ii). Taking together, these data suggest that fibrin fibers provide a relatively poor surface for newly adhering platelets, but can trap locally cleaved prothrombin.

Discussion

While GPVI has been identified as a receptor for fibrin and also fibrinogen⁷⁻⁹, the relative strength of the platelet-activating effect of fibrin via GPVI has not been examined in detail. It has been established that blood flow over immobilized collagens or collagen-related peptides via GPVI causes strong platelet activation responses, that is, a prolonged Ca^{2+} signal, high integrin activation, P-selectin expression, phosphatidyl-serine exposure, and massive thrombus formation^{21,38-40}. The present data, using a variety of immobilized fibrin surfaces, point to a weaker GPVI-dependent platelet-activating effect of blood flow over fibrin, in that fewer platelets adhered showing transient Ca^{2+} signals, residual P-selectin expression and limited phosphatidylserine exposure, altogether resulting in the formation of only small-sized microthrombi.

The microthrombus formation under flow appeared to be hardly influenced by producing the fibrin with or without added VWF-BP or FXIIIa. However, this does not rule out a role of VWF or FXIIIa in the thrombus-forming process, because fibrin can capture VWF from the blood plasma¹⁹, and FXIIIa can also be produced in coagulating plasma and released from activated platelets¹³. Evidence for a relative weakness of fibrin (in comparison to

collagen) as platelet-activating surfaces was further corroborated by experiments showing that fibrin fibers extending from immobilized platelets are relatively ineffective in trapping newly perfused platelets, when compared with the immobilized platelets themselves.

Comparative analysis of the microthrombi on fibrin-FXIIIa and collagen-III spots indicated that the platelets on fibrin had a lower activation state than those on collagen. Nevertheless, on both surfaces, inhibition of Syk (PRT-060318) or blockade of GPVI (Fab 9O12) suppressed the flow-dependent platelet adhesion, aggregate formation, and activation (P-selectin expression). In agreement with these findings, also light transmission aggregation studies using stirred platelet suspensions showed that the fibrin-induced aggregation process is abolished by both PRT-060318 and Fab 9O12.

Complete or partial defects in expression of integrin $\alpha\text{IIb}\beta 3$ (Glanzmann patients) resulted in an annulled platelet adhesion to fibrin under flow, which in case of partial deficiency was limited to the high shear rate condition. In addition, we could establish a role of GPIb-V-IX by using the blocking anti-GPIb α antibody RAG35³⁵. This antibody substantially but not completely decreased platelet adhesion to both fibrin-FXIIIa and collagen-III spots, while the remaining adhered platelets still displayed P-selectin expression. Together, these findings point to complementary and nonredundant roles of GPVI, $\alpha\text{IIb}\beta 3$, and GPIb-V-IX complex in the microthrombus formation on fibrin surfaces. Since the tyrosine kinase Syk is known to be phosphorylated and activated downstream of both GPVI and $\alpha\text{IIb}\beta 3$ ^{6,30,41}, our results suggest that concomitant activation via both receptors is required for formation of the microthrombi. This idea is supported by a previous study showing that Syk phosphorylation is a continuous process in murine thrombus growth, and that secondary Syk inhibition can annul platelet adhesion even on preformed thrombi under flow⁴². A nonredundant contribution of GPVI and $\alpha\text{IIb}\beta 3$ can also be derived from the observation that perfusion of blood from patients with GPVI

deficiency over fibrin spots resulted in an abolished aggregate formation, although individual platelets still adhered (unpublished data, but see Ref.⁴³).

Novel related observations were (1) the low phosphatidylserine exposure of platelets on fibrin (although still dependent on low-level GPVI), (2) the relative inability of thrombin to alter fibrin-dependent microthrombus formation, and (3) a low-level thrombin generation of platelets on fibrin in comparison to collagen. An explanation for these observations is the finding, supported by earlier studies,¹¹ that fibrin captures (fluorescent-labeled) thrombin, apparently without ability to cleave its substrate Z-GGR-ACM. This agrees with the earlier notion of irreversible thrombin binding to a fibrin network⁴⁴. A suggestion then is that under the present microfluidic conditions fibrin-bound thrombin is unable to activate platelets. Clearly, more research needs to be done to better understand this phenomenon. Hence, our present findings lead to the concept that on fibrin a low platelet GPVI activation and an inactivation of thrombin induces only weak support of thrombus formation; or in other words, that platelet interaction with fibrin in particular consolidates the process of thrombus formation. However, we cannot rule out that under certain (patho)physiological static or flow conditions the role of fibrin is enlarged⁴⁵.

The overall observation of fibrin-induced microthrombus formation suggests that fibrin fibers act as consolidating elements of the thrombus shield, such in contrast to vascular collagens which trigger the formation of larger size thrombi. Given that thrombus growth is regulated by secondary mediators, such as ADP and thromboxane A₂, which activate platelets in the thrombus core, it is not evident that the fibrin-GPVI interaction substitutes the high GPVI activation induced by collagens. A local inactivation of thrombin by fibrin may further contribute to this dampening process.

Nonstandard abbreviations and acronyms

FXIIIa	factor XIIIa
GPVI	glycoprotein VI

PPACK	D-Phe-Pro-Arg chloromethyl ketone
PRP	platelet-rich plasma
VWF	von Willebrand factor
VWF-BP	von Willebrand factor-binding peptide

Sources of funding

G. Perrella is supported by a joint PhD scholarship of Maastricht and Birmingham Universities. J. Huang and I. Provenziale are supported by the European Union's Horizon 2020 research and innovation program under the Marie Skłodowska-Curie grant agreement No. 766118, and are registered in the PhD programs of Maastricht and Santiago da Compostela Universities (J. Huang) or Maastricht and Reading Universities (I. Provenziale). S.P. Watson and R.A.S. Ariëns are supported by a Wellcome Trust Joint Investigator Award (204951/Z/16/Z). S.P. Watson holds a British Heart Foundation Chair (CH/03/003).

Disclosures

J.W.M. Heemskerk is founder and co-owner at FlowChamber b.v. The other authors report no conflicts.

References

1. Nieswandt B and Watson SP. Platelet-collagen interaction: is GPVI the central receptor? *Blood*. 2003; 102:449-461.
2. Versteeg HH, Heemskerk JW, Levi M and Reitsma PH. New fundamentals in hemostasis. *Physiol Rev*. 2013; 93:327-58.
3. Siljander PR, Munnix IC, Smethurst PA, Deckmyn H, Lindhout T, Ouwehand WH et al. Platelet receptor interplay regulates collagen-induced thrombus formation in flowing human blood. *Blood*. 2004; 103:1333-41.
4. Auger JM, Kuijpers MJ, Senis YA, Watson SP and Heemskerk JW. Adhesion of human and mouse platelets to collagen under shear: a unifying model. *FASEB J*. 2005; 19:825-7.

5. Pugh N, Maddox BD, Bihan D, Taylor KA, Mahaut-Smith MP and Farndale RW. Differential integrin activity mediated by platelet collagen receptor engagement under flow conditions. *Thromb Haemost.* 2017; 117:1588-1600.
6. Watson SP, Auger JM, McCarty OJ and Pearce AC. GPVI and integrin $\alpha\text{IIb}\beta\text{3}$ signaling in platelets. *J Thromb Haemost.* 2005; 3:1752-62.
7. Alshehri OM, Hughes CE, Montague S, Watson SK, Frampton J, Bender M et al. Fibrin activates GPVI in human and mouse platelets. *Blood.* 2015; 126:1601-1608.
8. Mammadova-Bach E, Ollivier V, Loyau S, Schaff M, Dumont B, Favier R et al. Platelet glycoprotein VI binds to polymerized fibrin and promotes thrombin generation. *Blood.* 2015; 126:683-91.
9. Mangin PH, Onselaer MB, Receveur N, Le Lay N, Hardy AT, Wilson C et al. Immobilized fibrinogen activates human platelets through glycoprotein VI. *Haematologica.* 2018; 103:898-907.
10. Falati S, Gross P, Merrill-Skoloff G, Furie BC and Furie B. Real-time in vivo imaging of platelets, tissue factor and fibrin during arterial thrombus formation in the mouse. *Nat Med.* 2002; 8:1175-81.
11. Berny MA, Munnix IC, Auger JM, Schols SE, Cosemans JM, Panizzi P et al. Spatial distribution of factor Xa, thrombin, and fibrin(ogen) on thrombi at venous shear. *PLoS One.* 2010; 5:e10415.
12. Swieringa F, Baaten CC, Verdoold R, Mastenbroek TG, Rijnveld N, Van der Laan KO et al. Platelet control of fibrin distribution and microelasticity in thrombus formation under flow. *Arterioscler Thromb Vasc Biol.* 2016; 36:692-9.
13. Mattheij NJ, Swieringa F, Mastenbroek TG, Berny-Lang MA, May F, Baaten CC et al. Coated platelets function in platelet-dependent fibrin formation via integrin $\alpha\text{IIb}\beta\text{3}$ and transglutaminase factor XIII. *Haematologica.* 2016; 101:427-36.
14. Zhang D, Ebrahim M, Adler K, Blanchet X, Jamasbi J, Megens RT et al. Glycoprotein VI is not a functional platelet receptor for fibrin formed in plasma or blood. *Thromb Haemost.* 2020; 120:977-93.
15. Lewis JC, Hantgan RR, Stevenson SC, Thornburg T, Kieffer N, Guichard J et al. Fibrinogen and glycoprotein IIb/IIIa localization during platelet adhesion. Localization to the granulomere and at sites of platelet interaction. *Am J Pathol.* 1990; 136:239-52.

16. Sánchez-Cortés J and Mrksich M. The platelet integrin $\alpha\text{IIb}\beta 3$ binds to the RGD and AGD motifs in fibrinogen. *Chem Biol.* 2009; 16:990-1000.
17. Dai A, Ye F, Taylor DW, Hu G, Ginsberg MH and Taylor KA. The structure of a full-length membrane-embedded integrin bound to a physiological ligand. *J Biol Chem.* 2015; 290:27168-75.
18. Van der Meijden PE, Heemskerk JW. Platelet biology and functions: new concepts and clinical perspectives. *Nat Rev Cardiol.* 2019; 16:166-179.
19. Miszta A, Pelkmans L, Lindhout T, Krishnamoorthy G, de Groot PG, Hemker CH et al. Thrombin-dependent incorporation of von Willebrand factor into a fibrin network. *J Biol Chem.* 2014; 289:35979-86.
20. Gilio K, Harper MT, Cosemans JM, Konopatskaya O, Munnix IC, Prinzen L et al. Functional divergence of platelet protein kinase C (PKC) isoforms in thrombus formation on collagen. *J Biol Chem.* 2010; 285:23410-9.
21. de Witt SM, Swieringa F, Cavill R, Lamers MM, Van Kruchten R, Mastenbroek T et al. Identification of platelet function defects by multi-parameter assessment of thrombus formation. *Nat Commun.* 2014; 5:4257.
22. Brouns SL, Van Geffen JP, Campello E, Swieringa F, Spiezia L, Van Oerle R et al. Platelet-primed interactions of coagulation and anticoagulation pathways in flow-dependent thrombus formation. *Sci Rep.* 2020; 10:11910.
23. Nagy M, Van Geffen JP, Stegner D, Adams DJ, Braun A et al. Comparative analysis of microfluidics thrombus formation in multiple genetically modified mice: link to thrombosis and hemostasis. *Front Cardiovasc Med.* 2019; 6:99.
24. Gotru K, Van Geffen JP, Nagy M, Mammadova-Bach E, Eilenberger J, Volz J et al. Defective Zn^{2+} homeostasis in mouse and human platelets with α - and δ -storage pool diseases. *Sci Rep.* 2019; 9:8333.
25. Van Geffen JP, Brouns SL, Batista J, McKinney H, Kempster C, Nagy M et al. High-throughput elucidation of thrombus formation reveals sources of platelet function variability. *Haematologica.* 2019; 104:1256-67.
26. Schindelin J, Arganda-Carreras I, Frise E, Kaynig V, Longair M, Pietzsch T et al. Fiji: an open-source platform for biological-image analysis. *Nat Methods.* 2012; 9:676-82.
27. Konings J, Hoving LR, Ariëns RS, Hethershaw EL, Ninivaggi M, Hardy LJ et al. The role of activated coagulation factor XII in overall clot stability and fibrinolysis. *Thromb Res.* 2015; 136:474-80.

28. Feijge MA, Van Pampus EC, Lacabartz-Porret C, Hamulyák K, Levy-Toledano S, Enouf J et al. Inter-individual variability in Ca^{2+} signaling in platelets from healthy volunteers: effects of aspirin and relationship with expression of endomembrane Ca^{2+} -ATPases. *Br J Haematol.* 1998; 102:850-9.
29. Heemskerk JW, Willems GM, Rook MB and Sage SO. Ragged spiking of free calcium in ADP-stimulated human platelets: regulation of puff-like calcium signals in vitro and ex vivo. *J Physiol.* 2001; 535:625-35.
30. Jooss NJ, De Simone I, Provenzale I, Fernandez DI, Brouns SL, Farndale RW et al. Role of platelet glycoprotein VI and tyrosine kinase Syk in thrombus formation on collagen-like surfaces. *Internatl J Mol Sci.* 2019; 20:2788.
31. Pugh N, Simpson AM, Smethurst PA, de Groot PG, Raynal N and Farndale RW. Synergism between platelet collagen receptors defined using receptor-specific collagen-mimetic peptide substrata in flowing blood. *Blood.* 2010; 115:5069-79.
32. Nagy M, Heemskerk JW and Swieringa F. Use of microfluidics to assess the platelet-based control of coagulation. *Platelets.* 2017; 28:441-8.
33. Swieringa F, Kuijpers MJ, Lamers MM, Van der Meijden PE and Heemskerk JW. Rate-limiting roles of the tenase complex of factors VIII and IX in platelet procoagulant activity and formation of platelet-fibrin thrombi under flow. *Haematologica.* 2015; 100:748-56.
34. Van der Meijden PE, Feijge MA, Swieringa F, Gilio K, Nergiz-Unal R, Hamulyák K et al. Key role of integrin $\alpha\text{IIb}\beta 3$ signaling to Syk kinase in tissue factor-induced thrombin generation. *Cell Mol Life Sci.* 2012; 69:3481-92.
35. Sixma JJ, Sakariassen KS, Stel HV, Houdijk WP, In der Maur DW, Hamer RJ et al. Functional domains on von Willebrand factor. Recognition of discrete tryptic fragments by monoclonal antibodies that inhibit interaction of von Willebrand factor with platelets and with collagen. *J Clin Invest.* 1984; 74:736-44.
36. Heemskerk JW, Vuist WM, Feijge MA, Reutelingsperger CP and Lindhout T. Collagen but not fibrinogen surfaces induce bleb formation, exposure of phosphatidylserine, and procoagulant activity of adherent platelets: evidence for regulation by protein tyrosine kinase-dependent Ca^{2+} responses. *Blood.* 1997; 90:2615-25.
37. Cosemans JM, Schols SE, Stefanini L, de Witt S, Feijge MA, Hamulyák K et al. Key role of glycoprotein Ib/V/IX and von Willebrand factor in platelet

- activation-dependent fibrin formation at low shear flow. *Blood*. 2011; 117:651-60.
38. Siljander P, Farndale RW, Feijge MA, Comfurius P, Kos S, Bevers EM et al. Platelet adhesion enhances the glycoprotein VI-dependent procoagulant response: Involvement of p38 MAP kinase and calpain. *Arterioscler Thromb Vasc Biol*. 2001; 21:618-27.
 39. Lecut C, Feijge MA, Cosemans JM, Jandrot-Perrus M and Heemskerk JW. Fibrillar type I collagens enhance platelet-dependent thrombin generation via glycoprotein VI with direct support of $\alpha 2\beta 1$ but not $\alpha 1\text{Ib}\beta 3$ integrin. *Thromb Haemost*. 2005; 94:107-14.
 40. Agbani EO, Van den Bosch MT, Brown E, Williams CM, Mattheij NJ, Cosemans JM et al. Coordinated membrane ballooning and procoagulant spreading in human platelets. *Circulation*. 2015; 132:1414-24.
 41. Suzuki-Inoue K, Wilde JI, Andrews RK, Auger JM, Siraganian RP, Sekiya F et al. Glycoproteins VI and Ib-IX-V stimulate tyrosine phosphorylation of tyrosine kinase Syk and phospholipase C $\gamma 2$ at distinct sites. *Biochem J*. 2004; 378:1023-9.
 42. Andre P, Morooka T, Sim D, Abe K, Lowell C, Nanda N et al. Critical role for Syk in responses to vascular injury. *Blood*. 2011; 118:5000-10.
 43. Nagy M, Perrella G, Dalby A, Becerra MF, Garcia Quintanilla L, Pike JA et al. Flow studies on human GPVI-deficient blood under coagulating and noncoagulating conditions. *Blood Adv*. 2020; 4:2953-61.
 44. Bänninger H, Lämmle B and Furlan M. Binding of α -thrombin to fibrin depends on the quality of the fibrin network. *Biochem J*. 1994; 298:156-63.
 45. Ahmed MU, Kaneva V, Loyau S, Nechipurenko D, Receveur N, le Bris M et al. Pharmacological blockade of glycoprotein VI promotes thrombus disaggregation in the absence of thrombin. *Arterioscler Thromb Vasc Biol*. 2020; 40:2127-42.

Supplementary materials of Chapter 6

Methods

Flow studies with FXIIIa or thrombin (receptor) inhibitors

Coverslips were coated for 1 hour with two spots, each 3-mm apart, that consisted of fibrin (upstream) and fibrin-FXIIIa (downstream), as described in the Methods. In short, fibrinogen (1 mg/mL, 0.5 μ L) was applied for 30 minutes, after which α -thrombin (20 nM, 1 μ L) was added for an additional 30 minutes. Where indicated, the thrombin was mixed with CaCl_2 (10 mM), FXIIIa (0.7 μ g/mL) and/or inhibitor T101 (20 μ M); and the mixture was applied on the fibrinogen spot. Whole blood flow was performed under conditions allowing coagulation at a total wall-shear rate of 1000 s^{-1} . To compare the effects of thrombin inhibitors, blood samples were preincubated for 10 minutes with vehicle or atopaxar (5 μ g/mL), recombinant hirudin (lepirudin 10 5 μ g/mL) and/or PPACK (40 μ M), then recalcified with 3.2 mM MgCl_2 (f.c.) and 6.3 mM CaCl_2 (f.c.) in Hepes buffer pH 7.45, and perfused through the flow-chamber at arterial shear rate (1000 s^{-1}). Fluorescent labels added per blood sample were DiOC₆ (platelet staining), AF568-annexin A5 (PS exposure), and AF647-anti-CD62P mAb (P-selectin expression). Brightfield and multicolor fluorescence images were taken every 2 minutes. Per donor, control and intervention conditions were repeated at least in duplicates. Collected time series of brightfield and fluorescence microscopic images were analysed by using pre-defined scripts¹. The scripts were formatted in the open source package Fiji².

Thrombin generation measurement and prothrombin staining

Coverslips were coated with spots of fibrin-FXIIIa (upstream) and collagen-I (downstream). Whole blood flow was perfused for 10 minutes under conditions allowing coagulation a total wall-shear rate of 1000 s^{-1} . Recalcified blood was perfused for 10 minutes, after which the thrombin-specific fluorogenic substrate Z-GGR-AMC (Z-Gly-Gly-Arg-AMC, 0.5 mM) was

added flow was continued for another 2 minutes. Fluorescence images were then taken under stasis every 2 minutes using a DAPI cube. To stain for labeled (pro)thrombin, thrombi were formed on similar spots under condition allowing coagulation, as described above. After 10 minutes of flow, the thrombi were post-perfused with Hepes buffer pH 7.45 containing CaCl_2 , 0.3 μM active-site labeled OG488-prothrombin (cleavable by factor Xa into OG488-thrombin)³ and TF (30 pM). Brightfield and fluorescence images were taken after rinse with Hepes buffer. Fluorescence microscopic images were analysed using pre-defined scripts.

Platelet adhesion to fibrin-forming spread platelets

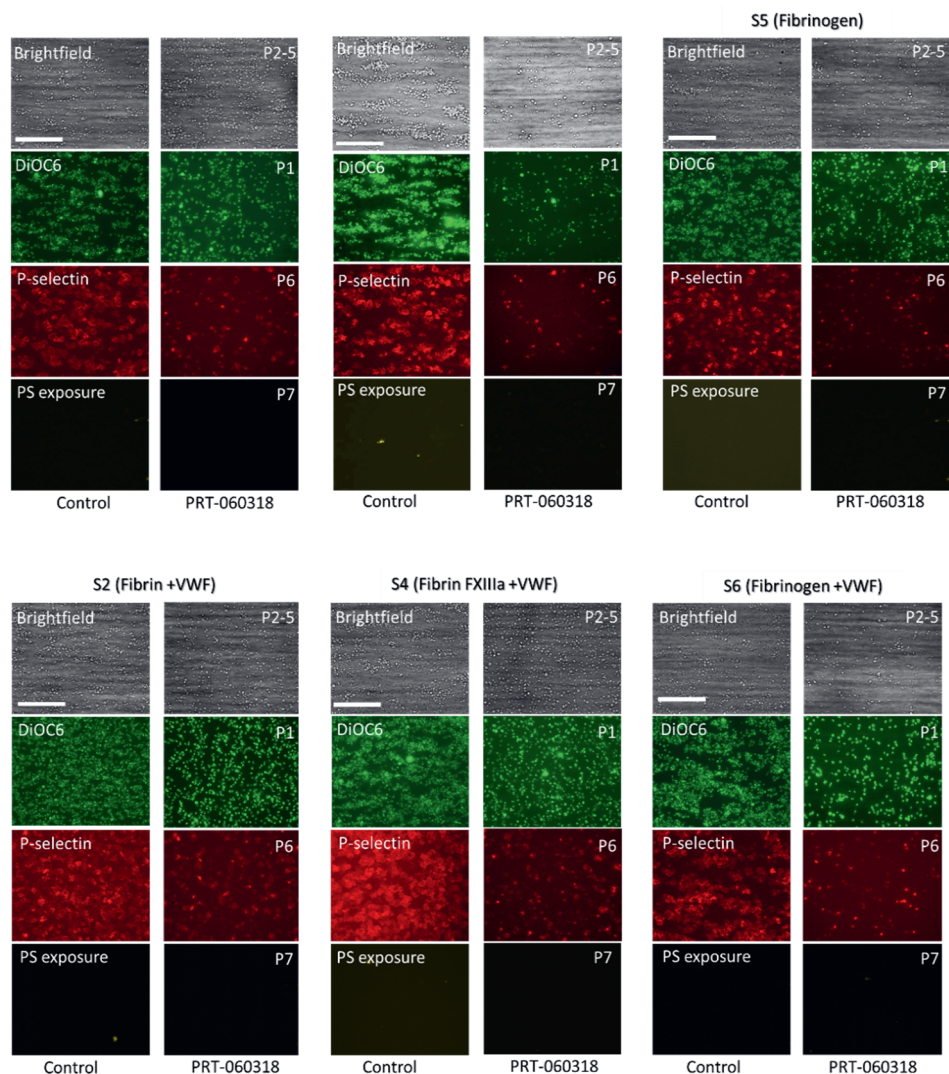
Washed platelets ($100 \times 10^9/\text{L}$) were allowed to spread on glass coverslips for 10 minutes, before blocking with 1% BSA in Hepes buffer pH 7.45. Plasma (citrate-anticoagulated) and CaCl_2 -containing medium (63 mM CaCl_2 and 32 mM MgCl_2 in Hepes buffer pH 7.45) were then co-perfused at low shear rate (250 s^{-1}) for 4 minutes, until fibrin fibres were appearing from the spread platelets. After stopping fibrin formation with heparin (1 U/mL), PPACK-anticoagulated whole blood was flowed over at 1000 s^{-1} , labeled with DiOC₆ (platelet staining), AF568-annexin A5 (PS exposure) and AF647-anti-CD62P mAb (P-selectin expression). During flow for 10 minutes, representative brightfield and tricolor fluorescence images, taken as overlays, were analyzed for fluorescence overlays after thresholding using the Colocalization Finder plugin of Fiji.

References

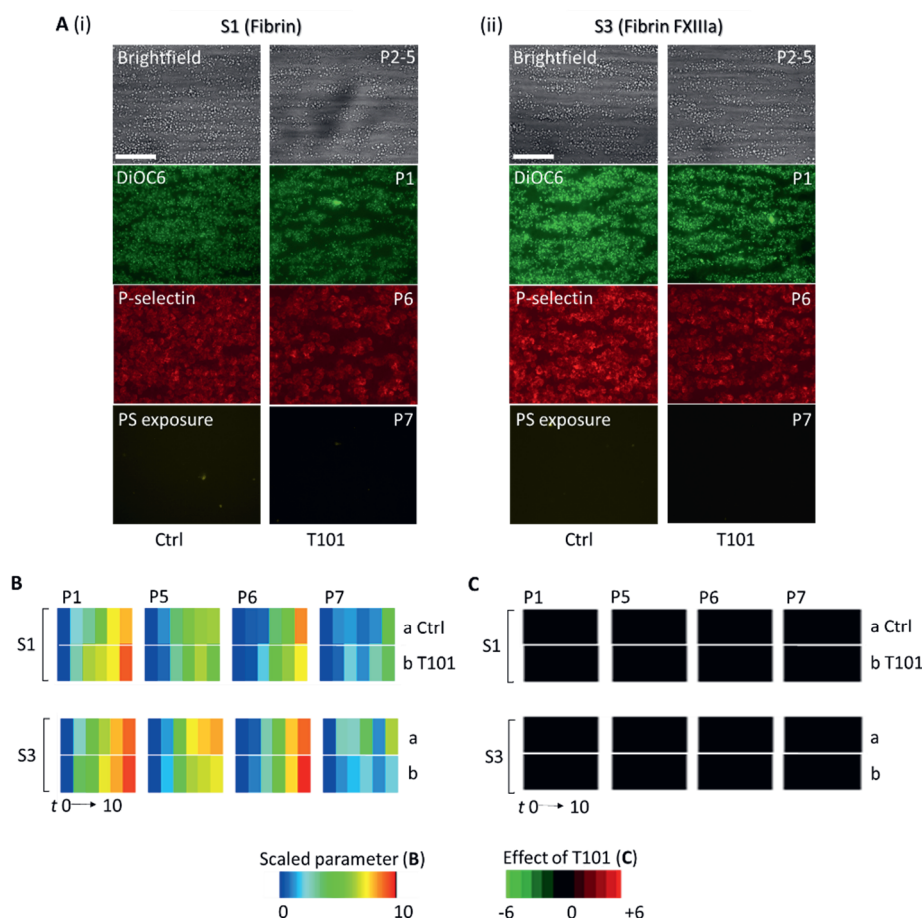
1. Van Geffen JP, Brouns SL, Batista J, McKinney H, Kempster C, Nagy M et al. High-throughput elucidation of thrombus formation reveals sources of platelet function variability. *Haematologica*. 2019;104:1256-67.
2. Schindelin J, Arganda-Carreras I, Frise E, Kaynig V, Longair M, Pietzsch T et al. Fiji: an open-source platform for biological-image analysis. *Nat. Methods*. 2012;9:676-82.

3. Berny MA, Munnix IC, Auger JM, Schols SE, Cosemans JM, Panizzi P et al. Spatial distribution of factor Xa, thrombin, and fibrin(ogen) on thrombi at venous shear. *Plos One*. 2010;5:e10415.

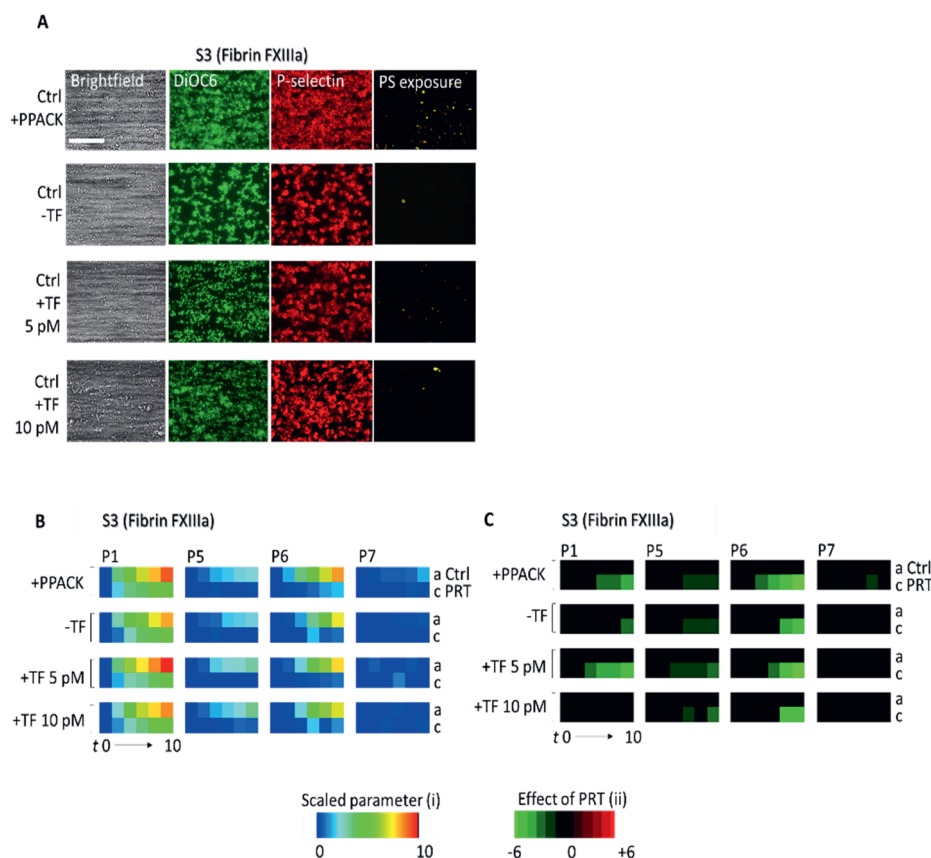
Supplementary figures of Chapter 6



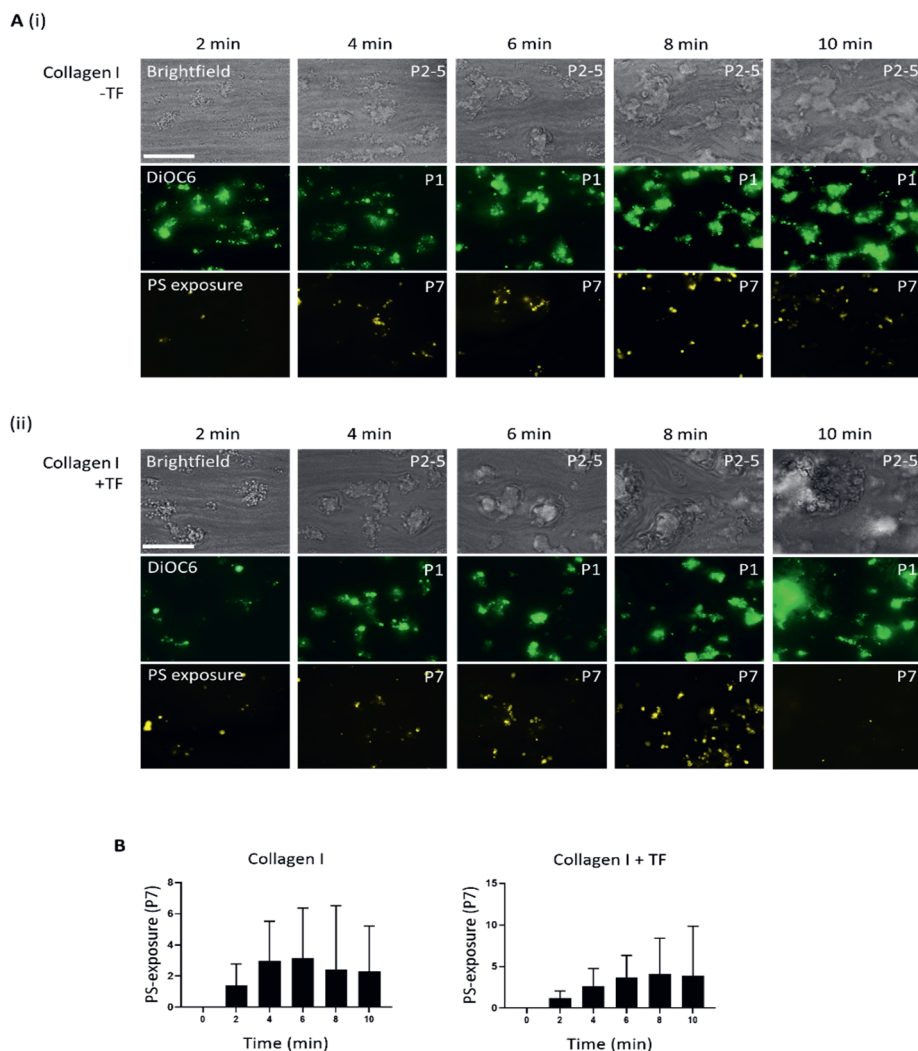
Suppl. Figure 1. Representative images of bilayered thrombi formed on various fibrin and fibrinogen surfaces with/without FXIIIa or VWF. Representative brightfield and fluorescence images ($n = 3-4$ donors) of fibrin (S1), fibrin + VWF-BP (S2), fibrin FXIIIa (S3), fibrin FXIIIa + VWF-BP (S4), fibrinogen (S5) and fibrinogen + VWF-BP (S6) with or without Syk inhibitor (PRT-060318, 10 μM) after 10 minutes of flow at arterial shear rate (1000 s^{-1}). Scale bar 50 μm .



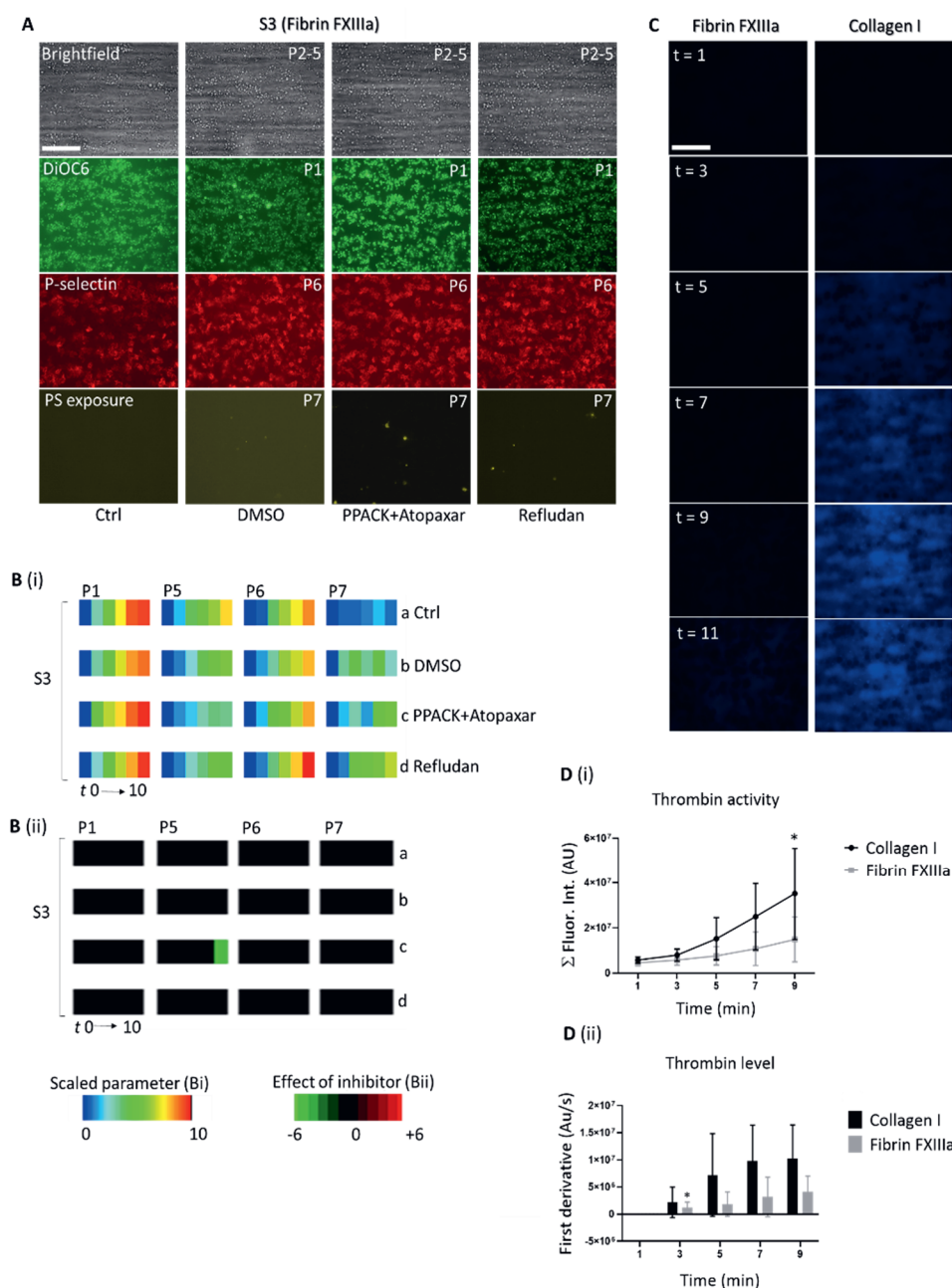
Suppl. Figure 2. Effect of factor XIIIa inhibition during fibrin formation on microthrombus formation. Spots of fibrin without (S1) or with co-coated FXIIIa (S3) were prepared, as in Methods. Inhibitor T101 (20 μ M) was added during fibrin formation, where indicated. Recalcified whole blood containing labels was flowed and parameters of thrombus formation were measured. **A**, Representative brightfield and fluorescence images after 10 minutes of flow over S1 (fibrin) (**A, i**) or S3 (fibrin-FXIIIa) (**A, ii**). **B**, Heatmaps of scaled image parameters (SAC%): P1 (DiOC₆), P5 (bi- or multilayer coverage), P6 (P-selectin) and P7 (PS exposure), demonstrating average effect of T101 per spot. Rainbow color code of scaled values from 0 (blue) to 10 (red). **C**, Subtraction heatmap showing effect of T101, for spots S1 and S3, filtered for significant changes ($n=3$; $P<0.05$, two-way ANOVA); black color indicates no significance.



Suppl. Figure 3. Role of Syk in regulation of microthrombus formation on fibrin spots at (non)coagulant conditions. Blood samples pre-incubated with vehicle (Ctrl) or Syk inhibitor (PRT, 10 μ M) were flowed over spots S3 (fibrin-FXIIIa) at 1000 s^{-1} . Microthrombi formed were imaged to obtain parameters P1 (adhesion via DiOC₆), P5 (bi- or multilayer size), P6 (P-selectin expression), and P7 (PS exposure). Effects of Syk inhibition were assessed per blood sample and parameter. **A**, Representative brightfield and fluorescence images per surface in the presence of PPACK or TF with/without PRT after 10 minutes of flow. **B**, Mean values from $n = 6$ blood samples were univariate scaled to 0-10. Heatmap of scaled parameters, demonstrating mean effects of Syk inhibition. Rainbow colour code indicates scaled values between 0 (blue) and 10 (red). **C**, Subtraction heatmap, representing effects of Syk inhibition, filtered for relevant changes ($n = 6$, $P < 0.05$, two-way ANOVA per surface and parameter). Color code represents decrease (green) or increase (red) in comparison to control. Scale bar 50 μ m.

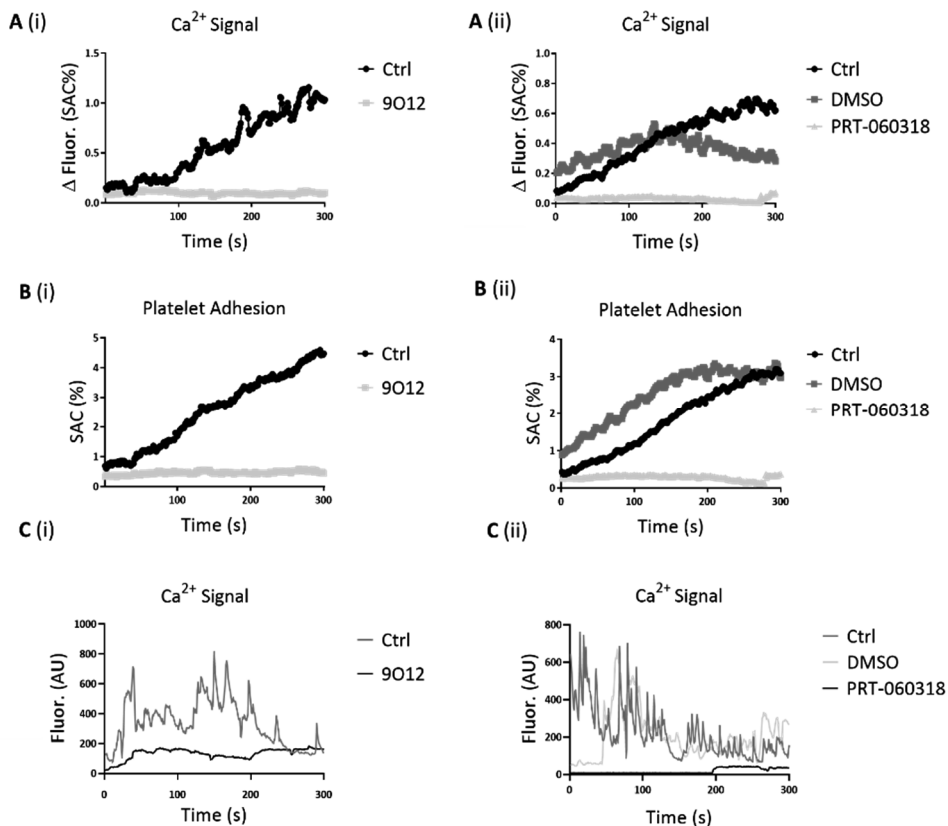


Suppl. Figure 4. Formation of multi-layered thrombi with phosphatidylserine (PS) exposure on collagen-I. Blood was flowed over collagen-I spots at shear rate of 1000 s^{-1} under coagulant conditions; tissue factor (TF) (10 pM, f.c.) was added to the recalcification buffer, where stated. Spots were imaged to obtain parameters P1 (DiOC₆) and P7 (PS exposure) over a time lapse of 10 minutes. **A**, Representative brightfield and fluorescence images of multilayered platelet thrombi formed on collagen-I (**A, i**), and collagen-I + TF (**A, ii**). Scale bar 50 μm . **B**, Graphs of PS exposure (P7) on collagen-I and on collagen-I + TF. Data are means \pm SD ($n = 10$).

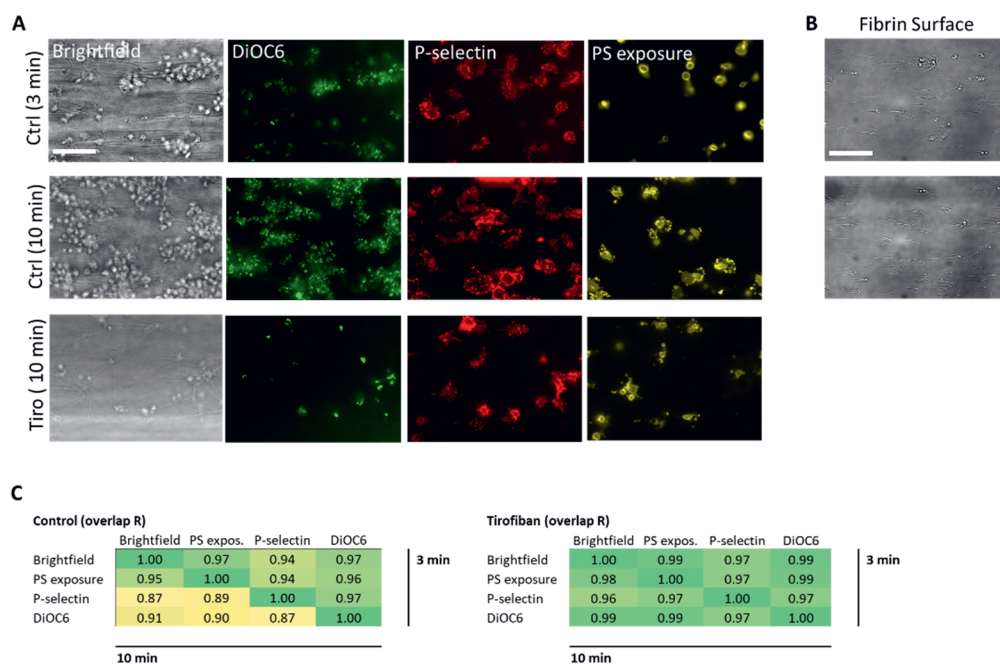


Suppl. Figure 5. Low contribution of thrombin to thrombus formation on fibrin surfaces. **A, B,** Recalcified, labeled whole blood was perfused over fibrin-FXIIIa spots at 1000 s^{-1} for 10 minutes, as for Figure 2. Blood samples were pre-treated with

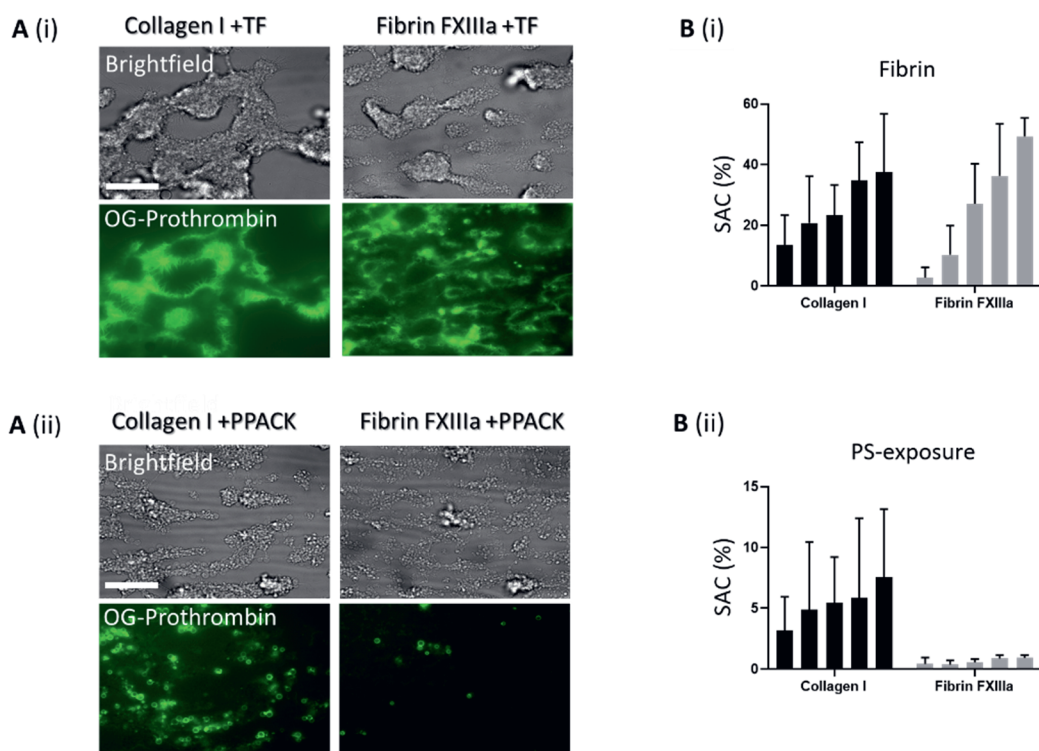
DMSO vehicle, lepirudin (10 $\mu\text{g/mL}$) or atopaxar (5 $\mu\text{g/mL}$) + PPACK (40 μM), as indicated. **A**, Representative images after 10 minutes of flow. Scale bar 50 μm . **B**, Microthrombi were analysed for parameters P1 (DiOC₆), P2 (bi- and multilayer score), P3 (P-selectin expression) and P4 (PS exposure) as a function of time. Scaled heatmaps of time-dependent changes, presented per parameter (**B, i**); and presented as subtraction heatmaps showing intervention effects after filtering for significance (green, $P < 0.05$ two-way ANOVA; black, not significant) (**B, ii**). **C-D**, Recalcified whole blood containing fluorogenic thrombin substrate Z-GGR-AMC (0.5 mM) was perfused over fibrin-FXIIIa and collagen-I spots at 1500 s^{-1} for 10 minutes. Subsequently, thrombin generation was measured under stasis from fluorescence accumulation per spot. **C**, Representative images taken every 2 minutes starting from 1 minute. **D**, Graph of integrated fluorescence intensity (**D, i**) and of first derivative indicating thrombin activity (**D, ii**). Thrombin generation comparing collagen and fibrin was measured for each time point. Means \pm SD ($n = 4$, $*P < 0.1$, Two-way ANOVA).



Suppl. Figure 6. Inhibition of GPVI or Syk affecting fibrin-induced Ca^{2+} fluxes in platelets under flow. Blood samples supplemented with autologous Fluo-4-loaded platelets were pre-incubated with vehicle (Ctrl), GPVI blocking antibody 9O12 or Syk inhibitor PRT-060318, and flowed over S3 spots (fibrin-FXIIIa). Fluorescence from adhered platelets was continuously recorded by confocal microscopy for 5 minutes. **A-B**, Movies analysed for fluorescence intensity above threshold fluorescence (Fluor.), i.e. representing elevated $[\text{Ca}^{2+}]_i$ above resting level (**A i and ii**), and for platelet adhesion as SAC% (**B i and ii**). Also shown are time traces of fluorescence changes in representative single platelets (**C i and ii**).



Suppl. Figure 7. Platelet adhesion and aggregation preferentially to immobilised platelets rather than to fibrin. Washed platelets were allowed to spread to glass coverslips, which were blocked with BSA-containing Hepes buffer pH 7.45, and then perfused with recalcified plasma to stimulate radial fibrin formation from the immobilized platelets. Subsequently, recalcified labeled (DiOC₆, anti-P-selectin and annexin A5) blood was flowed at shear rate 1000 s⁻¹, as for Figure 2. Integrin antagonist tirofiban (1 µg/mL) was present, where indicated. After 3 or 10 minutes, microscopic overlay images were taken from the same field. **A**, Representative brightfield and fluorescence images. **B**, Brightfield images of fibrin formed by the immobilized platelets. **C**, Matrix of overlap coefficients R of thresholded images, indicating similarity of positive pixels, for control and tirofiban conditions (n = 3). Note high pixel overlap of fluorescence from flowed DiOC₆ platelets with the P-selectin staining from the immobilized platelets; overlap further increased in the presence of tirofiban.



Suppl. Figure 8. Binding of cleaved OG488-prothrombin to fibrin in thrombi. Recalcified blood was perfused over fibrin-factor XIIa (FXIIIa) and collagen-I spots under coagulant (30 pM tissue factor, TF) or non-coagulant (20 μ M PPACK) conditions for 6 minutes at 1000 s^{-1} . The formed platelet thrombi were stained with OG488-prothrombin (green) in the presence of $CaCl_2$ and TF or PPACK, respectively. **A**, Representative brightfield and OG488-(pro)thrombin fluor-escence images from fibrin FXIIIa (**A, i**) and collagen-I (**A, ii**) spots. Scale bars 50 μ m. Note that with TF present the cleaved OG488-thrombin binds to fibrin-containing thrombi, whereas in the absence of coagulation (PPACK) the non-cleaved OG488-prothrombin only binds to balloon-shaped, PS-exposing platelets. **Bi-ii**, Graphs showing time-dependent increases in coverage of label in the presence of TF (OG488-thrombin) or PPACK (OG488-prothrombin). Mean + SD ($n=3$, $P<0.05$, two-way ANOVA).

Supplementary tables of Chapter 6

Major resource table

Antibodies

Target antigen	Vendor or Source	Catalog #	Working concentration	Lot #	Persistent ID / URL
Polyclonal anti-VWF-FITC Ab rabbit	DAKO (Michigan, MI, USA)	N.a.	20 µg/mL	N.a.	N.a.
AF488 donkey anti-rabbit IgG	Invitrogen ThermoFisher (Eindhoven, NL)	R37118	20 µg/mL	N.a.	https://www.thermofisher.com
mAb RAG35	Dr. J. van Mourik (CLB, Transfusion Service, Amsterdam, NL)	N.a.	20 µg/mL	N.a.	N.a.
Anti-GPVI Fab 9O12	Dr. M. Jandrot-Perrus (INSERM, University Paris Diderot, Paris, F)	N.a.	50 µg/mL	N.a.	N.a.
AF647-anti-human CD62P mAb	Biolegend (London, UK)	304916	0.5 µg/mL	N.a.	https://www.biolegend.com/en-us
AF568-annexin A5	ThermoFisher (Eindhoven, NL)	A13201	0.5 µg/mL	N.a.	https://www.thermofisher.com

Other

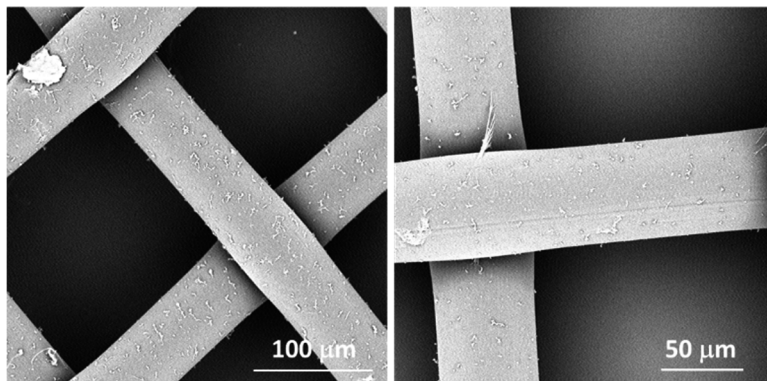
Description	Source / Repository	Persistent ID / URL
Membrane probe DiOC ₆	ThermoFisher (Eindhoven, NL)	https://www.thermofisher.com/order/catalog/product
Fluo-4 acetoxymethyl ester	ThermoFisher (Eindhoven, NL)	https://www.thermofisher.com/order/catalog/product/F14201
Pluronic	Invitrogen (Carlsbad CA, USA)	https://www.thermofisher.com/order/catalog/product/P3000OMP
D-Phe-Pro-Arg chloromethyl ketone (PPACK)	Santa Cruz Biotechnology (Santa Cruz, CA, USA)	https://www.scbt.com/p/ppack-dihydrochloride
Human fibrinogen	Enzyme Research Laboratories (Swansea, UK)	https://www.enzymeresearch.co.uk/product/human-fibrinogen-von-willebrand-factor-and-plasminogen-depleted
Human α -thrombin	Stago (Saint-Ouen-l'Aumône, F)	N.a.
Collagen-I Horm	Nycomed (Hoofddorp, NL)	https://www.takeda.com/de-at/hcps/diagnostika
Human collagen-III	Southern Biotechnology (Birmingham, AL, USA)	https://www.southernbiotech.com
VWF-BP	CambCol (Cambridge, UK)	http://www.cambcollabs.com
Tissue factor (rTF; Innovin)	Siemens (Erlangen, D)	https://www.yumpu.com/es

Table continuing on next page

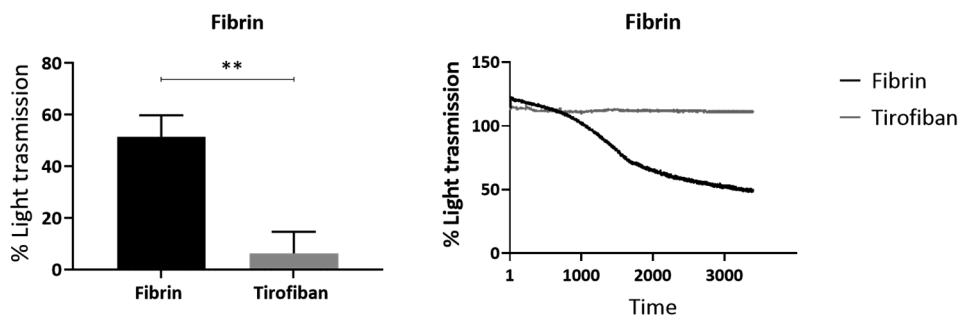
Description	Source / Repository	Persistent ID / URL
Syk inhibitor PRT-060318	Bio-Connect, (Huissen, NL)	https://www.bio-connect.nl/chemicals/prt-060318
Z-Gly-Gly-Arg-AMC	Bio-Connect (Huissen, NL)	https://www.bio-connect.nl/chemicals/z-gly-gly-arg-amc-acetate
Atopaxar	Axon Medchem (Groningen, NL)	https://www.axonmedchem.com/product/2030
Lepirudin	Abcam (Cambridge, UK)	https://www.abcam.com/recombinant-hirudin-protein-ab73660
FXIIa inhibitor T101	Zedira (Darmstadt, D)	https://zedira.com/Blood-coagulation/FXII-Inhibitors
OG488-prothrombin	Gift from Dr. P. Bock (Vanderbilt USM, Nashville, TE, USA)	N.a. Ref. ³

Appendix

Fibrinogen



Appendix Figure 1. Representative images of fibrinogen. Scanning electron microscopy (SEM) images of immobilised fibrinogen spot coated on a SEFAR filter.



Appendix Figure 2. Inhibition of integrin $\alpha IIb\beta 3$ in fibrin-activated platelets. Platelets in suspension were treated with integrin $\alpha IIb\beta 3$ inhibitor, tirofiban (5 $\mu\text{g/mL}$) for 10 minutes, before stimulation with fibrin. Platelet aggregation was monitored with conventional light transmission aggregometry. **A**, Quantitation of maximal aggregation upon stimulation with fibrin. **B**, Representative aggregation traces. Mean \pm SD ($n = 3$), ** $P < 0.005$ (two-tailed Student's unpaired t-test).

EMBARGOED

Chapter 7

Restrained glycoprotein VI-induced platelet signaling by tyrosine protein phosphatases independent of phospholipase C γ 2

Huang J, Fernández DI, You J, Wang X, Heemskerk JWM*, García Á*
(*equal contribution)

To be submitted

I performed experiments and analysed the data with D.I.F., J.Z. and X.W. I designed the experiments, conceptualized and wrote the manuscript with J.W.M.H. and A.G.

Chapter 8

Roles of focal adhesion kinase PTK2 and integrin $\alpha\text{IIb}\beta\text{3}$ signaling in collagen- and GPVI-dependent thrombus formation under shear

Huang J, Jooss NJ, Fernández DI, Sickmann A, García Á, Wichapong K,
Dijkgraaf I*, Heemskerk JWM*
(*equal contribution)

Int. J. Mol. Sci. 2022; 23:8688

Reprinted with permission

I designed and performed experiments and analysed the data with N.J., K.W., D.I.F. and I.D. I conceptualized and wrote the manuscript with I.D. and J.W.M.H. A.S., A.G. and J.W.M.H. provided funding and supervision.

Abstract

Glycoprotein (GP)VI and integrin $\alpha\text{IIb}\beta 3$ are a key signaling receptors in collagen-dependent platelet aggregation and in arterial thrombus formation under shear. The multiple downstream signaling pathways are still poorly understood. Here, we focused on disclosing the integrin-dependent roles of focal adhesion kinase (protein tyrosine kinase 2, PTK2), the shear-dependent collagen receptor GPR56 (*ADGRG1* gene), and calcium and integrin-binding protein 1 (CIB1). We designed and synthesized peptides that interfered with the integrin αIIb binding (pCIB and pCIB^m) or mimicked activation of GPR56 (pGRP). The results show that the combination of pGRP with PTK2 inhibition or of pGRP with pCIB > pCIB^m in additive ways suppressed collagen- and GPVI-dependent platelet activation, thrombus buildup and contraction. Microscopic thrombus formation was assessed by 8 parameters (with script descriptions enclosed). The suppressive rather than activating effects of pGRP were confined to blood flow at a high shear rate. Blockage of PTK2 or interference of CIB1 no more than slightly affected thrombus formation at a low shear rate. Peptides did not influence GPVI-induced aggregation and Ca^{2+} signaling in the absence of shear. Together, these data reveal a shear-dependent signaling axis of PTK2, integrin $\alpha\text{IIb}\beta 3$ and CIB1 in collagen- and GPVI-dependent thrombus formation, which is modulated by GPR56 and exclusively at high shear. This work thereby supports the role of PTK2 in integrin $\alpha\text{IIb}\beta 3$ activation and signaling.

Introduction

Collagen- and fibrin(ogen)-induced platelet activation and aggregation through glycoprotein VI (GPVI) has been recognized as controlling processes of *in vitro* and *in vivo* arterial thrombus formation, with only a limited role in hemostasis¹⁻³. GPVI is an immunoglobulin receptor that via the FcR γ -chain co-receptor, when triggered upon ligand binding, causes activation of a signal transduction pathway of protein tyrosine kinases, phosphatidylinositol-3-kinases and phospholipase $\text{C}\alpha_2$ (PLC α_2), to evoke granule release and activation of integrin $\alpha\text{IIb}\beta_3$ ⁴⁻⁶. Fibrinogen is the major ligand for integrin $\alpha\text{IIb}\beta_3$ to establish platelet aggregation and thrombus formation, in which the integrin can act in a non-redundant way with GPVI⁷⁻⁹.

Recent multiparameter microfluidics assays have provided first understanding of the molecular mechanisms, implicated in whole-blood thrombus formation involving GPVI¹⁰⁻¹². The heterogenous buildup of arterial thrombi takes place by a series of consecutive platelet activation events, *i.e.* flow-dependent platelet adhesion, integrin $\alpha\text{IIb}\beta_3$ activation, granular secretion, platelets aggregation and thrombus contraction and stabilization^{8,13}. Mouse studies have shown that several hundreds of platelet expressed genes and proteins contribute to collagen-dependent arterial thrombus formation, thus pointing to a high complexity of the underlying platelet signaling pathways¹⁴.

Knowing that multiple shear-dependent platelet adhesion mechanisms¹⁵ and platelet-platelet interactions¹¹ can determine the thrombus-forming process, we used our experience in the targeted design and synthesis of anti-platelet peptide^{13,15} to reveal the importance of less understood signaling pathways. In this context, a less well-studied protein kinase acting downstream of $\alpha\text{IIb}\beta_3$ in platelets is focal adhesion kinase PTK2 (PTK2, also known as focal adhesion kinase)¹⁶⁻¹⁸. In various cell types, including platelets, PTK2 is known to accumulate in focal adhesion sites formed upon stretching forces^{19,20}. In the mechanical force-dependent activation and

signaling of integrins, PTK2 was found to regulate the adhesion-dependent talin activity and actomyosin dynamics²¹. Interestingly, PTK2 has recently become a potential therapeutic target for some cancers^{22,23}.

Both peptide inhibition and mouse knockout studies have shown that platelet PTK2 can become activated upon fibrinogen binding via the calcium and integrin-binding protein 1 (CIB1, gene *CIB1*). Interaction of CIB1 with the α IIb chain appeared to regulate the integrin outside-in signaling²⁴⁻²⁷. Proteomic analyses have revealed that PTK2 and CIB1 are expressed at reasonable numbers of 2,956 and 780 copies/platelet, respectively^{28,29}. Yet, there is confusion if the role of CIB1 on platelets is stimulatory³⁰ or inhibitory³¹. Of note, the CIB1-PTK2 interaction occurs independently of tyrosine kinase Syk, which binds to the other β 3 integrin chain. In the absence of CIB1, platelet spreading on fibrinogen was found to be greatly impaired^{24,26}. Evidence for this role of CIB1 came in part from use of a α IIb cytoplasmic peptide (pCIB), entering platelets and interfering with the binding of CIB1 to α IIb, the peptide efficiently inhibited the human platelet spreading via the outside-in signaling mechanism²⁵. Mouse knockout studies further proved that CIB1 contributes to arterial thrombosis and hemostasis³⁰.

A novel shear force-dependent receptor on platelets is the G protein-coupled receptor 56 (GPR56, gene *ADGRG1*), signaling via G α 13 to allow platelet shape change³². In both human and mouse platelets, the *ADGRG1* mRNA is expressed at relatively high levels²⁹. In other cells, GPR56 appeared as an adhesive receptor for collagen type-III³³. In initial papers, identifying GPR56 as a shear-dependent collagen receptor, it appeared to become self-activated via its tethered ligand, after which signaling responses through other collagen receptors like GPVI were enforced^{32,34}. Knock-out mouse studies pointed to a moderate role of GPR56 in arterial thrombosis and hemostasis³². However, the precise requirements of GPR56 to support human thrombus formation on vascular collagens remained unclear.

In the present paper, we used a panel of inhibitors and synthesized peptides to re-investigate the roles of PTK2, CIB1 and GPR56 in shear-dependent

thrombus formation on a range of collagen surfaces with variable GPVI dependency.

Materials and Methods

Materials

Horm collagen type I derived from equine tendon was obtained from Nycomed (Hoofddorp, The Netherlands). Human placenta-derived collagen type III (1230-01S) was supplied by Southern Biotechnology (Birmingham, AL, USA). Human collagen type IV, FAK inhibitor 14 (FAK-IN14) and PF573228 were obtained from Sigma-Aldrich (Zwijndrecht, The Netherlands). PPACK (D-phenylalanyl-L-propyl-L-arginine chloromethyl ketone) came from Calbiochem (520222, Amsterdam, The Netherlands). Fura-2 acetoxymethyl ester and pluronic were from Invitrogen (Carlsbad, CA, USA). As fluorescent stains were used Alexa Fluor (AF)647-conjugated anti-human CD62P mAb (304918, Biolegend, London, UK), FITC-labeled fibrinogen (F0111, Dako, Amstelveen, The Netherlands), and AF568-labeled annexin A5 (A13202, ThermoFisher, Eindhoven, The Netherlands). Other reagents came from Sigma-Aldrich, or from sources described before⁴¹.

Preparation of blood and platelets

Blood was drawn from healthy volunteers through venipuncture. Donors had not received anti-platelet medication for at least two weeks, and gave full informed consent according to the declaration of Helsinki. Studies were approved by the local Medical Ethics Committee of Maastricht University Medical Centre⁺. Blood from donors was collected into 3.2% trisodium citrate (Vacurette tubes, Greiner Bio-One, Alphen a/d Rijn, The Netherlands). All blood samples had platelet counts within the reference ranges, such as measured by a Sysmex XN-9000 analyzer (Sysmex, Cho-ku, Kobe, Japan).

Platelet-rich plasma (PRP) and washed platelets were isolated, basically as described before⁴⁶. In brief, PRP was obtained from citrated blood by centrifugation at 240 g for 15 minutes. After addition of 1:10 vol/vol acid

citrate dextrose (ACD; 80 mM trisodium citrate, 183 mM glucose, 52 mM citric acid), this PRP was centrifuged at 5,500 g for 2 minutes. The pelleted platelets were resuspended into Hepes buffer pH 6.6 [10 mM Hepes, 136 mM NaCl, 2.7 mM KCl, 2 mM MgCl₂, 5.5 mM glucose and 0.1% bovine serum albumin (BSA)]. After addition of apyrase (1 U/mL) and 1:15 vol/vol ACD, another centrifugation step was performed to obtain washed platelets. The final platelet pellet was resuspended into Hepes buffer pH 7.45 (10 mM Hepes, 136 mM NaCl, 2.7 mM KCl, 2 mM MgCl₂, 5.5 mM glucose and 0.1% BSA) at requested platelet count as indicated below.

Selection and design of peptides

The 7-amino acid peptide TYFAVLM (pGRP), comprising the N-terminal tethered ligand of GPR56, was synthesized as described previously³³. Other peptides were synthesized to target the interaction site of the EF-hand domain of CIB1 with the integrin α IIb chain in the membrane-proximal hydrophobic 15-amino acids region^{47,48}. These included the wildtype CIB1-binding peptide Ace-LVLAMWKVGFFKRNRPPEEDDEEGQ-OH (pCIB), corresponding to the cytoplasmic C-terminus of the α IIb chain (Leu⁹⁸³-Glu¹⁰⁰⁸), which has been previously shown to be internalized into platelets²⁴. In addition, we designed and synthesized a more hydrophobic, mutated form Ace-LVRKMWQVGFYKRNRYPLEEDDEEGQ-OH (pCIB^m), and calculated the lowest binding free energy (BFE). For designing the latter, the structure of the α IIb chain was extracted from known NMR analyses (PDB ID: 2KNC), and this was virtually docked onto the binding pocket of CIB1 (PDB ID: 2LM5) by applications of the HADDOCK and HDock routines of the protein-protein docking WebServer^{49,50}. The retrieved docking poses were refined by performing molecular dynamics simulations, and BFE of these docking poses were also calculated and compared in order to determine a likely binding mode of pCIB-CIB1 complex. The docking solution which gave the lowest BFE, indicative of the most thermodynamically favorable conformation, was chosen as a template for improved *in silico* design peptide candidates^{51,52}. The virtually optimized CIB1-peptide complexes were subjected to

molecular dynamics simulations and BFE calculations to predict the most favorable peptide candidate, pCIB^m, using methods described before⁵³.

Solid-phase synthesis of peptides

The pCIB peptide was synthesized using automated microwave (CEM Liberty BLUE microwave peptide synthesizer) Fmoc-based synthesis on a Cl-MPA ProTide resin at 0.25 mmol scale. The modified peptide pCIB^m was also synthesized at 0.25 mmol scale, but using manual solid-phase peptide synthesis on a methylbenzhydrylamine polystyrene resin (ChemPep, Wellington, FL, USA), as described^{54,55}. For producing pCIB^m, 2-(6-chloro-1*H*-benzotriazol-1-yl)-1,1,3,3-tetramethylammonium hexafluoro-phosphate (Peptides International, Louisville, KY, USA) was used as coupling reagent. After cleavage of the produced peptide from resin using anhydrous hydrogen fluoride (GHC, Hamburg, Germany), the crude product was analyzed on a Waters (Milford, MA, USA) ultrahigh performance liquid chromatography mass spectrometric XEVO-G2QToF system. Both peptides were purified by semipreparative HPLC using a Vydac C₁₈ HPLC column (10×25 mm, 12 mL/min flow rate or 22×250 mm, 20 mL/min flow rate; Grace Davison Discovery Sciences, Deerfield, IL, USA) connected to a Waters Deltaprep System consisting of Prep LC Controller and a 2487 Dual wavelength absorbance detector (λ = 214 nm). To elute the peptides, an appropriate gradient of buffer B in buffer A was used, where buffer A was composed of 0.1% trifluoroacetic acid (Biosolve, Valkenswaard, The Netherlands) in H₂O/CH₃CN (95/5, v/v, Biosolve) and buffer B contained 0.1% trifluoroacetic acid in CH₃CN/H₂O (90/10, v/v).

Whole-blood thrombus formation

Microspots of collagen-I (M1), collagen-III (M2) and collagen-IV (M3) were applied by coating degreased coverslips with 0.5 μ L of 100 μ g/mL, as described previously¹⁰. After coating, the coverslips were incubated in a humid chamber overnight at 4°C, washed with saline, and blocked with 1% BAS-containing Hepes buffer pH 7.45 supplemented 30 minutes, before

assembling into the microfluidic chamber⁵⁶. In case of multiple microspots, the most active was located downstream, to prevent cross-activation of platelets¹⁰.

For the assessment of thrombus formation, samples of 500 μL citrated whole blood were pre-incubated with saline, or the indicated peptides or inhibitors for 10 minutes at room temperature. Immediately before perfusion, blood samples were supplemented with 40 μM PPACK and recalcified with 3.75 mM MgCl_2 and 7.5 mM CaCl_2 (f.c.). The recalcified blood was then flowed through a microspot-containing flow chamber for 3.5 minutes at wall shear rate of 1000 s^{-1} or 1600 s^{-1} , or for 6 minutes at wall shear rate of 150 s^{-1} . After flow, staining was started by a 2- minutes perfusion with AF647 anti-CD62P mAb (for P-selectin expression), FITC-fibrinogen (for integrin $\alpha\text{IIb}\beta 3$ activation), and AF568-annexin A5 (for phosphatidylserine exposure) in Hepes buffer pH 7.45 containing 2 mM CaCl_2 and 1 U/mL heparin, as described before¹¹. During staining, two brightfield images were captured per microspot. Subsequently, residual label was removed by post-perfusion with Hepes buffer pH 7.45 containing 2 mM CaCl_2 and 1 U/mL heparin, after which three representative multicolor fluorescence images were captured per microspot. All conditions were performed by duplicate runs with blood from at least 3 donors.

Microscopy and image analysis

Brightfield and fluorescence images were taken using an EVOS-FL microscope (Life Technologies, Bleiswijk, The Netherlands), equipped with Cy5, RFP and GFP LEDs, an Olympus UPLSAPO 60x oil-immersion objective, and a sensitive 1360×1024 pixel CCD camera¹¹. The images were analyzed using semi-automated scripts operating in Fiji (ImageJ) and a scoring procedure based on a preset of reference images⁴. Observers were blinded to the experimental condition. Per microspot, this gave five parameters from brightfield images (*P1-5*) and in one parameter from each of the three-color fluorescence images (*P6-8*), such as defined in Table 1.

Table 1. Overview of obtained parameters (P1-8) of thrombus formation from brightfield and fluorescence images. Measured ranges and scaling factor for heatmap analysis are also indicated. Abbreviations: PS, phosphatidylserine; SAC, surface area coverage. For details how the parameters were established using Fiji, see supplementary materials.

	Parameters	Range	Scaling
<i>Brightfield images</i>			
P1	Platelet adhesion (% SAC)	0-72.7	0-10
P2	Platelet aggregate coverage (% SAC)	0-29.8	0-10
P3	Thrombus morphological score	0-4.75	0-10
P4	Thrombus multilayer score	0-2.75	0-10
P5	Thrombus contraction score	0-2.75	0-10
<i>Fluorescence images</i>			
P6	PS exposure (% SAC)	0-22.2	0-10
P7	P-selectin expression (% SAC)	0-71.7	0-10
P8	Fibrinogen binding (% SAC)	0-45.7	0-10

Detailed information on the scripts and scoring procedures are given in the supplementary methods. This section also provides reference brightfield images, used for the scoring. In brief, P1 (platelet adhesion) represents the percentage of total surface-area-coverage (SAC%) occupied by platelets. P2 (platelet aggregate coverage) concerns the SAC% occupied by multilayered platelet aggregates. P3 (thrombus morphological score) P4 (thrombus multilayer score) and P5 (thrombus contraction score) describe the thrombus phenotype, such in comparison to reference images, ranging from 0,0,0 (essential absence of platelets) to 5,3,3 (large contracted, multilayered platelet aggregates). Finally, P6 (PS exposure), P7 (P-selectin expression) and P8 (fibrinogen binding) represent %SAC of platelets staining positively for the respective fluorescent probes.

Light transmission aggregometry

Aggregation of washed platelets ($250 \times 10^9/\text{L}$) was measured at 37°C under stirring at 1,200 rpm using a chronology aggregometer (Havertown, PA, USA). Platelet samples of 500 μL were pre-incubated with saline, tirofiban (1 $\mu\text{g}/\text{mL}$) or indicated inhibitors (peptides) for 10 minutes. Platelet activation was with indicated agonists at 37°C .

Cytosolic Ca^{2+} measurements

Washed platelets ($200 \times 10^9/\text{L}$) were loaded with a mixture of Fura-2 acetoxymethyl ester (3 μM) and pluronic (0.4 $\mu\text{g}/\text{mL}$) in a 40 minutes incubation at room temperature, as described elsewhere⁴¹. After centrifugation in the presence of 1:10 ACD and apyrase (1 U/mL), the dye-loaded cells were resuspended at the same concentration into Hepes buffer pH 7.45. Samples of 200 μL in 96-wells plates were pre-incubated either with saline, tirofiban (1 $\mu\text{g}/\text{mL}$), or indicated inhibitor (peptide) for 10 minutes at room temperature. Subsequently, 1 mM CaCl_2 was added, and after adaptation to 37°C , ratiometric changes in fluorescence (excitation wavelengths 340 and 380 nm, emission wavelength 510 nm) were measured per well with a FlexStation 3 (Molecular Devices, San Jose, CA, USA). Agonists collagen-I (10 $\mu\text{g}/\text{mL}$, f.c.) or CRP-XL (10 $\mu\text{g}/\text{mL}$, f.c.) were added by roboted pipetting. For optimal, diffusion-limited mixing, the speed of agonist injection was set at 125 $\mu\text{L}/\text{s}$ ⁴¹. Calibrated, nanomolar changes in cytosolic $[\text{Ca}^{2+}]_i$ were calculated as before^{57,58}. Measurements were performed in triplicate wells, with platelets isolated from at least 3 donors.

Statistics and data processing

Statistical analysis was performed with GraphPad Prism 8 software (San Diego, CA, USA). Figures were generated with the same package. Parameter values of thrombus formation from 2-3 corresponding images in the same run were averaged. In addition, parameters of duplicate flow runs were averaged obtain one parameter set per donor, microspot and condition⁴¹. For heatmap representation, mean parameter values across microspots

were univariate normalized $0-10^{11}$. For statistical analysis, values of control and inhibitor runs were compared per donor, using a paired Student's t-test. In the subtraction heatmaps, a conventional filter was set at P-values below 0.05^{41} .

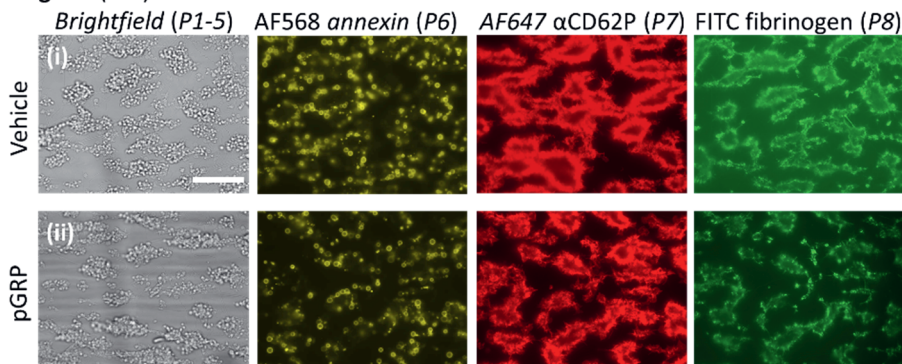
Results

Limited effect of the GPR56 peptide on collagen induced thrombus formation under shear

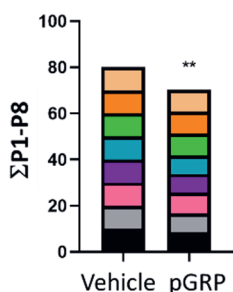
To investigate how the novel collagen receptor GPR56 contributes to platelet adhesion and thrombus-formation, we treated blood from healthy donors with the synthesized peptide pGRP (TYFAVLM, $50 \mu\text{g/mL}$), corresponding to the hidden tethered ligand of GPR56, and hence mimicking the shear-dependent activation of this receptor³². Perfusion of the blood was performed at arterial wall-shear rate of 1600 s^{-1} ^{11,35}. For platelet interaction, microspots of collagen-I, collagen-III and collagen-IV were used with decreasing GPVI dependency. As before, brightfield and multicolor microscopic images taken after perfusion were analyzed for eight parameters (Table 1), *i.e.* platelet adhesion (*P1*), platelet aggregation (*P2*), thrombus morphology, multilayer and contraction scores (*P3-5*), and platelet activation markers phosphatidylserine exposure (*P6*), P-selectin expression (*P7*) and integrin $\alpha\text{IIb}\beta 3$ activation (*P8*). An extended description of the scripts in Fiji to measure the continuous parameters and to obtain the discontinuous scores is given in the supplementary materials.

Representative images collected at end-stage for collagen-I (Figure 1A) and for collagen-III and -IV (Suppl. Figure 1A, B) indicated that treatment with pGRP did no more than slightly affect platelet adhesion and thrombus buildup (brightfield images) or platelet activation (3-color fluorescence images). Summative presentation of the univariate scaled parameter values pointed to inhibitory rather than stimulatory peptide effect, which was only significant for collagen-I and -IV (Figure 1B i-iii). Similar results were obtained at the standard high shear rate of 1000 s^{-1} . Control experiments did not point

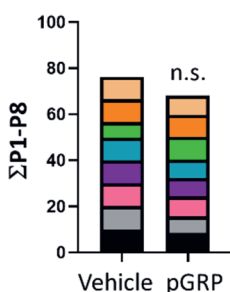
A Collagen-I (M1)



B (i) Collagen-I (M1)



(ii) Collagen-III (M2)



(iii) Collagen-IV (M3)

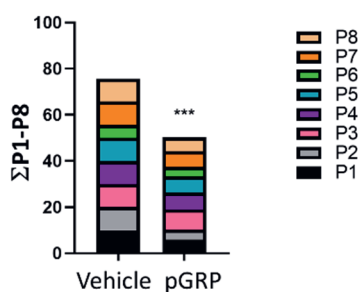


Figure 1. Effect of GPR56 interference on collagen-induced thrombus formation at high shear rate. Whole blood (700 μL) was pre-incubated with vehicle medium or pGRP peptide (50 $\mu\text{g}/\text{mL}$) for 10 minutes. After recalcification, blood samples were perfused over microspots of collagen-I, -III and -IV for 3.5 minutes at wall-shear rate of 1600 s^{-1} . Brightfield and fluorescence images were taken per microspot at end stage. **A**, Shown are representative microscopic images for collagen-I of: (i) vehicle control runs, or (ii) pGRP runs. Scale bar = 10 μm . Complementary images for thrombi on collagen-III and collagen-IV are given in Suppl. Figure 1. **B**, Cumulative plots per condition of scaled (0-10) image parameters: P1, platelet adhesion; P2, platelet aggregate coverage; P3-5, thrombus morphology, multilayer and contraction scores; platelet activation markers: P6, PS exposure; P7, P-selectin expression; P8, fibrinogen binding (see Table 1). Shown are means of duplicate runs for 3 donors. Mean values \pm SD, * $P < 0.05$, ** $P < 0.005$, *** $P < 0.001$, **** $P < 0.0001$ vs. vehicle (paired Student's t-test).

to a pGRP effect on collagen-induced platelet aggregation by conventional light transmission aggregometry (not shown, but see below).

Effects of the GPR56 peptide combined with PTK2 inhibition on thrombus formation under shear

Given the proposed mechanism of GPR56 in shear- and Gα13-dependent platelet activation³², we hypothesized that its role could be masked by integrin αIIbβ3 outside-in signaling, in which the focal adhesion kinase PTK2 plays a central role^{17,36,37}. To investigate this, we used two structurally different PTK2 inhibitors, PF573228 and FAK-IN14, of which the former was tested before on human platelets^{38,39}. Initial dose-response experiments (2.5-10 μM) indicated a more potent effect of PF573228 than of FAK-IN14 on collagen-induced platelet aggregation (Figure 2A, B), which agrees with published IC₅₀ values^{38,40}. As expected, under the slowly stirred conditions (1200 rpm providing a low shear rate) in light transmission aggregometry, the addition of pGRP did not further enhance the dose-dependent inhibitory effects of PF573228 or FAK-IN14 on platelet aggregation (Figure 2B).

To investigate how PTK2 inhibition affected whole-blood thrombus formation, we used the same microfluidic setup with collagen-I, -III and -IV. Blood samples were pretreated with 2.5-10 μM of PF573228 or FAK-IN14, and then perfused over the collagen spots at the standard high shear rate of 1000 s⁻¹. Inspection of microscopic images showed a consistent effect of PF573228 and FAK-IN14 at the highest dose applied by reducing platelet aggregate formation on collagen-I (Figure 3A i-iii). Subtraction heatmap analysis after parameter scaling showed that the reduction with either inhibitor extended to the majority of parameters, as well as from collagen-I and -III to collagen-IV (Figure 3B). This was confirmed by summation of the univariate scaled parameters P1-8, pointing to a significant reduction for PF573228 > FAK-IN14 (Suppl. Figure 2A-C, panels i).

We then examined the combined effect with the GPR56 peptide added. Surprisingly, the combination of pGRP with PF573228 or FAK-IN14 further

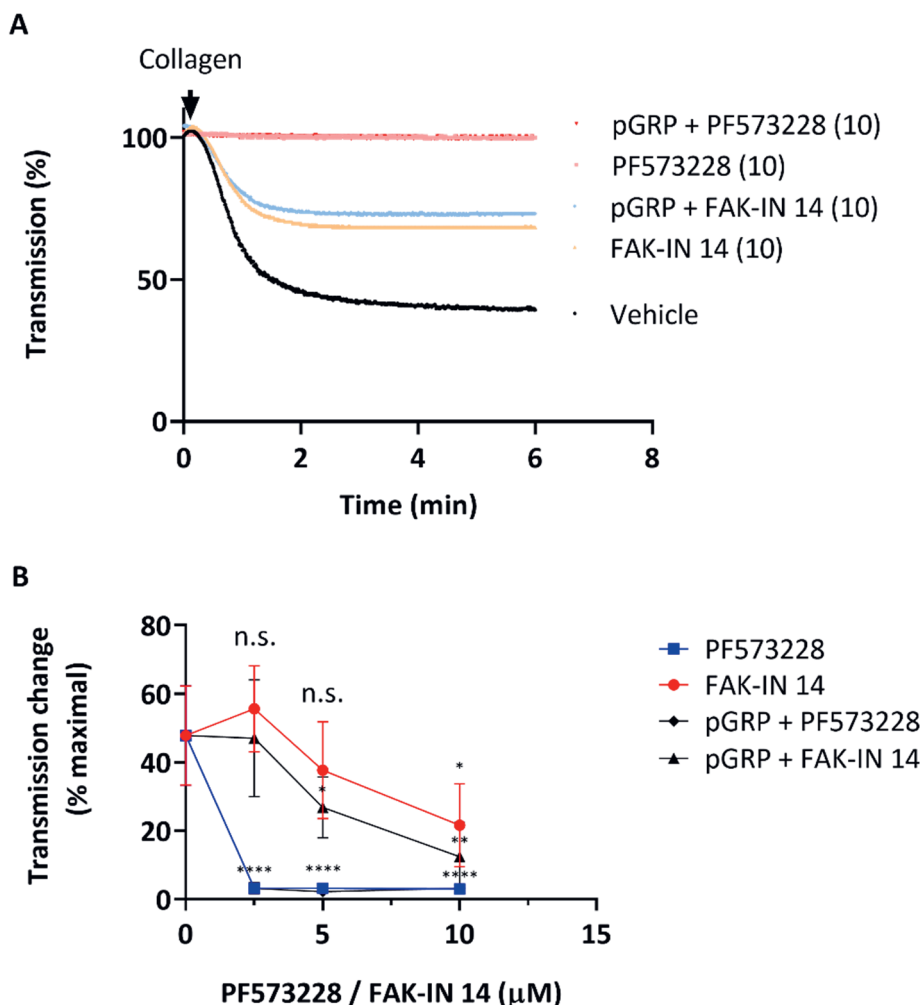


Figure 2. Effects of GPR56 and PTK2 interference on collagen-induced platelet aggregation. Washed platelets ($250 \times 10^9/L$) were incubated with vehicle (control), pGRP peptide ($50 \mu g/mL$) and indicated PTK2 inhibitor (2.5 - $10 \mu M$) for 10 minutes. Platelet aggregation was monitored by light transmission in response to collagen-I ($1 \mu g/mL$). **A**, Representative traces of collagen-induced aggregation. **B**, Dose-dependent effect of PTK2 inhibitors on maximal aggregation. Mean values \pm SD ($n=3$ donors). * $P<0.05$, ** $P<0.005$, *** $P<0.001$, **** $P<0.0001$ vs. vehicle (paired Student's *t*-test).

reduced platelet adhesion and aggregate size on collagen-I (Figure 3A iv-v), as well as on collagen-III and -IV (Suppl. Figure 3 ii-iii). In particular for PF573228, this reduction extended to a lower phosphatidylserine exposure, a marker of GPVI activity. This was also apparent from the subtraction heatmap of Figure 3B, showing larger effect sizes with the combined presence on all surfaces. Cumulative analysis of the scaled parameters confirmed that the reduction with pGRP was highest for PF573228 (Suppl. Figure 2).

Since activation of the GPR56 receptor is considered to act in a shear-dependent way, we compared the effects of PF573228 (5 μ M) alone or in combination with pGRP (50 μ g/mL) at high (1000 s^{-1}) and low (150 s^{-1}) shear rates. The composed subtraction heatmap versus the vehicle control condition pointed to an essential lack of effect by the combinations with pGRP at low shear rate, in contrast to the high-shear condition (Figure 4). This also appeared from the cumulation of scaled parameter values (Suppl. Figure 4). Taken together, these results pointed to a shear-dependent suppression of collagen-dependent thrombus by interfering with GPR56 plus PTK2 activity.

In silico design of CIB1-interfering peptide binding to integrin chain α IIb

Since PTK2 is known to be activated via integrin α IIb β 3 outside-in signaling, involving binding of CIB1 to the α IIb chain, we used the α IIb cytoplasmic peptide pCIB, which has been shown to enter into platelets and block the CIB1- α IIb interaction, as evidenced by the suppression of platelet spreading on fibrinogen^{24,26}. Virtual analysis of the binding mode of the 26 amino-acid pCIB to the binding pocket of CIB1 revealed a free binding energy of -43 kcal/mol (Figure 5A, B). Aiming to improve the predicted binding affinity of the peptide with CIB1, we rationally mutated several residues of pCIB in silico, which resulted in a list of mutant 31 peptides. Among these, the peptide pCIB^m with 5 mutations had the lowest binding free energy of -58 kcal/mol and predicted an unaltered interaction mode with CIB1 (Figure 5C).

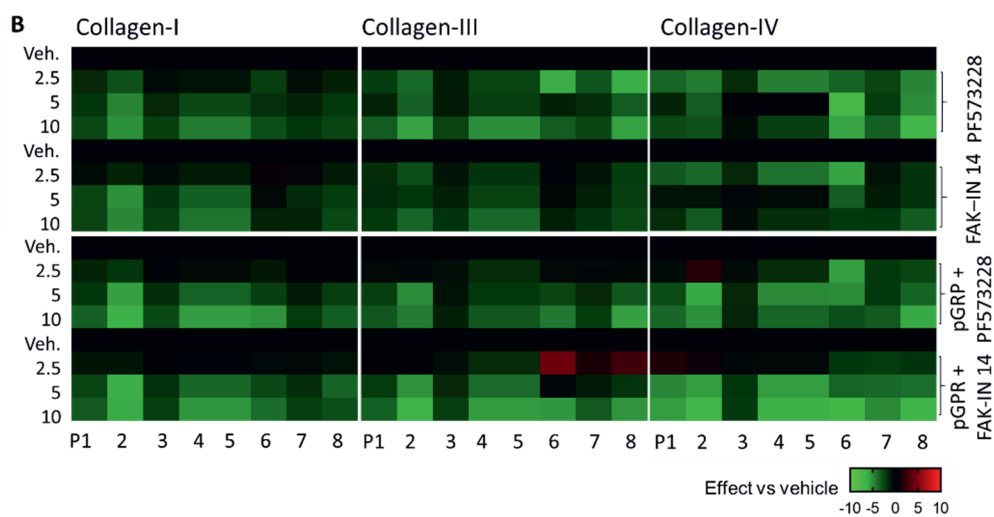
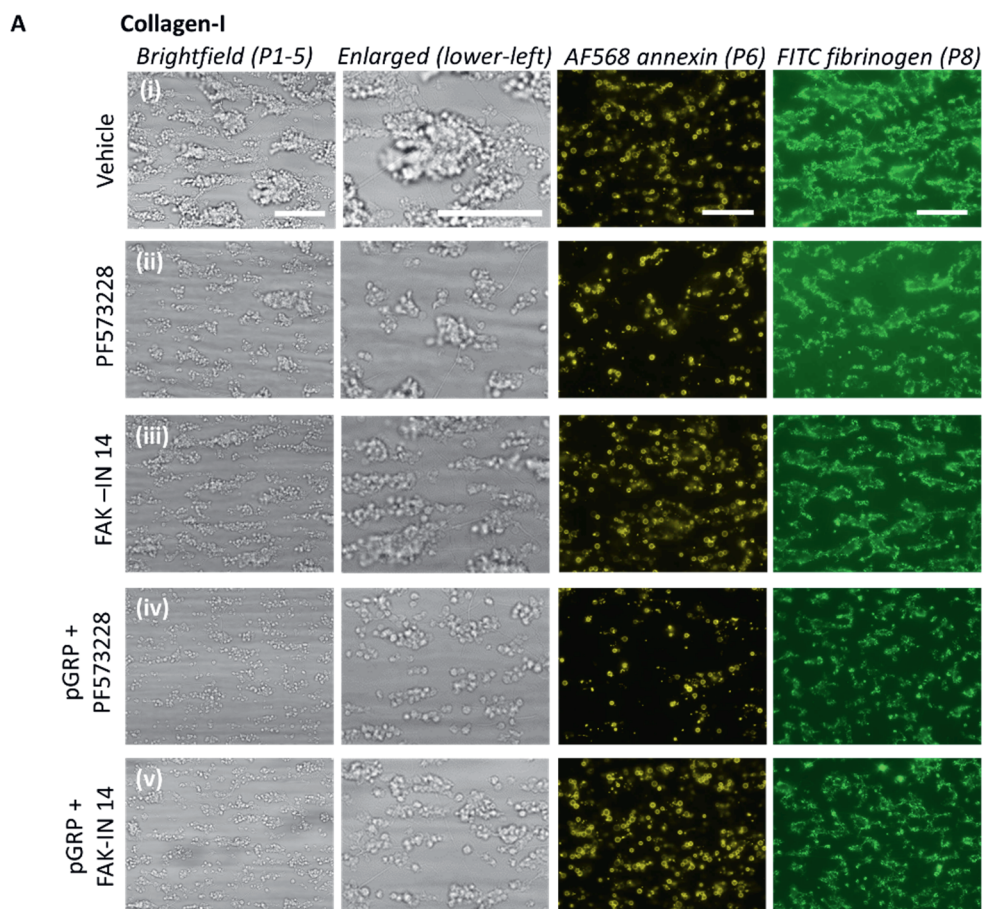


Figure 3. Effects of GPR56-binding peptide and PTK2 inhibition on collagen-induced thrombus formation. Whole blood samples were pre-incubated with vehicle medium (control) or indicated PTK2 inhibitor (PF573228 or FAK-IN14 at 2.5-10 μ M) with or without pGRP peptide (50 μ g/mL) for 10 minutes. After recalcification, the blood was perfused over collagen-I, -III and -IV for 3.5 minutes at standard shear rate of 1000 s^{-1} . End-stage brightfield and fluorescence images were analyzed for thrombus parameters P1-8. Enlarged images (lower-left corner) are indicated to visualize the formed platelet aggregates. **A**, Representative images for collagen-I of: (i) vehicle control, (ii) PF573228 (10 μ M), (iii) FAK-IN14 (10 μ M), (iv) pGRP + PF573228 runs, and (v) pGRP + FAK-IN14. Scale bar = 10 μ m. Representative images for collagen-III and collagen-IV are in Suppl. Figure 2. **B**, Subtraction heatmap representing control-subtracted scaled (0-10) parameters values for collagen-I, -III, and -IV microspots. Color code represents decrease (green) or increase (red) in comparison to control runs. Means of duplicate runs for 3 donors were compared per blood sample. For statistics, see Suppl. Figure 3.

We then chemically synthesized the previously used pCIB and the pCIB^m peptide for microfluidic assays. After purification, the measured masses of pCIB (3,104 Da) and pCIB^m (3,286 Da) corresponded well with the theoretical monoisotopic masses of 3,102 Da and 3,284 Da, respectively.

Effects of combined peptides interfering with GPR56 and CIB1 on thrombus formation under shear

For flow assays, the two synthesized CIB1-binding peptides were used at an affordable high dose for platelet-inhibiting peptides of 50 μ g/mL in whole blood¹⁵. Preincubation of blood with the pCIB or pCIB^m only resulted in no more than small visual effects on thrombus formation at microspots of collagen-I (Figure 6A i-iii). We also investigated the effects of combined application of pCIB or pCIB^m and pGRP. This combined treatment showed for collagen-I a reduction in platelet adhesion, thrombus buildup and platelet activation markers including exposed PS and P-selectin and activated integrin α IIb β 3, of which the reduction was more prominent for pCIB than for pCIB^m (Figure 6A iv-v). The stronger effect with pCIB was confirmed by

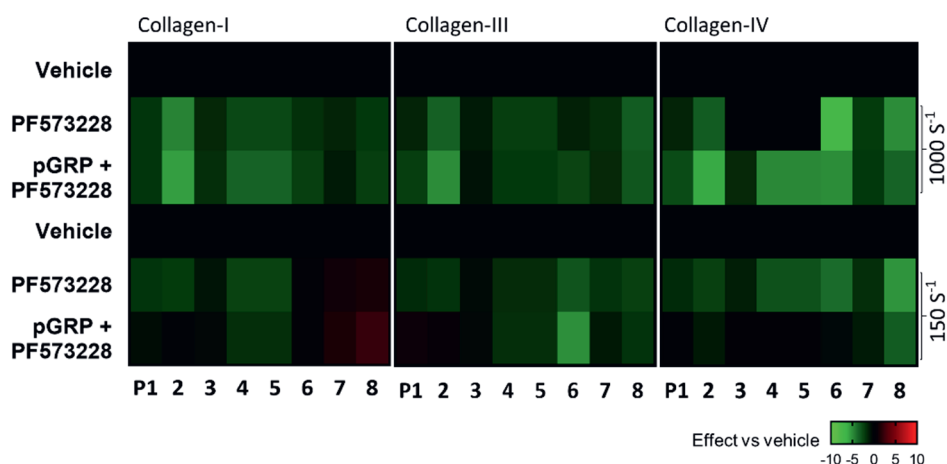


Figure 4. Shear rate dependency of GPR56 and PTK2 interference. Blood samples pre-incubated with vehicle (control) or PF573228 (5 μ M) with/ without pGRP (50 μ g/mL) for 10 minutes, and then perfused over collagen microspots for 3.5 or 6 minutes at wall-shear rate of 1000 s^{-1} or 150 s^{-1} respectively. Parameter analysis of recorded images was as for Figure 1. Shown is subtraction heatmap representing control-subtracted scaled (0-10) parameters values for collagen-I, -III, and -IV microspots. The color code represents decrease (green) or increase (red) in comparison to vehicle control runs.

statistical analysis of the parameters of platelet deposition (P1-2), thrombus characteristics (P3-5), and platelet activation (P6-8) (Figure 6B). Regarding collagen-III and -IV, representative images showed similar effects of the combined addition of peptides (Suppl. Figure 5A, B). Upon quantification, pGRP plus pCIB significantly reduce platelet deposition, thrombus characteristics, and platelet activation (Suppl. Figure 6A i-ii). A synergistic effect of pGRP + pCIB (but not pCIB^m) also appeared from the subtraction heatmap (Figure 7) and from cumulative plots of the scaled parameters (Suppl. Figure 6B i-iii). For all collagen types, effect sizes decreased in the order of pGRP + pCIB > pCIB > pGRP + pCIB^m > pCIB^m.

To assess shear dependency of these effects, we again evaluated the effects on thrombus formation inhibition of pGRP with/out pCIB or pCIB^m at high

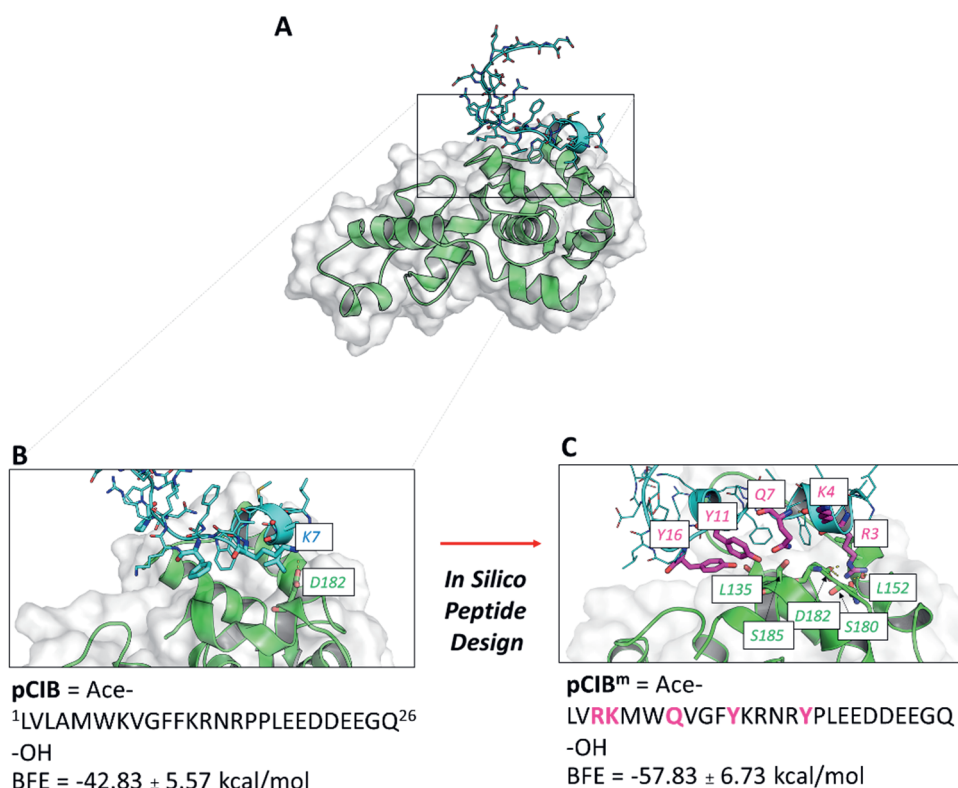


Figure 5. Molecular dynamics simulation of pCIB-CIB1 complex formation. **A**, Reported structure of CIB1 in complex with pCIB peptide, mimicking part of the intracellular $\alpha 1b$ chain. **B**, Calculated structure of pCIB-CIB1 complex obtained by molecular dynamics simulation. **C**, Structure of modified pCIB^m-CIB1 complex by molecular dynamics simulation. Color code: hydrogen bonds shown as yellow dashed lines; amino acid residues of the wildtype (**B**) and mutated (**C**) peptides are indicated in cyan and magenta, respectively; CIB1 residues are pictured in green. Also indicated per peptide is the calculated binding free energy (BFE).

(1000 s⁻¹) and low (150 s⁻¹) shear rates. The subtraction heatmap pointed to a consistently larger effect of the pGRP + pCIB combination, regardless of parameter and collagen type, at high shear rate than at low shear rate (Figure 7). This was confirmed by statistical parameter analysis (Supp. Figure 7).

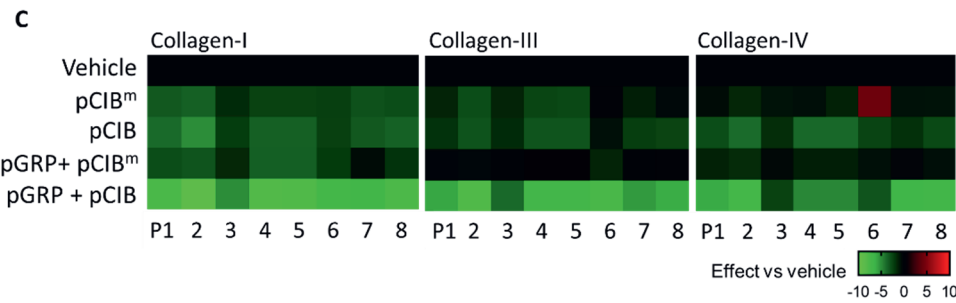
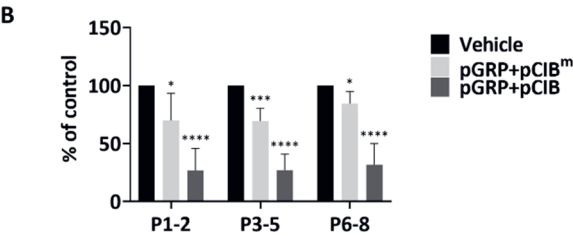
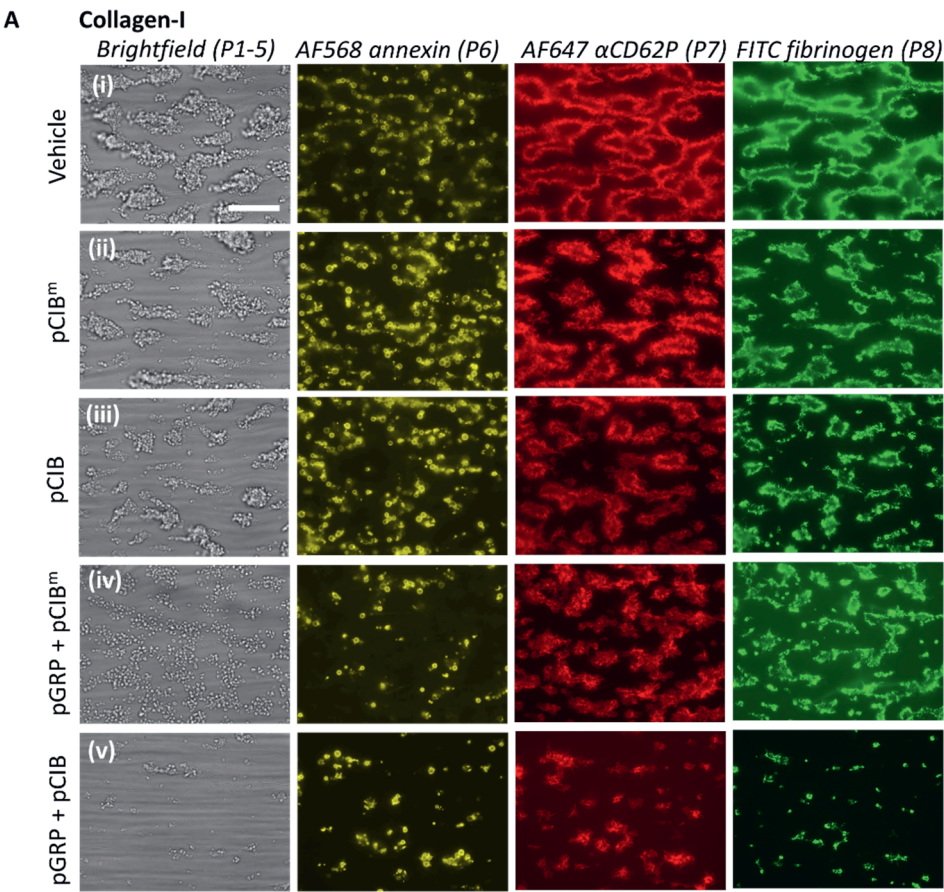


Figure 6. See upper page. Combined GPR56 and CIB1 peptides affecting collagen-induced thrombus formation. Blood samples were pre-incubated with vehicle medium (control) or indicated peptides pGRP, pCIB, pCIB^m (50 µg/mL each) for 10 minutes. Thrombus formation on collagen-I, -III and -IV was monitored. **A**, Representative images for collagen-I of: (i) vehicle control, (ii) pCIB^m, (iii) pCIB, (iv) pGRP + pCIB^m, or (v) pGRP + pCIB. Scale bar = 10 µm. **B**, Percentual effects of peptides on combined parameters of platelet deposition (P1-2), thrombus characteristics (P3-5) and platelet activation (P6-8) versus vehicle control condition. Additional images and raw data for collagen-III and collagen-IV are given in Suppl. Figures 5 and 6. **C**, Subtraction heatmap representing control-subtracted scaled (0-10) parameters values for collagen-I, -III, and -IV microspots. Color code represents decrease (green) or increase (red) in comparison to controls. Mean values ± SD (n=3 donors). *P<0.05, **P<0.005, ***P<0.001, ****P<0.0001 vs. vehicle (paired Student's t-test).

Absence of Peptide Effects on GPVI-Induced Platelet Aggregation and Ca²⁺ responses

Considering that the peptide-sensitive interaction of CIB1 with αIIbβ3 is thought to be confined to outside-in signaling²⁵, we checked the effects of pGRP in combination with pCIB or pCIB^m on GPVI-mediated platelet aggregation and intracellular Ca²⁺ responses. As a control, we used the common αIIbβ3 inhibitor tirofiban¹³. As expected, up to a concentration of 50 µg/mL, the peptide combination was unable to suppress the platelet aggregation response to collagen-I or CRP-XL (Figure 8A i-ii). Quantitative analysis only showed a minor significant aggregation inhibition by pCIB and pGRP + pCIB (Figure 8B). The control compound tirofiban completely blocked collagen-I- and CRP-XL-induced platelet aggregation. To investigate GPVI-induced Ca²⁺ responses, we examined fluorescence changes in response to the same agonists using Fura-2-loaded platelets, employing a 96 well-plate based assay and static condition⁴¹. In line with the aggregation results, we did not notice significant changes in [Ca²⁺]_i rises by pGRP alone or in combination with pCIB or pCIB^m (Figure 8C). These results pointed to

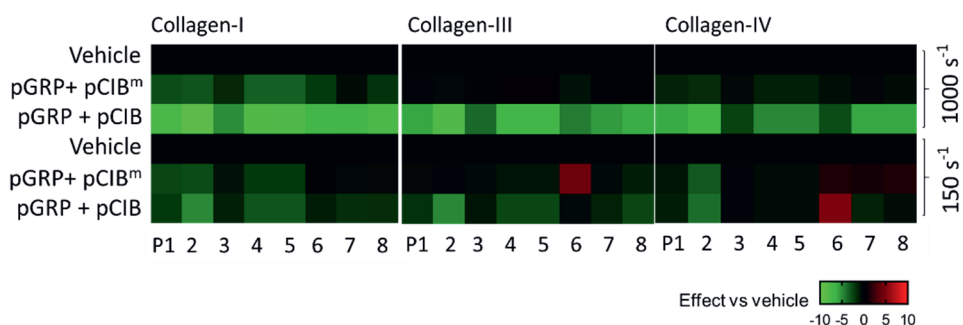


Figure 7. Shear rate dependency of GPR56 and CIB1 blockade. Blood samples pre-incubated with vehicle (control) or indicated peptides (50 $\mu\text{g/mL}$) for 10 minutes, and then perfused over collagen microspots for 3.5 minutes at 1000 s^{-1} or for 6 min at 150 s^{-1} . Shown is subtraction heatmap representing control-subtracted scaled (0-10) image parameters values for collagen-I, -III, and -IV microspots. Color code represents decrease (green) or increase (red) in comparison to vehicle control runs.

near absence of (combined) signaling effects of pGRP and pCIB on platelets under conditions of no or low shear.

Discussion

In this paper, we unraveled the roles of $\alpha\text{IIb}\beta 3$ integrin-dependent signaling involving PTK2, CIB1 and GPR56 in collagen-dependent thrombus formation under shear conditions. Our data support for this major platelet integrin, the recently recognized concept of integrin affinity and avidity regulation by mechanical forces²¹, in that the activation and signaling via $\alpha\text{IIb}\beta 3$ can be dampened by peptide-mimicking activation of the shear-dependent receptor GPR56. This would imply that external shear forces play a role in the concept of intracellular actomyosin-dependent mechanosensitive forces for $\alpha\text{IIb}\beta 3$ activation²¹. As we have recently shown¹⁵, the GPIIb α -VWF axis contributes to the formation of platelet aggregates under shear.

In our studies, we hypothesized that interference in integrin activation and signaling via PTK2 and CIB1 would affect the process of thrombus formation under shear. To investigate this, we used a range of collagens relevant for

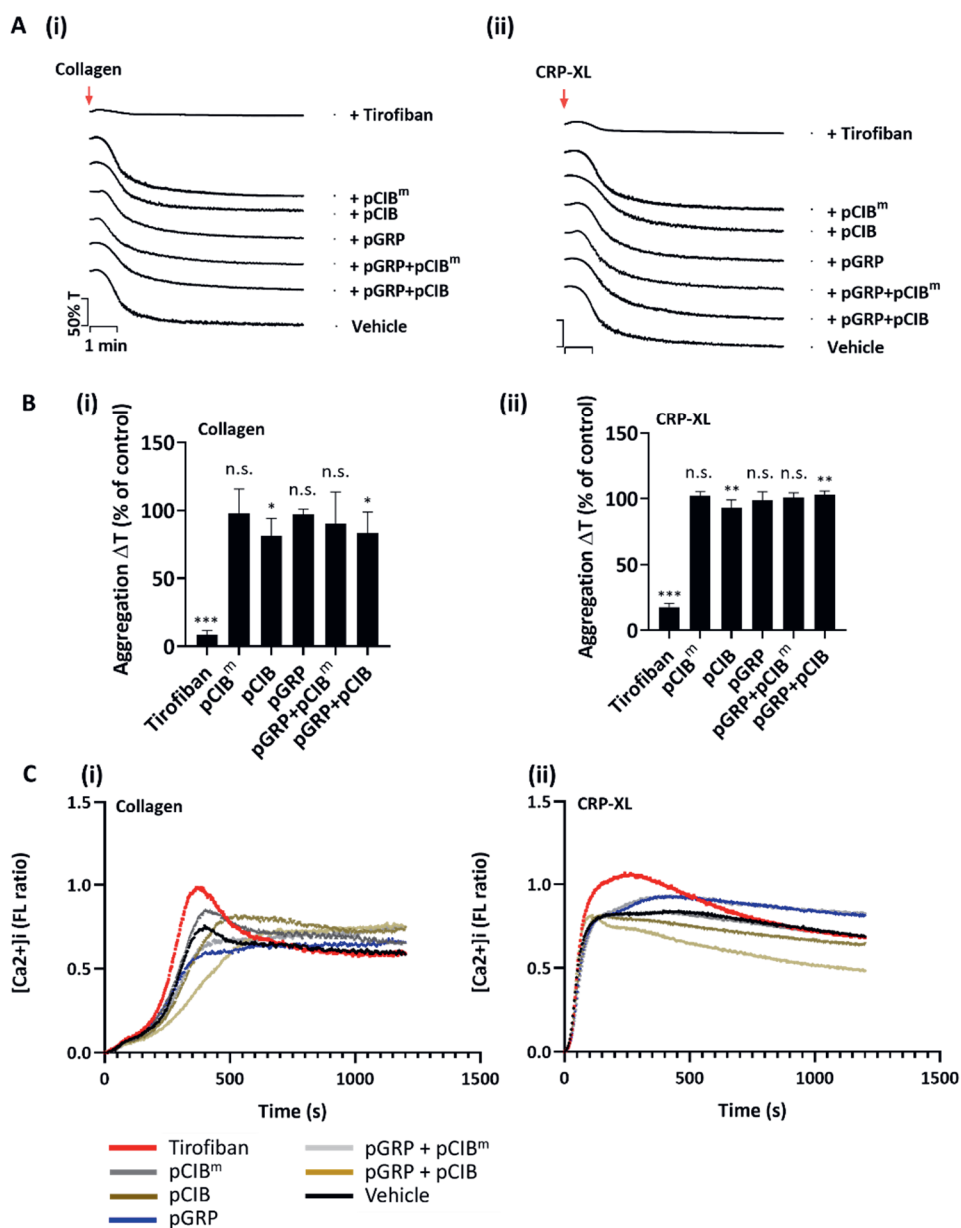


Figure 8. No effect of combined peptides pGRP and pCIB on collagen-induced platelet aggregation or Ca^{2+} fluxes. A, B, Platelet preparations ($250 \times 10^8/L$) were pre-incubated with vehicle control, tirofiban ($1 \mu g/mL$) or indicated peptides (50

$\mu\text{g/mL}$) for 10 minutes. Platelet aggregation was monitored by light transmission aggregometry in response to 1 $\mu\text{g/mL}$ collagen-I or (i) or 1 $\mu\text{g/mL}$ CRP-XL (ii). **A**, representative aggregation traces, and **(B)** normalized transmission changes. **C**, Fura-2-loaded platelets were pre-incubated with vehicle control, tirofiban (1 $\mu\text{g/mL}$), or indicated pep-tides (50 $\mu\text{g/mL}$) for 10 minutes, before adding to 96-wells plates. After supplementation of 1 mM CaCl_2 , loaded platelets were automatically stimulated with 10 $\mu\text{g/mL}$ by collagen-I (i) or 10 $\mu\text{g/mL}$ CRP-XL (ii). Dual wavelength 340/380 nm fluorescence changes per well were recorded in a FlexStation 3. Shown are representative $[\text{Ca}^{2+}]_i$ traces per agonist. Mean values \pm SD ($n = 3$ donors); * $P < 0.05$, ** $P < 0.005$, *** $P < 0.001$, **** $P < 0.0001$ vs. vehicle (paired Student's t-test).

the damaged vessel wall, e.g. the fibrillar Horm-type collagen I and human tissue-derived collagens-III and -IV. These collagen types were previously assigned to a high (I) or lower (III, IV) platelet GPVI-dependency⁴¹. Earlier work also indicated that the thrombi formed on all three collagens rely on Syk signaling, i.e. on tyrosine kinase activity through GPVI and in synergy with $\alpha\text{IIb}\beta 3$ signaling^{9,41}. As well-characterized PTK2 inhibitors, we used two structurally different compounds, PF573228 and FAK-IN14^{38,39}. We further chemically synthesized the 7 amino acid peptide pGRP, which is considered to mimic shear-dependent self-activation of GPR56³²; and furthermore a 26 amino acid peptide pCIB (wildtype), known to enter platelets and block the binding of CIB1 to the αIIb chain in outside-in signaling²⁶, as well as a four-time mutated form pCIB^m with calculated higher free binding energy.

Control experiments indicated that pGRP, pCIB or pCIB^m by itself did not influence collagen-induced platelet aggregation (integrin inside-out signaling) or Ca^{2+} fluxes, in agreement with a selective action on outside-in signaling. Yet, PTK2 inhibition did block collagen-induced platelet aggregation, pointing to a wider role of PTK2 in GPVI-dependent platelet activation. On the one hand, whole-blood flow experiments indicated that the inhibitors PF573228 and FAK-IN14 alone only slightly affected thrombus formation under high shear, which was also true for pGRP. On the other hand, when pGRP was combined with increasing doses of PF573228 or FAK-

IN14, this ultimately annulated the thrombus-forming process, extending over all three collagen preparations and diminishing the majority of parameters. Importantly, the thrombus-suppressing effect of pGRP plus the PTK2 inhibitor was prominent at a high shear rate (1000 s^{-1}) and substantially reduced at a low shear rate (150 s^{-1}).

Mouse knock-out and human platelet studies have confirmed that PTK2 signaling regulates platelet spreading on fibrinogen^{17,37}. Other early studies have shown that PTK2 phosphorylation - and likely activation - is a coordinated signaling event involving integrins as well as other receptors^{36,42}. This is in agreement with our current findings that PTK2 inhibition has a larger suppressive effect on GPVI-dependent platelet aggregation than CIB1 peptide interference. However, either type of inhibitor was similarly effective in antagonizing thrombus formation on the investigated collagens. Regarding CIB1, our results are furthermore compatible with the fact that genetic ablation of *Cib1* in mouse significantly delayed and destabilized *in vivo* arterial thrombus formation, while leaving *in vitro* platelet aggregation unaffected³⁰.

A remarkable finding was that the combination of the CIB1 peptide (pCIB or pCIB^m peptide) with the GPR56 peptide (pGRP) was required to suppress the thrombus-forming process on collagens. Herein, the combination of pGRP + pCIB had the strongest antithrombotic effect, *i.e.* larger than pGRP + pCIB^m or pGRP + PF573228/FAK-IN14. Given the BFE values of pCIB and pCIB^m, pCIB^m was expected to outperform pCIB. However, it appeared that pCIB^m was not more effective than its counterpart. This could be due to the fact that pCIB^m may adapt a more kinked conformation due to the mutation at Q7, Y11 and Y16, which may induce α -helix conformation of the peptide, resulting in less efficient CIB1-binding. Interestingly, CIB1 has also been reported to bind WASP, a protein with mutations in patients with the immunodeficiency Wiskott-Aldrich syndrome; the WASP-CIB1 complex was assigned a role in integrin $\alpha\text{IIb}\beta 3$ -dependent cell adhesion⁴³.

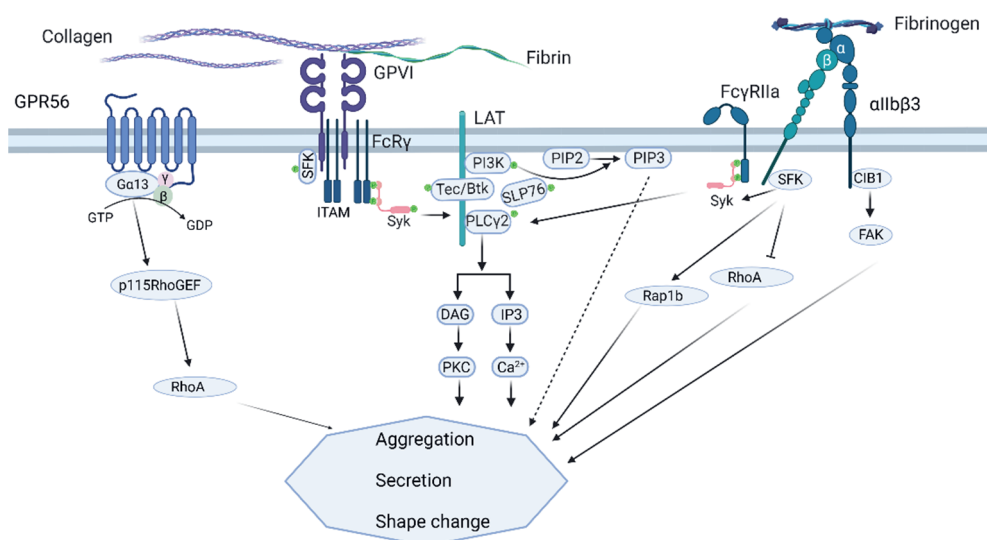


Figure 9. Scheme of proposed combined action of GPR56, GPVI and α IIb β 3 signaling in shear-dependent thrombus formation on collagen, consisting of platelet aggregation, secretion and shape change. (i) GPR56 signaling: small GTP-binding protein RhoA, activated by p115 RhoGEF (guanine nucleotide exchange factor). (ii) GPVI signaling via Fc γ co-receptor: SFK (Src-family kinases) and the tyrosine kinases Syk, Tec and Btk; phosphatidylinositol 3-kinase (PI3K); leading to activation of PLC γ 2, which generates the second messengers DAG (diacylglycerol) and IP $_3$ (inositol trisphosphate). (iii) α IIb β 3 outside-in signaling: SFK and CIB1 mediated activation, the latter triggering PTK2 (focal adhesion kinase FAK); small GTP-binding proteins Rap1b and RhoA transmit parts of the signal. For further explanation, see text.

The collective and consistent shear-dependent inhibitory rather than stimulatory effects of pGRP were unexpected. These findings suggest that the tethered ligand-mimicking peptide blocks rather than enhances a positive signaling role of the G α 13-linked GPR56 receptor; alternatively, in human platelets, this receptor restricts platelets activation. However, further studies will be needed to confirm this conclusion.

Overall, our findings point to a novel shear-dependent role of PTK2 and CIB1 in collagen-induced thrombus formation via integrin activation and signaling

that involves the GPR56 receptor (Figure 9). Our work thereby extends the previous studies on the separate roles of PTK2, CIB1 and GPR56. How precisely the presumed GPR56-G α 13 activity adds to the PTK2-CIB1- α IIb β 3 still need to be disclosed. Supported by earlier knock-out studies^{17,27,30,32} and the evaluation of multiple mouse genes in collagen-dependent thrombus formation *in vivo* and *in vitro*¹⁴, our findings now add another element to the complex signaling cascades in platelets required for the build-up of a stable contracted thrombus. Our work also extends the multitude of functions of GPR56 in immune regulation and tumor progression^{44,45}.

Supplementary materials

The following supporting information can be downloaded at: <https://www.mdpi.com/article/10.3390/ijms23158688/s1>.

Funding

JH, NJ and DIF are supported by the European Union's Horizon 2020 research and innovation program under the Marie Skłodowska-Curie grant agreement TAPAS No. 766118. JH and DIF are enrolled in a joint PhD project of the universities of Maastricht (NL) and Santiago de Compostela (ES), NJ is enrolled in a joint PhD project of the universities of Maastricht (NL) and Birmingham (UK). AG is supported by the Spanish Ministry of Science and Innovation (Grant No. PID2019–108727RB-I00), the Sociedad Española de Trombosis y Hemostasia (SETH), and the Consellería de Cultura, Educación e Ordenación Universitaria, Xunta de Galicia (Centro Singular de investigación de Galicia accreditation 2019–2022).

Institutional Review Board Statement

The study was approved by the local Medical Ethics Committees (Maastricht University Medical Centre, NL31480.068.10). All subjects gave full in-formed consent according to the Declaration of Helsinki and all methods were performed in accordance with the relevant guidelines and regulations.

Informed Consent Statement

Informed consent was obtained from all subjects involved in the study. According to ethical permission, all subjects gave blood without tracing to individuals.

Data Availability Statement

All data are included in the manuscript as figures, tables or supplement figures.

Conflicts of Interest

The authors declare no conflict of interest. The funders had no role in the design of the study; in the collection, analyses, or interpretation of data; in the writing of the manuscript, or in the decision to publish the results.

References

1. Versteeg HH, Heemskerk JW, Levi M and Reitsma PS. New fundamentals in hemostasis. *Physiol Rev.* 2013;93:327-358.
2. Nagy M, Perrella G, Dalby A, Becerra M, Garcia Quintanilla L, Pike J et al. Flow studies on human GPVI-deficient blood under coagulating and non-coagulating conditions. *Blood Adv.* 2020;4:2953-2961.
3. Huang J, Zhang P, Solari FA, Sickmann A, Garcia A, Jurk K et al. Molecular proteomics and signaling of human platelets in health and disease. *Int J Mol Sci.* 2021;22:9860.
4. Harbi MH, Smith CW, Nicolson PLR, Watson SP and Thomas MR. Novel antiplatelet strategies targeting GPVI, CLEC-2 and tyrosine kinases. *Platelets.* 2021; 32: 29-41.
5. Sokol J, Skerenova M, Biringer K, Simurda T, Kubisz P and Stasko J. Glycoprotein VI gene variants affect pregnancy loss in patients with platelet hyperaggregability. *Clin Appl Thromb Hemost.* 2018; 24: 202S-208S.
6. Fernandez DI, Kuijpers MJ and Heemskerk JW. Platelet calcium signaling by G-protein coupled and ITAM-linked receptors regulating anoctamin-6 and procoagulant activity. *Platelets.* 2021; 32: 863-871.

7. Slater A, Perrella G, Onselaer MB, Martin EM, Gauer JS, Xu RG et al. Does fibrin(ogen) bind to monomeric or dimeric GPVI, or not at all? *Platelets*. 2019;30:281-289.
8. Van der Meijden PE and Heemskerk JW. Platelet biology and functions: new concepts and future clinical perspectives *Nat Rev Cardiol*. 2019;16:166-179.
9. Perrella G, Huang J, Provenzale I, Swieringa F, Heubel-Moenen FC, Farndale RW et al. Non-redundant roles of platelet glycoprotein VI and integrin $\alpha\text{IIb}\beta 3$ in fibrin-mediated microthrombus formation. *Arterioscler Thromb Vasc Biol*. 2021;41:e97-e111.
10. De Witt SM, Swieringa F, Cavill R, Lamers MM, Van Kruchten R, Mastenbroek T et al. Identification of platelet function defects by multi-parameter assessment of thrombus formation. *Nat Commun*. 2014;5:4257.
11. Van Geffen JP, Brouns SL, Batista J, McKinney H, Kempster C, Nagy M et al. High-throughput elucidation of thrombus formation reveals sources of platelet function variability. *Haematologica*. 2019;104:1256-1267.
12. Navarro S, Stegner D, Nieswandt B, Heemskerk JW and Kuijpers MEJ. Temporal roles of platelet and coagulation pathways in collagen and tissue factor induced thrombus formation. *Int J Mol Sci*. 2021;23:358.
13. Van den Kerkhof DL, Nagy M, Wichapong K, Brouns SL, Heemskerk JW, Hackeng TM et al. Inhibition of platelet adhesion, thrombus formation and fibrin formation by a potent $\alpha\text{IIb}\beta 3$ integrin inhibitor. *Res Pract Thromb Haemost*. 2020;5:231-242.
14. Baaten CC, Meacham S, de Witt SM, Feijge MA, Adams DJ, Akkerman JW et al. A synthesis approach of mouse studies to identify genes and proteins in arterial thrombosis and bleeding. *Blood*. 2018;132:e35-e46.
15. Hrdinova J, Fernández DI, Ercig B, Tullemans BM, Suylen DP, Agten SM et al. Structure-based cyclic glycoprotein Iba-derived peptides interfering with von Willebrand factor binding affecting platelet aggregation under shear. *Int J Mol Sci*. 2022;23:2046.
16. Achison M, Elton CM, Hargreaves PG, Knight CG, Barnes MJ and Farndale RW. Integrin-independent tyrosine phosphorylation of p125Fak in human platelets stimulated by collagen. *J Biol Chem*. 2001;276:3167-3174.
17. Hitchcock IS, Fox NE, Prévost N, Sear K, Shattil SJ and Kaushansky K. Roles of focal adhesion kinase (FAK) in megakaryopoiesis and platelet function: studies

- using a megakaryocyte lineage specific FAK knockout. *Blood*. 2008;111:596-604.
18. Guidetti GF, Torti M, Canobbio I. Focal adhesion kinases in platelet function and thrombosis. *Arterioscler Thromb Vasc Biol*. 2019;39:857-868.
 19. Mekrache M, Bachelot-Loza C, Ajzenberg N, Saci A, Legendre P and Baruch D. Activation of pp125FAK by type 2B recombinant von Willebrand factor binding to platelet GPIb at a high shear rate occurs independently of α IIb β 3 engagement. *Blood*. 2003;101:4363-4371.
 20. Tapial MP, López NP and Lietha D. FAK structure and regulation by membrane interactions and force in focal adhesions. *Biomolecules*. 2020;10:179.
 21. Sun Z, Costell M and Fässler R. Integrin activation by talin, kindlin and mechanical forces. *Nat Cell Biol*. 2019;21:25-31.
 22. Levy A, Alhazzani K, Dondapati P, Alaseem A, Cheema K, Thallapureddy K et al. Focal adhesion kinase in ovarian cancer: a potential therapeutic target for platinum and taxane-resistant tumors. *Curr Cancer Drug Targets*. 2019;19:179-188.
 23. Qiang YY, Li CZ, Sun R, Zheng LS, Peng LX, Yang JP et al. Along with its favorable prognostic role, CLCA2 inhibits growth and metastasis of nasopharyngeal carcinoma cells via inhibition of FAK/ERK signaling. *J Exp Clin Cancer Res*. 2018;37:34.
 24. Naik MU and Naik UP. Calcium-and integrin-binding protein regulates focal adhesion kinase activity during platelet spreading on immobilized fibrinogen. *Blood*. 2003;102:3629-3636.
 25. Naik UP and Naik MU. Association of CIB with GPIIb/IIIa during outside-in signaling is required for platelet spreading on fibrinogen. *Blood*. 2003;102:1355-1362.
 26. Naik MU, Naik TU, Summer R and Naik UP. Binding of CIB1 to the α IIb tail of α IIb β 3 is required for FAK recruitment and activation in platelets. *Plos One*. 2017;12:e0176602.
 27. Denofrio JC, Yuan W, Temple BR, Gentry HR and Parise LV. Characterization of calcium- and integrin-binding protein 1 (CIB1) knockout platelets: potential compensation by CIB family members. *Thromb Haemost*. 2008;100:847-856.
 28. Burkhart JM, Vaudel M, Gambaryan S, Radau S, Walter U, Martens L et al. The first comprehensive and quantitative analysis of human platelet protein

- composition allows the comparative analysis of structural and functional pathways. *Blood*. 2012;120:e73-e82.
29. Huang J, Swieringa F, Solari FA, Provenzale I, Grassi L, De Simone I et al. Assessment of a complete and classified platelet proteome from genome-wide transcripts of human platelets and megakaryocytes covering platelet functions. *Sci Rep*. 2021;11:12358.
 30. Naik MU, Nigam A, Manrai P, Millili P, Czymmek K, Sullivan M et al. CIB1 deficiency results in impaired thrombosis: the potential role of CIB1 in outside-in signaling through integrin $\alpha\text{IIb}\beta\text{3}$. *J Thromb Haemost*. 2009;7:1906-1914.
 31. Yuan W, Leisner TM, McFadden AW, Wang Z, Larson MK, Clark S et al. CIB1 is an endogenous inhibitor of agonist-induced integrin $\alpha\text{IIb}\beta\text{3}$ activation. *J Cell Biol*. 2006;172:169-175.
 32. Yeung J, Adili R, Stringham EN, Luo R, Vizurraga A, Rosselli-Murai LK et al. GPR56/ADGRG1 is a platelet collagen-responsive GPCR and hemostatic sensor of shear force. *Proc Natl Acad Sci USA*. 2020;117:28275-28286.
 33. Luo R, Jin Z, Deng Y, Strokes N and Piao X. Disease-associated mutations prevent GPR56-collagen III interaction. *Plos One*. 2012;7:e29818.
 34. Hers I and Mundell SJ. GPR56, a novel platelet collagen receptor that loves stress. *J Thromb Haemost*. 2021;19:1848-1851.
 35. Provenzale I, Brouns SL, Van der Meijden PE, Swieringa F and Heemskerk JW. Whole blood based multiparameter assessment of thrombus formation in a standard microfluidic device to proxy in vivo haemostasis and thrombosis. *Micromachines*. 2019;10:e787.
 36. Lipfert L, Haimovich B, Schaller MD, Cobb BS, Parsons JT and Brugge JS. Integrin-dependent phosphorylation and activation of the protein tyrosine kinase pp125FAK in platelets. *J Cell Biol*. 1992;119:905-912.
 37. Ji P and Haimovich B. Integrin $\alpha\text{IIb}\beta\text{3}$ -mediated pp125FAK phosphorylation and platelet spreading on fibrinogen are regulated by PI 3-kinase. *Biochim Biophys Acta*. 1999;1448:543-552.
 38. Jones ML, Shawe-Taylor AJ, Williams CM and Poole AW. Characterization of a novel focal adhesion kinase inhibitor in human platelets. *Biochem Biophys Res Commun*. 2009;389:198-203.
 39. Golubovskaya V, Curtin L, Groman A, Sexton S and Cance WG. In vivo toxicity, metabolism and pharmacokinetic properties of FAK inhibitor 14 or Y15

- (1,2,4,5-benzenetetramine tetrahydrochloride). *Arch Toxicol.* 2015;89:1095-1101.
40. Slack-Davis JK, Martin KH, Tilghman RW, Iwanicki M, Ung EJ, Autry C et al. Cellular characterization of a novel focal adhesion kinase inhibitor. *J Biol Chem.* 2007;282:14845-14852.
 41. Jooss NJ, De Simone I, Provenzale I, Fernández DI, Brouns SL, Farndale RW et al. Role of platelet glycoprotein VI and tyrosine kinase Syk in thrombus formation on collagen-like surfaces. *Int J Mol Sci.* 2019;20:E2788.
 42. Shattil SJ, Haimovich B, Cunningham M, Lipfert L, Parsons JT, Ginsberg MH et al. Tyrosine phosphorylation of pp125FAK in platelets requires coordinated signaling through integrin and agonist receptors. *J Biol Chem.* 1994;269:14738-14745.
 43. Tsuboi S, Nonoyama S and Ochs HD. Wiskott-Aldrich syndrome protein is involved in $\alpha\text{IIb}\beta\text{3}$ -mediated cell adhesion. *EMBO Rep.* 2006;7:506-511.
 44. Ng KF, Chen TC, Stacey M and Lin HH. Role of ADGRG1/GPR56 in tumor progression. *Cells.* 2021;10:3352.
 45. Singh AK and Lin HH. The role of GPR56/ADGRG1 in health and disease. *Biomed J.* 2021;44:534-547.
 46. Swieringa F, Solari FA, Pagel O, Beck F, Huang J, Feijge MA et al. Impaired iloprost-induced platelet inhibition and phosphoproteome changes in patients with confirmed pseudohypoparathyroidism type Ia, linked to genetic mutations in GNAS. *Sci Rep.* 2020;10:11389.
 47. Barry WT, Boudignon-Proudhon C, Shock DD, McFadden A, Weiss JM, Sondek J et al. Molecular basis of CIB binding to the integrin αIIb cytoplasmic domain. *J Biol Chem.* 2002;277:28877-28883.
 48. Yamniuk AP, Nguyen LT, Hoang TT and Vogel HJ. Metal ion binding properties and conformational states of calcium- and integrin-binding protein. *Biochemistry.* 2004;43:2558-2568.
 49. Van Zundert GC, Rodrigues JP, Trellet M, Schmitz C, Kastiris PL, Karaca E et al. The HADDOCK2.2 webserver: user-friendly integrative modeling of biomolecular complexes. *J Mol Biol.* 2016;428:720-725.
 50. Yan Y, Tao H, He J and Huang SY. The HDock server for integrated protein-protein docking. *Nat Protoc.* 2020;15:1829-1852.

51. Wichapong K, Alard JE, Ortega-Gomez A, Weber C, Hackeng TM, Soehnlein O et al. Structure-based design of peptidic inhibitors of the interaction between CC chemokine ligand 5 (CCL5) and human neutrophil peptides 1 (HNP1). *J Med Chem.* 2016;59:4289-4301.
52. Eckardt V, Miller MC, Blanchet X, Duan R, Leberzammer J, Duchene J et al. Chemokines and galectins form heterodimers to modulate inflammation. *EMBO Rep.* 2020;21:e47852.
53. Wichapong K, Silvestre-Roig C, Braster Q, Schumski A, Soehnlein O and Nicolaes GA. Structure-based peptide design targeting intrinsically disordered proteins: novel histone H4 and H2A peptidic inhibitors. *Comput Struct Biotechnol J.* 2021;19:934-948.
54. Dawson PE, Muir TW, Clark-Lewis I and Kent SB. Synthesis of proteins by native chemical ligation. *Science.* 1994;266:776-9.
55. Hackeng TM, Griffin JH and Dawson PE. Protein synthesis by native chemical ligation: expanded scope by using straightforward methodology. *Proc Natl Acad Sci USA.* 1999;96:10068-10073.
56. Van Kruchten R, Cossemans JM and Heemskerk JW. Measurement of whole blood thrombus formation using parallel-plate flow chambers - a practical guide. *Platelets.* 2012;23:229-242.
57. Feijge MA, Lacabartz-Porret C, Van Pampus EC, Hamulyàk K, Lévy-Toledano S, Enouf J et al. Contribution of thromboxane and endomembrane Ca^{2+} -ATPases to variability in Ca^{2+} signaling of platelets from healthy volunteers. *Platelets.* 1998;9:179-83.
58. Fernández DI, Provenziale I, Cheung HYF, Van Groningen J, Tullemans BM, Veninga A et al. Ultra-high-throughput Ca^{2+} assay in platelets to distinguish ITAM-linked and G-protein-coupled receptor activation. *iScience.* 2021;25:103718.

Supplementary materials of Chapter 8

Supplementary methods of Chapter 8

Image processing for multiparameter assessment of thrombus formation

Microscopic images (EVOS microscope) were separately acquired in brightfield, RFP (probe AF568), CY5 (probe AF647) and GFP (probe FITC) channels, resulting in 8-bit black-white images for brightfield and overlaid 24-bit gray-level fluorescence images in each of the fluorescent channels. All images were analyzed using Fiji software with pre-written scripts for each individual channel. In brief, the scripts opened a set of images using a for-loop. In this loop, the background level was homogenized using a fast Fourier transform bandpass (FFTB) filter. This was followed by manual adjusting a threshold setting and measuring the surface area coverage. For brightfield images, in addition a series of 'Gray morphology' conversions was applied to reduce striping and to improve the detection accuracy. The applied conversion steps were as follows: a diamond large-sized close, followed by a medium-sized circle close, and a small circle-shaped dilate. The first step increased the selected pixels, yet stronger in regions with many neighboring pixels; the second step rounded the shapes and additionally reduced straight lines; and the final step could be manually adjusted to match the overlap with the original images and the magnification used in the microscope. Prior to analysis, the RGB images per color channel were subjected to an FFTB filter with a size to have minimal impact on the structures, and yet flatten the background areas for good analysis. For both the brightfield and CY5 images, large structures were filtered down to 60 pixels; for RFP images large structures were filtered down to 150 pixels; and for GFP images large structures were filtered down to 200 pixels. Small structures were not filtered down as these contained details of interest within platelets.

Reference brightfield images for scoring parameters P3-5

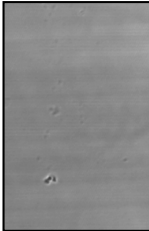
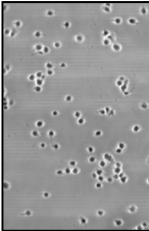
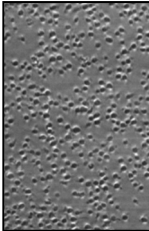
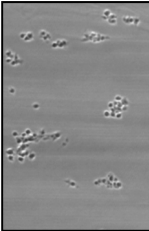
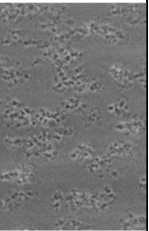
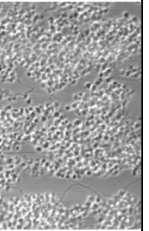
The following microscopic brightfield images were used as a reference for scoring of parameters. Note that scoring was done including halve points.

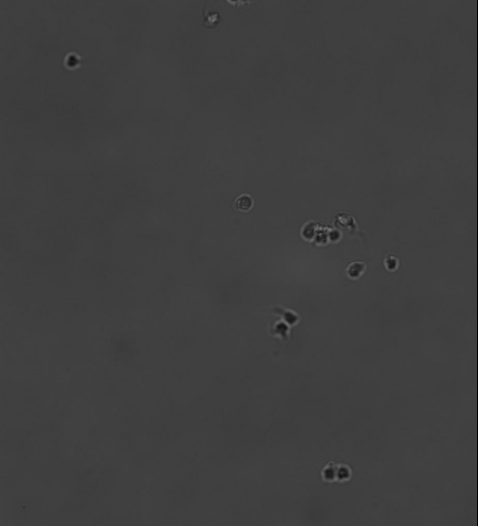
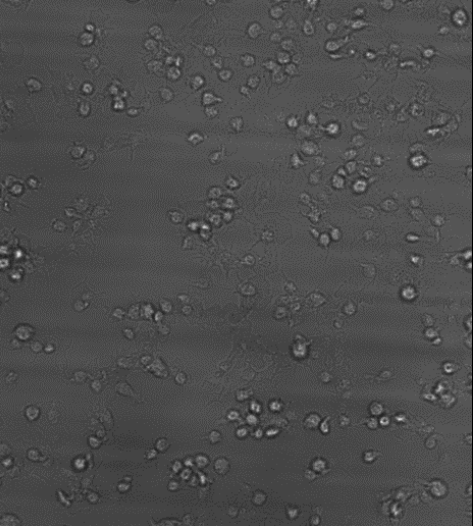
P3: Thrombus morphological score (range 0-5)

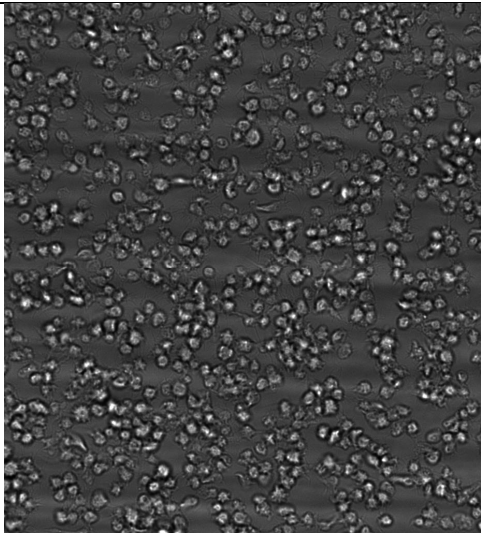
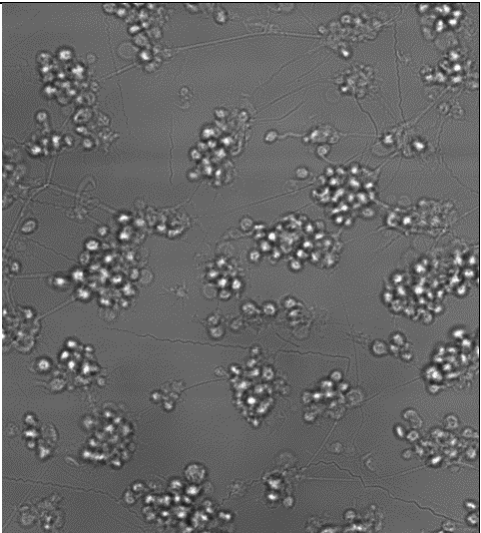
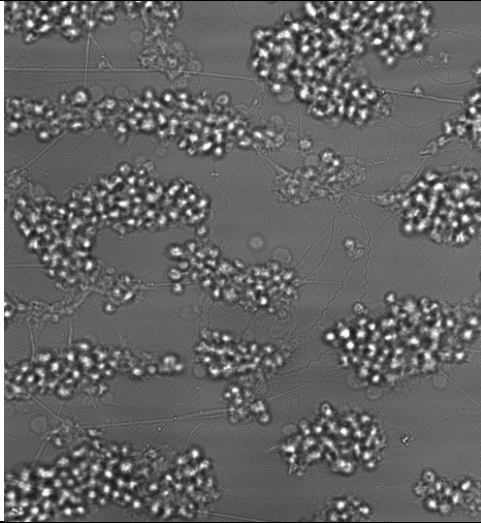
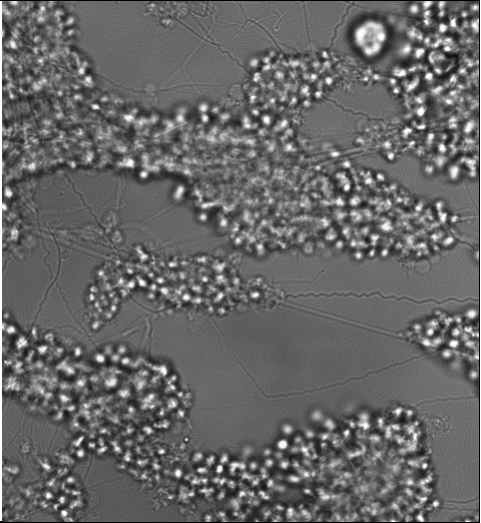
P4: Thrombus multilayer score (range 0-3)

P5: Thrombin contraction score (range 0-3)

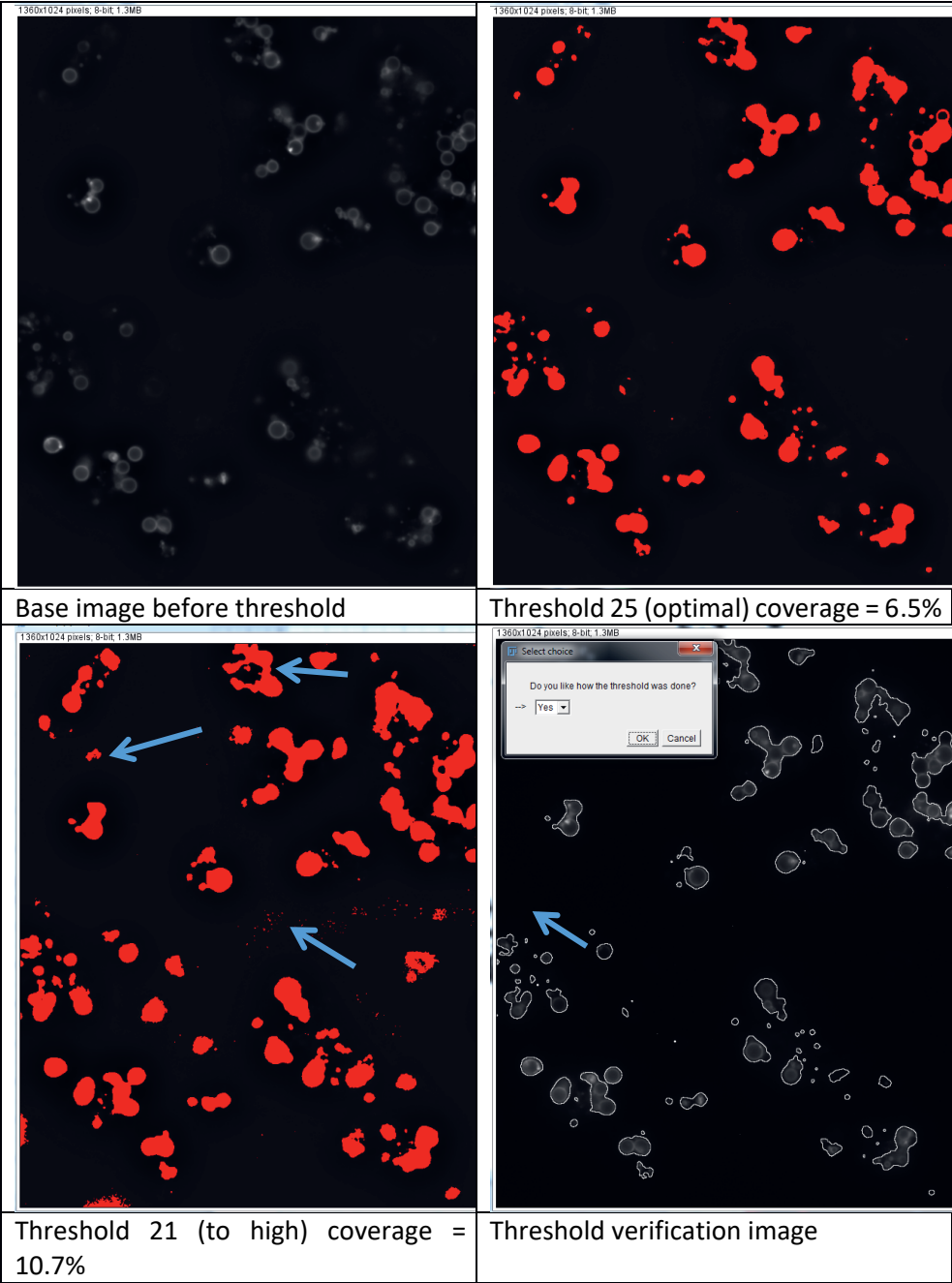
Scoring for P3: Thrombus morphology

0	1	2	3	4	5
					
No adhesion	Single platelets	Platelet monolayer	Small aggregates	Medium aggregates	Large aggregates

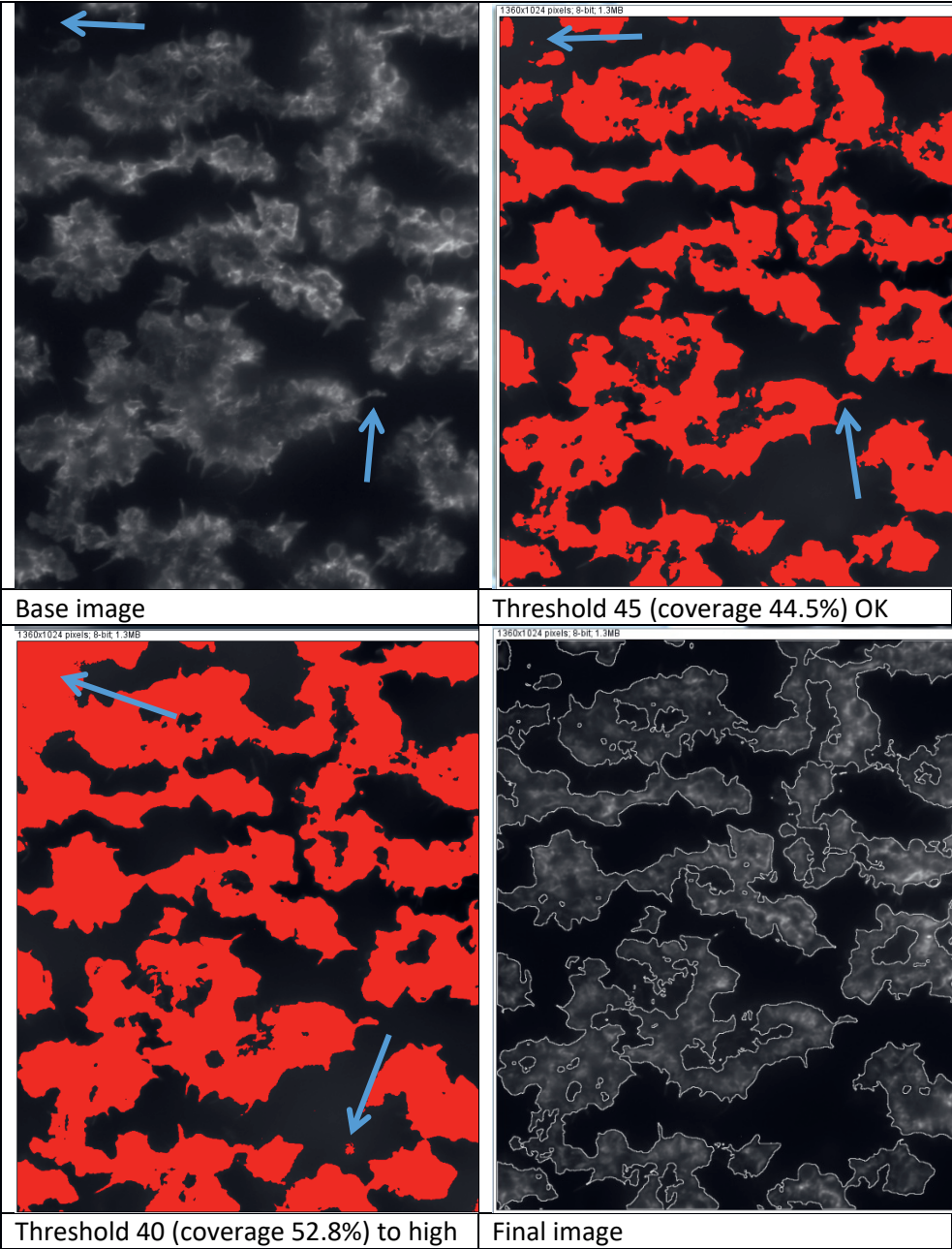
	
Morphological Score 0 (<15 platelets) Contraction score 0 Multilayer score 0	Morphological Score 1 (>15 platelets) Contraction score 0 Multilayer score 0

	
Morphological score 2 Contraction score 0 Multilayer score 0	Morphological score 3 Contraction score 1 Multilayer score 1
	
Morphological score 4 Contraction score 2 Multilayer score 2	Morphological score 5 Contraction score 3 Multilayer score 3 <i>Leukocyte count 1</i>

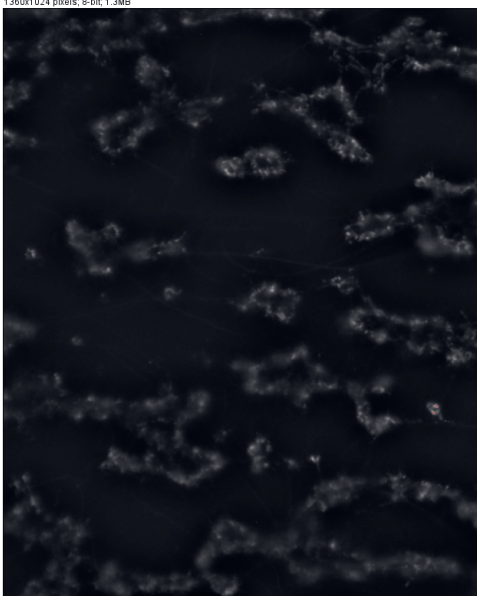
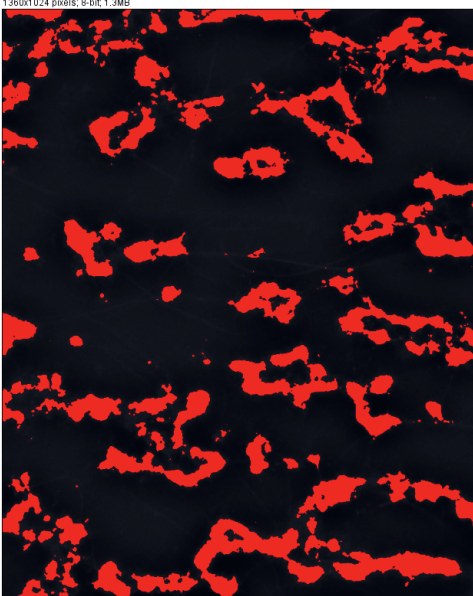
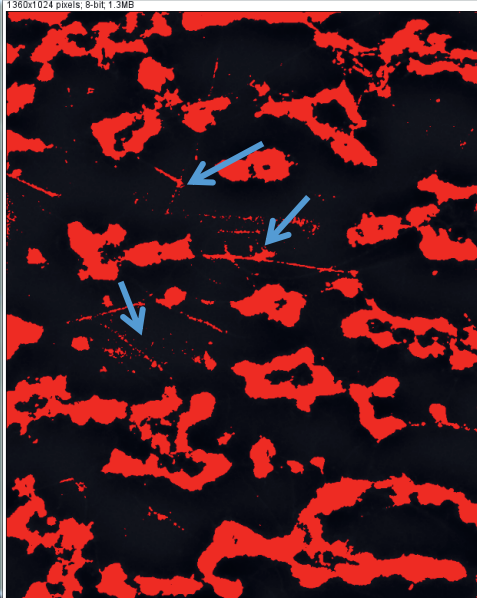

Performance of script for PS exposure (P6)



Performance of script for P-selectin expression (P7)

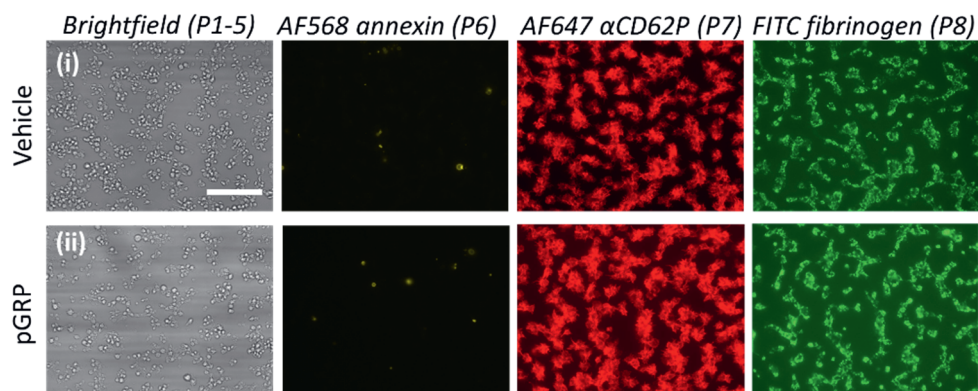


Performance of script for fibrinogen binding (P8)

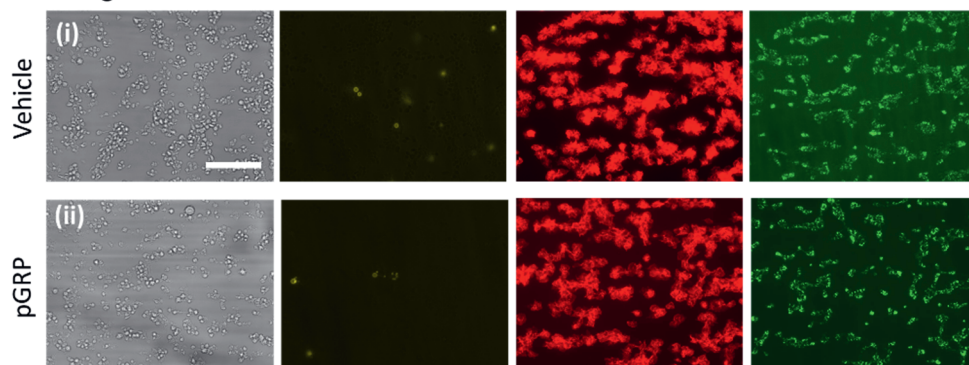
	
Base image	Threshold 33 (18.4%) correct
	
Threshold 29 (24.4%) to high background	End image

Supplementary figures and tables of Chapter 8

A Collagen-III

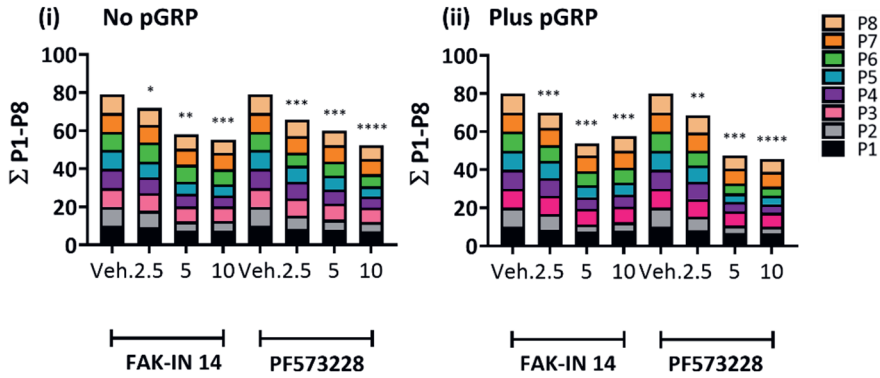


B Collagen-IV

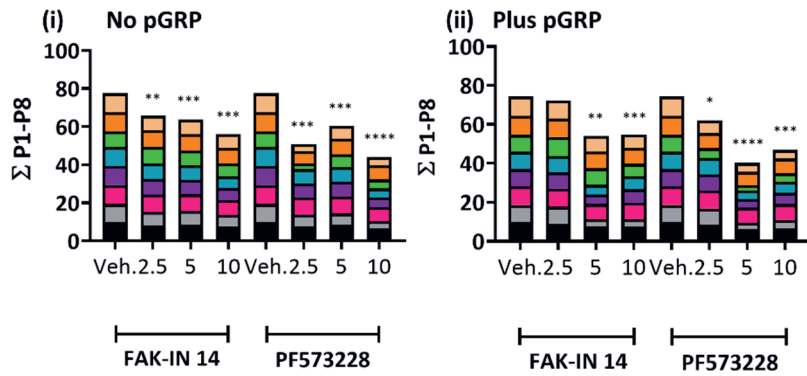


Suppl. Figure 1. Effects of GPR56-blocking peptide on collagen-dependent thrombus formation. Whole blood (700 μ L) was pre-incubated with vehicle medium or pGRP peptide (50 μ g/mL) for 10 minutes. After recalcification, the blood was perfused over microspots of collagen-I, -III and -IV for 3.5 minutes at wall-shear rate of 1600 s^{-1} . Brightfield and tri-color fluorescence images were taken per microspot at end stage. Shown are representative microscopic images for collagen-III (**A**) and collagen-IV (**B**) of: (i) vehicle control, or (ii) pGRP. Scale bar = 10 μ m.

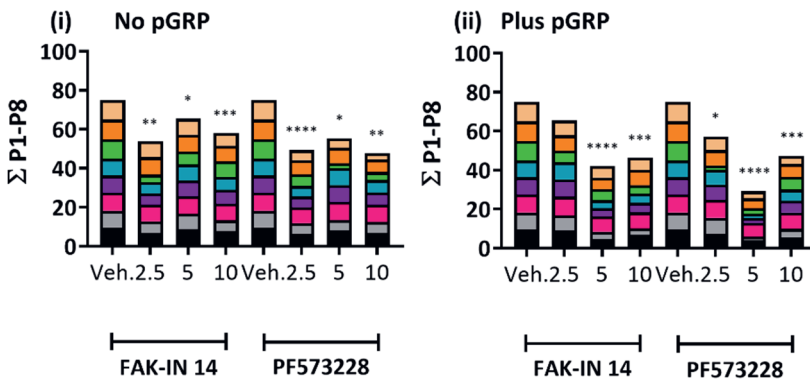
A Collagen-I



B Collagen-III

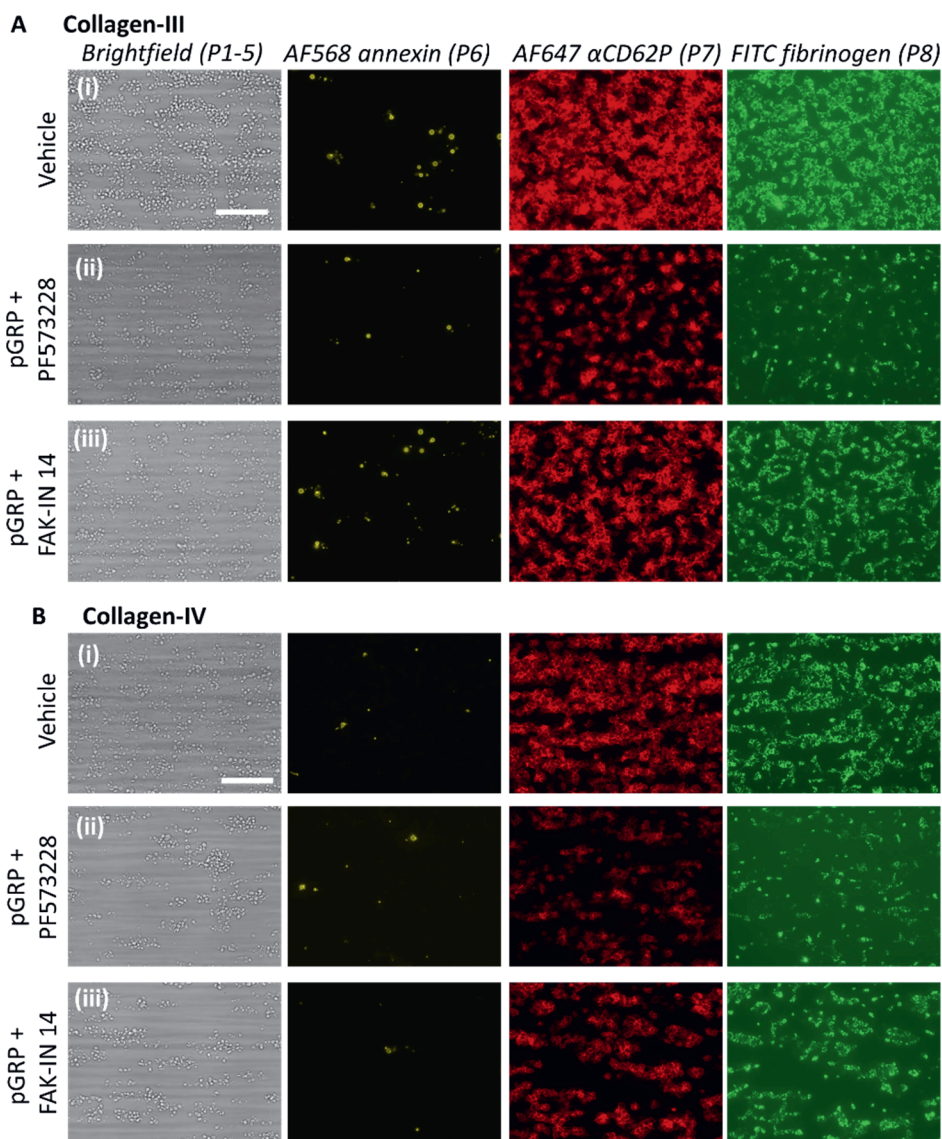


C Collagen-IV



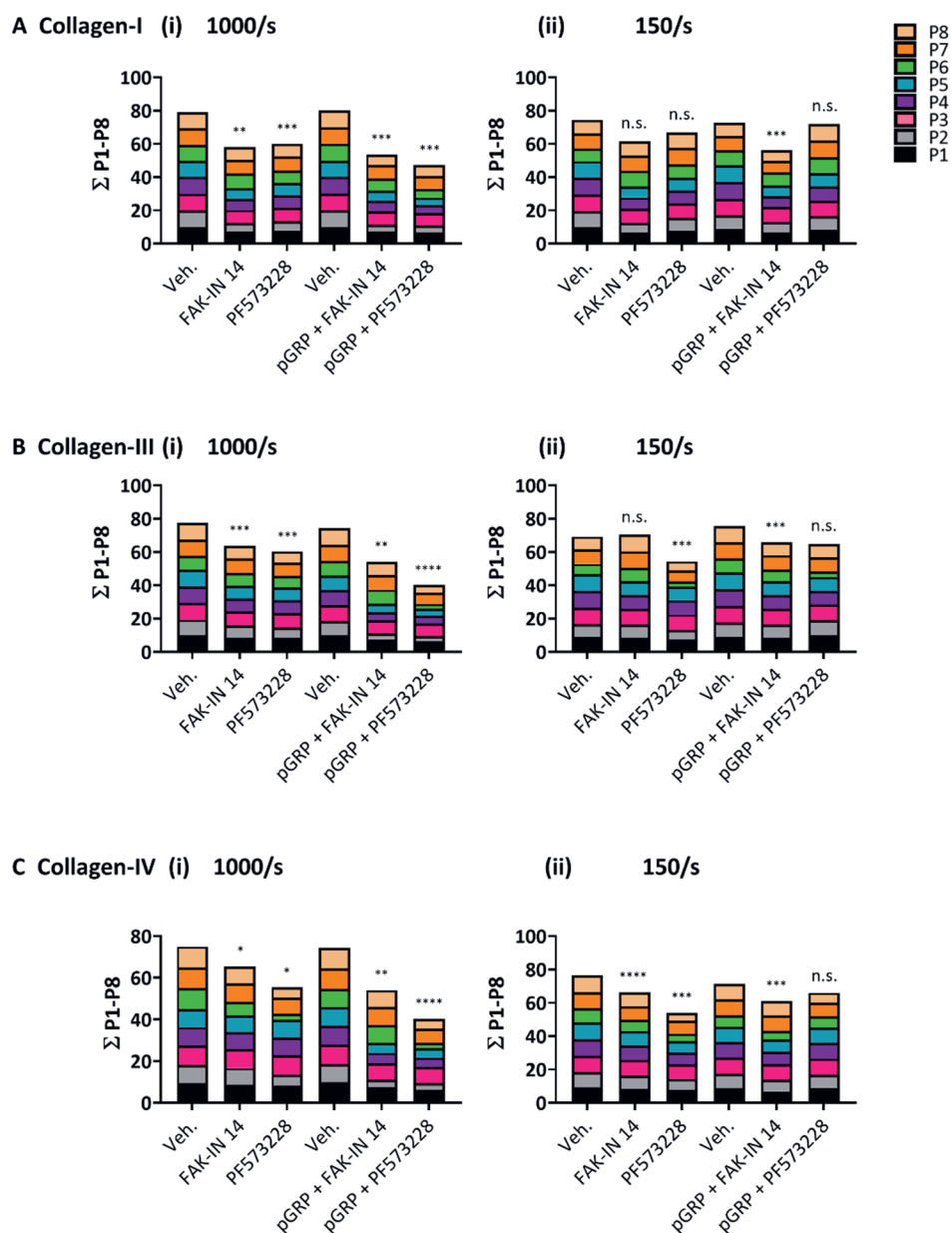
Suppl. Figure 2. Quantitative effect of GPR56-blocking peptide and PTK2 inhibition on collagen-dependent thrombus formation. Whole-blood flow runs over collagen-

*I, collagen-III and collagen-IV, and analyzed as for Figure 3. Preincubation of PTK2 was with FAK-IN14 or PF573228 (2.5-10 μ M) with(out) pGRP peptide (50 μ g/mL). Shown are cumulative plots per condition of scaled (0-10) image parameters: P1, platelet adhesion; P2, platelet aggregate coverage; P3-5, thrombus morphology, multilayer and contraction scores; platelet activation markers: P6, PS exposure; P7, P-selectin expression; P8, fibrinogen binding. Means of duplicate runs for 3-5 donors. Mean values compared per sample using a paired Student's t-test, * $P < 0.05$, ** $P < 0.005$, *** $P < 0.001$, **** $P < 0.0001$.*



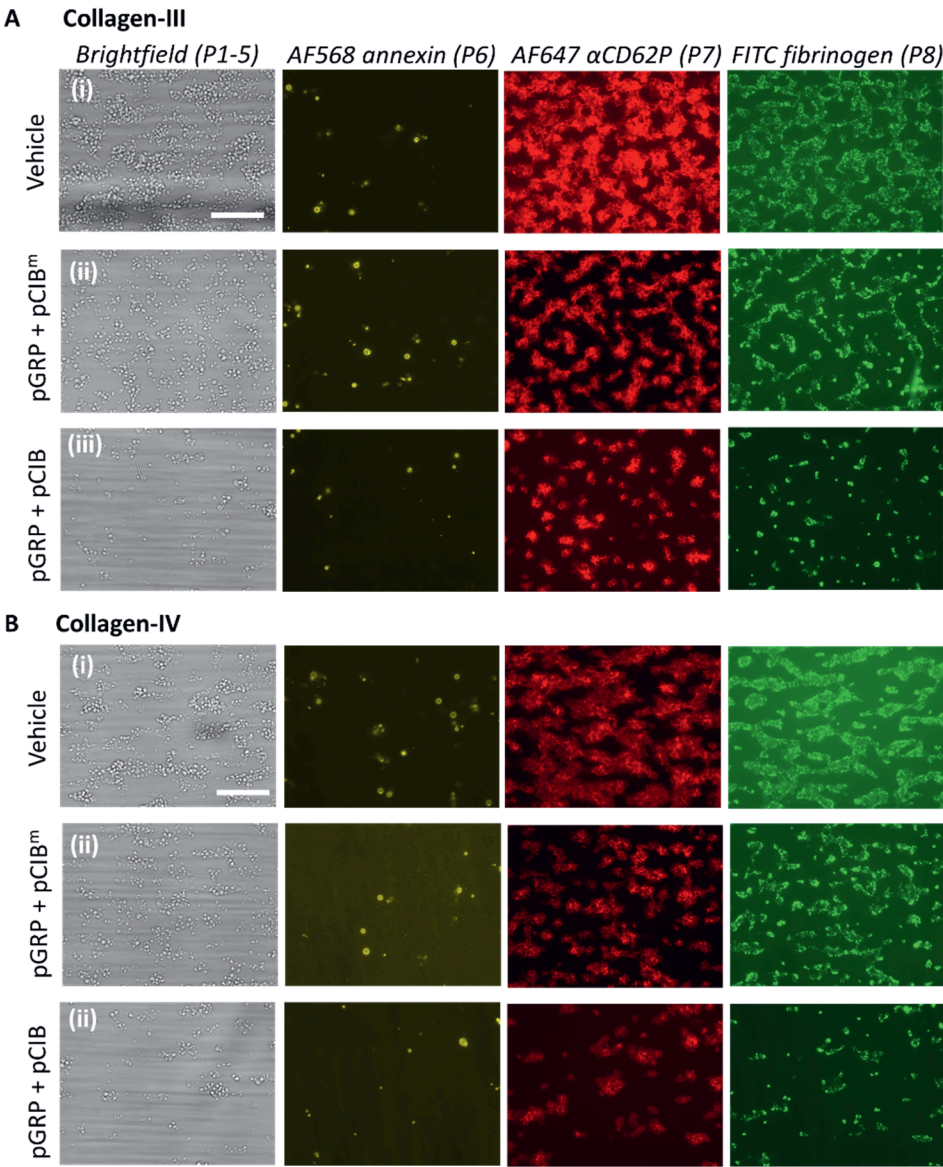
Suppl. Figure 3. Effect of GPR56-blocking peptide and PTK2 inhibition on collagen-dependent thrombus formation. Whole blood samples were pre-incubated with vehicle medium (control) or indicated PTK2 inhibitor (PF573228 or FAK-IN14, 10 μ M) with or without pGRP peptide (50 μ g/mL) for 10 minutes. After recalcification, the blood was perfused over collagen-I, -III and -IV microspots for 3.5 minutes at

*standard shear rate of 1000 s^{-1} . Representative end-stage brightfield and tri-color fluorescence images from microspots with collagen-III **(A)** and collagen-IV **(B)**. Shown are runs of control (i), pGRP + PF573228 (iv) and pGRP + FAK-IN14 (iii). Scale bar = $10\text{ }\mu\text{m}$.*



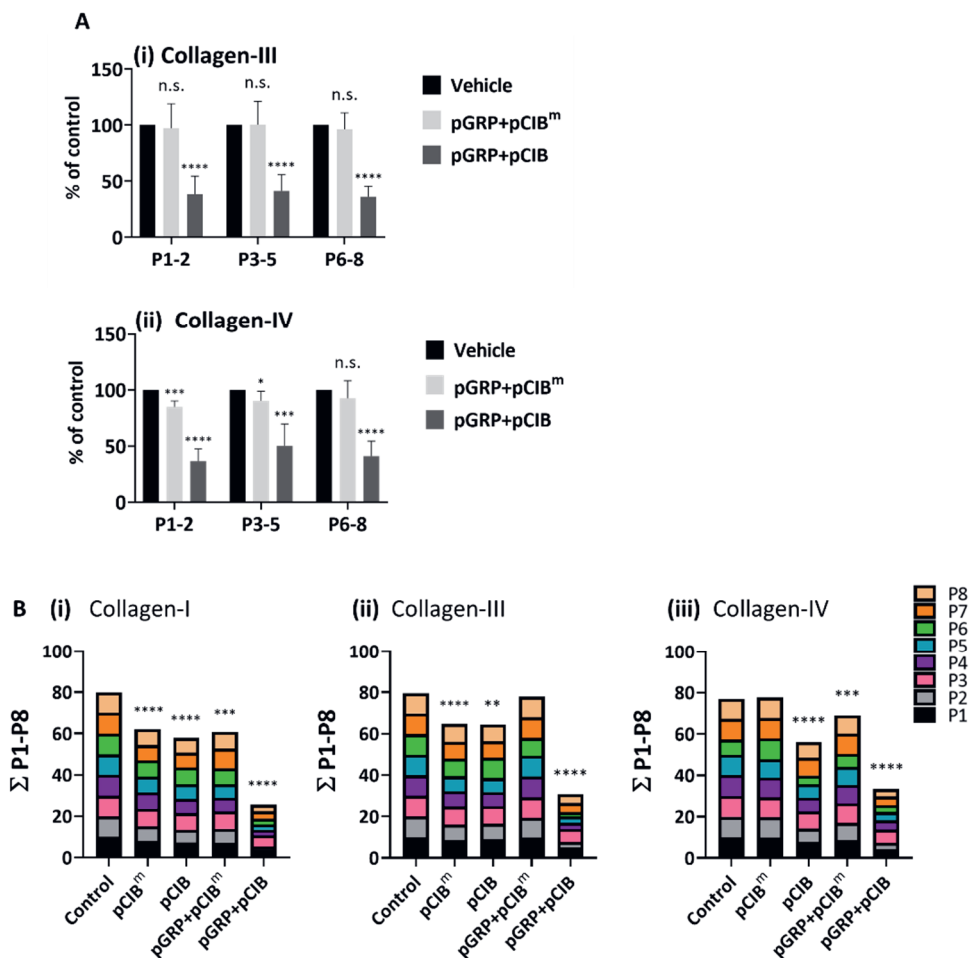
Suppl. Figure 4. Quantitation of shear rate dependency of GPR56 and PTK2 inhibition. Blood samples pre-incubated with vehicle (control) or PF573228 (5 μ M) with/without pGRP (50 μ g/mL) for 10 minutes, and then perfused over microspots

*of collagen-I, collagen-III and collagen-IV for 3.5 minutes at 1000 s⁻¹ or for 6 minutes at 150 s⁻¹ (see Figure 4). Shown are cumulative plots per condition of scaled (0-10) parameters P1-8. Means of duplicate runs for 3-5 donors. Mean values were compared per each blood sample using a paired Student's t-test, *P<0.05, **P<0.005, ***P<0.001, ****P<0.0001.*



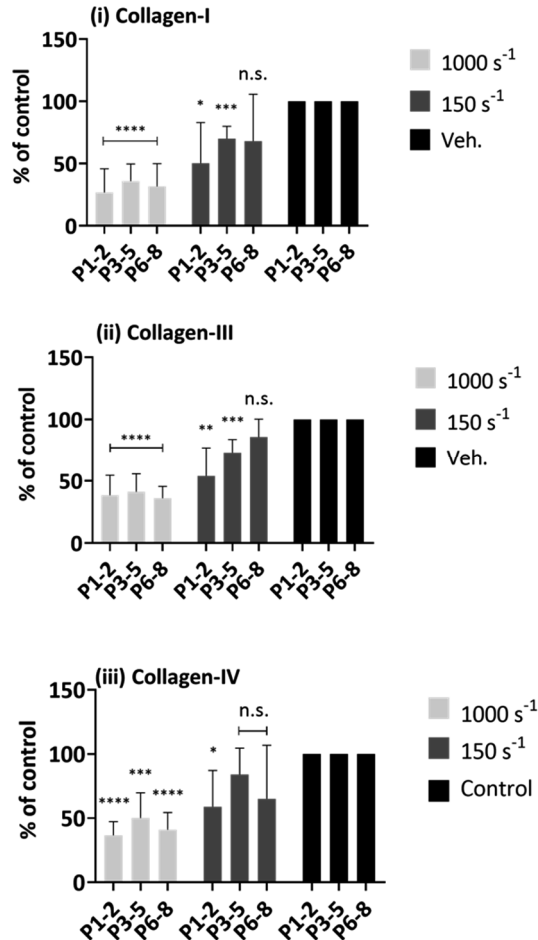
Suppl. Figure 5. Combined effects of GPR56- and CIB1-blocking peptides on collagen-induced thrombus formation. Whole blood samples were pre-incubated with vehicle (control) or indicated peptides pGRP, pCIB, pCIP^m (50 μ g/mL each) for 10 minutes. After recalcification, the blood was perfused over microspots of

collagen-I, -III and -IV for 3.5 minutes at 1000 s^{-1} (as in Figure 6). Brightfield and tri-color fluorescence images were taken per microspot at end stage. Representative images for collagen-III **(A)** and collagen-IV **(B)** of: (i) control runs, (ii) pGRP + pCIB runs, or (iii) pGRP + pCIB^m runs. Scale bar = 10 μm . Results from duplicate runs for 3-5 donors.



Suppl. Figure 6. Quantitative effects of GPR56- and CIB1-blocking peptides on collagen-dependent thrombus formation. Experimental setup as in Suppl. Figure 6. **A**, Percentual effects of peptides on combined parameters of platelet deposition (P1-2), thrombus characteristics (P3-5) and platelet activation (P6-8) versus vehicle control condition for collagen-III (i) and collagen-IV (ii). **B**, Cumulative plots per condition of scaled (0-10) parameters P1-8. Means of duplicate runs for 3-5 donors. Mean values were compared per each blood sample using a paired Student's t-test, * $P < 0.05$, ** $P < 0.005$, *** $P < 0.001$, **** $P < 0.0001$.

A



Suppl. Figure 7. Quantitative effects of rate dependency of GPR56 and CIB1 blockade. Experimental setup as in Figure 7. Blood samples pre-incubated with indicated inhibitors, and perfused over microspots of collagen-I, collagen-III and collagen-IV for 3.5 minutes at 1000 s⁻¹ or for 6 minutes at 150 s⁻¹. Shown are cumulative plots per condition of scaled (0-10) parameters P1-8. Means of duplicate runs for 3-5 donors. Mean values were compared per each blood sample using a paired Student's t-test, *P<0.05, **P<0.005, ***P<0.001, ****P<0.0001.

Chapter 9

General discussion

Cardiovascular diseases (CVD) are among the greatest threats to human health¹. In CVD, especially arterial thrombosis is a leading cause of death^{2,3}. It is well recognized that platelets play a key role in the onset and establishment of arterial thrombus formation, and they also crucial for normal hemostasis⁴. Platelets furthermore contribute to several other physiological and pathological processes, including thrombo-inflammation, cancer metastasis and vascular integrity^{5,6}. In the last decade, the platelet glycoprotein (GP)VI receptor has gained increased attention, as it is involved in nearly all of these pathological processes, whereas its role in hemostasis is minor⁷. This insight has raised the interest of GPVI as a novel antithrombotic target, potentially leading to drugs not causing major bleeding as a side effect. In spite of all the research, not much is known of the signaling mechanisms that restrain GPVI activity in platelets. Advanced mass spectrometric techniques are valuable here, since these provide in-depth insight into the protein phosphorylation changes, such as induced by GPVI, in activated and inhibited platelets⁸⁻¹⁰.

In the present thesis, I aim to provide a comprehensive overview of the complete platelet proteome and to elucidate the restraining mechanisms of GPVI-mediated thrombus formation by proteomics analyses and microfluidic assays. **Chapters 2-8** thus provide in-depth information on platelet multi-omics and on novel factors that regulate GPVI-induced platelet activation and thrombus formation. In more detail, the focus of my work is on: *(i)* overviewing the literature on platelet proteomics; *(ii)* trying to assess the complete platelet proteome by taking advantage of the genome-wide human platelet and megakaryocytes transcriptomes; *(iii)* extending this information to the mouse platelet proteome and transcriptome for comparison; *(iv)* link the omics insights to examine the controlling mechanisms of GPVI-induced platelet activation such in combination of with the fibrinogen receptor, integrin $\alpha\text{IIb}\beta\text{3}$.

Overviewing the field of platelet proteomics

Before diving into the experimental work, **Chapter 2** provides an overview of key platelet signaling pathways and it introduces how molecular proteomics can help to develop novel insight into platelet functions in health and disease. From the 67 reviewed publications on human platelet proteomics, it becomes clear that thousands of proteins have a role in platelet formation or function, and that many of these proteins contain phosphorylation sites that are regulated in activated or inhibited platelets. The phospho-site regulation holds for all conventional triggers of platelet activation, including collagen-like substances (via GPVI), von Willebrand factor (via GPIb-V-IX), thrombin (via the receptors PAR1 and PAR4), ADP (via the receptors P2Y₁ and P2Y₁₂), thromboxane A₂ (inhibited with aspirin) and the CLEC2 receptor with partly unclear ligands. The continuous development of mass spectrometric techniques has enabled these and even more regulated other types of post-translational modifications. Overviewing the detailing on advancements brought by these techniques, two aspects are important to mention: *(i)* the numbers of identified proteins and modification sites still vary widely between papers, depending on the purpose of the researchers, *(ii)* in spite of the large amounts of proteins and phosphorylation sites identified, the really important targets in key signaling pathways are still mostly unclear.

In this respect, we reported in **Chapter 2** on the limitations and challenges of current proteomics research in understanding the platelet (sub)proteome and the proteins associated with platelet signaling and activation, also taking into account metabolic, regulatory and structural aspects of platelets. The conclusion is that we need more confirmation and standardization of the proteomics outputs and, in addition, need powerful bioinformatics tools for in-depth analysis of the relevance for platelet function. It is to be expected that in the future, mass-spectrometry-based proteomics will develop to even more useful tools for detecting novel biomarkers for (abnormal) platelet activity in CVD and in response to medication in the clinic.

Global quantitative comparison of human and mouse platelet proteomes and transcriptomes

Because the anucleated platelets have attained a final differentiation stage and are limited in messenger translation, they form a relatively homogenous human cell source¹¹. By consequence, functional changes of platelets need to be regulated by post-translational modifications (PTM) such as protein phosphorylation, acylation, glycosylation, cleavage and ubiquitinylation. This provides an attractive opportunity for mass spectrometry-based analysis of protein modifications for investigating the regulatory activation pathways inside of a responsive platelet^{6,12}.

Platelets are unable to transcribe nuclear DNA, but they still contain an abundant and complex RNA transcriptome, including species of mRNAs, pre-mRNAs, RNAs from pseudogenes, micro-RNAs and circular RNAs^{11, 13, 14}. Although the proteome and the transcriptome of human platelets have been studied by various groups in the last decade, a comprehensive multi-omics comparison has not yet been made. In this thesis, we set on to systematically assess the quantitative (human) platelet proteome in comparison to the quantified platelet and megakaryocyte transcriptomes by combining multiple published datasets. In **Chapter 3**, the work was performed in collaboration with the owners of the datasets, *i.e.* the Blueprint Consortium (M. Frontini, Cambridge). In addition, we brought in a novel way of (UniProt-based) classification of proteins depending on the protein's main intracellular localization and function. This classification scheme, together with the transcriptome data, was used to establish a prediction model for the full platelet proteome, which we could also validate.

In **Chapter 3** we further describe that the human platelet and megakaryocyte transcriptomes are highly correlated, especially for the protein-coding genes. This similarity suggests a more or less random transfer of mRNAs from megakaryocytes to the formed platelets. This suggestion agrees with data from others that the gene expression levels in platelet to a certain extent reflect the megakaryocyte transcriptional status^{15,16}. Our

findings in addition demonstrate that the quantitative platelet proteome, as far as known, is less well correlated with the platelet or megakaryocyte transcriptome, which is consistent with a similar conclusion for bacteria and mouse tissues^{17,18}.

Our functional class analysis pointed out that the high appearance in the proteome of cytoskeleton intermediate proteins and secretory proteins with essentially absent mRNA levels can be explained by unavoidable contamination of samples with plasma proteins (present in the platelet open canicular system) and human keratins (likely coming from individuals responsible for the sample workup).

The earlier literature was still confusing on the degree of correlation between the human platelet proteome and transcriptome. In 2004, this correlation was estimated as high as 69%, but this percentage was limited to measurements of only 82 secreted proteins¹⁹. Later, Londin *et al.* performed a comprehensive quantitative comparison on a larger set of platelet proteins, and reported a much weaker connection ($R \approx 0.30$) between quantified mRNA (based on RNA-Seq analysis) and protein abundance levels²⁰. The work of that group indicated that the majority of identified proteins had detectable levels of mRNA, but not *vice versa*²⁰, a conclusion that is in agreement with the present findings. Our first platelet proteome-transcriptome database of **Chapter 3** contains more than 57k genome-wide transcripts corresponding to an expected proteome of around 15k protein-coding transcripts. Since so far only 5.2k unique platelet proteins have been identified, this means that around 10k proteins are 'missing', *i.e.* absent from the theoretical proteome. In quantitative terms, our analysis indicated that platelet proteins with highest copy numbers consistently had high mRNA levels, while proteins with lower copy numbers had more variable mRNA levels. Taking into account the high correlation with the megakaryocyte transcriptome, this may suggest a single gene/messenger-specific regulation of translation in the megakaryocyte.

Our assignment of gene products into protein functional classes pointed to three restraining factors, responsible for the low protein identification in platelets. These were: (i) a (peri)nuclear localization of a protein in the megakaryocyte; (ii) a low megakaryocytic transcription level, or (iii) a low mRNA translation level. These factors agreed with findings by the group of Rowley, Weyrich and co-workers. This group made a comparison with detectable mRNA species, and pointed out that 96% of the 3,993 identified proteins corresponded to detectable mRNA, of which 87% were expressed well in platelets²¹. Conversely, of the highly expressed transcripts also 84% corresponded to an identified protein. Together, these findings demonstrate that those proteins with both a high transcription and high translation in the megakaryocyte are more likely to be identified in platelets by proteomics techniques.

To gain a more comprehensive understanding of platelet proteome and transcriptome, in **Chapter 4** we added more datasets of human and mouse platelet transcriptomes and linked these to the corresponding platelet proteomes. The updated comparison of multiple transcriptomes showed high correlations within species ($R > 0.90$). However, correlations between species were lower both for the levels of mRNA ($R = 0.61$) and proteins ($R = 0.65$). This applied to essentially all protein function classes. Our work in this chapter extends a previous inter-species comparison, based on smaller datasets. Herein, the correlation between human and mouse platelet mRNA expression levels was lower ($R = 0.44$) for mRNA levels with relevant expression (defined as >0.3 rpkm)²². Also for human and rat platelets, a high similarity for the static ‘core’ and ‘evolutionary’ proteins has been revealed by comparative quantitative proteomics analysis²³.

Our own data show a remarkably high overlap between the identified human and mouse platelet proteomes, and an even higher overlap between the presence of human and mouse platelet mRNA transcripts (84%). This overlap was highest for the most abundant transcripts (96%), which again is an extension of the conclusion on overall similarity from Rowley *et al.*²². On

the other hand, our data point to specific inter-species differences in the presence or absence of certain transcripts. We figured out 184 differences between human and mouse, including for PAR3, the thrombin receptor that is only expressed on mouse platelets. Functional classes analysis revealed that differences were especially present in transcripts for membrane receptors and channels, and for signaling & adapter proteins. A restricted, only qualitative analysis of the human and mouse platelet transcriptome indeed indicated typical inter-species differences in the platelet signaling cascade²⁴.

Signaling restraining mechanisms of platelet GPVI

The activation processes of platelets in thrombosis and hemostasis are driven by intracellular signaling cascades. Mass spectrometry-based proteomics provides a useful way for detecting key regulatory elements in platelet signaling by monitoring alterations in protein expression and protein phosphorylation. In **Chapter 5**, we quantified 2,516 phosphorylation sites in platelets from seven patients with pseudohypoparathyroidism type 1a (Albright hereditary osteodystrophy syndrome or AHO syndrome). This syndrome is linked to a mutation in the *GNAS* gene locus, encoding for the G α s protein. Of the phosphorylation sites in the patients' platelets, 453 appeared to be iloprost-regulated. The majority of the up-regulated phospho-proteins were protein kinase A-dependent, while changes in the global platelet proteome were minor. The conclusion of a highly regulated phosphoproteome but a stable global proteome is consistent with other research on the platelets from patients with Scott syndrome or Gray platelet syndrome. In the Scott platelets, stimulation of GPVI and thrombin receptors caused an overall increase in phosphorylation level, while only 2.5% of the proteins were changed in global protein expression¹⁰. In Gray syndromic platelets (lacking granules), only 83 out of 2200 quantified proteins were found to be differential expressed. This suggested that most of the platelet proteins were similarly expressed in the patients and controls, except for the proteins regulating granule formation or involved in Ca²⁺ mobilization²⁵.

Loroch *et al.*, investigating the platelet proteome of Glanzmann patients, applied targeted mass-spectrometric methods (iTRAQ-labeling and parallel reaction monitoring, PRM) for the quantification of several possible integrin-linked proteins, including the coagulation factor XIII B chain (F13B), plasminogen (PLMN) and laminin subunit $\alpha 4$ (LAMA4)²⁶. While these proteins along with fibrinogen and the integrin αIIb and $\beta 3$ chains were altered, again the majority of the platelet proteome was unchanged. Taken together with our findings, it seems that in patients with platelet-related disorders the global platelet proteome is almost unchanged, except for some typical deviations. On the other hand, as we and others reported, quantification of phosphorylation changes in activated platelets did reveal important activation changes in the platelets from specific patient groups. Together, this argues for more precise proteomic-based quantification methods for monitoring such phosphorylation changes than the ones provided by current techniques. High-throughput analysis and zero variance in proteomic sample preparation applied to platelets will be an important step forward²⁷.

Apart from phospho-proteomics, Western blotting is widely used for the analysis of platelet signaling pathways. In **Chapter 7**, we investigated the signaling regulation of a postulated restraining mechanism for platelet activation in GPVI-induced platelet activation (Figure 1). Pharmacological inhibition of the protein tyrosine phosphatases Shp1/2 showed an increased platelet aggregation in response to low doses of CRP-XL, as well as a reversal of the blockage effect of phosphoinositide 3-kinase (PI3K).

These findings matched the earlier postulated suppressive role of Shp2 (gene *PTPN11*) in GPVI- and ITAM-regulated platelet signaling²⁸. On the other hand, in combined Shp1- and Shp2-deficient mouse platelets, a reduced to normal platelet aggregation, respectively, was observed in response to CRP-XL²⁹. The latter reduction was explained by a lower GPVI expression on the deficient platelets, which hence differs from effects of combined Shp1/2 inhibition. In the same study, it was reported that in

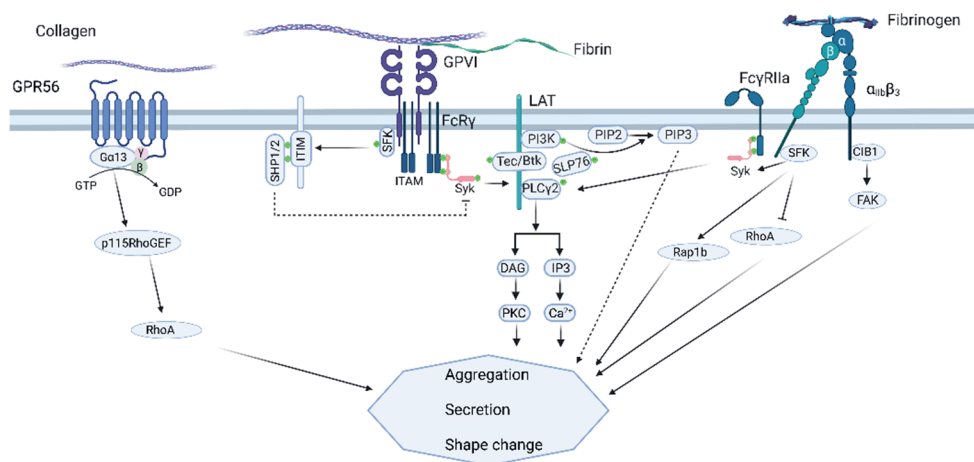


Figure 1. Summative representation of GPVI- and α IIb β 3-related platelet signaling cascades upon stimulation by collagen, fibrin or fibrinogen. The binding of collagen (fibrin) to GPVI and the dimeric ITAM-containing Fc γ R chain activates Src family kinases (SFK) and Syk, resulting the assembly of a LAT signalosome to recruit adaptors including PLC γ 2, PI3K, Tec/Btk. The activation of PI3K isoforms catalyzes the generation of the phospholipid messenger PIP3, and the PLC γ 2 activation leads to Ca²⁺ mobilization. ITIM-containing receptors provide docking sites for Shp1/2 to inhibit ITAM-mediated platelet activation, but only under certain conditions. The activated integrin α IIb β 3 by binding to fibrinogen helps to sustain platelet aggregation, secretion and shape change through SFK, CIB1, FAK (i.e., PTK2) and the GTPase Rap1b. The receptor GPR56 is activated by binding to collagen at high shear rate and may regulate platelet activation via RhoA. Key abbreviations: DAG, diacylglycerol; FAK, focal adhesion kinase; IP3, inositol 3-phosphate; PI3K, phosphoinositide 3-kinase; PCK, protein kinase C. Figure created by Biorender.com.

platelets from Shp1-deficient mice (gene *Ptpn6*) the tyrosine phosphorylation levels of PLC γ 2 Tyr¹²¹⁷, Src Tyr⁴¹⁸ and Syk Tyr⁵¹⁹⁺⁵²⁰ were reduced upon stimulation of CRP-XL, while there was no difference in Shp2-deficient platelets²⁹. In our experiments of **Chapter 7**, we did not detect an altered phosphorylation level of PLC γ 2 at Tyr⁷⁵⁹, Src at Tyr⁴¹⁹, or Syk at Tyr⁵²⁵⁺⁵²⁶ after blocking of Shp1/2 in the GPVI-stimulated human platelets via collagen-related peptide. Interestingly, the phosphorylations of Src Tyr⁴¹⁹

and PLC γ 2 Tyr⁷⁵⁹ were reduced rather than increased in the combined presence of both Shp1/2 and phosphoinositide 3-kinase (PI3K) blockers. In addition, we observed an unchanged collagen-induced platelet aggregation in response to Shp inhibition, which agrees with a report by other authors³⁰. The differential responses of platelets to collagen-related peptide or collagen can be explained by the adjacent role of platelet integrin α 2 β 1 in binding to collagen. Overall, we concluded that the isoform Shp2 is regulatory at suppressed PI3K activity in GPVI-specific platelet responses via a mechanism not involving PLC γ 2 phosphorylation and activation. However, this work will need confirmation using isoform-specific inhibitors of Shp1 or Shp2.

Role of GPVI in arterial thrombosis and hemostasis

In the past decades, the evidence for a role of the platelet-specific receptor GPVI in arterial thrombus formation has accumulated. One of the first reports on this came from *in vivo* studies with mice where GPVI was blocked by the antibody JAQ1, while causing a no more than moderate increase in tail bleeding time³¹. The recognition that mouse GPVI has a major role in arterial thrombosis, but a minor role in hemostasis made GPVI an interesting antithrombotic target³². However, the mechanisms and signaling pathways of GPVI-dependent platelet activation in thrombosis are still incompletely understood. To explore these, we investigated the contribution of two less well identified pathways in GPVI signaling and thrombus formation.

In **Chapter 6**, we examined the role of GPVI in fibrin- and fibrinogen-mediated thrombus formation under flow. On surfaces of immobilized fibrin or fibrinogen, we found that GPVI induced the formation of microthrombi at arterial shear rates under coagulant conditions. The study also indicated that integrin α IIb β 3 next to GPVI contributes to the fibrin(ogen)-dependent platelet adhesion and activation (Figure 1). This finding was confirmed with blood samples from Glanzmann patients, lacking the integrin. In addition, we observed that fibrin-induced platelet aggregation, Ca²⁺ mobilization and granule secretion were partly reduced, when the GPVI was blocked by Fab

9O12, while these responses were fully suppressed when the signaling via Syk was blocked. Since Syk is a common protein tyrosine kinase activated downstream of GPIIb-V-IX, GPVI and α IIB β 3, we checked for inhibition of GPIIb-V-IX, which showed no more than mild effects on platelet activation. Together, this work suggested that in the fibrin-induced thrombus formation, the roles of GPVI and integrin α IIB β 3 are nonredundant, meaning that both GPVI and α IIB β 3 are necessary for microthrombus formation. This conclusion is consistent with previous research that the shear-dependent thrombus formation in mouse *in vivo* becomes abolished upon blockage of Syk³³. Taken together, our findings allow to support an earlier conclusion that platelet GPVI can become (weakly) activated by fibrin³⁴.

To further explore the relationship between integrin α IIB β 3 and collagen-GPVI-mediated thrombus formation under flow, in **Chapter 8** we explored the combined contributions of the shear-dependent collagen receptor GPR56 with an integrin-dependent pathway involving calcium and integrin-binding protein 1 (CIB1)³⁵ and focal adhesion kinase (PTK2) in thrombus formation *in vitro* (Figure 1). For this purpose, we designed and synthesized peptides interfering with the interaction of CIB1 with α IIB β 3 (pCIB and pCIB^m) or with GPR56 (pGRP). We observed that the thrombus formation on collagen surfaces at high shear rate (1600 s⁻¹) was slightly reduced in the presence of pGRP, thus in agreement with the postulated role of GPR56 as a shear-force dependent receptor³⁶. Interestingly, we also observed that the addition of PTK2 inhibitors drastically enhanced the inhibitory effect of pGRP on the thrombus formation. This suggested that the role of GPR56 may be obscured by the known α IIB β 3-dependent activation through PTK2³⁷. In contrast, in slowly stirred suspensions of aggregating platelets, we did not see a synergistical effect of pGRP with PTK2 inhibitor. Further experiments then indicated that the combination of pCIB with pGRP had similar but less strong effects under shear as PTK2 inhibition, allowing us to postulate a shear- and integrin α IIB β 3-dependent novel role of CIB1 and PTK2 in collagen- and GPVI-mediated thrombus formation.

Conclusion and future perspectives

In this thesis, I provide a global reconstruction of the full transcriptomes and proteomes of human and mouse platelets, including a comprehensive qualitative and quantitative comparison between the platelet/megakaryocyte transcriptome and proteome per 21 (or 22) assigned protein function classes. My work has elucidated both qualitative and quantitative inter-species differences of the (theoretical) platelet proteomes and transcriptomes. In addition, I describe some novel approaches to reveal the inhibitory mechanisms of collagen- and GPVI-mediated thrombus formation.

Altogether, this thesis provides several novel insights: *(i)* the protein composition rather than the expression levels in platelets is related to the transcriptome of platelets and megakaryocytes, in a way that proteins with both a high transcription and translation in the megakaryocyte are more likely to be identified by proteomics techniques; *(ii)* the platelet proteins and protein-coding transcripts show high inter-species overlap, while correlations are relatively low on a quantitative base; *(iii)* only several key proteins appear to be altered in platelet-related disorders or platelet with specific treatment; *(iv)* the tyrosine phosphatase pathways of Shp1/2 only under certain conditions restrains the GPVI-induced platelet activation; and *(v)* the outside-in signaling pathway of integrin $\alpha\text{IIb}\beta\text{3}$, CIB1 and PTK2 positively contributes to collagen- and (likely) fibrin-induced thrombus formation via GPVI.

Currently, based on transcriptome analysis, no more than half of the proteins that are expected in human or mouse platelets has been identified. Accordingly, the full platelet proteome is not yet known, likely due to the technical and instrument limitations. This limitation sets a brake on investigating the precise regulation of the platelet signaling pathways. We envision that the newest developments of mass-spectrometric techniques, instrumentation and analysis methods will overcome this limitation. As a result, with the more complete platelet global proteome and regulated

platelet phosphoproteome established, application to the research field of platelet signaling and to the clinic will become easier and more user-friendly. Concerning GPVI as a novel antithrombotic target, in spite of the fact that this platelet receptor has been studied for such a long time, anti-GPVI drugs are still in the early phase of clinical testing. Today, glenzocimab (based on the 9O12 Fab) and revacept are the GPVI-related drugs with first promising results in clinical trial. My hope is that the GPVI-related signaling pathways examined in this thesis will help to better understand the potential and perhaps limitations of these anti-GPVI drugs.

References

1. Yusuf S, Wood D, Ralston J and Reddy KS. The World Heart Federation's vision for worldwide cardiovascular disease prevention. *Lancet*. 2015;386:399-402.
2. Alkarithi G, Duval C, Shi Y, Macrae FL and Ariëns RAS. Thrombus structural composition in cardiovascular disease. *Arterioscler Thromb Vasc Biol*. 2021;41:2370-2383.
3. Gregson J, Kaptoge S, Bolton T, Pennells L, Willeit P, Burgess S et al. Cardiovascular risk factors associated with venous thromboembolism. *JAMA Cardiol*. 2019;4:163-173.
4. Van der Meijden PE and Heemskerk JW. Platelet biology and functions: new concepts and clinical perspectives. *Nat Rev Cardiol*. 2019;16:166-179.
5. Perrella G, Nagy M, Watson SP and Heemskerk JW. Platelet GPVI (glycoprotein VI) and thrombotic complications in the venous system. *Arterioscler Thromb Vasc Biol*. 2021;41:2681-2692.
6. Huang J, Zhang P, Solari FA, Sickmann A, Garcia A, Jurk K et al. Molecular proteomics and signaling of human platelets in health and disease. *Int J Mol Sci*. 2021;22:9860.
7. Rayes J, Watson SP and Nieswandt B. Functional significance of the platelet immune receptors GPVI and CLEC-2. *J Clin Invest*. 2019;129:12-23.
8. Beck F, Geiger J, Gambaryan S, Solari FA, Dell'Aica M, Lorocho S et al. Temporal quantitative phosphoproteomics of ADP stimulation reveals novel central nodes in platelet activation and inhibition. *Blood*. 2017;129:e1-e12.

9. Burkhardt JM, Vaudel M, Gambaryan S, Radau S, Walter U, Martens L et al. The first comprehensive and quantitative analysis of human platelet protein composition allows the comparative analysis of structural and functional pathways. *Blood*. 2012;120:e73-82.
10. Solari FA, Mattheij NJ, Burkhardt JM, Swieringa F, Collins PW, Cosemans JM et al. Combined quantification of the global proteome, phosphoproteome, and proteolytic cleavage to characterize altered platelet functions in the human Scott syndrome. *Mol Cell Proteomics*. 2016;15:3154-3169.
11. Bray PF, McKenzie SE, Edelstein LC, Nagalla S, Delgrosso K, Ertel A et al. The complex transcriptional landscape of the anucleate human platelet. *BMC Genomics*. 2013;14:1.
12. Burkhardt JM, Gambaryan S, Watson SP, Jurk K, Walter U, Sickmann A et al. What can proteomics tell us about platelets? *Circ Res*. 2014;114:1204-19.
13. Nassa G, Giurato G, Cimmino G, Rizzo F, Ravo M, Salvati A et al. Splicing of platelet resident pre-mRNAs upon activation by physiological stimuli results in functionally relevant proteome modifications. *Sci Rep*. 2018;8:498.
14. Denis MM, Tolley ND, Bunting M, Schwartz H, Jiang H, Lindemann S et al. Escaping the nuclear confines: signal-dependent pre-mRNA splicing in anucleate platelets. *Cell*. 2005;122:379-391.
15. Schubert S, Weyrich AS and Rowley JW. A tour through the transcriptional landscape of platelets. *Blood*. 2014;124:493-502.
16. Rondina MT and Weyrich AS. Regulation of the genetic code in megakaryocytes and platelets. *J Thromb Haemost*. 2015;13 Suppl 1:S26-32.
17. Bathke J, Konzer A, Remes B, McIntosh M and Klug G. Comparative analyses of the variation of the transcriptome and proteome of *Rhodobacter sphaeroides* throughout growth. *BMC Genomics*. 2019;20:358.
18. Ghazalpour A, Bennett B, Petyuk VA, Orozco L, Hagopian R, Mungrue IN et al. Comparative analysis of proteome and transcriptome variation in mouse. *PLoS Genet*. 2011;7:e1001393.
19. McRedmond JP, Park SD, Reilly DF, Coppinger JA, Maguire PB, Shields DC et al. Integration of proteomics and genomics in platelets: a profile of platelet proteins and platelet-specific genes. *Mol Cell Proteomics*. 2004;3:133-144.
20. Londin ER, Hatzimichael E, Loher P, Edelstein L, Shaw C, Delgrosso K et al. The human platelet: strong transcriptome correlations among individuals associate weakly with the platelet proteome. *Biol Direct*. 2014;9:3.

21. Rowley JW and Weyrich AS. Coordinate expression of transcripts and proteins in platelets. *Blood*. 2013;121:5255-5256.
22. Rowley JW, Oler AJ, Tolley ND, Hunter BN, Low EN, Nix DA et al. Genome-wide RNA-seq analysis of human and mouse platelet transcriptomes. *Blood*. 2011;118:e101-e111.
23. Yu Y, Leng T, Yun D, Liu N, Yao J, Dai Y et al. Global analysis of the rat and human platelet proteome - the molecular blueprint for illustrating multi-functional platelets and cross-species function evolution. *Proteomics*. 2010;10:2444-2457.
24. Balkenhol J, Kaldorf KV, Mammadova-Bach E, Braun A, Nieswandt B, Dittrich M et al. Comparison of the central human and mouse platelet signaling cascade by systems biological analysis. *BMC Genomics*. 2020;21:897.
25. Bergemalm D, Ramström S, Kardeby C, Hultenby K, Eremo AG, Sihlbom C et al. Platelet proteome and function in X-linked thrombocytopenia with thalassemia and *in silico* comparisons with gray platelet syndrome. *Haematologica*. 2021;106:2947-2959.
26. Lorocho S, Trabold K, Gambaryan S, Reiß C, Schwierczek K, Fleming I et al. Alterations of the platelet proteome in type I Glanzmann thrombasthenia caused by different homozygous delG frameshift mutations in ITGA2B. *Thromb Haemost*. 2017;117:556-569.
27. Lorocho S, Kopczynski D, Schneider AC, Schumbrutzki C, Feldmann I, Panagiotidis E et al. Towards zero variance in proteomics sample preparation: positive pressure FASP in 96-well format enables highly reproducible, time- and cost-efficient analysis of sample cohorts. *J Proteome Res*. 2022;21:1181-1188.
28. Pao LI, Badour K, Siminovitch KA and Neel BG. Nonreceptor protein-tyrosine phosphatases in immune cell signaling. *Annu Rev Immunol*. 2007;25:473-523.
29. Mazharian A, Mori J, Wang Y-J, Heising S, Neel BG, Watson SP et al. Megakaryocyte-specific deletion of the protein-tyrosine phosphatases Shp1 and Shp2 causes abnormal megakaryocyte development, platelet production, and function. *Blood*. 2013;121:4205-4220.
30. Koch E, Pircher J, Czermak T, Gaitzsch E, Alig S, Mannell H et al. The endothelial tyrosine phosphatase Shp1 plays an important role for vascular haemostasis in TNF α -induced inflammation in vivo. *Mediators Inflamm*. 2013;2013:279781-279781.

31. Nieswandt B, Schulte V, Bergmeier W, Mokhtari-Nejad R, Rackebrandt K, Cazenave JP et al. Long-term antithrombotic protection by in vivo depletion of platelet glycoprotein VI in mice. *J Exp Med*. 2001;193:459-469.
32. Baaten CCFMJ, Meacham S, de Witt SM, Feijge MAH, Adams DJ, Akkerman JW et al. A synthesis approach of mouse studies to identify genes and proteins in arterial thrombosis and bleeding. *Blood*. 2018;132:e35-e46.
33. Andre P, Morooka T, Sim D, Abe K, Lowell C, Nanda N et al. Critical role for Syk in responses to vascular injury. *Blood*. 2011;118:5000-5010.
34. Mammadova-Bach E, Ollivier V, Loyau S, Schaff M, Dumont B, Favier R et al. Platelet glycoprotein VI binds to polymerized fibrin and promotes thrombin generation. *Blood*. 2015;126:683-691.
35. Naik UP and Naik MU. Association of CIB with GPIIb/IIIa during outside-in signaling is required for platelet spreading on fibrinogen. *Blood*. 2003;102:1355-62.
36. Yeung J, Adili R, Stringham EN, Luo R, Vizurraga A, Rosselli-Murai LK et al. GPR56/ADGRG1 is a platelet collagen-responsive GPCR and hemostatic sensor of shear force. *Proc Natl Acad Sci USA*. 2020;117:28275-28286.
37. Hitchcock IS, Fox NE, Prévost N, Sear K, Shattil SJ and Kaushansky K. Roles of focal adhesion kinase (FAK) in megakaryopoiesis and platelet function: studies using a megakaryocyte lineage specific FAK knockout. *Blood*. 2008;111:596-604.

Chapter 10

Summary

Samenvatting

Resumo

总结

Impact

Curriculum vitae

Publications

Acknowledgements

Summary

Platelets play a key role in several physiological and pathological processes including hemostasis, arterial thrombosis, inflammation, vascular integrity and cancer metastasis. Upon vascular injury, they form a plug or thrombus to prevent excessive blood loss, and in thrombosis they form an occlusive blood clot. Glycoprotein VI (GPVI), as the major signaling collagen receptor on platelets, is currently considered as a novel antithrombotic target due to its established role in murine arterial thrombosis but a limited role in bleeding. In spite of multiple investigations, aspects of the mechanisms of collagen- and GPVI-mediated platelet activation are still unclear. Because of their anucleate structure, the majority of protein activities in activated platelets are regulated by post-translational modifications (PTMs). For this reason, high-resolution mass spectrometry-based proteomic techniques have become powerful tools to systematically discover and understand changes in protein phosphorylations and integrate these into receptor-mediated protein signaling cascades. The central aims of this thesis were to reveal the composition of the complete platelet proteome and to elucidate novel mechanisms and pathways of GPVI-induced platelet activation and thrombus formation.

Chapter 1 provides a general introduction of the contribution of platelets to thrombosis and hemostasis. Particular attention is paid here to the roles of GPVI, the GPVI-related signaling pathways, and the use of platelet proteomics. As a detailed overview of the application of proteomics methods to platelet research, the review **Chapter 2** lists and discusses all published work on human platelet proteomes, platelet signaling, and specific applications brought in by molecular proteomic research in health and disease. The chapter summarizes the findings from 67 publications related to human platelet proteome studies since 2010, and details relevant signaling pathways mediated by activating receptors on platelets, including the collagen receptor GPVI, the von Willebrand factor (VWF) receptor GPIb-V-IX, the podoplanin receptor CLEC-2, the thrombin receptors PAR1 and PAR4, the ADP receptors P2Y₁ and P2Y₁₂, the thromboxane A₂ receptor TP,

and furthermore the fibrin(ogen) receptor integrin $\alpha\text{IIb}\beta 3$. In addition, we included information related to the platelet inhibitory agents, prostacyclin and nitric oxide. Regarding signaling pathways, we overviewed current developments in platelet proteomics techniques. Applications of these techniques to monitor protein changes appeared to extend from platelet ageing, platelet-related congenital disorders to platelet alterations in cardiovascular disease. We also reported current limitations and challenges of the proteomics methods for established a full platelet (sub)proteome related to signal transduction, metabolism, platelet structure and survival. It is stated that, in the future, mass-spectrometry-based proteomics promise to be one of the powerful tools for detecting biomarkers related to platelet abnormalities, and use in the clinic.

Since the full platelet proteome in relation to the platelet transcriptome was not established, in **Chapter 3** we provided a comprehensive quantitative comparison of these omics set based on the leading Blueprint dataset (Cambridge, UK) and six published proteomes from the Leibnitz Institute ISAS in Dortmund. This comparison led to a prediction model for the full or theoretical platelet proteome. In this chapter, we established a current human platelet proteome database of more than 5,200 identified unique proteins, and combined with the genome-wide RNA-Seq platelet and megakaryocyte transcriptomes of >54k transcripts. All the potentially expressed platelet mRNAs and proteins were classified into 21 protein function categories, depending on the intracellular location and the assumed function as annotated in the UniProt database. Quantitative comparison of the human platelet and megakaryocyte transcriptomes indicated a high correlation, especially for the protein-coding transcripts. Furthermore, a quantitative comparison between the platelet proteome and transcriptome data showed a triangular pattern, indicating that a high translation corresponded to a high transcription level, but not *vice versa*. These results were consistent with the distribution patterns of platelet transcripts, in that the fraction of mRNAs with corresponding identified proteins increased with

the mean gene expression level. On the other hand, in the not-identified parts of the platelet proteome, the majority of the corresponding transcripts had low gene expression levels, regardless of the function classes.

Our function class-based analysis of proteome and transcriptome indicated three restraining factors for a limited protein identification in platelets by mass spectrometry-based proteomics; these are: (i) (peri)nuclear localization; (ii) low transcription levels, and (iii) low translation levels. This information was used to build a prediction model based with three restraining factors, leading to an achievable platelet proteome of 10 k proteins. The prediction model could be validated by a new analysis with the platelet pool from 30 healthy subjects.

As a next step, to gain a more comprehensive understanding of the proteome and transcriptome, we extended our analysis to the classified transcriptomes of both human and mouse platelets, and linked these to the available proteome datasets. Accordingly, in **Chapter 4**, we integrated eight RNA-Seq datasets from human platelets and two datasets from mouse platelets, altogether resulting in 54,357 human transcripts with 20,125 of protein-coding genes, and 17,317 mouse protein-coding transcripts. Our results indicated that, in spite of some heterogeneity in sample in transcriptome profiling, the platelet transcriptome is highly correlated for datasets within species. On the other hand, in between species the correlation was low for both the transcriptomes and proteomes, regardless of the assigned function classes. Despite this, the qualitative overlap was high between human and mouse regarding the proteins with estimated copy numbers, and regarding the orthologous mRNAs, especially for the high abundant transcripts. On the other hand, several many species-unique transcripts and proteins were identified, of which 184 with major inter-species differences, including PAR3 as a thrombin receptor known to be only present in mouse platelets. The protein function class analysis pointed out that the most different proteins were enriched in the classes of membrane receptors & channels, and signaling & adapter proteins.

An interesting application of mass spectrometry-based proteomics is to monitor protein changes in the platelets from patients with platelet-related disorders. In **Chapter 5**, we revealed the phosphoproteome changes in platelets from seven patients with Albright hereditary osteodystrophy syndrome (AHO or pseudohypoparathyroidism type Ia). The AHO syndrome is linked to a loss-of-function mutation in the *GNAS* gene locus, encoding for the Gs α protein, which is involved in activation of adenylate cyclase (AC) and cAMP-dependent protein kinase A (PKA); *i.e.* a major platelet-inhibition pathway. In this chapter, 453 iloprost-regulated phosphorylation sites were detected out of 2,516 identified phosphorylation sites, of which 50 were differentially regulated between patients and healthy control subjects. The iloprost upregulated proteins were in majority proven to be PKA-dependent. The proteome changes were: (i) linked to a defective G α s and PKA activity, (ii) related to changes in platelet function, and (iii) evaluated for the potential of discriminating patients with *GNAS* mutations between AHO and non-AHO. However, despite the dramatic changes in the patients' platelet phosphoproteome, the global protein expression showed only slight alterations. In spite of these findings, the results also pointed to the need of more precise proteomic quantification methods for monitoring the dynamic changes in protein phosphorylation.

As the major signaling collagen receptor, GPVI plays an important role in murine arterial thrombosis, meaning that it is important to know the positive and negative regulatory signaling pathways downstream of GPVI. In **Chapter 6**, we focused on the joint roles of GPVI and integrin α IIb β 3 in fibrin(ogen)-induced thrombus formation under flow conditions. It was noticed that a fibrin or fibrinogen surface only moderately stimulated GPVI, resulting in limited platelet aggregation and microthrombus formation at arterial shear rate. In addition, blockage studies of GPVI or Syk demonstrated a non-redundant role of GPVI and integrin α IIb β 3 in the fibrin-induced thrombus formation. Similar observations were made with the blood from Glanzmann

patients, whose platelets lack $\alpha\text{IIb}\beta 3$. Accordingly, our data pointed to a partial overlap of the clinical-relevant antagonism of GPVI and $\alpha\text{IIb}\beta 3$.

In **Chapter 7**, we investigated the how the supposed negative regulation of GPVI by the tyrosine phosphatases Shp1 and Shp2, influenced the GPVI-induced platelet activation. We found that the combined inhibition of Shp1/2 by NSC87877 increased the platelet aggregation induced by a low dose of collagen-related peptide. In addition, NSC87877 rescued the inhibitory effects of blocked phosphoinositide 3-kinase (PI3K) on platelet aggregation. However, western blot analysis indicated that the phosphorylations of PLC γ 2 Tyr⁷⁵⁹ and Src Tyr⁴¹⁹ were reduced by the combined inhibition of Shp1/2 and PI3K. In contrast, the phosphorylation of Syk Tyr⁵²⁵⁺⁵²⁶ remained unaltered. Taken together, these findings suggested that Shp1/2 compensates for the absence of PI3K activity in mediating integrin activation and PLC γ 2 phosphorylation, although the sign of change was different. Likely, this underscores a negative role of Shp2 (in integrin activation) and a positive role of Shp1 (in the PLC pathway).

In order to better understand the contributions of GPVI and integrin $\alpha\text{IIb}\beta 3$ in collagen-induced thrombus formation, in **Chapter 8** we conducted research to the integrin-dependent roles of focal adhesion kinase PTK2, calcium and integrin-binding protein 1 (CIB1) and the shear-dependent collagen receptor GPR56. For this purpose, we designed and synthesized peptides that were proven to interfere with the αIIb -CIB1 binding (pCIB and pCIB^m) or mimicked the activation of GPR56 (pGRP). We noticed that pGRP at high shear rate showed suppressive effects on collagen-mediated thrombus formation, rather than activating effects. Furthermore, the simultaneous blockage of PTK2 caused an even higher suppression of thrombus formation. And the same was true for the CIB1 interfering peptides, pCIB and pCIB^m. On the other hand, no peptide effects were observed for GPVI-induced platelet aggregation or Ca²⁺ mobilization, in the absence of shear. Together, these findings pointed to a shear-dependent role of PTK2,

CIB1 and integrin $\alpha\text{IIb}\beta 3$ in collagen- and GPVI-mediated platelet activation and thrombus formation.

In **Chapter 9**, the most important findings are critically discussed and placed within the framework of the current literature. It is stated that the current work provides a powerful tool for further investigating the platelet protein composition and to reveal the relations of the platelet proteome and transcriptome across human and mouse. There is still a new avenue to open by mass-spectrometry based proteomics methods, also to help further elucidating the positive and negative pathways underlying GPVI-induced thrombus formation in hemostasis and thrombosis; and furthermore to help identifying GPVI antagonist, such as developed in the H2020 TAPAS program for antithrombotic studies.

Samenvatting

Bloedplaatjes spelen een sleutelrol in meerdere fysiologische en pathofysiologische processen, waaronder hemostase, arteriële trombose, ontsteking, vasculaire integriteit en metastases. Bij vaatwandschade vormen ze een prop of trombus om daarmee overmatig bloedverlies te voorkomen, en bij trombose klonteren ze samen tot een occlusief bloedstolsel. Glycoproteïne VI (GPVI), als de belangrijkste signalerende collageenreceptor op bloedplaatjes, wordt momenteel beschouwd als een nieuw antitrombotisch doelwit vanwege diens bewezen rol bij arteriële trombose van de muis, met daarbij een beperkte rol in de hemostase. Ondanks uitgebreid onderzoek is een deel van het mechanisme van collageen- en GPVI-gemedieerde bloedplaatjes-activering nog steeds onduidelijk. Door afwezigheid van een celkern worden eiwitten in geactiveerde bloedplaatjes grotendeels gereguleerd door post-translationele modificaties (PTM's). Inmiddels zijn op massaspectrometrie gebaseerde proteoom-technieken met een hoge resolutie krachtige hulpmiddelen geworden om veranderingen in eiwitfosforylering in bloedplaatjes te begrijpen en om deze te integreren in receptor-afhankelijke eiwitsignaleringscascades. Centrale doelstellingen van dit proefschrift zijn om de samenstelling van het complete bloedplaatjes-proteoom te bepalen en om nieuwe mechanismen en routes van GPVI-geïnduceerde bloedplaatjesactivering en thrombusvorming op te helderen.

Hoofdstuk 1 verschaft een algemene introductie van de bijdragen van bloedplaatjes aan trombose en hemostase. Bijzondere aandacht is besteed aan de rol van GPVI, de GPVI-gerelateerde signaleringsroutes en het gebruik van bloedplaatjes-proteomics. **Hoofdstuk 2** bevat een gedetailleerd overzicht van de toepassingen van proteomics-methoden in het bloedplaatjesonderzoek. Een sommatie is gegeven van het gepubliceerde werk over proteoom-analyses van humane bloedplaatjes, de signaleringsroutes en specifieke toepassingen in het kader van gezondheid en ziekte. Hoofdstuk 2 bevat daarmee de bevindingen van 67 publicaties met betrekking tot studies aan het bloedplaatjesproteoom sinds 2010. Een

beschrijving wordt gegeven van de meest bekende signaleringsroutes, die worden aangestuurd via relevante receptoren, waaronder de collageenreceptor GPVI, de von Willebrand-factor (VWF)-receptor GPIb-V-IX, de podoplanine receptor CLEC-2, de trombine-receptoren PAR1 en PAR4, de ADP-receptoren P2Y₁ en P2Y₁₂, de tromboxaan A₂-receptor TP, en verder de fibrinogeen (en fibrine) receptor integrine $\alpha\text{IIb}\beta 3$. Daarnaast hebben wij informatie opgenomen over bloedplaatjesremmende middelen, met name prostacycline en stikstofmonoxide. Met betrekking tot signaleringsroutes geven we een overzicht van huidige ontwikkelingen in de proteomics-technieken. Toepassingen hierin om eiwitveranderingen te monitoren blijken te gaan van bloedplaatjesveroudering, aangeboren aandoeningen en bloedplaatjesveranderingen bij hart- en vaatziekten. Rapport is ook gemaakt van huidige beperkingen en uitdagingen in het proteomics-veld voor het vaststellen van een volledig bloedplaatjes (sub)proteoom en de samenhang daarmee voor signaaltransductie, metabolisme, cellulaire structuur en veroudering. Gesteld is dat toekomstige op massaspectrometrie gebaseerde proteomics-technieken krachtige hulpmiddelen zullen zijn voor het detecteren van biomarkers, die duiden op bloedplaatjesafwijkingen en nuttig kunnen zijn in de kliniek.

Omdat het volledige bloedplaatjesproteoom in relatie tot het transcriptoom nog niet was bepaald, hebben we in **hoofdstuk 3** een kwantitatieve vergelijking gemaakt van deze omics datasets op basis van de toonaangevende Blueprint gegevens (Cambridge, VK) en zes proteomen, gepubliceerd door het Leibnitz instituut ISAS in Dortmund. Deze vergelijking heeft geresulteerd in een voorspellingsmodel voor het volledige of theoretische bloedplaatjesproteoom. In dit hoofdstuk hebben wij een proteoom-database opgezet van het humane bloedplaatjes-proteoom met meer dan 5.200 geïdentificeerde unieke eiwitten, en deze gecombineerd met genoombrede RNA-Seq datasets van bloedplaatjes- en megakaryocyt-transcriptomen met daarin meer dan 54,000 transcripten. Alle potentieel tot expressie gebrachte mRNA's en eiwitten van bloedplaatjes zijn

geclassificeerd in 21 eiwitfunctie-categorieën, op basis van hun intracellulaire locatie en de veronderstelde functie op grond van de standaard UniProt-database. Kwantitatieve vergelijking van de transcriptomen van humane bloedplaatjes en megakaryocyten duidde op een hoge onderlinge correlatie, met name wat betreft de eiwitcoderende transcripten. De vergelijking tussen het bloedplaatjes-proteoom en het corresponderende transcriptoom liet een driehoekig patroon zien, waaruit afgeleid werd dat een hoge translatie naar eiwit het gevolg is van een hoog mRNA transcriptieniveau, maar niet omgekeerd. De resultaten bleken consistent met de distributiepatronen van bloedplaatjestranscripten, in die zin dat de fracties van mRNA's voor geïdentificeerde eiwitten toenam met het gemiddelde genexpressie-niveau. Echter in niet-geïdentificeerde delen van het bloedplaatjes-proteoom hadden de meeste transcripten een laag genexpressieniveau, onafhankelijk van de bepaalde functieklassen.

Onze functionele classificatie van eiwitten en transcripten gaf drie beperkende factoren aan voor de afwezigheid van bepaalde eiwitten in bloedplaatjes op basis van massaspectrometrie tot dusver: (i) een (peri)nucleaire lokalisatie; (ii) een laag transcriptieniveau, en (iii) een laag translatieniveau. Met behulp van deze informatie konden we een voorspellingsmodel bouwen, dat gebaseerd was op deze drie beperkende factoren. Dit leidde tot een haalbaar bloedplaatjesproteoom van 10,000 eiwitten. Het voorspellingsmodel kon vervolgens worden gevalideerd door een nieuwe proteoom-analyse met een pool van bloedplaatjes afkomstig van 30 gezonde proefpersonen.

Als een volgende stap om meer grip te krijgen op het proteoom en transcriptoom in bloedplaatjes, hebben wij de analyses uitgebreid tot de geclassificeerde transcriptomen van zowel humane als muizenbloedplaatjes, en deze gekoppeld aan beschikbare proteoom-datasets. **Hoofdstuk 4** geeft een beschrijving en vergelijking van RNA-Seq analyses met humane bloedplaatjes en twee datasets van muizenbloedplaatjes, hetgeen resulteerde in 54.357 humane transcripten van 20.125

eiwitcoderende genen, en in 17.317 corresponderende transcripten voor muizenewitten. De analyses gaf aan dat, ondanks enige heterogeniteit bij de monsterbereiding en transcriptoomprofieling, het bloedplaatjestranscriptoom van beide species sterk gecorreleerd is. Aan de andere kant bleek de correlatie tussen species laag bij kwantitatieve vergelijking van het transcriptoom en proteoom, onafhankelijk van de functieklasse. Desondanks was de kwalitatieve overlap tussen mens en muis hoog voor wat betreft de ewitten met bekende kopieaantallen en de corresponderende mRNA's, met name voor de veel voorkomende transcripten. Aan de andere kant konden we diverse unieke transcripten en ewitten identificeren in humane of muizenplaatjes. Hiervan hadden er 184 grote verschillen tussen de species, waaronder de trombinereceptor PAR3, waarvan bekend was dat deze alleen tot expressie komt in de bloedplaatjes van muizen. De analyse van eiwitfunctieklassen wees uit dat de meest verschillende ewitten voorkwamen in de klassen van membraanreceptoren en -kanalen, en signalerings- en adapterewitten.

Een interessante toepassing van de op massaspectrometrie gebaseerde proteomics is het bepalen van eiwitveranderingen in de bloedplaatjes van patiënten met bloedplaatjesgerelateerde aandoeningen. In **hoofdstuk 5** hebben wij de fosfoproteoom-veranderingen in bloedplaatjes bepaald van een zevental patiënten met het osteodystrofiesyndroom van Albright (AHO of pseudohypoparathyreoïdie type Ia). Het AHO-syndroom is gerelateerd aan een *loss-of-function* mutatie in de *GNAS*-genlocus, welke codeert voor het G α s-eiwit, dat betrokken is bij de activering van adenylaacyclase (AC) en cAMP-afhankelijk proteïne-kinase A (PKA). Deze signaleringroute is belangrijk voor het onderdrukken van de bloedplaatjesactivering. In dit hoofdstuk zijn 453 iloprost-gereguleerde eiwitfosforylerings-plaatsen bepaald uit een totaal van 2.516 fosforyleringen, waarvan er 50 differentieel gereguleerd waren tussen patiënten en gezonde controlepersonen. Van de iloprost opgereguleerde ewitten kon in de meeste gevallen aangetoond worden dat deze PKA-afhankelijk waren. De gevonden

proteoomveranderingen waren daarmee: (i) gekoppeld aan een defecte G α s- en PKA-activiteit, (ii) gerelateerd aan veranderingen in de bloedplaatjesfuncties, en (iii) in staat om een onderscheid te maken tussen patiënten met AHO of niet-AHO *GNAS*-mutaties. Ondanks de grote veranderingen in het fosfoproteoom van de bloedplaatjes van de patiënten, vertoonde de globale eiwitexpressie slechts kleine veranderingen. Onze resultaten wijzen echter ook op de noodzaak tot nauwkeurigere proteoom kwantificatiemethoden voor het bepalen van de eiwitfosforylering in bloedplaatjes.

Als belangrijkste signalerende collageenreceptor speelt GPVI een rol bij de experimentele arteriële trombose in muizen. Daarnaast is het belangrijk is om de positieve en negatieve regulerende signaleringsroutes via GPVI te kennen. In **hoofdstuk 6** hebben wij ons gericht op een gemeenschappelijke rol van GPVI en integrine α IIb β 3 in de trombusvorming onder stromingscondities op een fibrine- of fibrinogeen-oppervlak. Opvallend was dat deze oppervlakken slechts een matige stimulering van GPVI bewerkstelligden, hetgeen resulteerde in beperkte bloedplaatjesaggregatie en microtrombusvorming bij arteriële afschuifsnelheden. Verder toonden farmacologische interventiestudies gericht op GPVI of Syk aan, dat GPVI en integrine α IIb β 3 een niet-redundante rol hebben in de door fibrine geïnduceerde trombusvorming. Soortgelijke waarnemingen werden gedaan met het bloed van Glanzmann-patiënten, bij wie α IIb β 3 afwezig is op bloedplaatjes. Daarmee duiden onze gegevens op gedeeltelijke overlap van een klinisch relevante antagonisme van GPVI en α IIb β 3.

In **hoofdstuk 7** hebben wij onderzocht hoe de veronderstelde negatieve regulatie van GPVI door de tyrosinefosfatasen Shp1 en Shp2 van invloed is op de GPVI-geïnduceerde bloedplaatjesactivering. Vastgesteld werd dat de gecombineerde remming van Shp1/2 door de drug NSC87877 leidde tot een verhoging van de plaatjesaggregatie, wanneer die opgewekt werd door een lage dosis collageen-gerelateerd peptide. Bovendien neutraliseerde NSC87877 de remmende effecten van een geblokkeerde fosfoinositide 3-

kinase (PI3K) op de aggregatie van bloedplaatjes. Western-blot-analyse gaf echter aan dat de fosforylering van PLC γ 2 Tyr⁷⁵⁹ en Src Tyr⁴¹⁹ verminderde door de gecombineerde remming van Shp1/2 en PI3K. Daarentegen bleef de fosforylering van Syk Tyr⁵²⁵⁺⁵²⁶ ongewijzigd. Samengevat suggereren deze bevindingen dat Shp1/2 een afwezigheid van PI3K-activiteit compenseert bij zowel de integrine-activering als de PLC γ 2-fosforylering. De resultaten zijn in overeenstemming met een negatieve rol van Shp2 (in integrine-activering) en een positieve rol van Shp1 (in de fosfolipase-C route).

Om de bijdragen van GPVI en integrine α Ib β 3 aan collageen-geïnduceerde trombusvorming beter te begrijpen, beschrijft **hoofdstuk 8** een onderzoek naar de integrine-afhankelijke rol van *focal adhesion kinase* PTK2, calcium en integrine-bindend eiwit 1 (CIB1) en de *shear*-afhankelijke collageenreceptor GPR56. Voor dit doel hebben we peptiden ontworpen en gesynthetiseerd, waarvan aangetoond was dat deze interfereren met de α Ib-CIB1-binding (pCIB en pCIB^m) of met de activering van GPR56 (pGRP). Het bleek dat pGRP bij hoge afschuifsnelheden een remmend effect vertoonde op de collageen-gemedieerde trombusvorming, in plaats van een verwacht activerend effect. Bovendien zorgde de gelijktijdige blokkering van PTK2 voor een nog sterkere onderdrukking van de trombusvorming. En datzelfde gold voor de CIB1-interfererende peptiden, pCIB en pCIB^m. Aan de andere kant konden wij geen peptide-effecten meten in de GPVI-geïnduceerde bloedplaatjesaggregatie of Ca²⁺-mobilisatie, onder statische condities. Samen duiden deze bevindingen op een *shear*-afhankelijke rol van PTK2, CIB1 en integrine α Ib β 3 bij de collageen- en GPVI-gemedieerde bloedplaatjesactivering en trombusvorming.

In **hoofdstuk 9** zijn de belangrijkste bevindingen uit mijn proefschrift kritisch besproken en in het kader geplaatst van de huidige literatuur. Conclusie is in alle bescheidenheid dat het huidige werk een krachtig hulpmiddel biedt voor verder onderzoek naar de eiwitsamenstelling van bloedplaatjes in mens en muis, alsmede in relatie tot het bloedplaatjestranscriptoom. Op massaspectrometrie gebaseerde proteomics-methoden bieden nog steeds

nieuwe openingen voor bepaling van de positieve en negatieve reguleringspaden van GPVI-geïnduceerde trombusvorming bij hemostase en trombose. Bovendien kunnen deze helpen bij het identificeren van nieuwe GPVI-antagonisten voor antitrombotisch onderzoek, zoals ontwikkeld in het H2020 TAPAS-programma.

Resumo

As plaquetas desempeñan un papel fundamental en varios procesos fisiolóxicos e patolóxicos, incluíndo a hemostase, a trombose arterial, a inflamación, a integridade vascular e a metástase do cancro. Tras a lesión vascular, forman un tapón ou trombo para evitar a perda excesiva de sangue, e na trombose forman un coágulo de sangue oclusivo. A glicoproteína VI (GPVI), principal receptor de coláxeno de sinalización das plaquetas, considérase actualmente como unha nova diana antitrombótica debido ao seu papel descrito na trombose arterial murina, pero cun papel limitado no sangrado. Ademais, observouse un sangrado leve en pacientes deficientes en GPVI. A pesar das múltiples investigación levadas a cabo, aínda non están claros aspectos dos mecanismos da activación plaquetaria mediada por coláxeno e GPVI. Debido á súa estrutura anucleada, a maioría das actividades proteicas das plaquetas activadas están reguladas por modificacións postraducionais (PTM). Por este motivo, as técnicas proteómicas baseadas en espectrometría de masas de alta resolución convertéronse en ferramentas poderosas para descubrir e comprender de forma sistemática os cambios nas fosforilacións de proteínas que regulan cascadas de sinalización mediadas por receptores. Os obxectivos centrais desta tese foron revelar a composición do proteoma plaquetario completo e dilucidar novos mecanismos e vías de activación plaquetaria inducidas por GPVI e o seu papel na formación de trombos.

O **capítulo 1** ofrece unha introdución xeral da contribución das plaquetas á trombose e á hemostase. Préstase especial atención aquí aos papeis do GPVI, á vía de sinalización relacionada co GPVI e ao uso da proteómica plaquetaria. Como unha visión xeral detallada da aplicación dos métodos de proteómica á investigación de plaquetas, o **capítulo 2** enumera e analiza todos os traballos publicados sobre proteomas plaquetarios humanos, sinalización plaquetaria e aplicacións específicas que a investigación da proteómica molecular en saúde e enfermidades ofrece. O capítulo resume os descubrimentos de 67 publicacións relacionadas cos estudos de proteomas plaquetarios humanos desde 2010, e detalla as vías de sinalización

relevantes mediadas pola activación de receptores nas plaquetas, incluíndo o receptor de coláxeno GPVI, o receptor do factor von Willebrand (VWF) GPIb-V-IX, o receptor de podoplanina CLEC-2, os receptores de trombina PAR1 e PAR4, os receptores de ADP P2Y₁ e P2Y₁₂, o receptor de tromboxano A₂ TP e, ademais, o receptor de fibrina (óxeno) integrina α IIb β 3. Ademais, inclúese información relacionada cos axentes inhibidores plaquetarios, a prostaciclina e o óxido nítrico. En canto ás vías de sinalización, analizamos os desenvolvementos máis recentes nas técnicas de proteómica plaquetaria. As aplicacións destas técnicas para o estudo dos cambios proteicos expándense desde o envellecemento plaquetario e os trastornos conxénitos relacionados coas plaquetas ata as alteracións plaquetarias nas enfermidades cardiovasculares. Tamén informamos das limitacións e desafíos actuais dos métodos proteómicos para establecer un (sub)proteoma plaquetario completo relacionado coa transdución do sinal, o metabolismo, a estrutura plaquetaria e a supervivencia. Indícase que, no futuro, a proteómica baseada na espectrometría de masas promete ser unha das ferramentas máis poderosas para detectar biomarcadores relacionados con anomalías plaquetarias, con potencial uso na clínica.

Dado que non se estableceu o proteoma plaquetario completo en relación co transcriptoma plaquetario, no **capítulo 3** ofrecécese unha comparación cuantitativa completa deste conxunto ómico baseado no conxunto de datos presentados no Blueprint (Cambridge, Reino Unido) e seis proteomas publicados polo Instituto Leibnitz ISAS de Dortmund. Esta comparación levou a un modelo de predición para o proteoma plaquetario completo ou teórico. Neste capítulo, establecemos unha base de datos actual de proteomas plaquetarios humanos de máis de 5200 proteínas únicas identificadas e combinadas cos transcriptomas de plaquetas e megacariocitos de RNA-Seq en todo o xenoma de transcritos > 54k. Todos os mRNA e proteínas de plaquetas potencialmente expresados clasificáronse en 21 categorías de funcións proteicas, dependendo da localización intracelular e da función asumida, tal como se anota na base de

datos UniProt. A comparación cuantitativa dos transcriptomas de plaquetas e megacariocitos humanos amosou unha alta correlación, especialmente para os transcripts que codifican proteínas. Ademais, unha comparación cuantitativa entre os datos do proteoma plaquetario e do transcriptoma mostrou un patrón triangular, o que indica que unha tradución elevada correspondía a un nivel de transcrición elevado, pero non á inversa. Estes resultados foron consistentes cos patróns de distribución dos transcritos plaquetarios, xa que a fracción de mRNA coas proteínas identificadas correspondentes aumentou co nivel medio de expresión xénica. Por outra banda, nas partes non identificadas do proteoma plaquetario, a maioría dos transcritos correspondentes tiñan niveis de expresión xénica baixos, independentemente das clases de función.

A nosa análise baseada na clase de función do proteoma e do transcriptoma indicou tres factores de restrición para unha identificación limitada de proteínas nas plaquetas mediante proteómica baseada en espectrometría de masas; estes son: (i) localización (peri)nuclear; (ii) baixos niveis de transcrición e (iii) baixos niveis de tradución. Esta información utilizouse para construír un modelo de predición baseado en tres factores de restrición, o que leva a un proteoma plaquetario alcanzable de proteínas de 10 k. O modelo de predición podería validarse mediante unha nova análise co conxunto de plaquetas de 30 suxeitos sans.

Como seguinte paso, para obter unha comprensión máis completa do proteoma e do transcriptoma, estendemos a nosa análise aos transcriptomas clasificados de plaquetas humanas e de rato, e relacionámoslos cos conxuntos de datos de proteomas dispoñibles. En consecuencia, no **capítulo 4**, integramos oito conxuntos de datos de RNA-Seq de plaquetas humanas e dous conxuntos de datos de plaquetas de rato, o que resultou en total 54357 transcricións humanas con 20125 xenes codificantes de proteínas e 17317 transcricións de proteínas de rato. Os nosos resultados indicaron que, a pesar da heteroxeneidade da mostra no perfil do transcriptoma, o transcriptoma plaquetario está moi

correlacionado dentro das especies. Por outra banda, entre especies a correlación foi baixa tanto para os transcriptomas como para os proteomas, independentemente das clases de función asignadas. A pesar diso, a superposición cualitativa foi alta entre humanos e ratos no que se refire ás proteínas cun número de copias estimado, e no que respecta aos mRNA ortólogos, especialmente para as transcricións abundantes. Por outra banda, identificáronse varios tránscritos e proteínas únicas de especies en humanos e ratos respectivamente, das cales 184 amosaron grandes diferenzas entre especies, incluíndo PAR3 como receptor de trombina que se sabe que só está presente nas plaquetas do rato. A análise da clase de función das proteínas sinalou que as proteínas máis diferentes estaban enriquecidas nas clases de receptores e canles de membrana e proteínas de sinalización e adaptadores.

Unha aplicación interesante da proteómica baseada na espectrometría de masas é controlar os cambios de proteínas nas plaquetas de pacientes con trastornos relacionados coas plaquetas. No **capítulo 5**, revelamos os cambios de fosfoproteoma nas plaquetas de sete pacientes con síndrome de osteodistrofia hereditaria de Albright (AHO ou pseudohipo-paratiroidismo tipo Ia). A síndrome AHO está ligada a unha mutación con perda de función no locus do xene *GNAS*, que codifica para a proteína *Gαs*, que está implicada na activación da adenilato ciclase (AC) e da proteína quinase A (PKA) dependente de cAMP; é dicir, unha vía principal de inhibición plaquetaria. Neste capítulo, detectáronse 453 sitios de fosforilación regulados por iloprost dos 2516 sitios de fosforilación identificados, dos cales 50 foron regulados de forma diferenciada entre pacientes e suxeitos control sans. Probouse na súa maioría que as proteínas reguladas por iloprost eran dependentes de PKA. Os cambios no proteoma foron: (i) vinculados a unha actividade defectuosa de *Gαs* e PKA, (ii) relacionados con cambios na función plaquetaria e (iii) avaliados polo potencial de discriminar pacientes con mutacións *GNAS* entre AHO e non AHO. Non obstante, a pesar dos cambios dramáticos no fosfoproteoma plaquetario dos pacientes, a expresión global da proteína só mostrou leves alteracións. A pesar destes achados, os

resultados tamén apuntaron á necesidade de métodos de cuantificación proteómica máis precisos para controlar os cambios dinámicos na fosforilación de proteínas.

Como o principal receptor de coláxeno, o GPVI xoga un papel importante na trombose arterial murina, o que significa que é importante coñecer as vías de sinalización reguladora positiva e negativa augas abaixo do GPVI. No **capítulo 6** centrámonos nos papeis conxuntos de GPVI e integrina $\alpha\text{IIb}\beta 3$ na formación de trombos inducidos por fibrina (óxeno) en condicións de fluxo. Observouse que unha superficie de fibrina ou fibrinóxeno só estimulaba moderadamente o GPVI, o que resultaba nunha agregación plaquetaria limitada e formación de microtrombos a velocidade de cizallamento arterial. Ademais, os estudos de bloqueo de GPVI ou Syk demostraron un papel non redundante da GPVI e da integrina $\alpha\text{IIb}\beta 3$ na formación de trombos inducidos pola fibrina. Observacións similares foron feitas con sangue de pacientes coa enfermidade de Glanzmann, cuxas plaquetas carecen de $\alpha\text{IIb}\beta 3$. En consecuencia, os nosos datos apuntaron a unha superposición parcial do antagonismo clínico relevante de GPVI e $\alpha\text{IIb}\beta 3$.

No **capítulo 7**, investigamos como a suposta regulación negativa de GPVI polas tirosina fosfatasas Shp1 e Shp2 inflúe na activación plaquetaria inducida por GPVI. Descubrimos que a inhibición combinada de Shp1/2 por NSC87877 aumentou a agregación plaquetaria inducida por unha baixa dose do agonista específico de GPVI, *collagen-related peptide* (CRP-XL) (CRP-XL). Ademais, NSC87877 rescatou os efectos inhibidores do bloqueo da fosfoinosítido 3-quinasa (PI3K) sobre a agregación plaquetaria. Non obstante, as análises de western blot indicaron que as fosforilacións de PLC γ 2 Tyr⁷⁵⁹ e Src Tyr⁴¹⁹ reducíronse pola inhibición combinada de Shp1/2 e PI3K. Pola contra, a fosforilación de Syk Tyr⁵²⁵⁺⁵²⁶ permaneceu inalterada. En conxunto, estes achados suxiren que Shp1/2 compensa a ausencia de actividade de PI3K na mediación da activación da integrina e da fosforilación de PLC γ 2, aínda que o signo do cambio foi diferente. Probablemente, isto

subliña un papel negativo de Shp2 (na activación da integrina) e un papel positivo de Shp1 (na vía PLC).

Para comprender mellor as contribucións de GPVI e integrina $\alpha\text{IIb}\beta 3$ na formación de trombos inducidos por coláxeno, no **capítulo 8** realizamos unha investigación sobre o efecto dos papeis dependentes da integrina da quinase de adhesión focal PTK2, o calcio e a proteína de unión á integrina 1 (CIB1) e o receptor de coláxeno GPR56 dependente do cizallamento na formación de trombos inducidos polo coláxeno. Para este fin, deseñamos e sintetizamos péptidos que se demostrou que interferían coa unión αIIb -CIB1 (pCIB e pCIB^m) ou que imitaban a activación de GPR56 (pGRP). Observamos que o pGRP a alta velocidade de cizallamento mostraba efectos supresores na formación de trombos mediados por coláxeno, en lugar de efectos de activación. Ademais, o bloqueo simultáneo de PTK2 provocou unha supresión aínda maior da formación de trombos. E o mesmo ocorreu cos péptidos interferentes CIB1, pCIB e pCIB^m. Por outra banda, non se observaron efectos peptídicos para a agregación plaquetaria inducida por GPVI ou a mobilización de Ca^{2+} , en ausencia de cizallamento. Xuntos, estes achados apuntaron a un papel dependente do cizallamento de PTK2, CIB1 e integrina $\alpha\text{IIb}\beta 3$ na activación plaquetaria e formación de trombos mediada por coláxeno e GPVI.

No **capítulo 9**, os achados máis importantes son discutidos de forma crítica e sitúanse no marco da literatura actual. Indícase que o traballo actual proporciona unha poderosa ferramenta para investigar máis a composición das proteínas plaquetarias e revelar as relacións do proteoma plaquetario e do transcriptoma entre humanos e ratos. O traballo realizado abre novas vías para aplicar métodos proteómicos baseados na espectrometría de masas á Bioloxía plaquetaria, e tamén para axudar a dilucidar aínda máis as vías positivas e negativas subxacentes á formación de trombos inducidas por GPVI na hemostase e a trombose; e ademais axudar a identificar un antagonista de GPVI.

总结

血小板在多种生理和病理过程中发挥关键作用，包括参与止血与动脉血栓形成、参与炎症过程、影响血管完整性和癌症转移等。在血管损伤时，它们会形成血栓以防止失血过多；但是这一闭塞性血凝块亦会引起血栓。糖蛋白 VI(GPVI)作为血小板上主要的胶原蛋白受体，目前已在小鼠实验中被证实能引起动脉血栓形成，但是 GPVI 的缺失并不会造成出血风险；当 GPVI 在人体中突变或者缺失亦会引起轻度出血，因此 GPVI 目前被认为是一种新的抗血栓靶点。尽管对胶原蛋白和 GPVI 诱导血小板激活进行了大量研究，但胶原蛋白和 GPVI 介导的血小板活化机制仍有许多未知部分。由于特殊的无核结构，血小板中的大部分蛋白质活动受翻译后修饰 (PTM) 的调节。因此，基于高分辨率质谱的蛋白质组学技术已成为系统地鉴定和理解蛋白质磷酸化变化并将其整合到受体介导的蛋白质信号级联中的强大工具。本论文的主要目标是揭示完整的血小板蛋白质组的组成，并阐明 GPVI 诱导的血小板活化和血栓形成的新的途径和新的机制。

第 1 章概括了血小板特别是糖蛋白受体 GPVI 在血栓形成和止血过程中的作用，以及如何应用血小板蛋白质组学对血小板进行特定或者全面的研究。作为蛋白质组学方法在血小板研究中应用的详细概述，**第 2 章**列出并讨论了自 2010 年以来的所有已发表 67 篇的关于人类血小板蛋白质组、以及分子蛋白质组学研究在疾病和血小板信号传导中的特定应用的工作，并详细介绍了被激活的血小板上受体介导的相关信号通路，包括胶原蛋白受体 GPVI、血管性血友病因子(VWF)受体 GPIb-V-IX、podoplanin 受体 CLEC-2、凝血酶受体 PAR1 和 PAR4、ADP 受体 P2Y₁ 和 P2Y₁₂、血栓素 A₂ 受体 TP，以及纤维蛋白(原)受体整合素 α IIb β 3。此外，我们还介绍了与血小板相关的抑制途径，包括前列环素和一氧化氮相关的抑制途径以及血小板抑制剂所抑制的各种途径，同时还概述了血小板蛋白质组学技术的当前发展，以及其在血小板信号传导通路上的应用，包括监测血小板老化相关的蛋白质变化和血小板相关先天性疾病以及心血管疾病中的血小板蛋白的改变。我们还综合介绍了目前蛋白质组学方法在建立与信号转导、代谢、血小板结构和存活相关

的完整血小板(亚)蛋白质组方面的目前的局限和未来的挑战。综上所述, 基于质谱的蛋白质组学有望成为检测与血小板异常相关的生物标志物的最强大工具之一, 并有临床中研究中发挥重大作用。

由于尚未建立与血小板转录组相关的完整血小板蛋白质组, 在**第3章**中, 我们对血小板的转录组学和蛋白组学进行了全面的定量比较, 并以此构建了(理论上)完整血小板蛋白质组的预测模型。首先, 我们基于多特蒙德莱布尼茨研究所 ISAS 发表的六个蛋白质组数据建立了一个当前人类血小板蛋白质组数据库, 其中包含超过 5200 个已鉴定的特异性蛋白质, 同时, 我们将其与含有超过 5 万 4 千个血小板及巨核细胞转录组的 Blueprint 数据库(英国剑桥)结合起来进行综合比较分析。随后, 根据 UniProt 数据库中注释的细胞内位置和功能, 我们将所有可能表达的血小板 mRNA 和蛋白质分为 21 类。通过比较, 我们发现血小板和巨核细胞转录组高度相关, 尤其在能够编码蛋白质的转录本之间。此外, 血小板蛋白质组和转录组数据之间的定量比较呈现出三角形模型, 这一模式表明具有较高翻译水平的蛋白质往往也具有较高的转录水平, 但反之则不然。这些结果也在血小板转录组的分布分析中得以证明, 已鉴定到的蛋白质的 mRNA 平均基因表达水平均较高, 而未鉴定到的血小板蛋白质中, 大多数相应的转录物具有相对较低的基因表达水平。

通过功能类别分析, 我们发现了限制蛋白质被鉴定到的三个因素, 分别是: (i)(周)核定位; (ii)低转录水平, (iii)低翻译水平。基于这三个限制因素, 我们构建了一个包含约有一万个血小板蛋白质的血小板全蛋白组预测模型。同时使用最新的包含 30 个健康受试者的血小板蛋白质组学数据对这一预测模型进行验证。

为了更全面地了解血小板蛋白质组和转录组, 我们对不同物种间的血小板转录组和蛋白组进行了全面综合的分类比较。在**第4章**中, 我们整合了来自人类血小板的 8 个 RNA-Seq 数据集, 得到了 54357 个人类转录本, 其中 20125 个基因能够编码蛋白质, 同时整合了来自小鼠血小板的两个数据集, 获得 17317 个小鼠蛋白质编码转录本。结果表明, 尽管转录组分析中存在一些样本异质性, 血小板转录组的种内相

关性极高，而种间相关性则大为降低，这一结论在血小板蛋白组中也成立。尽管如此，血小板的蛋白质和直系同源 mRNA 在不同物种之间高度重叠，尤其高丰度表达的 mRNA。然而，不同物种之间仍包含非常多的物种特异性蛋白质或转录本，在我们的数据集中发现 184 种具有明显种间差异的蛋白质/转录本，包括已知仅存在于小鼠血小板中的凝血酶受体 PAR3。对这些物种特异性蛋白质进行功能类别分析发现，差异最大的蛋白质主要集中在膜受体与膜通道蛋白和信号与衔接蛋白中。

蛋白质组学的一个重要应用是监测患有血小板相关疾病的患者血小板中的蛋白质变化。在**第 5 章**中，我们揭示了 7 名 Albright 遗传性营养不良综合征(AHO, Ia 型假性甲状旁腺功能减退症)患者血小板中磷酸化蛋白质组的变化。AHO 综合征与 GNAS 基因位点的功能丧失突变有关，该突变编码 Gs α 蛋白，该蛋白参与腺苷酸环化酶(AC)和 cAMP 依赖性蛋白激酶 A(PKA)的激活，这是血小板中主要的激活抑制途径。在本章中，共鉴定到 2516 个磷酸化位点，包括 453 个受伊洛前列素调节的磷酸化位点，其中有 50 个磷酸化位点在患者和健康对照受试者之间差异表达。同时，我们证实大部分被伊洛前列素刺激而上调的蛋白质都与 PKA 信号传导途径相关。最为重要的是，我们发现发生表达差异的蛋白质主要与以下几种途径相关：(i)与有缺陷的 Gs α 和 PKA 活性有关，(ii)与血小板功能的变化有关，(iii)参与评估 AHO 和非 AHO 之间具有 GNAS 突变的患者的可能性。同时我们发现，尽管患者的血小板磷酸化蛋白质组发生了巨大变化，但全蛋白质组仅显示出微小的变化。这一结果表明我们需要更精确的蛋白质组学定量方法来监测蛋白质磷酸化的动态变化。

作为胶原蛋白的主要信号传导受体，GPVI 在小鼠动脉血栓形成中起重要作用，这意味着了解 GPVI 下游的信号通路的调控非常重要。在**第 6 章**中，我们重点讨论了 GPVI 和整合素 α IIb β 3 在流动条件下受纤维蛋白(原)诱导激活的血栓形成中的联合作用。我们注意到 GPVI 在纤维蛋白或纤维蛋白原表面被微微激活，从而有限的引起血小板聚集及在动脉剪切速率下的促进微小血栓形成。此外，当抑制 GPVI 或 Syk 后发

现了 GPVI 和整合素 $\alpha\text{IIb}\beta 3$ 在纤维蛋白诱导的血栓形成中的非冗余作用。这一发现在缺乏 $\alpha\text{IIb}\beta 3$ 的 Glanzmann 患者的血小板中得到证实，这表明 GPVI 和 $\alpha\text{IIb}\beta 3$ 的临床相关拮抗作用存在部分重叠。

在第 7 章中，我们研究了可能对 GPVI 进行负调节的酪氨酸磷酸酶 Shp1 和 Shp2 如何影响 GPVI 诱导的血小板活化。我们发现 Shp1/2 被 NSC87877 联合抑制后，由低剂量 GPVI 特异性激动剂胶原相关肽(CRP-XL)诱导的血小板聚集增加了。此外，NSC87877 还可以拯救因抑制磷酸肌醇-3-激酶 (PI3K)而对血小板聚集产生的抑制作用。然而，western blot 实验表明 PLC γ 2 Tyr⁷⁵⁹ 和 Src Tyr⁴¹⁹ 的磷酸化水平因 Shp1/2 和 PI3K 的联合抑制而降低，而 Syk Tyr⁵²⁵⁺⁵²⁶ 的磷酸化水平保持不变。这些发现表明 Shp1/2 在介导整合素激活和 PLC γ 2 磷酸化方面弥补了 PI3K 活性的缺失。这一现象有可能是由于 Shp2(在整合素激活中)的负面作用和 Shp1(在 PLC 信号通路中)的积极作用所造成的。

为了更好地理解 GPVI 和整合素 $\alpha\text{IIb}\beta 3$ 在胶原诱导的血栓形成中的作用，在第 8 章中，我们研究了黏着斑激酶 PTK2、钙和整合素结合蛋白 1(CIB1)和剪切速率依赖性胶原受体 GPR56 对胶原诱导的血栓形成的影响。为此，我们设计并合成了经证实可干扰 αIIb -CIB1 结合(pCIB 和 pCIB^m)或模拟 GPR56(pGRP)激活的肽段。我们注意到高剪切速率下的 pGRP 对胶原介导的血栓形成具有抑制作用，而不是激活作用。此外，PTK2 能够与 pGRP 共同作用以提高对血栓形成的抑制作用。CIB1 干扰肽 pCIB 和 pCIB^m 与 pGRP 共同作用也具有相同的抑制效果。另一方面，在没有剪切速率的情况下，GPVI 则不能诱导的血小板聚集或 Ca^{2+} 释放。这些发现阐明了 PTK2、CIB1 和整合素 $\alpha\text{IIb}\beta 3$ 在胶原蛋白和 GPVI 介导的血小板活化和血栓形成中的剪切速率依赖性作用。

第 9 章主要对论文中最重要的发现结合已发表的文章进行了批判性讨论。这篇论文目前的工作为进一步研究血小板蛋白组成和揭示不同物种间血小板蛋白质组和转录组之间的关系提供了强有力的工具。同时，利用基于质谱的蛋白质组学方法有助于进一步阐明 GPVI 诱导的止血和血栓形成的正负调控途径，帮助识别 GPVI 拮抗剂，以为将来更

深入的抗血栓研究提供基础。

Impact

Cardiovascular diseases (CVD) provide the great threaten to man, of which thrombosis in the arteries or veins are still leading causes of death¹⁻³. Platelets are the smallest anucleate blood cells that are released by megakaryocytes in the bone marrow⁴. Platelets fulfill a key role in the formation of a thrombus or clot and also support the blood coagulation system. Hence, the formation of a platelet plug prevents excessive blood loss when a blood vessel is damaged or ruptured⁵. However, dysfunctional platelet activation in thrombus formation at a ruptured site of an atherosclerotic plaque can cause pathological occlusive thrombus formation, which predisposes for stroke or heart infarction. Currently, antiplatelet drugs are widely used in the clinical treatment after arterial thrombosis, including aspirin, clopidogrel, prasugrel and ticagrelor⁶. However, all these antithrombotic drugs are associated with a risk of bleeding, and their efficacy can vary greatly between individuals.

Glycoprotein VI (GPVI) is the major signaling collagen receptor on the surface of platelets, which induces thrombus formation by binding to collagen directly, or by binding to fibrin in second instance. In GPVI-deficient mouse, only a moderate increase of the bleeding time was observed, while arterial thrombosis was substantially impaired. This points to a crucial role of GPVI in arterial thrombosis with limited contribution to hemostasis; and this makes GPVI to a novel potential antithrombotic target⁷. As indicated below, this thesis on human platelets aims to contribute to the support for a selective antithrombotic action mechanism through GPVI signaling inhibition or through GPVI blockage.

Because of their anucleate structure, platelet signaling activities are regulated by post-translational modifications (PTMs). To unravel these, mass spectrometry-based proteomics analyses are becoming one of the powerful tools for defining the protein alterations and receptor-mediated signaling cascades in platelets^{8,9}. Here, we revealed the full composition of platelet proteome by a global comparison of platelet proteomes and transcriptomes. The generated large datasets – also to compare human and mouse platelets

– can now be used to elucidate the mechanisms of GPVI-induced thrombus formation, and ultimately for determining protein targets downstream of GPVI for use in the clinic.

With the development of state-of-the-art mass spectrometers, proteomics techniques are increasingly applied in the research of platelet protein composition, platelet signaling cascades and platelet-related diseases. The overview on these aspects in **Chapter 2** provides in-depth insight into earlier and current proteomics methods for detecting protein changes in patients after antiplatelet treatment or presenting with a platelet-based disorder. However, in spite of this wide use of proteomics methods, still only part of the platelet proteins has been identified in comparison to the detected mRNAs, likely to limitations in the proteomic techniques. To get a comprehensive idea on the theoretical platelet protein composition, we conducted a quantitative global comparison of the human and mouse platelet proteomes and the corresponding platelet (and megakaryocyte) transcriptomes, which assisted in our understanding the variety of functions carried out by platelets (**Chapters 3 and 4**). For the latter purpose, we developed an integrative platelet protein function classification scheme.

Throughout this work, three restraining factors for the hitherto limited protein identification by mass spectrometry-based proteomics were seen. These were: (i) (peri)nuclear localization; (ii) low transcription and (iii) low translation of the expected (megakaryocytic) proteins. Based on these restraining factors, we could establish and validate a prediction model for the full platelet proteome, in which around 10,000 platelet proteins are expected out of the more than 20,000 predicted ones with any corresponding transcript level. In addition, we confirmed a high correlation between the human platelet and megakaryocyte transcriptomes, and even higher correlations between several included datasets of human platelet transcriptomes. However, the composed mouse platelet transcriptome was less well correlated with the median human platelet transcriptome; and the same was true for the two platelet proteomes. On the other hand, the

overlap of orthologous transcripts between the two species was very high, especially for the highest abundance transcripts. The same also held for the highest abundant human and mouse platelet proteins. Together, these studies thus provided a better understanding of the (complete) platelet proteome with the help of platelet transcriptome information.

Platelet proteomics can also be used for monitoring proteins changes in platelet related diseases. In **Chapter 5**, using stable isotope labeling we detected a panel of 50 differently iloprost-regulated protein phosphorylation sites in platelets from patients with Albright hereditary osteodystrophy syndrome (AHO syndrome), and we confirmed that the upregulated proteins were protein kinase A-dependent. This indicated that indeed platelet phosphoproteome analysis can help to understand alterations in platelet function in such patients.

In **Chapters 6-8**, we investigated signaling pathways that may enhance or restrain the GPVI-induced processes of platelet activation and thrombus formation. In **Chapter 6**, we observed that the activating role of GPVI was only moderately activated by binding to fibrin(ogen), by only triggering microthrombus formation on surfaces of fibrin or fibrinogen upon whole-blood flow. The blockage effects of GPVI fiber or Syk let us conclude for a nonredundant role of GPVI and the integrin $\alpha\text{IIb}\beta\text{3}$ in fibrin-induced thrombus formation. Stated otherwise, our data suggest a partial overlap of the effects of clinical-relevant antagonisms of GPVI and $\alpha\text{IIb}\beta\text{3}$.

In **Chapter 7**, we established that the pharmacological inhibition of the Src homology 2 domain containing protein tyrosine phosphatases, Shp1 and Shp2, under certain conditions, enhanced GPVI-induced platelet aggregation. This was the case in response to a low dose of CRP-XL, and upon blockage of the phosphoinositide 3-kinase (PI3K) pathway which is required for integrin activation. However, the blockage of Shp1/2 did not affect the signaling immediately below GPVI, while the combined inhibition of Shp1/2 and PI3K reduced rather than increased the phosphorylation of Src Tyr⁴¹⁹ and phospholipase $\text{C}\gamma\text{2}$ (PLC γ2) Tyr⁷⁵⁹. These findings suggested that both

isoforms Shp1/2 compensate for the absence of PI3K activity in mediating integrin activation and PLC γ 2 phosphorylation. Likely, this underscores a specific negative role of Shp2 (in integrin activation) and a positive role of Shp1 (on the PLC pathway).

In **Chapter 8**, we established that a peptide mimicking activation of the shear-dependent collagen receptor GPR56 (pGRP) showed suppressive rather than enhancing effects on collagen-mediated thrombus formation, in a way confined to a high wall-shear rate, as is relevant for arterial thrombosis. Simultaneous blockage of the focal adhesion kinase PTK2 caused a synergistical suppression of the thrombus formation. In the same chapter, we found that interfering peptides with the calcium and integrin-binding protein 1 (CIB1), pCIB and pCIB^m were able to suppress collagen-induced thrombus formation only at high shear rate. These findings pointed to a shear-dependent role of PTK2, CIB1 and integrin α IIb β 3 in collagen- and GPVI-mediated platelet activation and thrombus formation.

Overall, this thesis provides a powerful tool for further investigating the platelet protein composition and to reveal the relations of the platelet proteome and transcriptome across human and mouse. In addition, this thesis provides novel insights into the precise regulation and mechanism of the GPVI-mediated signaling and thrombus formation. Therefore, I am confident that my findings will give a better background for understanding the possibilities and limitations for GPVI-related antithrombotic drugs in CVD.

References

1. Alkarithi G, Duval C, Shi Y, Macrae FL and Ariëns RAS. Thrombus structural composition in cardiovascular disease. *Arterioscler Thromb Vasc Biol.* 2021;41:2370-2383.
2. Yusuf S, Wood D, Ralston J and Reddy KS. The World Heart Federation's vision for worldwide cardiovascular disease prevention. *Lancet.* 2015;386:399-402.
3. Gregson J, Kaptoge S, Bolton T, Pennells L, Willeit P, Burgess S et al. Cardiovascular risk factors associated with venous thromboembolism. *JAMA*

- Cardiol.* 2019;4:163-173.
4. Sim X, Poncz M, Gadue P and French DL. Understanding platelet generation from megakaryocytes: implications for in vitro-derived platelets. *Blood.* 2016;127:1227-1233.
 5. Van der Meijden PE and Heemskerk JW. Platelet biology and functions: new concepts and clinical perspectives. *Nat Rev Cardiol.* 2019;16:166-179.
 6. Wijeyeratne YD and Heptinstall S. Anti-platelet therapy: ADP receptor antagonists. *Br J Clin Pharmacol.* 2011;72:647-657.
 7. Nieswandt B, Schulte V, Bergmeier W, Mokhtari-Nejad R, Rackebrandt K, Cazenave JP et al. Long-term antithrombotic protection by in vivo depletion of platelet glycoprotein VI in mice. *J Exp Med.* 2001;193:459-469.
 8. Shevchuk O, Begonja AJ, Gambaryan S, Totzeck M, Rassaf T, Huber TB et al. Proteomics: a tool to study platelet function. *Int J Mol Sci.* 2021;22:4776.
 9. Burkhart JM, Gambaryan S, Watson SP, Jurk K, Walter U, Sickmann A et al. What can proteomics tell us about platelets? *Circ Res.* 2014;114:1204-19.

Curriculum vitae

Jingnan Huang was born on August 3rd 1993 in Henan, China. In 2010 she started her bachelor study of Biotechnology at the Hainan University, China, where she got her bachelor's degree in 2014. After receiving her bachelor's degree, she moved to Fudan University (China) to start a master of Biochemistry and Molecular Biology under the supervisor of Prof. Xumin Zhang. In 2017, she obtained her master's degree at Fudan University with honours. After her master, she worked as a technician at Shanghai Jiaotong University School of Medicine in Shanghai. During this period, she was in charge of the proteomics sample preparations and instrument maintenance. In 2018, she started the PhD project, which was part of the joint doctoral programme between Leibniz-Institut für Analytische Wissenschaften-ISAS-e.V., ISAS in Dortmund (Germany), the University of Maastricht (the Netherlands) and the University of Santiago de Compostela (Spain), under the joint supervision of Prof. Johan Heemskerk, Prof. Albert Sickmann, Dr. Ángel García and Prof. Hugo ten Cate. In 2018-2021, she performed research in the fields of analysis of platelet proteomics and transcriptomics, and in experimental thrombosis and haemostasis, as described in this thesis. During her PhD period, she started in protein dynamics group of Prof. Albert Sickmann in Dortmund. Afterwards, she moved to Maastricht University under the supervisor of Prof. Johan Heemskerk and Prof. Hugo ten Cate, while in 2021, she left to Santiago de Compostela for working in the platelet proteomics group of Dr. Ángel García. To complete her studies, she came back to Maastricht to finish her project in the platelet group of Prof. Johan Heemskerk.

Publications

Publications

1. Zhang Y, He Q, Ye J, Li Y, Huang L, Li Q, **Huang J**, Lu J and Zhang X. Systematic optimization of C-terminal amine-based isotope labeling of substrates approach for deep screening of C-terminome. **Analyt Chem.** 2015 Oct 20;87(20):10354-61.
2. Ye J, Zhang Y, Huang L, Li Q, **Huang J**, Lu J, Li Y and Zhang X. An optimized guanidination method for large-scale proteomic studies. **Proteomics.** 2016 Jul;16(13):1837-46.
3. Zhang Y, Li Q, **Huang J**, Wu Z, Huang J, Huang L, Li Y, Ye J and Zhang X. An approach to incorporate multi-enzyme digestion into C-TAILS for C-terminomics studies. **Proteomics.** 2018 Jan;18(1):201700034.
4. **Huang J**, Wang J, Li Q, Zhang Y and Zhang X. Enzyme and Chemical Assisted N-Terminal blocked peptide analysis, ENCHANT, as a selective proteomics approach complementary to the conventional shotgun approach. **J Proteome Res.** 2018 Jan 5;17(1):212-221.
5. Wu Z, Huang J, **Huang J**, Li Q and Zhang X. Lys-C/Arg-C, a more specific and efficient digestion approach for proteomics studies. **Analyt Chem.** 2018 Aug 21;90(16):9700-9707.
6. Li Q, Zhang Y, **Huang J**, Wu Z, Tang L, Huang L and Zhang X. Basic strong cation exchange chromatography, BaSCX, a highly efficient approach for C-terminomic studies using LysargiNase digestion. **Analyt Chem.** 2020 Apr 7;92(7):4742-4748.
7. Swieringa F, Solari FA, Pagel O, Beck F, **Huang J**, Feijge MAH, Jurk K, Korver-keularts IMLW, Mattheij NJA, Faber J, Pohlenz J, Russo A, Stumpel CTRM, Schrande DE, Zieger B, van der Meijden PEJ and Heemskerk JWM. Impaired iloprost-induced platelet inhibition and phosphoproteome changes in patients with confirmed pseudohypoparathyroidism type Ia, linked to genetic mutations in GNAS. **Sci Rep.** 2020 Jul 9;10(1):11389.

8. Li Q, Zhang Y, Wu Z, **Huang J**, Yue N, Huang L and Zhang X. Tyrosine-EDC conjugation, an undesirable side effect of the EDC-catalyzed carboxyl labeling approach. **Analyt Chem**. 2021 Jan 19;93(2):697-703.
9. Perrella G, **Huang J**, Provenzale I, Swieringa F, Heubel-Moenen FCJ, Farndale RW, Roest M, van der Meijden PEJ, Thomas M, Ariëns RAS, Jandrot-Perrus M, Watson SP and Heemskerk JWM. Nonredundant roles of platelet glycoprotein VI and integrin $\alpha\text{IIb}\beta 3$ in fibrin-mediated microthrombus formation. **Arterioscler Thromb Vasc Biol**. 2021 Feb;41(2):e97-e111.
10. **Huang J**, Swieringa F, Solari FA, Provenzale I, Grassi L, De Simone I, Baaten CCFMJ, Cavill R, Sickmann A, Frontini M and Heemskerk JWM. Assessment of a complete and classified platelet proteome from genome-wide transcripts of human platelets and megakaryocytes covering platelet functions. **Sci Rep**. 2021 Jun 11;11(1):12358.
11. **Huang J**, Zhang P, Solari FA, Sickmann A, García Á, Jurk K and Heemskerk JWM. Molecular proteomics and signaling of human platelets in health and disease. **Int J Mol Sci**. 2021 Sep 13;22(18):9860.
12. **Huang J**, Jooss NJ, Fernández DI, Sickmann A, García Á, Wichapong K, Dijkgraaf I, Heemskerk JWM. Roles of focal adhesion kinase PTK2 and integrin $\alpha\text{IIb}\beta 3$ signaling in collagen- and GPVI-dependent thrombus formation under shear. **Int J Mol Sci**. 2022 Aug 4; 23(15):8688
13. **Huang J**, Fernández DI, Zou J, Wang X, Heemskerk JWM, García Á. Restrained glycoprotein VI-induced platelet signaling by tyrosine protein phosphatases independent of phospholipase $\text{C}\gamma 2$. To be submitted.
14. **Huang J**, Swieringa F, Solari FA, Provenzale I, Grassi L, De Simone I, Baaten CCFMJ, Cavill R, Middleton E, Sickmann A, Rondina MT, Frontini M, Heemskerk JWM. A classified reference genome-wide transcriptome and proteome of human and mouse platelets revealing high qualitative similarity. To be submitted.

Abstracts

1. **Huang J***, Swieringa F*, Provenzale I, Grassi L, Solari FA, Cavill R, Sickmann A**, Frontini M**, Heemskerk JWM**. Towards functional assignment of the full platelet proteome and transcriptome. Congress of the International Society on Thrombosis and Haemostasis (ISTH), Milan, Italy, 2020.
2. **Huang J**, Swieringa F*, Solari FA*, Provenzale I, Grassi L, Baaten CCFMJ, Cavill R, Sickmann A**, Frontini M**, Heemskerk JWM**. Towards functional assignment of the full platelet proteome and transcriptome. Human Proteome Organization (HUPO), Stockholm, Sweden, 2020
3. **Huang J**, Jooss JJ, Fernández DI, García Á, Heemskerk JWM. Role of novel shear-dependent receptor GPR56 and integrin-linked CIB in GPVI-dependent thrombus formation and signaling. CiMUS workshop, Santiago de Compostela, Spain, 2021
4. Fernández DI, **Huang J**, Kuijpers MJE, Heemskerk JWM, García Á. Intracellular suppressive pathways of collagen-induced GPVI activation: effects on thrombus formation. CiMUS workshop, Santiago de Compostela, Spain, 2021

Posters

1. **Huang J**. Innovative methods to study proteomic signatures of glycoprotein receptor signaling. Centrum für Thrombose und Hämostase (CTH) retreat, Bonn, Germany, 2019. (Oral)
2. **Huang J**. Towards functional assignment of the full platelet proteome and transcriptome. Congress of the International Society on Thrombosis and Haemostasis (ISTH), Milan, Italy, 2020. (Poster)
3. **Huang J**. Towards functional assignment of the full platelet proteome and transcriptome. Human Proteome Organization (HUPO), Stockholm, Sweden, 2020. (Poster)

4. **Huang J.** Role of novel shear-dependent receptor GPR56 and integrin-linked CIB in GPVI-dependent thrombus formation and signaling. CiMUS workshop, Santiago de Compostela, Spain, 2021 (Oral)

Acknowledgements

I want to thank my four brilliant supervisors, **Prof. Johan Heemskerk**, **Dr. Ángel García**, **Prof. Albert Sickmann** and **Prof. Hugo ten Cate**, for their selfless help, their patience, their precious advices and supports during my PhD period. My promoter **Prof. Johan Heemskerk**, you are the best supervisor in the world in my viewpoint, I can't achieve such fruitful results during my PhD without your help and support. You are always there to help me, to encourage me, I can't imagine what my PhD would have been without you. I appreciate that I have the chance to complete my PhD under your supervision, thank you very much for guiding me for the last three years, I'll remember this experience forever. I also want to thank my promoter in ISAS, Germany, **Prof. Albert Sickmann**, thank you very much for giving this chance to work in ISAS. My co-promotor **Dr. Ángel García**, thank you very much for all your help in Santiago de Compostela, I'll never forget the days I spent in Santiago and the knowledges I obtained in our platelet proteomics group. My co-promotor **Prof. Hugo ten Cate**, thank you a lot for your kind support in Maastricht.

A big thank you goes to **Gina**, who welcomed me warmly when I moved to Maastricht and taught me everything about 'flow chamber', for the nice trips in the Netherlands, nice picnic in Maastricht and best Pizza I've ever eaten. **Frauke**, who taught me a lot about large-scale data analysis and provided all the help I needed. I also would like to thank **Funda**, for the Turkish coffee, traditional Turkish cuisine, and fantastic travel in Germany and Belgium. A special thanks to **Delia**, who shared great times with me in Maastricht and Santiago, for her excellent collaboration in the lab and for her relaxing travels in the Netherlands and Spain. **Natalie**, who gave me a lot of help and advice on experiments, thank you so much! I also want to thank all my roommates in Maastricht, **Isabella** for nicely help when I moved to Maastricht, **Alicia** for the advices in the experiment, **Danielle** for the very timely translation of the Dutch news and **Ilaria** for driving. I would also like to thank for everything to the colleagues of the platelet team: **Sanne** for the help with heatmaps, **Constance** for making network figures, **Bibian** for

always helping me find antibodies in the lab, **Claudia, Mieke and Giorgia** for taking blood. A big thank you to **Judith, Marijke and Simone** for all the supports in the lab, thank you very much!

I also would like to thank all the colleagues in ISAS, Dortmund, I have thoroughly enjoyed my eight months at ISAS. I want to thank **Stefan** for warmly welcomed in the first day of Dortmund and all the help in my experiments, **Fiorella** for revising my proteomics paper, **Laxmikanth Kollipara (Lucky)** for teaching me to do proteomics experiment.

A special thank you goes to all my colleagues in University of Santiago de Compostela, it's a wonderful and fruitful 7-month work in platelet proteomics group. I would like to thank **Sara** for the help with microscope and aggregation experiment, **Lidia** for arranging donors and experiments.

A very special thank goes to all my Chinese friends in Maastricht, Dortmund and Santiago de Compostela. 首先非常感谢邹今幂(Jinmi)对我工作生活中所有的帮助，作为实验室最开始差不多同时进实验室的唯二的中国人，我们一起相互帮助做实验，相互献血，同时也蹭了你家不少的饭，非常开心能够跟你在马城做了那么久的同事！作为多重同事，十分感谢张任丰(Hilaire)对我所有的帮助，无论是在 ISAS 还是在 UM，或是在 TAPAS 项目中，我们都有非常良好的合作关系，能够有机会跟你一起做实验我真的非常开心，同时也十分感谢你每次旅行中的优秀的规划，希望有机会能够再次一起出行。我还要感谢我在 Santiago 的 TAPAS 小伙伴王雪晴(Xueqing)，说实话，我实在无法想象如果没有你，我自己一个人在 Santiago 该怎么过，哈哈。非常感谢你在 Santiago 给我的所有帮助，无论是实验上还是生活上。略有遗憾的就是疫情开始之后我们就再也没有一起出去玩过了，非常怀念疫情之前的各种旅游，以后有机会我会再去欧洲找你玩的，哈哈。我还要感谢 ISAS 的中国小伙伴，李婷婷(Tingting)，陈粟源(Suyuan)，张鹏宇(Pengyu)，因为有你们，所以才有我在 ISAS 将近八个月的美好时光，也是因为你们，我才能获得更多的学习交流的信息。我还要感谢我在 Maastricht 的师姐们，刘小松(Song)，桑亚秋(Yaqiu)，感谢你们对我工作中的帮助，更加感谢你们

的大餐，哈哈！想要感谢的人还有很多，想要说的话也有很多，纸短情长。人生没有不散的宴席，终是到了分别的岔路口，希望未来的我们无论都能在各自的领域认真生活，开心工作，努力成为自己的光。

最后我还要感谢我的家人朋友这么些年对我的支持，没有你们，我想我很难在异国他乡坚持这几年。Finally, the sincerest thanks to all of my friends and my family. I would like to thank my parents and brother for giving me all the love and support I needed to complete the PhD, my dearest friends **Kaili, Rui, Ruixia, Yang, Qingqing** and **Lin**, who always support and encourage me to do whatever I want to do. They have made my life better and fearless.